INTERLAMINAR TENSILE STRENGTH AND MODE I FRACTURE TOUGHNESS OF DIFFERENT ANGLE-PLY CFRP AND GFRP COMPOSITE LAMINATES

A THESIS SUBMITTED TO
THE GRADUATE SCHOOL OF NATURAL AND APPLIED SCIENCES
OF
MIDDLE EAST TECHNICAL UNIVERSITY

BY

BURAK OGÜN YAVUZ

IN PARTIAL FULFILLMENT OF THE REQUIREMENTS
FOR
THE DEGREE OF MASTER OF SCIENCE
IN
AEROSPACE ENGINEERING

SEPTEMBER 2019

Approval of the thesis:

INTERLAMINAR TENSILE STRENGTH AND MODE I FRACTURE TOUGHNESS OF DIFFERENT ANGLE-PLY CFRP AND GFRP COMPOSITE LAMINATES

submitted by **BURAK OGÜN YAVUZ** in partial fulfillment of the requirements for the degree of **Master of Science in Aerospace Engineering Department, Middle East Technical University** by,

Prof. Dr. Halil Kalıpçılar
Dean, Graduate School of **Natural and Applied Sciences** _____

Prof. Dr. İsmail Hakkı Tuncer
Head of Department, **Aerospace Engineering** _____

Assoc. Prof. Dr. Demirkan Çöker
Supervisor, **Aerospace Engineering, METU** _____

Prof. Dr. Levend Parnas
Co-Supervisor, **Mechanical Engineering, TED University** _____

Examining Committee Members:

Prof. Dr. Altan Kayran
Aerospace Engineering, METU _____

Assoc. Prof. Dr. Demirkan Çöker
Aerospace Engineering, METU _____

Prof. Dr. Levend Parnas
Mechanical Engineering, TED University _____

Assist. Prof. Dr. Gökhan Özgen
Mechanical Engineering, METU _____

Assoc. Prof. Dr. Hüsnü Dal
Mechanical Engineering, METU _____

Date: 09.09.2019

I hereby declare that all information in this document has been obtained and presented in accordance with academic rules and ethical conduct. I also declare that, as required by these rules and conduct, I have fully cited and referenced all material and results that are not original to this work.

Name, Surname: Burak Ogün Yavuz

Signature:

ABSTRACT

INTERLAMINAR TENSILE STRENGTH AND MODE I FRACTURE TOUGHNESS OF DIFFERENT ANGLE-PLY CFRP AND GFRP COMPOSITE LAMINATES

Yavuz, Burak Ogün
Master of Science, Aerospace Engineering
Supervisor: Assoc. Prof. Dr. Demirkan Çöker
Co-Supervisor: Prof. Dr. Levend Parnas

September 2019, 160 pages

Delamination is one of the main failure mechanisms in composite structures. Initiation and propagation of delamination are controlled by interface parameters including the interlaminar strength and fracture toughness, respectively. Hence, it is crucial to use the correct values of these parameters in the design and analysis of components such as composite tapered beams and curved beams. In this study, the effect of ply orientation on the interlaminar tensile strength and Mode I fracture toughness for CFRP, and GFRP laminates are investigated. For this purpose, curved beam strength (CBS) experiments are conducted on CFRP and GFRP laminates with 0˚/0˚, 25˚/-25˚, 45˚/-45˚ and 65˚/-65˚ interfaces and double cantilever beam (DCB) experiments are conducted on CFRP, and GFRP laminates with 0˚//0˚, 25˚//-25˚, 45˚//-45˚, 45˚//45˚, 65˚//65˚, and 90˚//90˚ interfaces.

Keywords: Interlaminar Tensile Strength, Fracture Toughness, CBS Test, Mode I, DCB Test

ÖZ

KARBON VE CAM DESTEKLİ KOMPOZİTLERDE DEĞİŞİK AÇILI LAMİNALARIN ARAYÜZLERİNİN, LAMİNALAR ARASI ÇEKME MUKAVEMETİNE VE MOD I KIRILMA TOKLUĞUNA ETKİSİ

Yavuz, Burak Ogün
Yüksek Lisans, Havacılık ve Uzay Mühendisliği
Tez Danışmanı: Doç. Dr. Demirkan Çöker
Ortak Tez Danışmanı: Prof. Dr. Levend Parnas

Eylül 2019, 160 sayfa

Delaminasyon, kompozit yapılardaki ana kırılma mekanizmalarından biridir. Delaminasyonun başlatılması ve yayılması sırası ile laminalar arası mukavemet ve laminalar arası kırılma tokluğu ile belirlenir. Bu nedenle, bu parametrelerin daralan kesit kompozit ve eğri şekilli kompozit bileşenlerin tasarımında ve analizinde doğru değerleri ile kullanılması çok önemlidir. Bu çalışmada, karbon ve cam destekli kompozitlerde değişik açılı laminaların arayüzleririn, laminalar arası çekme mukavemetine ve Mod I kırılma tokluğuna etkisi deneysel olarak incelenmiştir. Bu amaçla, 0˚ / 0˚, 25˚ / -25˚, 45˚ / -45˚ ve 65˚ / -65˚ arayüzleri ile CFRP ve GFRP laminatlarında kavisli kiriş dayanımı (CBS) deneyleri yapılmıştır. Çift çıkma kiriş (DCB) deneyleri CFRP ve GFRP laminatlar ile 0˚//0˚, 25˚//-25˚, 45˚//-45˚, 45˚//45˚, 65˚//65˚, and 90˚//90˚ arayüzlerinde gerçekleştirilir.

Anahtar Kelimeler: Laminalar Arası Çekme Dayanımı, Kırılma Tokluğu, CBS Deneyi, Mod I, DCB Deneyi

To reach a better world

ACKNOWLEDGEMENTS

First of all, I would like to express my deepest gratitude to my advisor, Assoc. Prof. Dr. Demirkan Çöker, for his tireless guidance, criticism, encouragement, and drive in helping me to achieve my M.Sc. study. I would like to thank my co-supervisor and the coordinator of our DKTM project, Prof. Dr. Levend Parnas, for giving to me the chance to study with him in both academic and business life. I appreciate all of his contributions that he gave to me, despite his very limited time, not only his recommendations but also by him being a role-model in his way of thinking, both academically and personally.

I would like to express sincere appreciation to the examining jury members, Prof. Dr. Altan Kayran, Assoc. Prof. Dr. Hüsnü Dal and Assist. Prof. Dr. Gökhan Özgen for their valuable comments and criticism, and the time they patiently devoted to this study. I would also like to acknowledge Assoc. Prof. Dr. Oğuz Uzol for offering me a peaceful working area and the opportunity to use METUWIND facilities.

I would like to thank the members of the Coker Research Group, Ahmet Çevik, Burcu Taşdemir, Tamer Tahir Ata, Miraç Onur Bozkurt, Can Muyan, Aydın Amireghbali, and Emine Burçin Özen for making this difficult time fun, their irreplaceable friendship, assistance and guidance throughout this study.

Some special words of gratitude go to my friends Hasan Yetgin, Begüm Çicek, Deniz Arslan and Kutay Çetin who have always been a major source of support when things would get a bit discouraging. Thanks, guys, for always being there for me. Also, I would like to thank my friends Irmak Subaşı and Tuba Mumcu for helping, supporting, and guiding me in my long master's degree study. And, I thank my friends Saeid Hosseinpour Dashatan and Mohsen Poorzeinolabedin, from the DKTM project, who shared their experience and knowledge with me. I appreciate my friends at the company Denise Parnas, Nimet Vuran, and Ertuğ Keleşoğlu for having a good time together, both at work and life outside. In the last stage, I would also like to

acknowledge my friends Parisa Moradi, Serhat Onur Çakmak and Arzu Aslaner who were in the same thesis period as me, for not making me feel alone in this process.

Last but not least, I would like to express my deepest thanks to my precious family. I am indebted to my father Hasan and my mother Huriye for their endless encouragement, love, and eternal faith in me, to my beloved brother Doruk Okan for his invaluable support, to my grandma the angel of the family Fatma Özel for her warm thoughts and eternal prayers, and to my grandpa, Ali Yavuz, for his love and for showing me the way to be a good person. Thank you for standing beside me in every step I took. I also would like to thank my uncle, Mustafa Zafer Özel and his wife Karen Özel, for helping me in the writing process of my thesis and guiding me in my academic career.

Finally, this work is financially supported by the Turkish Aerospace Industries, Inc. by a special grant from The Under secretariat for Defense Industries (SSM) under grant number DKTM 2015/05. The authors would like to thank RUZGEM – METU Center for Wind Energy for the use of their facilities. I also especially thank my companies, Leopar Composite and Teknolus Energy. I also would like to thank Erkan Önder, who is the owner of Teknolus Energy, for giving me this opportunity to create my thesis.

TABLE OF CONTENTS

LIST OF TABLES

TABLES

LIST OF FIGURES

FIGURES

LIST OF ABBREVIATIONS

ABBREVIATIONS

ASTM	American society for testing and materials
C3D8R	8 node brick element with reduced integration
CBS	Curved beam strength
CFRP	Carbon fiber reinforced polymer
CNC	Computer numerical control
DCB	Double cantilever beam
GFRP	Glass fiber reinforced polymer
ILTS	Interlaminar tensile strength
Mode I	Opening mode
Mode II	In-plane shear mode
UD	Unidirectional

LIST OF SYMBOLS

SYMBOLS

$\%$	Percent / fraction
σ_r^{max}	Interlaminar tensile strength
//	Initial crack location in laminate
°	Degree
±	Plus-minus
Δ	Delta (the difference between two data points)
a	Crack length
A_1	Slope of the a/h vs $C^{1/3}$ graph
B	Width of the double cantilever beam specimen
C	Compliance of one leg of double cantilever beam specimen
$℃$	Degree celsius
cm	Centimeter
Cos	Cosines
D	The diameter of the roller of the curved beam strength fixture
d_x	Distance between rollers of the fixture in the lateral axis
d_y	Stroke of the test machine
E^c_{11}	Compressive elastic modulus in the fiber direction
E^c_{22}	Compressive elastic modulus in the transverse direction

E^c_{33}	Compressive elastic modulus in the thickness direction
E^t_{11}	Tensile elastic modulus in the fiber direction
E^t_{22}	Tensile elastic modulus in the transverse direction
E^t_{33}	Tensile elastic modulus in the thickness direction
G_I	Fracture toughness (opening mode)
h	Thickness of the one leg of double cantilever beam specimen
L	Length of the specimen
l	Length of the specimen
l_0	Length of one leg of curved beam strength specimen between two rollers
l_b	Distance between bottom roller of curved beam strength experiment's fixture
l_t	Distance between top roller of curved beam strength experiment's fixture
M	Moment
P	Load
ϕ	The angle of the one leg of curved beam strength specimen with respect to ground
P_b	Perpendicular load applied to the specimen
r_i	Inner radius
r_o	Outer radius
S_{11}	Stress in the fiber direction
S_{12}	Shear strength in 1-2 plane or shear stress

S_{13}	Shear strength in 1-3 plane or shear stress
S_{22}	Stress in the transverse direction
S_{23}	Shear strength in 2-3 plane or shear stress
S_{33}	Stress in the thickness direction
S^c_{11}	Compressive strength in the fiber direction
S^c_{22}	Compressive strength in the transverse direction
S^c_{33}	Compressive strength in the thickness direction
S^t_{11}	Tensile strength in the fiber direction
S^t_{22}	Tensile strength in the transverse direction
S^t_{33}	Tensile strength in the thickness direction
t	Thickness of the specimen
Tan	Tangent
U	Energy
w	Width of curved beam specimen
α	Crack correction length
Θ	Angle
v_{12}	Poisson's ratio in transverse direction due to strain in the fiber direction
v_{13}	Poisson's ratio in thickness direction due to strain in the fiber direction
v_{23}	Poisson's ratio in thickness direction due to strain in the transverse direction
ρ	Density

CHAPTER 1

INTRODUCTION

This chapter starts with a definition of composites. Secondly, the importance of the composites will be mentioned. Thirdly failure in a composite structure is defined. Then the important properties which determine the failure of a composite structure are explained. Finally, the most important failure type; delamination, in composite structures will be explained.

1.1. Composite

Composite means “placed together”. Principally, composite materials consist of two or more separate materials combined in a macroscopic structural unit. Also, it is a physical combination of two or more different phases. Composite materials are used because of the unique and desirable properties of combined materials. The difference between composites and alloy comes from homogeneity. Even if alloys are also a combination of different materials, they are macroscopically homogenous, so they are not composites. The microscopic picture of one carbon-fiber reinforced polymer composite is shown in Figure 1.1.

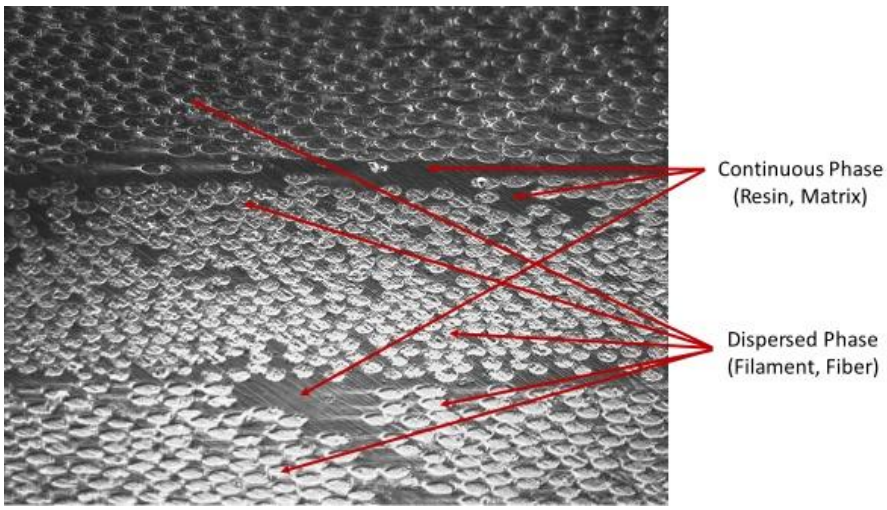

Figure 1.1. Microscopic picture of fiber and matrix composite

Composite materials are used for their advantageous properties. They have a high level of stiffness, high strength, are lightweight, have high fatigue resistance, design flexibility, and greater corrosion resistance relative to steel. For fiber-matrix composites, fibers provide strength and stiffness, while the matrix provides load transfer from fiber to fiber and, also, dimensional stability. Using composite parts decreases part count, so this decreases the number of fasteners or connections required. The capability of using different fiber orientations provides design flexibility. There are three forms of composite: fibrous, particulate and laminated. Laminated composites are examined in this study. For laminated composites, there are four main fiber types; boron, carbon, aramid, and glass. Furthermore, there are two main mesh types: fabric and unidirectional. Unidirectional laminates were produced for this study. There are two main groups of matrix called thermoset and thermoplastic. The thermoset matrix has irreversible chemical bonding while the thermoplastic one has reversible chemical bonding. The most used matrix is epoxy, which is thermoset due to its mechanical properties. In this study, glass and carbon are used as fiber types and epoxy as the matrix type. For fiber-reinforced polymer type composites, fibers are used for their high strength and modulus, while resin (polymer) is used for bonding of these fibers which provide load transfer from fiber to fiber.

1.2. Delamination Failure of Unidirectional Composite Laminates

Laminated composites are used in many important areas such as in vehicles, sports parts, military structures, etc. The importance of these applications makes the failure of composites a significant concern. For unidirectional laminates, three forms of failure can occur, which are: matrix crack, fiber crack, and delamination, as seen in Figure 1.2. In the picture, there are 90-degree and 0-degree laminas, 0-degree fibers, seen as long white lines, while 90-degree fibers are seen as white dots. Darker regions correspond to resin (matrix). Breakage of only the resin is matrix failure, breakage of both resin and fiber is fiber failure. The separation of layers with matrix failure corresponds to delamination.

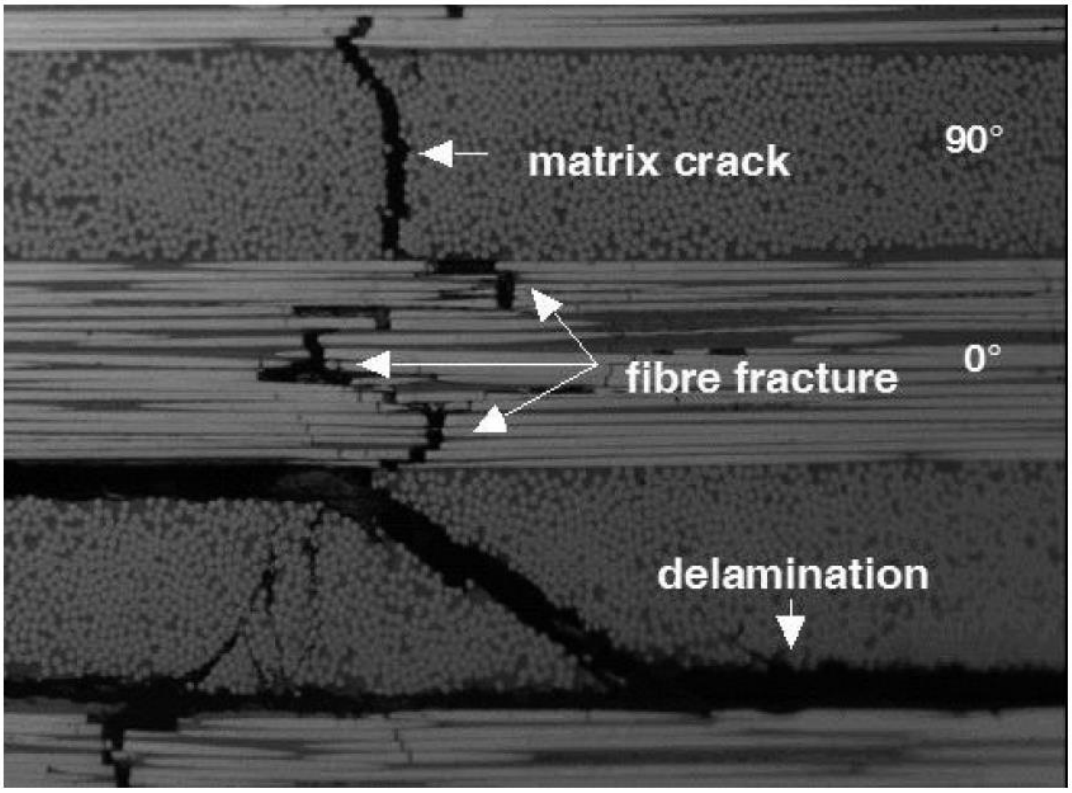

Figure 1.2. Three forms of failure in unidirectional laminates [51]

Two main properties determine delamination, one is interlaminar stress, the other is fracture toughness. Interlaminar stress determines the initiation of delamination. Fracture toughness controls the propagation of delamination. Principal directions are seen in Figure 1.3. These properties are third direction properties. Interlaminar tensile strength (ILTS) is a property in the interface plane and the third direction, while interlaminar shear (ILSS) strength is in the first and second directions. Interlaminar tensile strength is the property that determines the initiation of delamination under tensile stress, while interlaminar shear strength is the property that determines the initiation of delamination under shear stress.

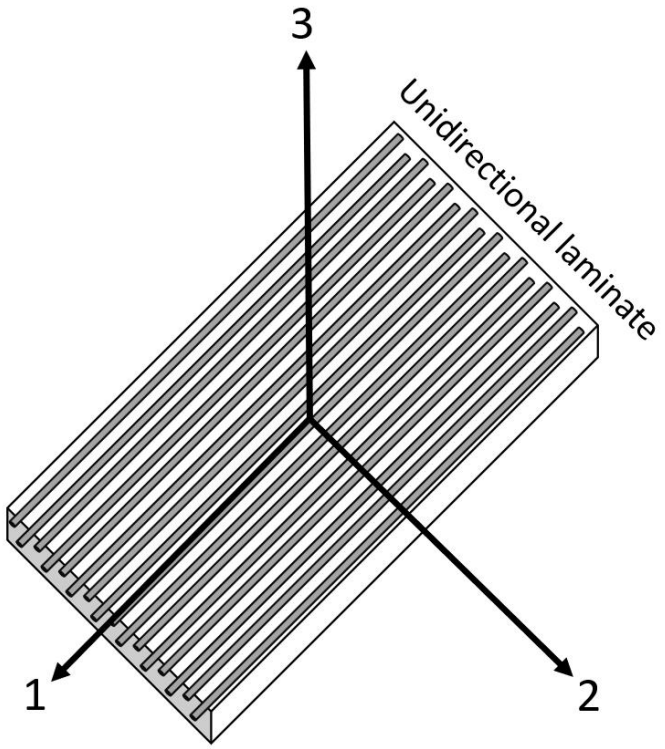

Figure 1.3. Principal directions in unidirectional composites

After the crack starts with interlaminar stresses, the infinitesimal crack front is formed. The second main property is fracture toughness, which controls the propagation of the infinitesimal crack. It has three different modes which are; opening (Mode I), in-plane shear (Mode II), and out-of-plane shear (Mode III), as illustrated in Figure 1.4.

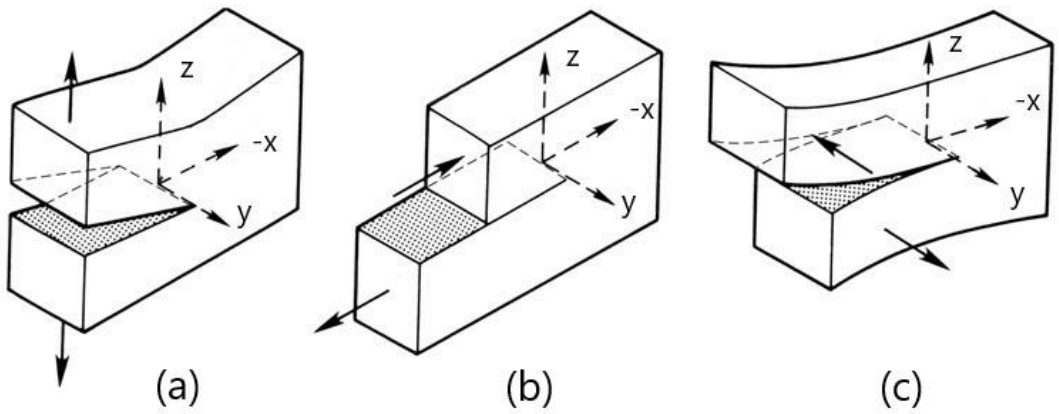

Figure 1.4. (a) Mode I, (b) Mode II, and (c) Mode III fracture modes

These mechanical properties have been obtained from experimental studies. Curved beam strength experiments (CBS) are done to determine interlaminar tensile strength (ILTS) and short beam experiments with 3 point bending are completed to examine interlaminar shear strength (ILSS). The double cantilever beam (DCB) test is carried out for Mode I fracture toughness, while the end-notched flexure (ENF) test is accomplished for Mode II fracture toughness. Composite laminates are produced with different lay-up orientations to perform under different loading conditions. For complex designs, any degree layer composite can be compacted with any other degree layer composite, such as; 0/0, 0/45 and, 0/90. In the business world, the properties which are mentioned above are obtained only for the 0/0 interface. In this study, ILTS and Mode-I fracture toughness of different interface angles are examined to show that using 0/0 properties for all interfaces is not correct. The experimental study is divided into two chapters: one for ILTS, and another for Mode-I fracture toughness results.

CHAPTER 2

INTERLAMINAR TENSILE STRENGTH OF DIFFERENT ANGLE-PLY CFRP AND GFRP COMPOSITES

2.1. Introduction

The use of composite structures has been increasing year by year. This attaches importance to failure mechanisms of their structures. Delamination, which is a separation of laminates in a composite structure, is one of the main failure mechanisms due to it being the weakest plane in the composite structure having 3% of strength in the fiber direction [1]. Being such, interlaminar interfaces are the weakest plane in the composite structure, and their failure can be the reason for a dramatic decrease in load-carrying capacity in curved beam structures.

Initiation and propagation of delamination are controlled by interlaminar strength and fracture toughness, respectively. Interlaminar tensile strength (ILTS) is a property that determines the initiation of delamination through the direction of the thickness. There are several methods to assess ILTS in the literature. The direct load method and 3-point bending method to measure ILTS are compared by Hara et al. [2]. They recommend a 3-point loading method because of easy production and simple calculation method in comparison to the direct load method, which has stress concentration, multi-axial stress creation, and volume effect problems. As a result, the volume effect on ILTS was clearly shown in this study. Moroni et al. [3] measured ILTS of co-cured and co-bonded CFRP joints with the direct load method. Cui et al. [4] compared methods using a direct load specimen, diametrical compression disk, a semi-circular/elliptical specimen, a ring/curved beam specimen, an L-beam specimen, pure moment on curved beam and a four-point curved beam specimen. They suggested a different type of curved beam strength (CBS) specimen, which is loaded with pure

moment load as per the ASTM standard D6415/D6415M [5]. This Four-Point curved beam method has an advantage for both specimen production and test set-up. Additionally, a CBS specimen [5] is an appropriate choice for a volumetric comparison. As it is mentioned, there are three primary test types, which are the direct load test, 3-point bending test, and the CBS test. Firstly, less material is needed to produce the CBS specimen. Secondly, they are close in thickness to real structures. Finally, there is no stress concentration and alignment problems compared to the direct load method. Therefore, the best method is the CBS test. Thus, many studies about ILTS used CBS specimens. Yet, the CBS experiment is not only for determining ILTS but also is related to the max load-carrying capacity of the L shaped composite under pure moment load. Some studies compared CBS values of different lay-up orientations however these do not show the ILTS values of the different interfaces.

Curved beam test studies to measure ILTS are reviewed in this section. Hao et al. [6] investigated thickness and curved beam radios/thickness effect on ILTS value, which decreases with an increase in thickness that is a volumetric effect. Even though different angle-ply lay-ups were used in the study, all delaminations were found to occur at 0/0 interfaces. According to the author, the reason is that the fracture toughness of the 0/0 interface is lower than the other interfaces. However, comparing the ILTS values with fracture toughness is not applicable. Moreover, some studies tried to produce stronger interface properties. The effect of carbon nanotubes was studied by Arca [7]. Interestingly ILTS is decreased by the addition of carbon nanotubes, while fracture toughness increased. Hence these results show that ILTS is not always related to fracture toughness. Stitching is another way of strengthening the interlaminar properties as shown by Ranz et al. [8] whilst the thickness effect is demonstrated by three different thickness CBS specimens. Stitching, which is done in the center of CBS specimen where max interlaminar tensile strength is created, is very effective on ILTS values. Up to 40% increase is founded on thin specimens. In addition, ILTS values are profoundly affected by specimen production [9]. It can

change with porosity, fiber resin ratio, geometric quality of the specimen, and types of resin-fiber.

Consequently, delamination failure is important in composite components such as curved beam, tapered beam and beam under impact loading where interlaminar tensile stresses play an important role in their failure [10, 11, 12, 13]. Kedward et al. [1] give also the example of interlaminar failures and emphasize that this must be solved in the design process to prevent future failures. Hence, it is crucial to use the correct values of these interface parameters in the design and analysis of these components. Although there are many studies about ILTS and CBS, the effect of angle-ply on ILTS has not been studied. In this paper, CBS experiments are conducted on CFRP and GFRP 0/0, 25/-25, 45/-45, and 65/-65 interfaces in order to find the ILTS of these interfaces.

2.2. Experimental Procedure

Mode I experiments were conducted using the double cantilever beam (DCB) specimen according to ASTM D6415/D6415M. Specimen preparation, experimental protocol, post-processing data and interlaminar stress analysis of the experimental study are mentioned in this section.

2.2.1. Specimen Preparation

The main composite part for five specimens was produced in an autoclave with prepreg carbon and glass unidirectional composite layers using the hand lay-up technique. $[\pm\Theta]_{20}$ lay-up configuration was used for both carbon and glass specimens with Θ=0, 25, 45, and 65. During the lay-up process, layers were compacted after placement of every three layers. After the final vacuum process, the curing process took place in an autoclave. The autoclave worked with 6 bar pressure and 0.45 bar vacuum pressure. Specimens were cured at 120 ℃ in the autoclave for 2 hours in the chamfer. Then, the cured part was cut using a water jet cutter into 25mm wide pieces in order to prevent edge cracks, which occurs when a CNC machining process is applied. These specimens have a 6.4 mm inner radius of curvature and their legs were more than 90 mm. Thicknesses of the cut specimens were different for CFRP and

GFRP which was 5 mm and 9 mm thickness respectively. The glass prepreg layer thickness was double the thickness of the carbon prepreg layer thickness. Both glass and carbon specimens are seen in Figure 2.1. The thickness difference and the other properties for the analysis section of CFRP and GFRP prepregs are shown in Table 2.1 and Table 2.2.

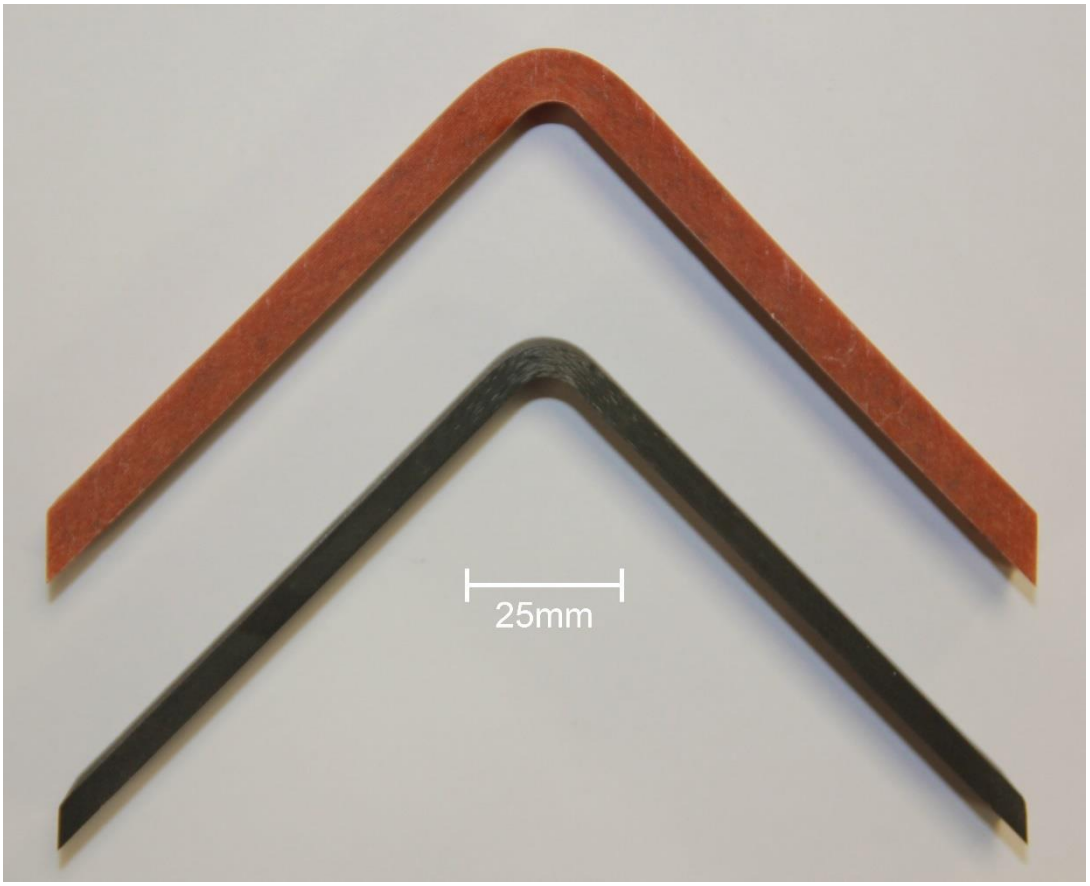

Figure 2.1. CBS specimens

Table 2.1. Material properties of CFRP UD prepregs (HEXPLY 913 132 HTA Carbon)

Density	ρ= 1.52 (g/cm^3)
Ply Thickness	0.136 mm
Fiber Volume Fraction	58.4 %
Elastic	E^t_{11}=140 GPa, E^t_{22}=E^t_{33} =9 GPa, E^c_{11}=110 GPa,
	E^c_{22}=E^c_{33} =10 GPa, ν_{12}=ν_{13}=0,35, ν_{23}=0,12,
	G_{11}=G_{22}=G_{33} =5 GPa
Strength	S^t_{11}=2000 MPa, S^t_{22}=65 MPa, S^c_{11}=1500 MPa,
	S^c_{22}=S^c_{33}=220 MPa, S_{12}= S_{13}=S_{23} =110 MPa,

Table 2.2. Material properties of GFRP UD prepregs (Hexcel S2 Glass UD/913)

Density	ρ= 1.85 (g/cm^3)
Ply Thickness	0.244 mm
Fiber Volume Fraction	50.5 %
Elastic	E^t_{11}=50 GPa, E^t_{22}=E^t_{33} =12 GPa, E^c_{11}=40 GPa,
	E^c_{22}=E^c_{33} =12 GPa, ν_{12}=ν_{13}=0,3 ν_{23}=0,1
	G_{11}=G_{22}=G_{33}=4 GPa
Strength	S^t_{11}=1400 MPa, S^t_{22}=50 MPa, S^c_{11}=1100 MPa,
	S^c_{22}=S^c_{33}=200 MPa, S_{12}= S_{13}=S_{23} =90 MPa

Before the experiment, according to ASTM standard D6415/D6415M (Ref 3), the specimen can be painted with a white color in order to see cracks and delaminations on the specimen. However, each lamina and matrix crack could not be examined with a microscope with the white color. For this reason, specimens in this study were sanded and polished for microscopic investigation. However, the process was not done for all specimens because it is a time-consuming process. Microscopic views of all lay-ups and materials are shown in Figure 2.2.

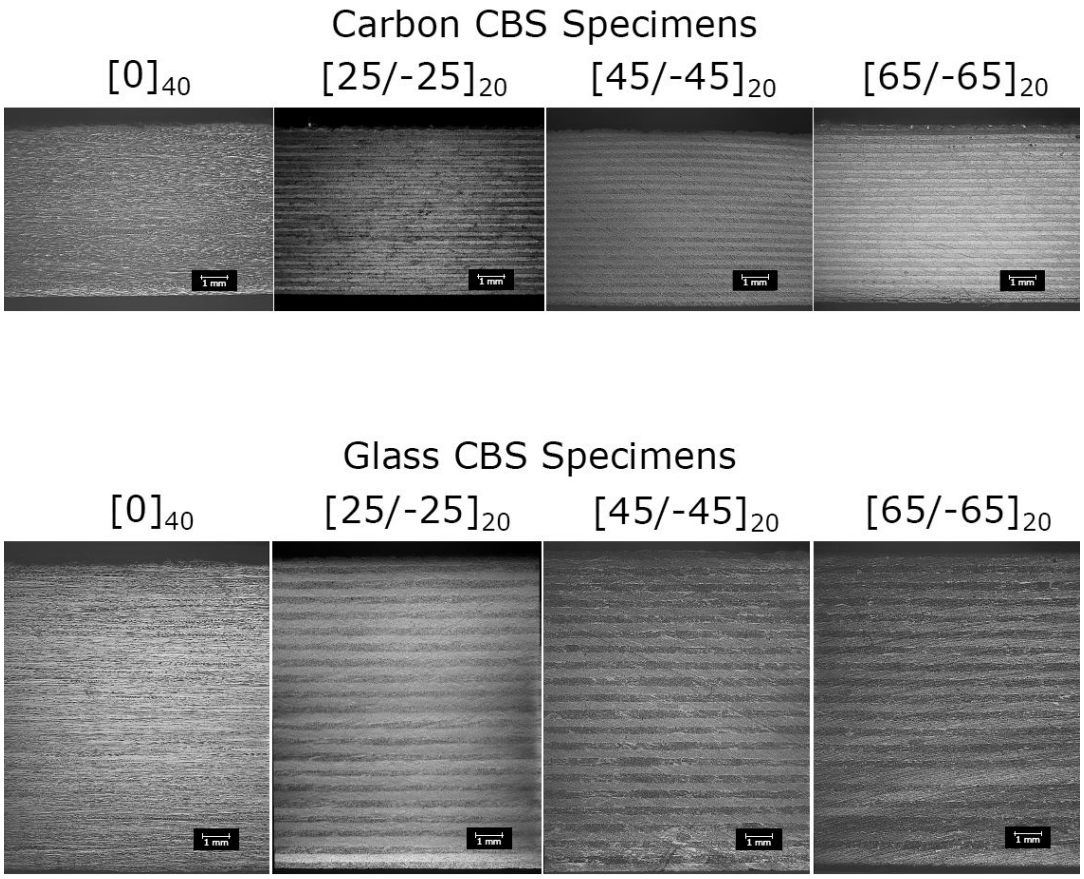

Figure 2.2. Microscopic pictures of all specimens

2.2.2. Experimental Protocol

According to the ASTM D6415/D6415M standard (Ref 3), a CBS specimen was loaded with the pure moment using a Shimadzu 10 kN test machine. The experimental set-up, prepared according to the standard is seen in Figure 2.3. The standard suggests a fixture which has four rollers that are supported between bearings. These bearings help rollers to rotate during the deformation of CBS specimen. The fixture is aligned with a ±0.05 mm error of the roller's locations. Error in the fixture can lead to uneven stress distribution through the thickness and change the initial delamination location. There are two essential dimensions for rollers; one is l_t, which is a distance between the top roller, and the second is l_b, which is a distance between the bottom roller. The standard suggests l_t= 75 mm and l_b=100 mm; however, 75 mm is too much if the

specimen stiffness is not enough to create the moment which creates delamination. Accordingly, the fixture which has l_t= 35 mm and l_b= 100 mm was used for $[\pm 65]_{20}$ CFRP and GFRP CBS specimens, because the full stroke of the standard fixture did not create delamination on $[\pm 65]_{20}$ CFRP specimens. In order to achieve delamination in CFRP $[\pm 65]_{20}$ specimens, different types of fixtures were tried. These fixtures are demonstrated in Figure 2.6. As a result of these trials, the rotation allowance of the fixture was very important. If the rotation friction is high or rotation is not allowed at the narrow rollers, loading is concentrated at the contact point where the narrow fixture touches the specimen. So, the specimen is tried to bend at the narrow rollers rather than at the center of the specimen. Secondly, if rotation is not allowed at the wide fixture, there is a stick and slip motion during the experiment and due to uneven stick and slip on both sides, there is an uneven stress distribution at the two legs. In order to prevent stick and slip motion, a lubricant can be used between fixtures and the specimen. As mentioned above, getting a narrow fixture distance to low values helps to create more moment at a low stroke. However, if the l_t value is too low, it will create compressive stress in the curved region. Then, there will be a calculation mistake or cracks due to this high compressive stress. As a result, the decided fixtures in Figure 2.5 has rollers with bearings and two different l_t values for different specimens. Experiments for the two fixtures with CFRP $[\pm 45]_{20}$ specimens were carried out for 1 specimen only per each fixture, due to lack of specimens. While the ILTS at the modified fixture is 38.1 MPa, the ILTS at the standard fixture is 41 MPa. This 3 MPa difference is within the experimental scattering range, so both of the fixtures can be used for the ILTS experiment.

Figure 2.3. Experimental set-up

The specimens were located on their fixture according to specimen type, that $[\pm 65]_{20}$ was placed on the modified fixture and the others were placed on the standard fixture as seen in Figure 2.5. Loading was applied with 0.5mm/min stroke speed using a 10 kN Shimadzu electro-mechanic test machine. Load and displacement values were taken from the machine at 20 *Hz*. The experiment was continued until the load drop when the delamination which had occurred reached 50 *%* of the max load. After the load drop, specimens were unloaded at the max speed of the machine.

2.2.3. Post-Processing of Data

The CBS experiments showed ILTS of the delaminated interfaces. Dimensions were used in the formulation as shown in figure 1.4. l_t is the top roller's distance. l_t was 35 mm for $[\pm 65]_{20}$ specimens and 75 mm for the other specimens. l_b is the bottom roller's distance; it was constant for all specimens and 100 mm in length. ϕ is the angle of one leg with respect to the ground which was initially 45˚. It is an important parameter that is calculated from the stroke of the machine (d_y). D is the diameter of the fixture, which was 8 mm for the fixture. P is the load, which was read from the machine load cell.

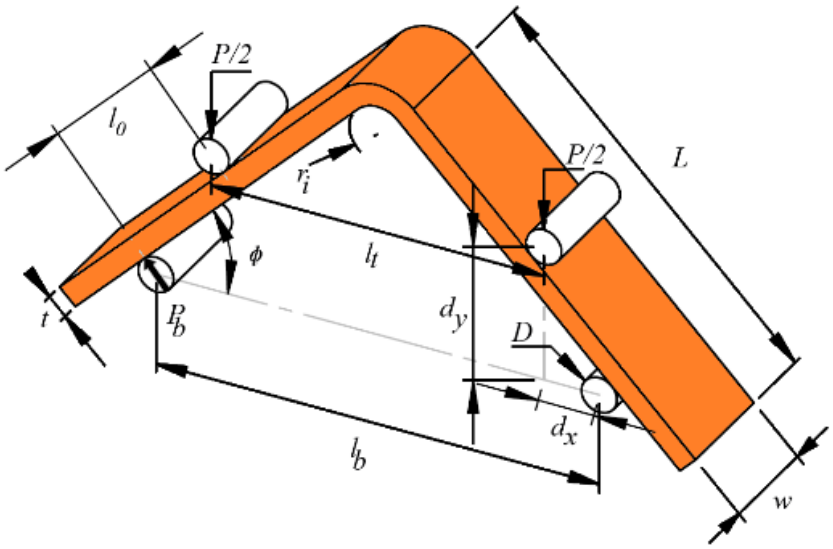

Figure 2.4. Dimensions of the specimen and the fixture

When the first delamination occurs as a huge load drop in the load-displacement graph, the max load right before the delamination is taken as a P (load) in the formulation in 1 and 2. r_i is inner, and r_o is the outer radius of the CBS specimen and t is the thickness of the specimen. ILTS is calculated from the CBS of the specimen at first delamination according to the ASTM D6415/D6415M standard.

$$CBS = \frac{M}{w} = \frac{P_b l_0}{w} = \left(\frac{P}{2w\cos\phi}\right)\left(\frac{d_x}{\cos\phi} + (D+t)\tan\phi\right) \quad (1)$$

$$ILTS = \sigma_r^{max} = \frac{3CBS}{2t\sqrt{r_i r_o}} \quad (2)$$

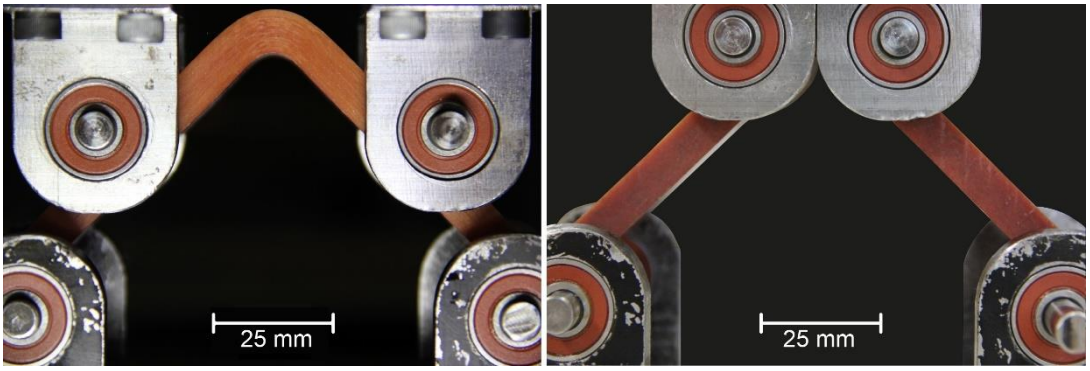

(a) Standard fixture (b) Modified fixture

Figure 2.5. l_t =75 mm and 35 mm fixtures respectively

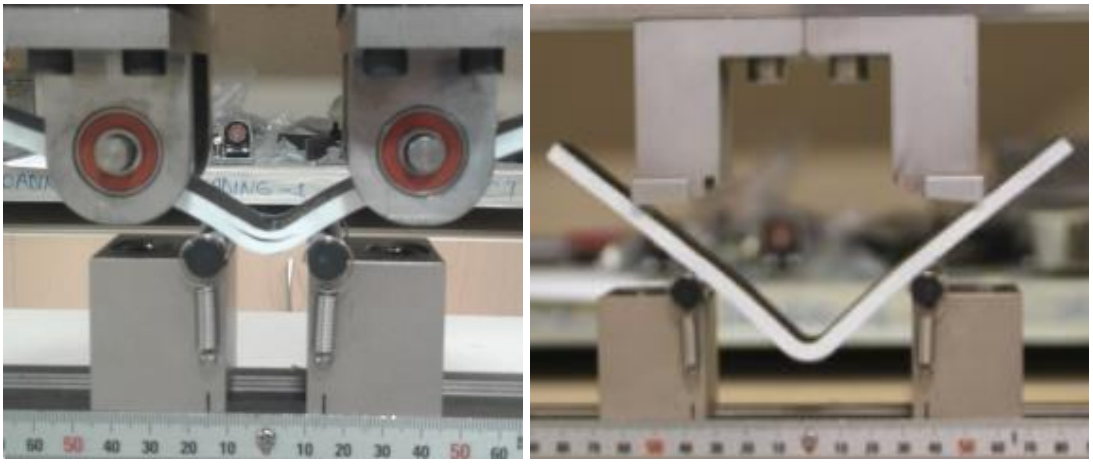

Figure 2.6. Fixture trials

2.2.4. Interlaminar Stress Analysis

For the angle ply CBS specimen under pure moment load, there is shear stress between layers due to the mismatch of the adjacent layers. In order to see the effect of the shear stress on the failure region, the curved region of the CBS specimen was modeled in the Abaqus program with the same dimensions and layup orientation. C3D8R type of mesh was used. For each layer, one cube element was used in the thickness direction in Figure 2.7. No failure model was used for this analysis, only stresses were controlled. The CFRP $[\pm 65]_{20}$ CBS specimen was modeled using the elastic properties in Table 2.1. Pure moment load was applied at the end of the curved region of the

specimen. The Pure moment load was equal to the failure load of the CBS specimen which was 15 Nm. The result of this analysis is mentioned in this section.

65/-65 lay-ups create shear load at interface under tensile or compressive loads. In order to show the shear does not affect the ILTS, analysis of the CBS specimen was carried out in Abaqus 16. Lay-up is $[\pm 65]_{20}$. The same moment which was applied at the failure point of the specimen is applied in the analysis.

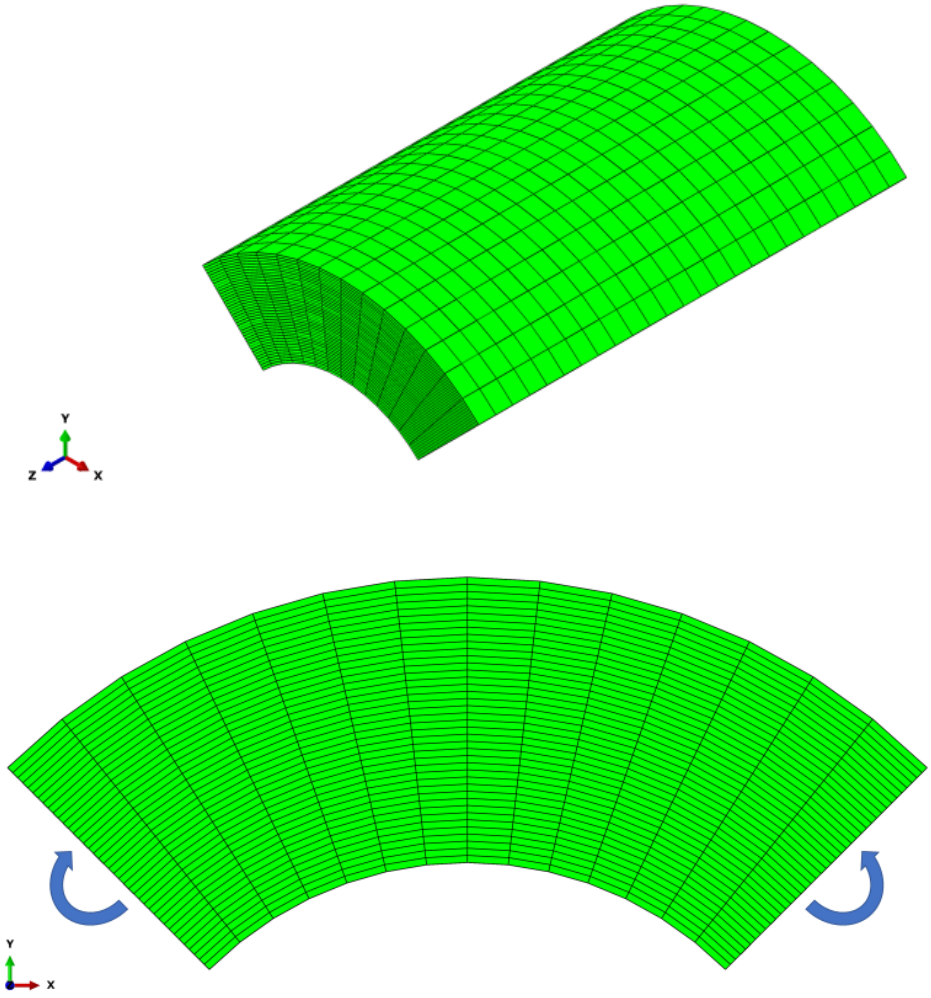

Figure 2.7. Carbon $[\pm 65]_{20}$ CBS Analysis Model and Applied Moment

Max inter-laminar tensile stress (S_{33}) is created around the center of the specimen. A section view at the YZ plane highlighting the S_{33} values is shown in Figure 2.8. Maximum S_{33} is created at the 15th layer from the bottom.

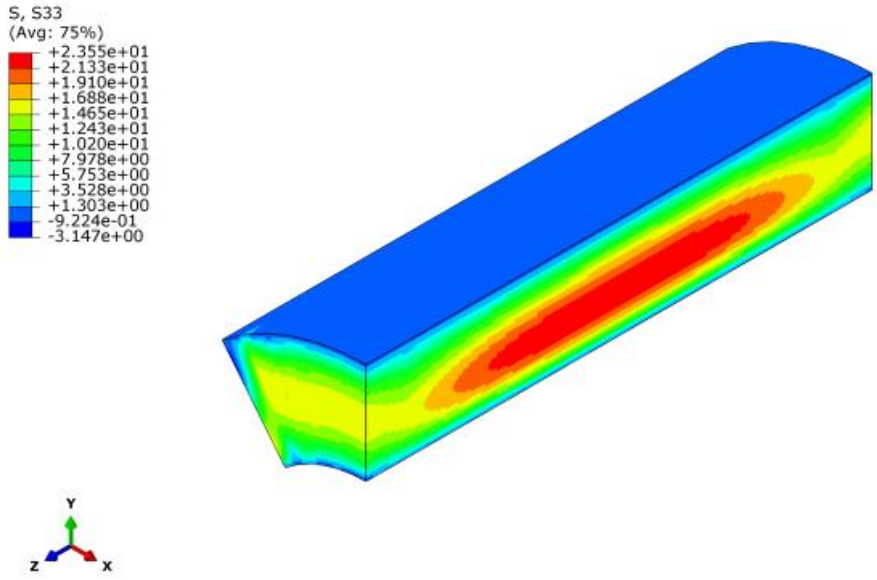

Figure 2.8. Carbon $[\pm 65]_{20}$ CBS analysis S_{33} (center section view at YZ plane)

In Figure 2.9 and Figure 2.10, only S_{33} of the 15th layer which is interlaminar tensile stress and S_{23} of the 15th layer which is interlaminar shear stress shown. According to this analysis max interlaminar tensile stress is at the center of the width. Because of that, delamination will start at the center. Shear value at the center is close to 0, which means shear does not affect the initiation of delamination. Shear strength is more dominant near the edges. Interlaminar shear strength of CFRP and GFRP laminates are 100 MPa and 76 MPa respectively according to the data provided by the manufacturer.

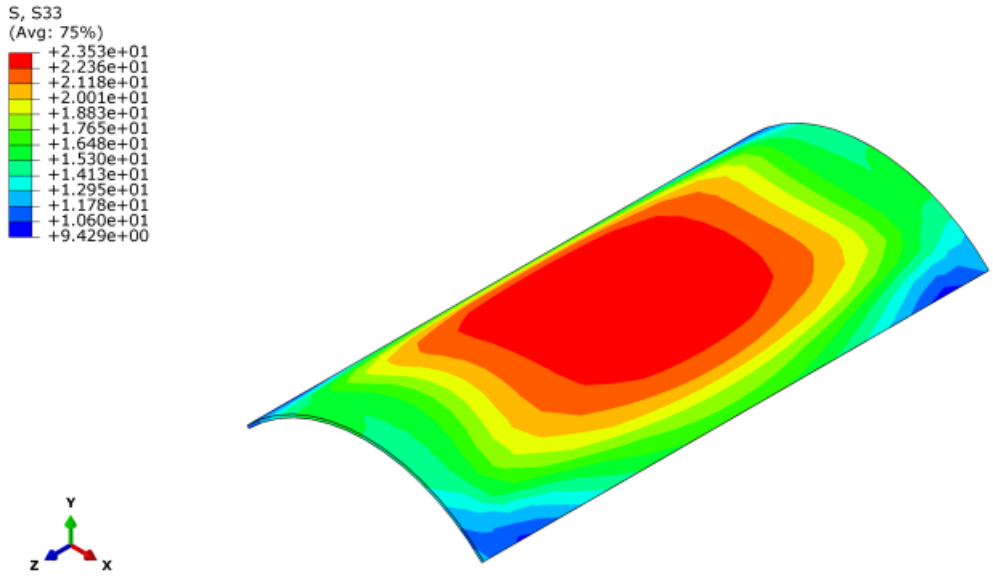

Figure 2.9. Carbon $[\pm 65]_{20}$ CBS analysis S_{33} (center max stress layer)

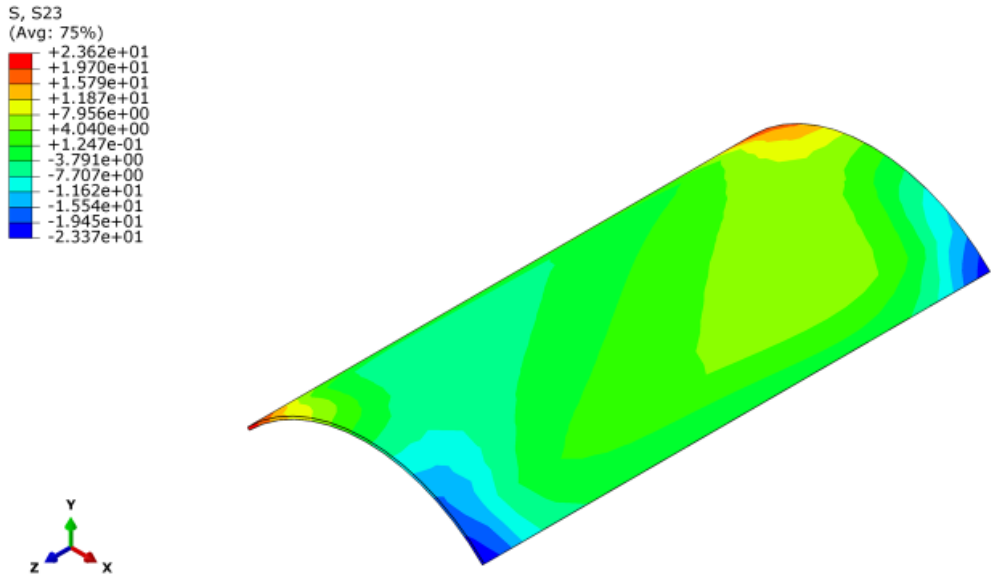

Figure 2.10. Carbon $[\pm 65]_{20}$ CBS analysis S_{23} (max stress layer)

2.3. Results

In this section, load-displacement graphs, delamination onset pictures, and microscopic views of CBS specimens are presented for all lay-ups of both carbon and glass specimens. Then, ILTS values taken at first delamination are given for all specimens. Results are shown in the following sections according to the lay-up angle for each fiber type used. Furthermore, interlaminar stress analysis with Abaqus is also mentioned in this section. The test matrix is seen in Table 2.3. The lay-up orientations of specimens, materials used for these lay-up orientations, numbers of experiments that were accomplished and fixtures used in experiments are demonstrated in the test matrix. Only one experiment using CFRP $[\pm 25]_{20}$ specimens was accomplished in the modified fixture unlike the other $[\pm 25]_{20}$ specimens.

Table 2.3. Test matrix

Lay-up orientation	Material	Numbers of experiments	Experiment Fixture
$[0]_{40}$	CFRP/GFRP	3/3	Standard
$[\pm 25]_{20}$	CFRP /GFRP	2+1 /3	Standard+Modified /Standard
$[\pm 45]_{20}$	CFRP/GFRP	3/3	Standard
$[\pm 65]_{20}$	CFRP/GFRP	3/3	Modified

2.3.1. ILTS Result of CFRP Specimens

In this section, ILTS of 4 different lay-up orientations for CFRP CBS specimens are shown with their load-displacement results and pictures.

2.3.1.1. ILTS of $[0]_{40}$ CFRP Specimens

As is mentioned in the method section, $[0]_{40}$ CFRP CBS specimens are loaded with a four-point bending fixture. A pure bending moment is applied to specimens. l_t and l_b values are 75 and 100 mm, respectively, as given in the standard (Ref 3). Load-displacement plots for three specimens tested are shown in Figure 2.11. Slopes of curves in the elastic region are seen to be almost the same. However, failure loads are observed to be changing from 3500 N to 4500 N. The failure, which is in the form of delaminations, shows itself with a load drop of about 3000 N for all specimens. These load drops correspond to more than 75% of max loads. Because of that, immediately afterwards, the test was stopped since the ASTM D6415/D6415M standard recommends the loading to continue until a 50% load drop is reached. Since ILTS is defined as the value which corresponds to the initiation of delamination and CBS is calculated based on the first load drop, ILTS is calculated by using CBS as given in (Ref 3). From the specimens used in this test program, ILTS was calculated, on average, to be 87.6 MPa.

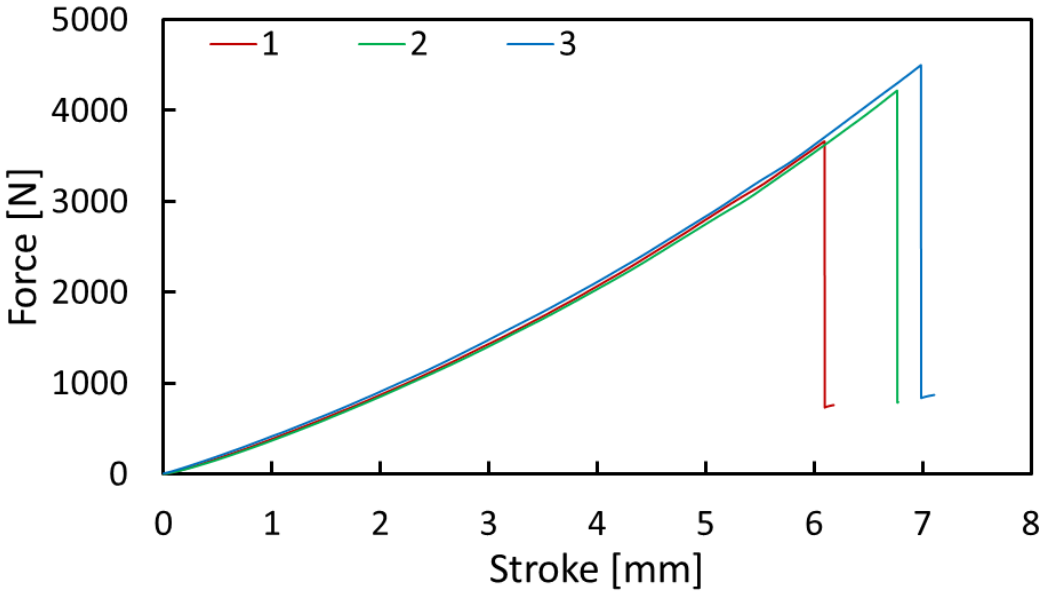

Figure 2.11. Load-displacement graph for $[0]_{40}$ CFRP CBS specimens

One of the reasons for the variation in the maximum load values is suggested to be due to the manufacturing defects in CBS specimens. ILTS is a property that is known to be dependent on production parameters. There is a certain nonlinearity before failure, which comes out as a function of angle Φ. There is a difference between the load P_b which is which forming the bending moment and load P, which is measured by the machine. It is represented by the following formula;

$$P = 2P_b \cos \Phi \tag{3}$$

In the majority of three tests, multiple delaminations were observed which occurred during the first load drop. They can be clearly seen in Figure 2.12 along with a picture of their microscopic view. In the microscopic pictures, however, ply interfaces that are supposed to be resin rich cannot be clearly identified. This is not unusual for 0-degree laminates with similar volumetric fiber ratios.

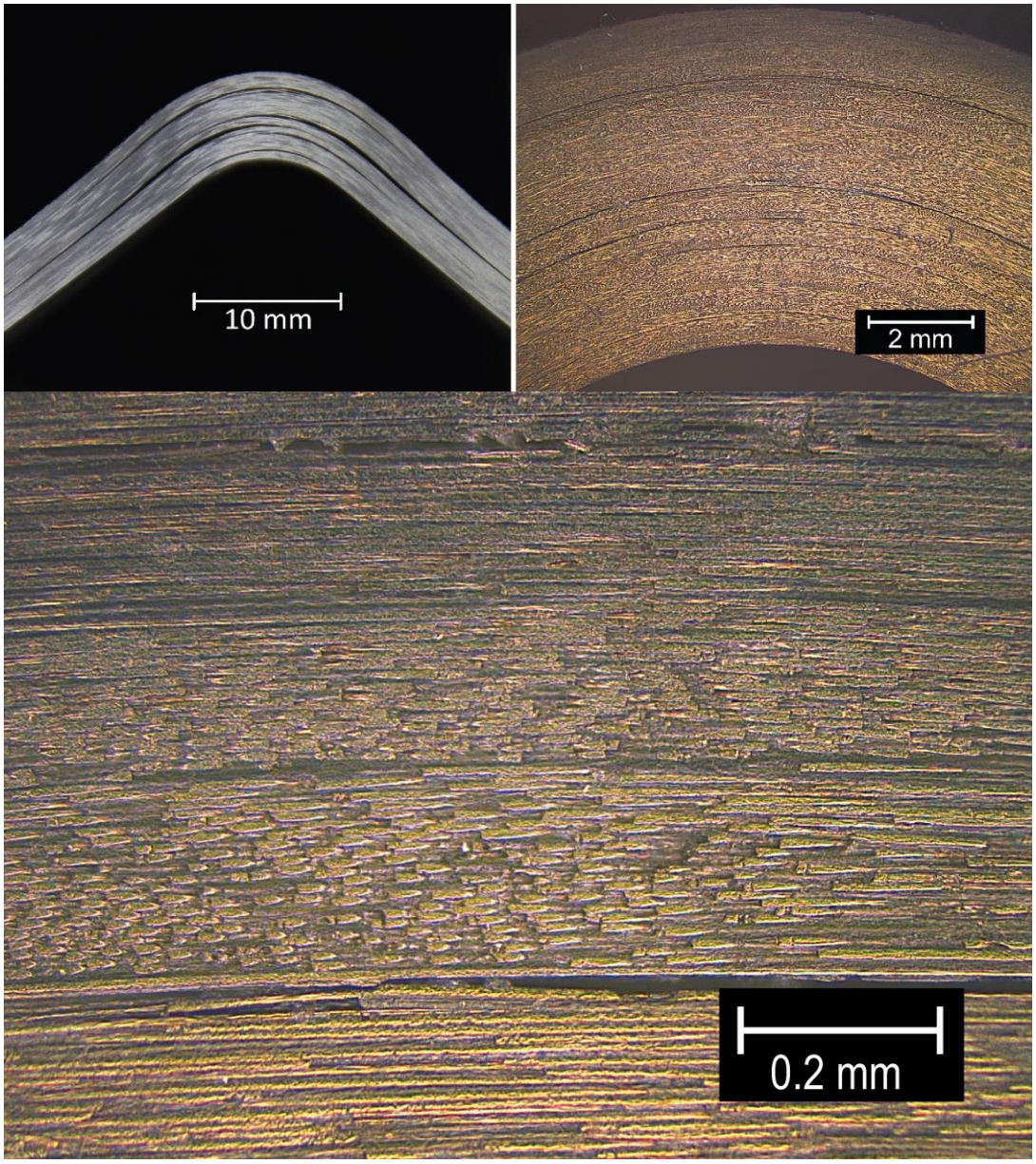

Figure 2.12. Photo of delamination onset and microscopic views of the $[0]_{40}$ CFRP specimen (failure microscopic photos)

2.3.1.2. ILTS of $[\pm 25]_{20}$ CFRP Specimens

Two of the $[\pm 25]_{20}$ CFRP specimens were loaded with the standard fixture, while one of the specimens was loaded with the modified fixture. The standard fixture specimens (which are number one and two in Figure 2.13) failed around 4500 N. The modified one failed around 2000 N. l_t was 75 mm for the standard fixture while it was 35 mm for the modified fixture. There are little load drops close to the delamination which appears as a huge load drops. These little load drops correspond to ply failure rather than delamination. The modified fixture was tried to prevent the ply failures which are seen in the figure. ILTS of these specimens was calculated according to the data where the big load drop occurred. As an average value, 96 MPa was obtained as an interlaminar strength of 25/-25 interface.

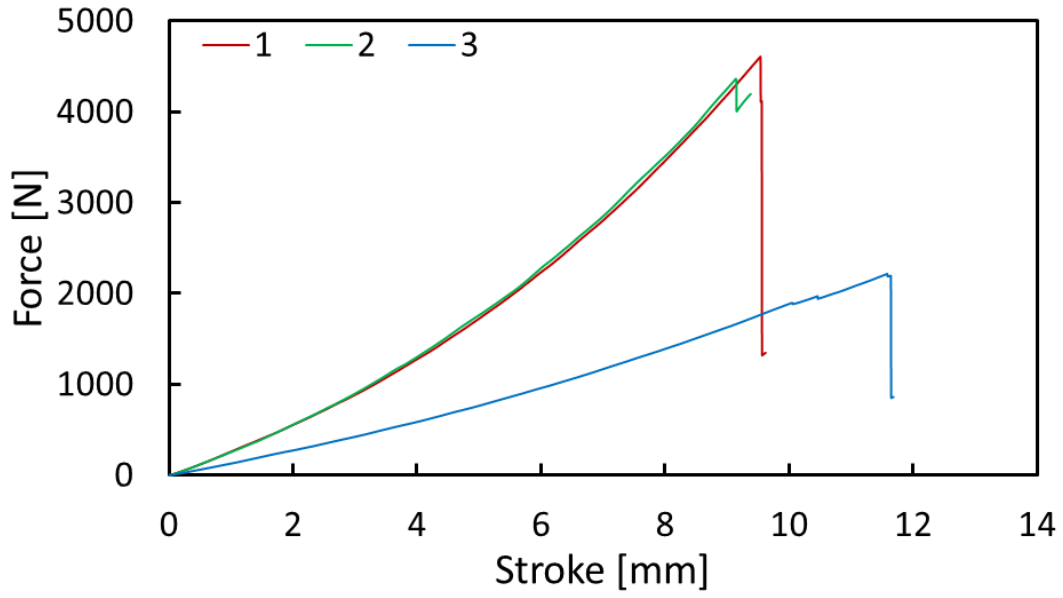

Figure 2.13. Load-displacement graph for $[\pm 25]_{20}$ CFRP CBS specimens

One or two delaminations occurred in these experiments. The main delamination occurred at the interface and the ply failure finished in the direction of the thickness. The main delamination and ply failures are demonstrated in Figure 2.14. The main failure of the ply seemed like a compressive failure in one direction. The failed plies

are pushed out from the main laminate. Because of this ply failure, calculated ILTS is lower than the real values.

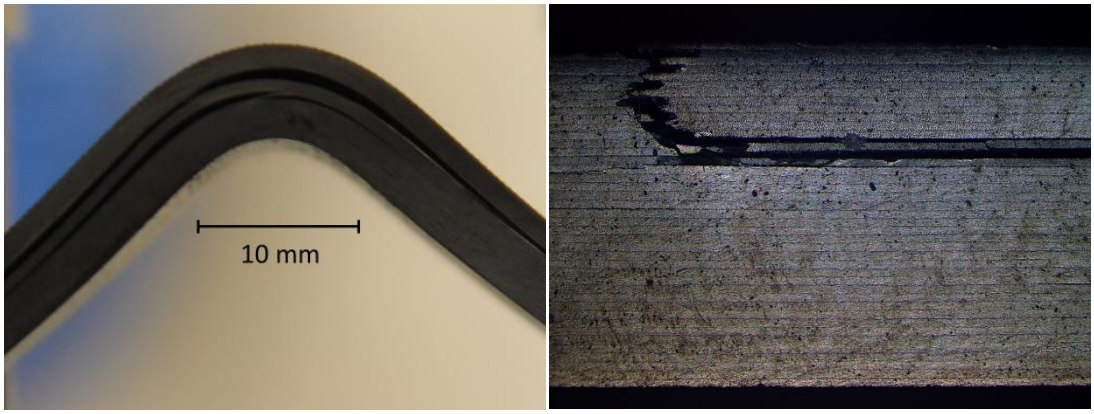

Figure 2.14. Photo of delamination onset and microscopic view of the compressive failure of the $[\pm 25]_{20}$ CFRP specimen

2.3.1.3. ILTS of $[\pm 45]_{20}$ CFRP Specimens

These specimens are similarly loaded with the four-point bending fixture where geometric parameters l_t and l_b are the same as with the standard fixture which is l_t=75 mm in Figure 2.5. For this set of specimens, the load-displacement curves show very similar patterns in terms of maximum load, slopes and load drops as given in Figure 2.15. The load drops are from about 3000 N and to about 2250 N for all specimens. After the first load drops, the loading was stopped as dictated by the standard (Ref 3) since a 75% load drop had been reached.

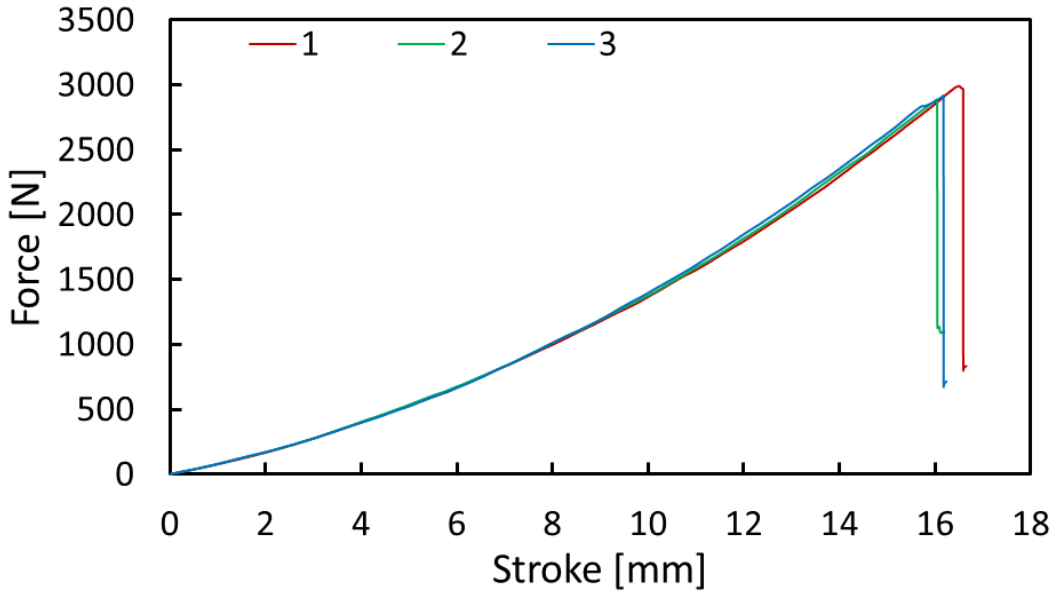

Figure 2.15. Load-displacement graph for $[\pm 45]_{20}$ CFRP CBS specimens

Delaminations occur at higher displacement values compared with $[0]_{40}$ specimens. There is also a similar non-linearity in stiffness before failure. However, it is more significant since deformations to failure are higher in this case which corresponds to lower Φ angles.

Multiple delaminations occurring during the load drop are believed to be the main reason behind the huge stress waves after the delamination. Similarly, CBS values of specimens are calculated based on the maximum load value at the first load-drop. ILTS for these specimens is calculated to be 41.5 MPa on average. The delamination onset and microscopic view are shown in Figure 2.16. Opposite to the previous case, resin-rich regions at the interfaces can be clearly seen for this specimen.

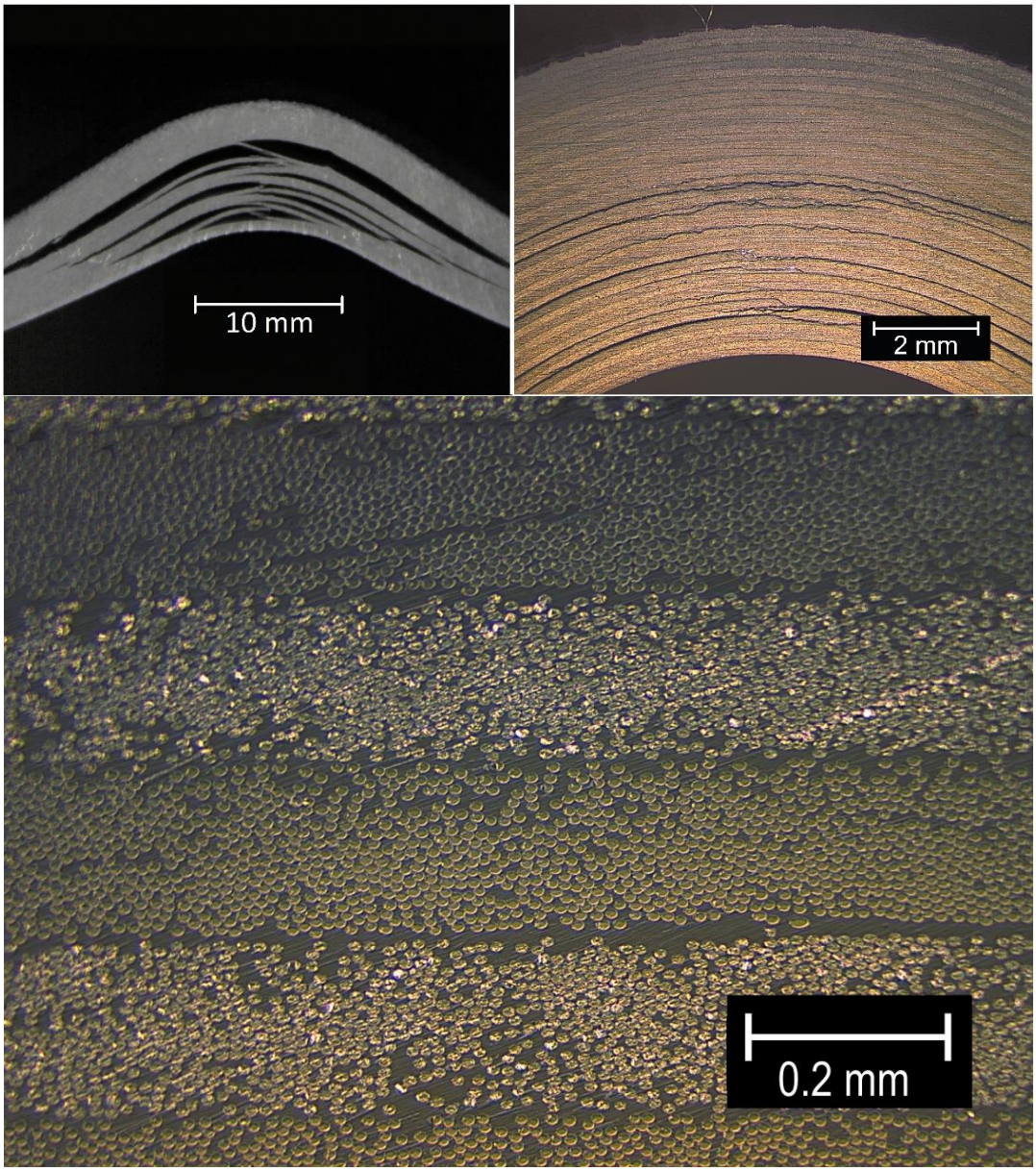

Figure 2.16. Photo of delamination on-set and microscopic views of the $[\pm 45]_{20}$ CFRP specimen

In addition, in order to see the progression of multiple delaminations and see where the first delamination occurred, a high-speed camera was used to catch the high-speed delamination. The specimen was sanded and painted with a white color due to visualization problems. However, the specimen used in the high-speed camera experiment had a lay-up orientation error and also had fixture alignment errors about 1.5 mm in the direction of the width. It was about a 3.5-degree error in the fixture so

the first interface in which the delamination occurred was affected by these errors. According to literature, the crack must be starting at 2/5 of the thickness from the bottom. The speed of the camera was arranged to 525000 frames per second. Each frame time was about 2 microseconds. Progressive delamination can be seen in Figure 2.17. The first frame shows that the crack started at 1/5 of the thickness of the specimen. The first delamination was affected by the errors in the specimen and fixture. There was stress release due to the first delamination, stress was increased at the other interfaces, so consecutive delaminations occur in one load drop. All delaminations happened in 0.6 milliseconds. As a result, even if the load drop was seen as a single load drop, the delamination was progressive. Moreover, the alignment of the fixture was important as it could have led to delamination at the different interfaces. Because of this, all experiments were repeated using the aligned fixture.

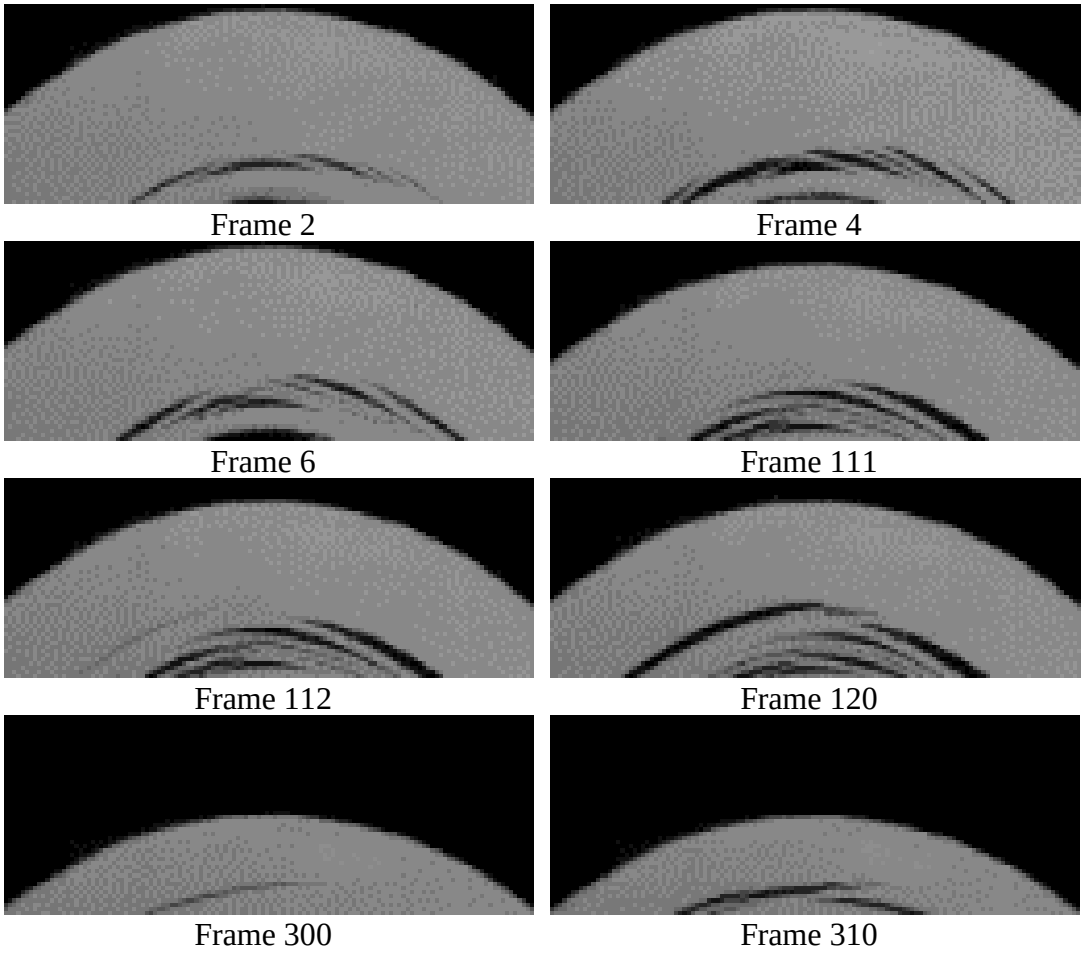

Figure 2.17. C-CBS-45—45-5-MF10741 specimen's CBS experiment with high-speed frames

2.3.1.4. ILTS of $[\pm 65]_{20}$ CFRP Specimens

Different to previous cases, these specimens were loaded with the modified fixture in Figure 2.5. The specimen had much lower stiffness than previous ones such that, the fixture dimensions were not enough to cause any delamination even at the maximum stroke of the test machine. The load-displacement curves are shown in Figure 2.18. A similar stiffness nonlinearity as before is observed here as well until a point where a different phenomenon is observed at around 13-mm stroke. A change of slope is found around this point where a corresponding matrix cracking is observed in specimens. Matrix cracks first form at the bottom surface which is the tension side of the specimen and then they grow into the inner layers as shown in Figure 2.19. The following small

changes in the slope of the load-displacement curve in Figure 2.18, corresponds to these matrix cracks as shown with a red ellipse in Figure 2.19. When matrix cracks reach the high interlaminar stress zone, delamination starts at this region illustrated with a red arrow in Figure 2.19. This corresponds to the point of the large drop in Figure 10. All specimens have matrix cracks around 450N where a knee is seen in the load-displacement plot and delamination around 600N where a sudden load drop occurs. The experiment was stopped at the first large load drop.

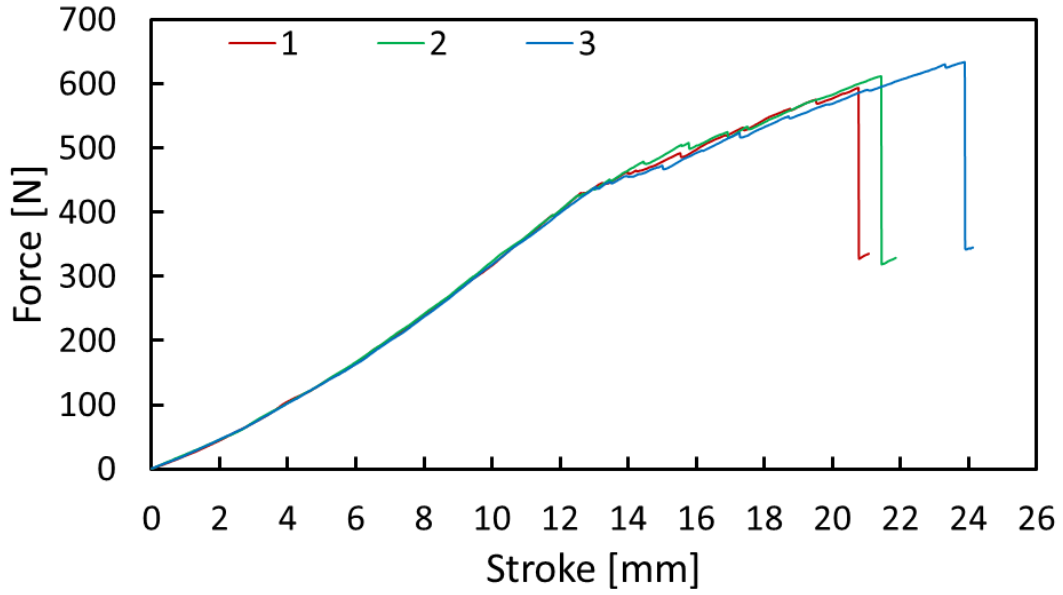

Figure 2.18. Load-displacement graph for $[\pm 65]_{20}$ CFRP CBS specimens

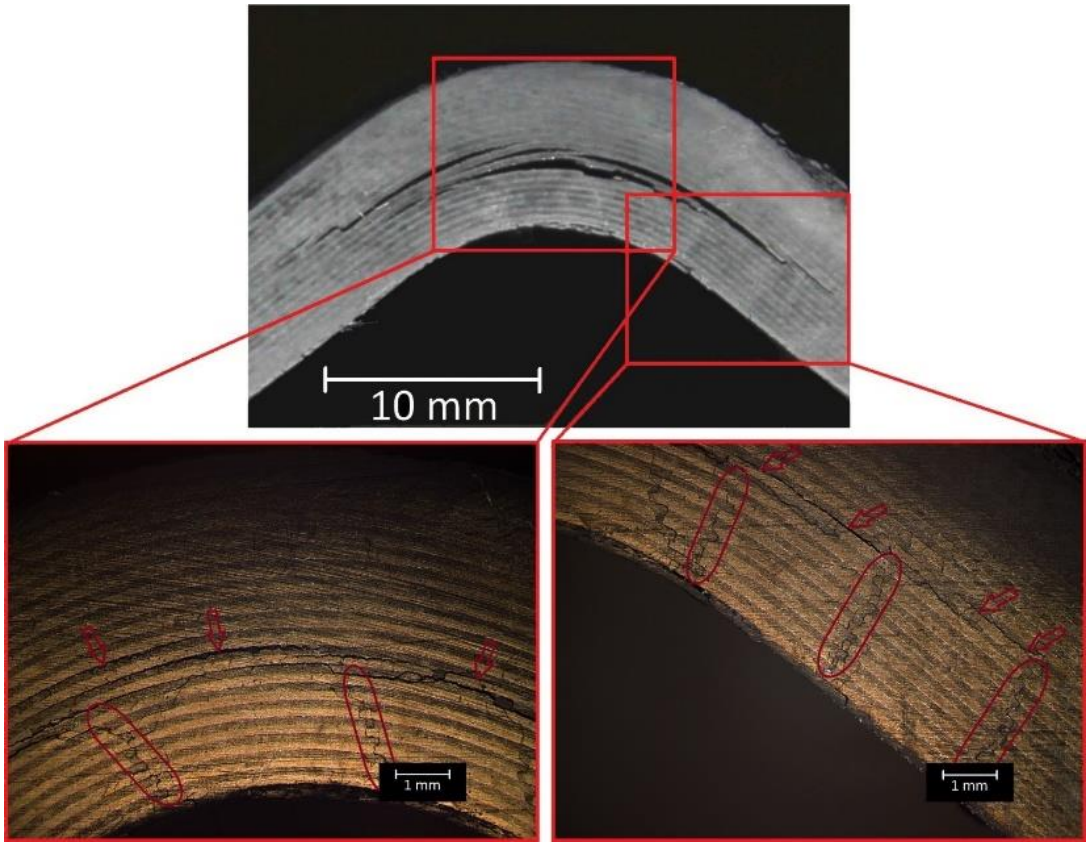

Figure 2.19. Matrix cracks and delamination of $[\pm 65]_{20}$ CFRP CBS specimens

The area under the curve is relatively small compared to $[\pm 45]_{20}$ and $[0]_{40}$. Single delamination is believed to be due to this low energy that is stored during the loading. An average of 20.4 MPa is calculated for these specimens as the ILTS value. However, this value is actually for the case where first there are matrix cracks generated, which leads to delamination. Therefore, it does not really represent the ILTS of the specimen. As shown in Figure 2, resin-rich regions are relatively smaller compared with $[\pm 45]_{20}$ specimens, and large compared to specimens of $[0]_{40}$. This resin region difference may be due to the fact that there is a difference of 50° between adjacent fibers in ±65° system, while adjacent layers in $[\pm 45]_{20}$ specimens are 90° apart.

2.3.2. ILTS Result of GFRP Specimens

In this section, ILTSs of three different lay-up orientations for GFRP CBS specimens are shown with their load-displacement results and pictures.

2.3.2.1. ILTS of $[0]_{40}$ GFRP Specimens

Similarly, the same fixture was used for these specimens which have l_t = 75 mm and l_b = 100 mm as shown in Figure 2.5. Glass specimens exhibited higher stiffnesses before failure as seen in Figure 2.20. The double-layer thickness of GFRP material is the reason for this difference. Non-linearity in the curve before failure seems to be very limited since the first delamination happens at comparatively very low displacement values. A scattering of maximum load values is also seen for GFRP $[0]_{40}$ CBS specimens. The average failure load is about 3000 N, and the load drops as much as 1800 N during the first delamination.

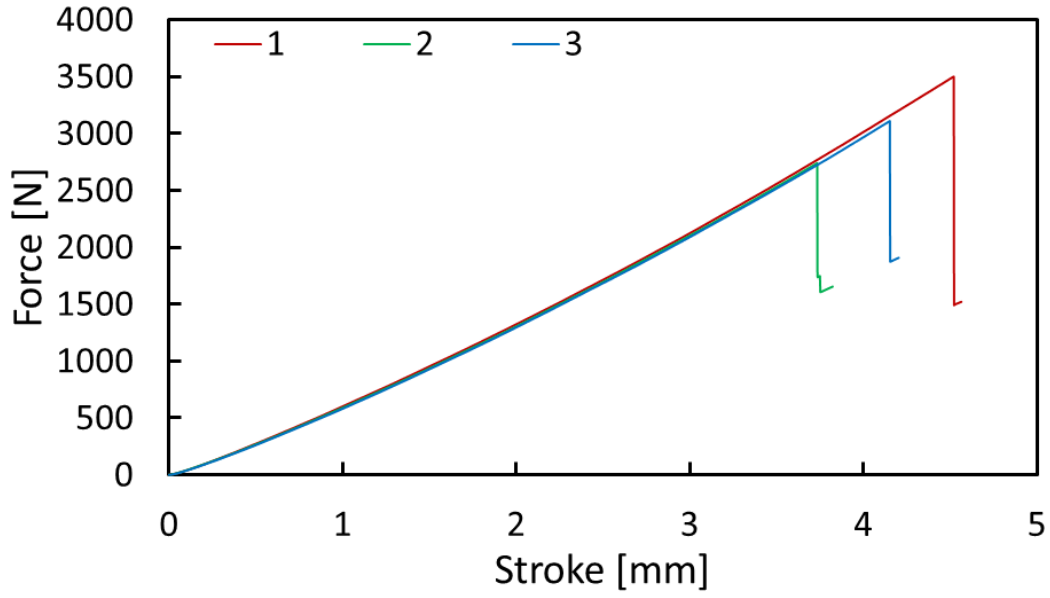

Figure 2.20. Load-displacement graph for $[0]_{40}$ GFRP CBS specimens

ILTS value for these specimens is calculated to be 45.7 MPa on average. Either single or double delaminations are observed for these specimens. This could be due to higher fracture toughness and relatively low energy release at the first load drop since they

have a relatively small area under the load-displacement curve. Delamination onset and microscopic view are shown in Figure 2.21. In the microscopic view, resin-rich regions can clearly be seen, unlike CFRP laminates. For these specimens, resin content is 8% more in volume than carbon specimens. Another reason is that the prepreg layers of GFRP happen to be relatively thicker and therefore, they created more resin-rich regions. This thickness problem also causes difficulty in laying and compaction of plies, this increases the likelihood of more resin-rich regions.

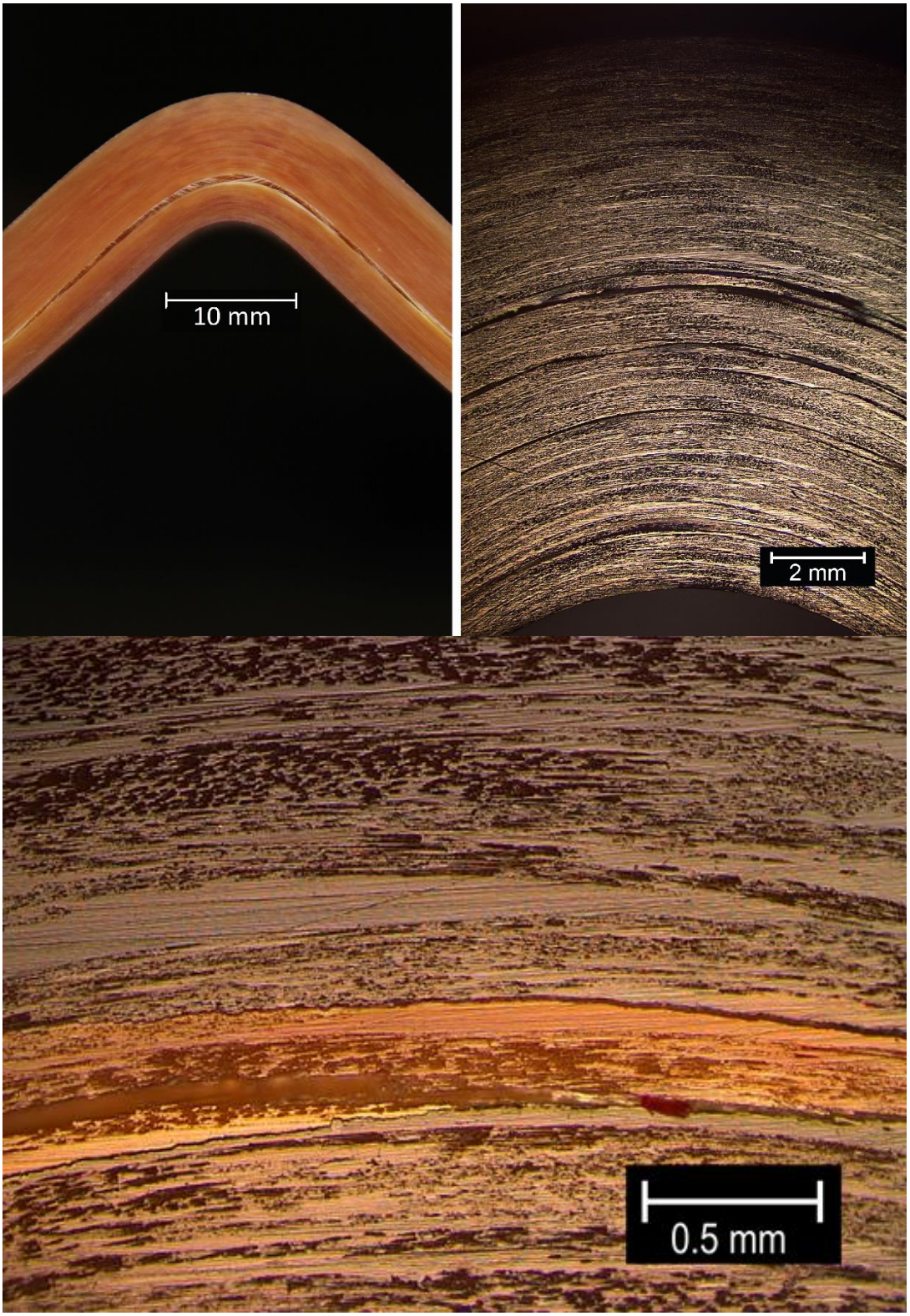

Figure 2.21. Photo of delamination onset and microscopic views of $[0]_{40}$ GFRP specimen

Furthermore, when the experiment continued, further delaminations occurred with multiple load drop rather than one load drop which is different from the CFRP specimens. In the ASTM D6415/D6415M standard, CBS is calculated when the load drop is half of the maximum load at the experiment. However, this specimen has an increasing load curve trend with further delamination in Figure 2.22.

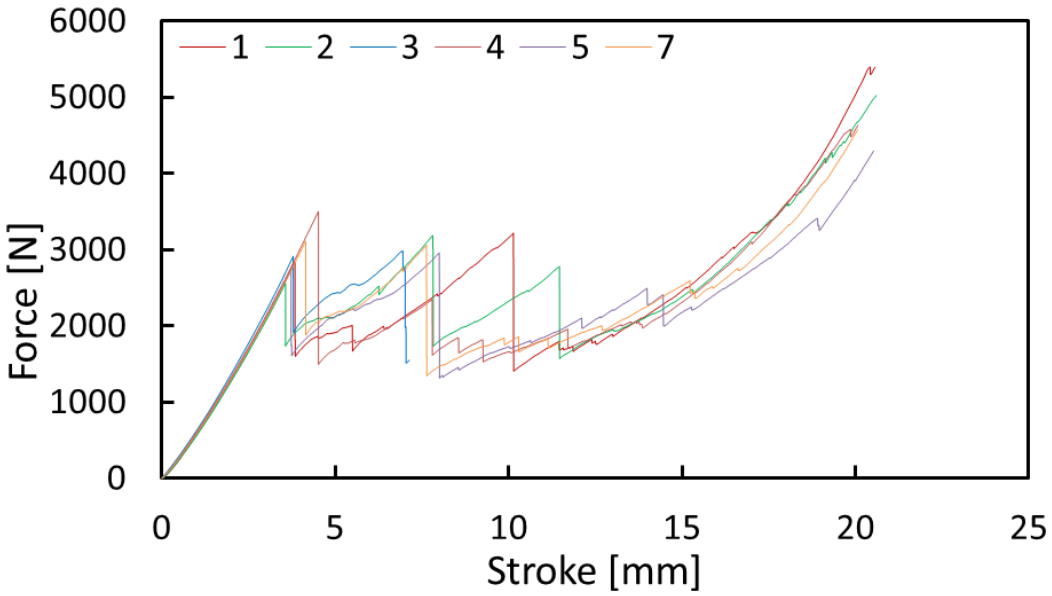

Figure 2.22. Load-displacement graphs of further delamination for seven 0/0 GFRP laminates

This phenomenon seems like CBS of the specimens increased with further delaminations. The reason for that is the first delamination of the specimens cannot propagate through the specimen, due to compressive stress at the top rollers. Delamination starts at the center of the specimen then propagates in the legs. The compressive stress prevents the Mode I type fracture. So, the high load values do not have to be used in the calculation of CBS and ILTS values. Further delamination pictures are seen in Figure 2.23.

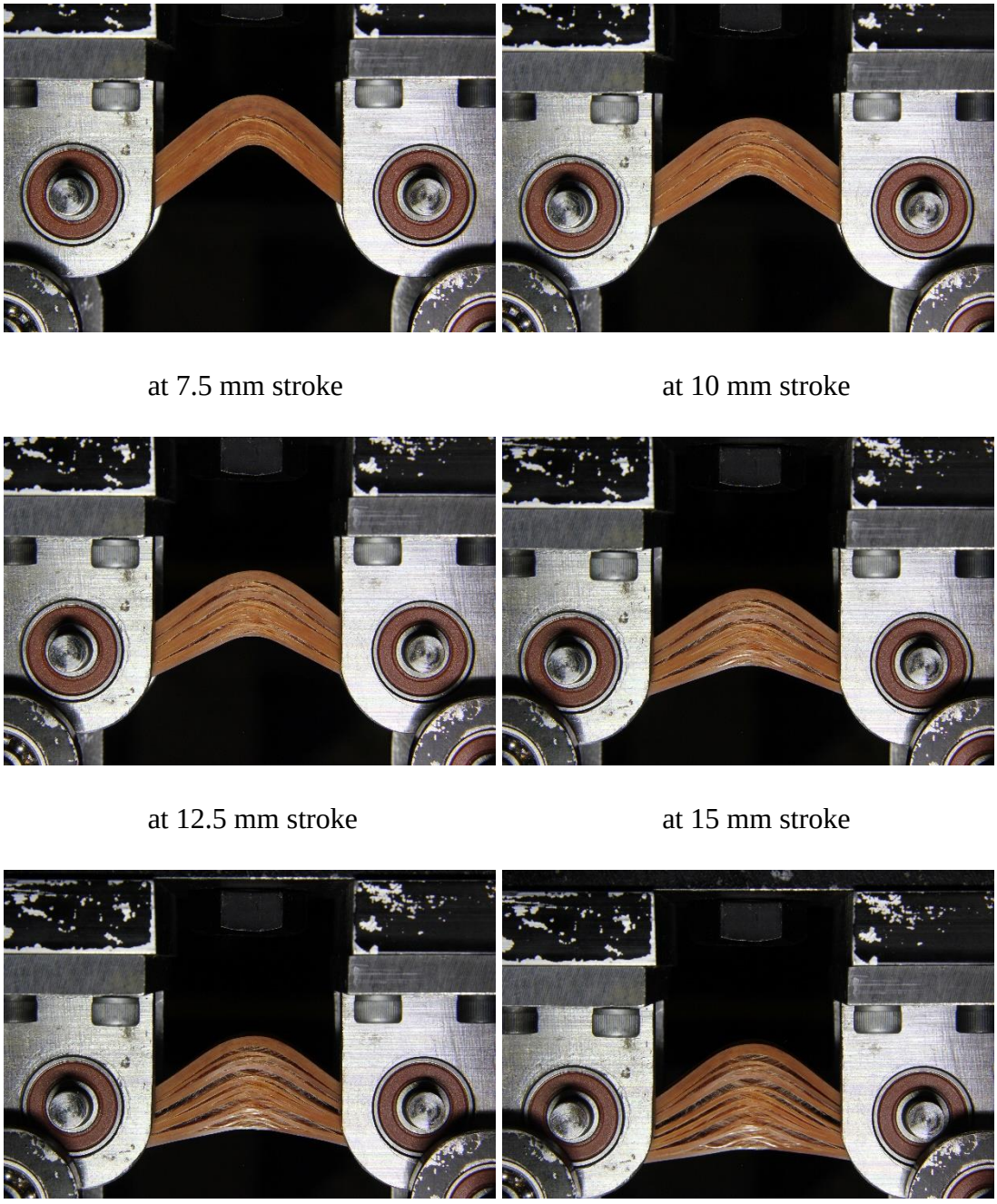

at 7.5 mm stroke at 10 mm stroke

at 12.5 mm stroke at 15 mm stroke

at 17.5 mm stroke at 20 mm stroke

Figure 2.23. Delamination progression in 0/0 GFRP specimen 1

This phenomenon shows that preventing the propagation of the delamination or preventing the delamination will increase the CBS to high values. As mentioned in the introduction section, stitching is the best way to increase CBS.

2.3.2.2. ILTS of $[\pm 25]_{20}$ GFRP Specimens

Three specimens were tested for $[\pm 25]_{20}$ GFRP laminates. All experiments were accomplished on the standard fixtures. Loads at failure were around 3750 N as shown in Figure 2.24. After failure, the load drops around 1750 N. Loading curves of these specimens fit well with each other. The only failure is delamination for all specimens, so the calculated values are acceptable. ILTS values are calculated according to these load drops. 56.3 MPa is calculated as an average value of three experiments.

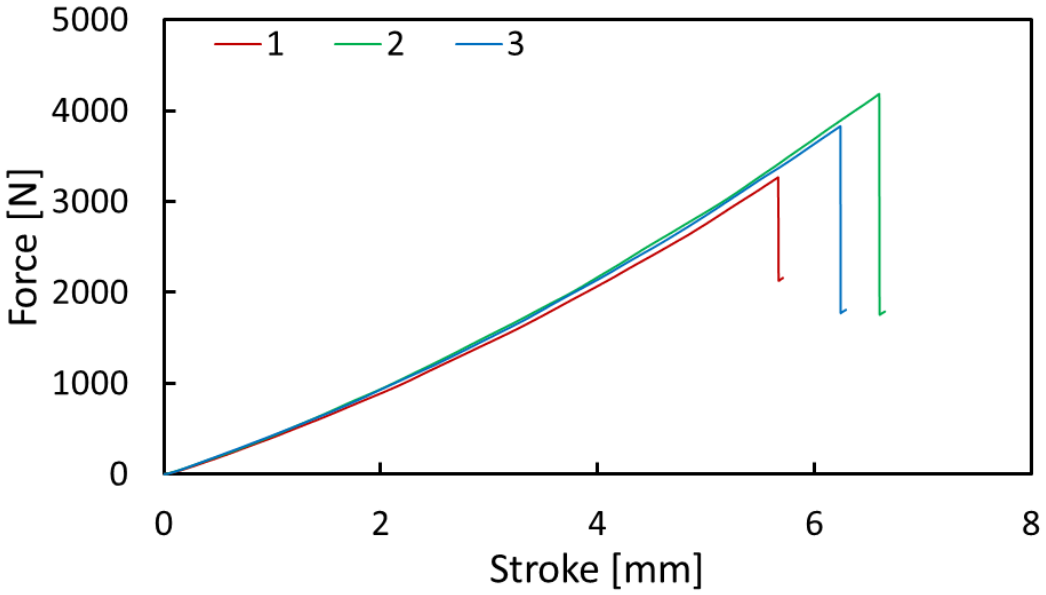

Figure 2.24. Load-displacement graph for $[\pm 25]_{20}$ GFRP CBS specimens

The delamination and microscopic photos of specimen number 2 are demonstrated in Figure 2.25. One main delamination occurred for these specimens and other failure types were not observed. The calculated values are true for this reason. The resin-rich region is also seen for these specimens in the microscopic pictures.

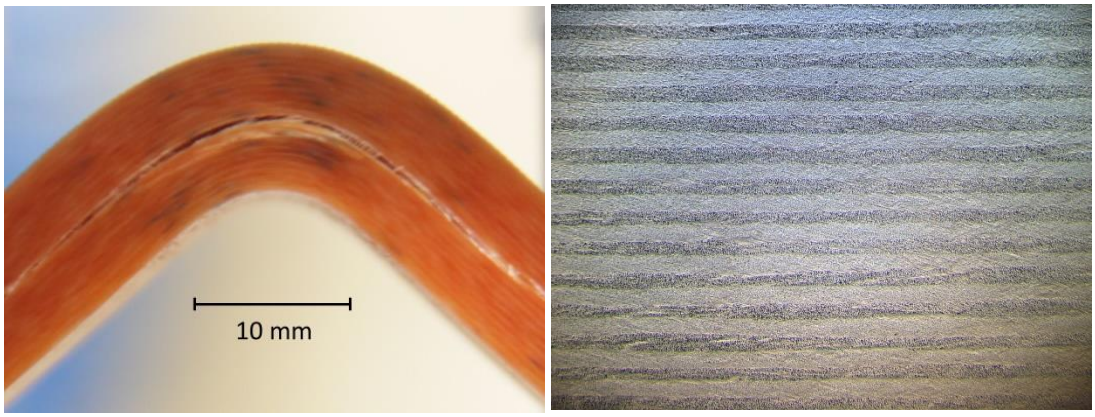

Figure 2.25. Photo of delamination and microscopic view of the $[\pm 25]_{20}$ CFRP specimen

2.3.2.3. ILTS of $[\pm 45]_{20}$ GFRP Specimens

CBS specimens with $[\pm 45]_{20}$ layups were also tested with the ASTM D6415/D6415M standard fixture. Relatively low scattering was observed for load values corresponding to the first delamination, which was 4250 N on average for this specimen set. Single delamination occurred accompanied by the first load drop similar to the behavior in $[0]_{40}$ GFRP CBS specimens. Load drops have a variation from 1250 N to 2500 N as in Figure 2.26.

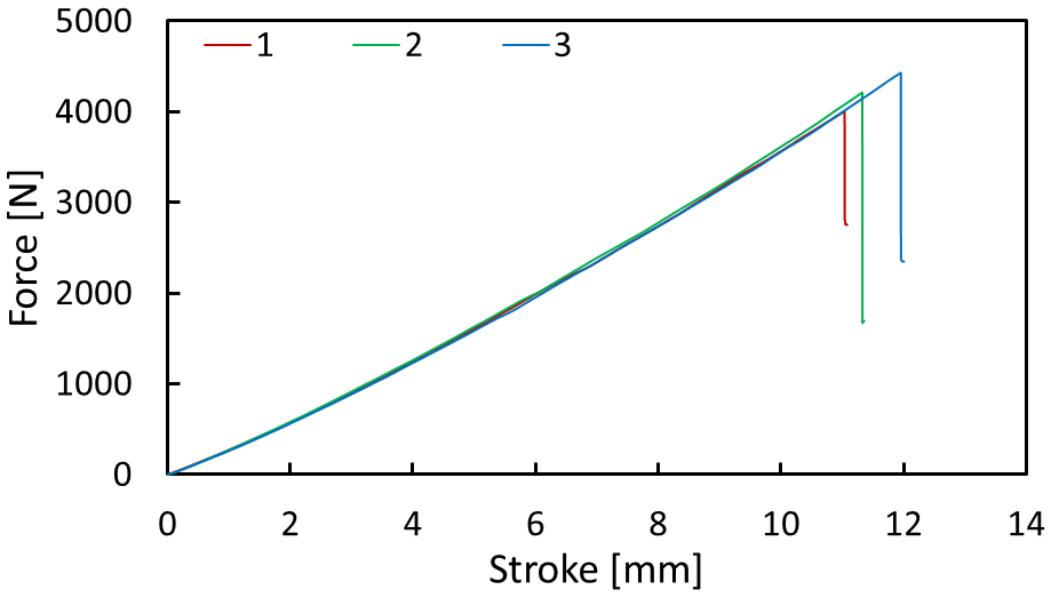

Figure 2.26. Load-displacement graph for $[\pm 45]_{20}$ GFRP CBS specimens

An average of 43.5 MPa is calculated as ILTS for these specimens. A view of major delamination and also a microscopic view of the same surface outside of the damaged zone are shown in Figure 2.27. Resin rich regions around layer interfaces are more visible compared with other specimens (Figure 2.2). A large difference between adjacent layers for this type of specimen and thicker GFRP prepregs is believed to be the reason for the creation of such resin-rich area formation.

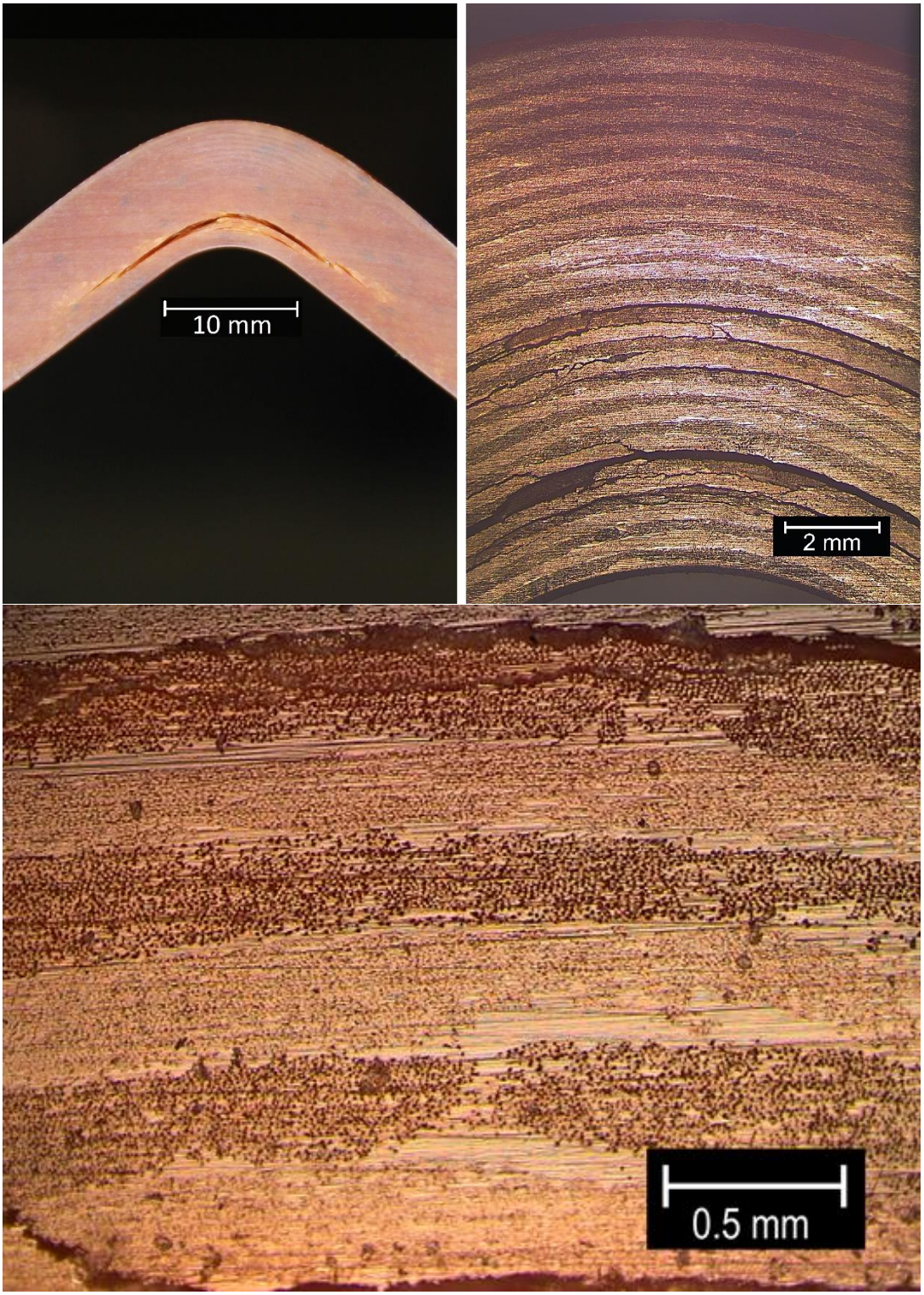

Figure 2.27. Photo of delamination and microscopic views of the $[\pm 45]_{20}$ CFRP specimen

2.3.2.4. ILTS of $[\pm 65]_{20}$ GFRP Specimen

Similar to CFRP $[\pm 65]_{20}$ specimens, corresponding $[\pm 65]_{20}$ GFRP CBS specimens were loaded with the modified four-point bending fixture, with l_t changed to 35 mm. Although specimens had enough stiffness for conducting the test on the standard fixture, in order to have better comparison and to reduce the number of matrix cracks that happen before delamination, the modified fixture geometry was used. The load-displacement curve is almost linear before matrix cracks start as shown in Figure 2.28. After passing around 500 N, matrix cracks start occurring in inner layers of the specimen and growing into the mid-layer.

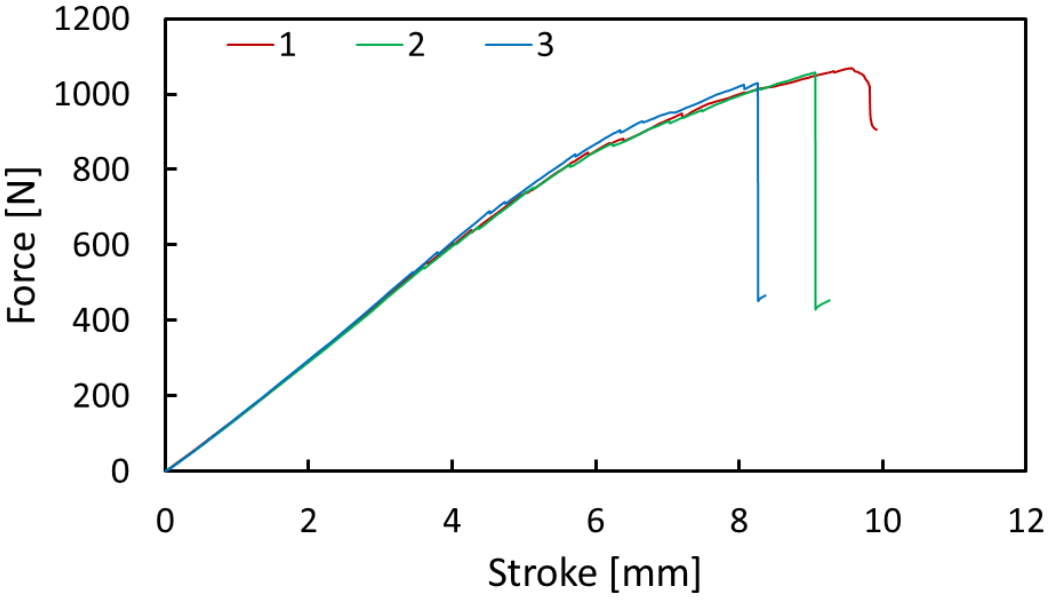

Figure 2.28. Load-displacement graph for $[\pm 65]_{20}$ GFRP CBS

Matrix cracks on the GFRP specimens are noticeable with a huge color change mostly below the mid-layer in Figure 2.30. These matrix cracks grow and eventually develop to delamination which is pronounced by a corresponding large load drop at about 1000N.

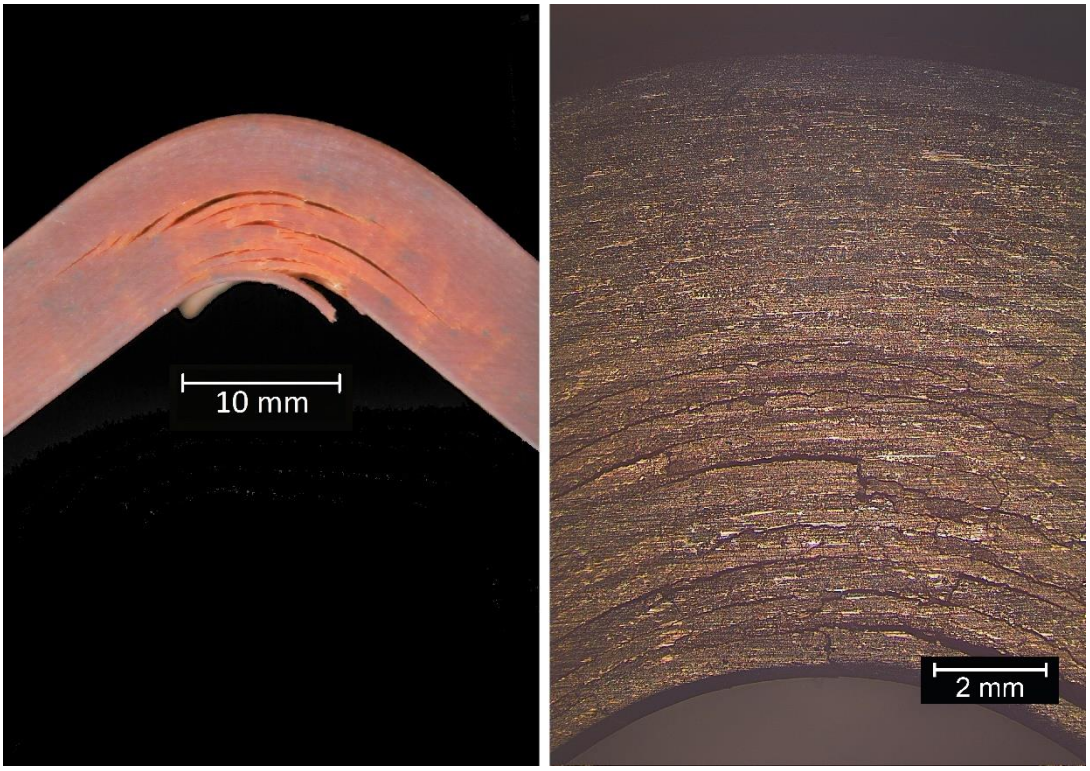

Figure 2.29. Photo of delaminations and microscopic view of $[\pm 65]_{20}$ CFRP specimen

Matrix cracks for this layup are believed to somehow cause premature delamination of the specimens. This, in turn, is the reason for the relatively low ILTS value obtained which averages at 25.8 MPa. Thus, it does not represent the ILTS of this layup, a different layup with 25/-25 interface is proposed. As is mentioned in the CFRP results, the 65/-65 interface has less resin-rich zones than 45/-45 and more than 0/0.

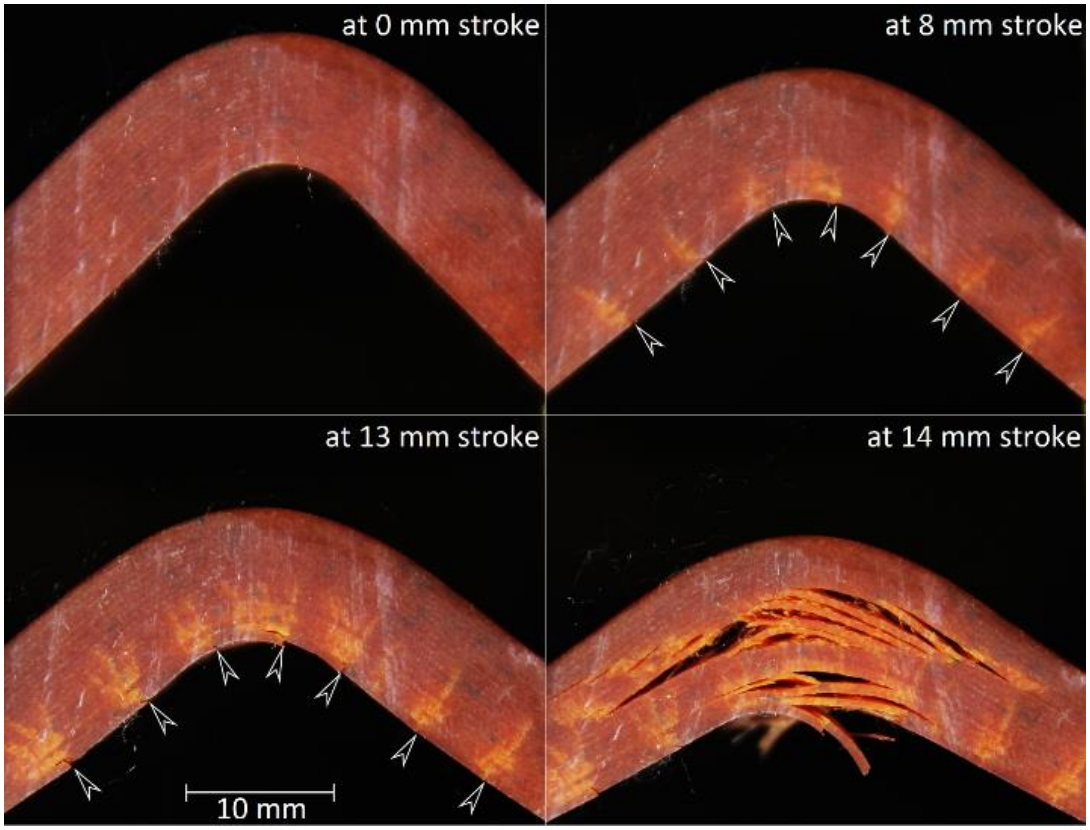

Figure 2.30. Matrix cracks formed and followed by delamination in GFRP $[\pm 65]_{20}$ specimens

2.3.3. Summary of Results

According to the ASTM D6415/D6415M standard [Ref 3], the ILTS value has to be calculated at the first large load drop. ILTS and CBS values obtained in this test program for CFRP and GFRP are presented in Figure 2.31 and, Figure 2.32 respectively. CBS values are calculated according to the first delamination load so they are related to ILTS values, which are also calculated at the first delamination load, of the specimens. Side photos of delaminations of all experiments are shown in Figure 0.1, Figure 0.2, Figure 0.3 and Figure 0.4 in the appendix section.

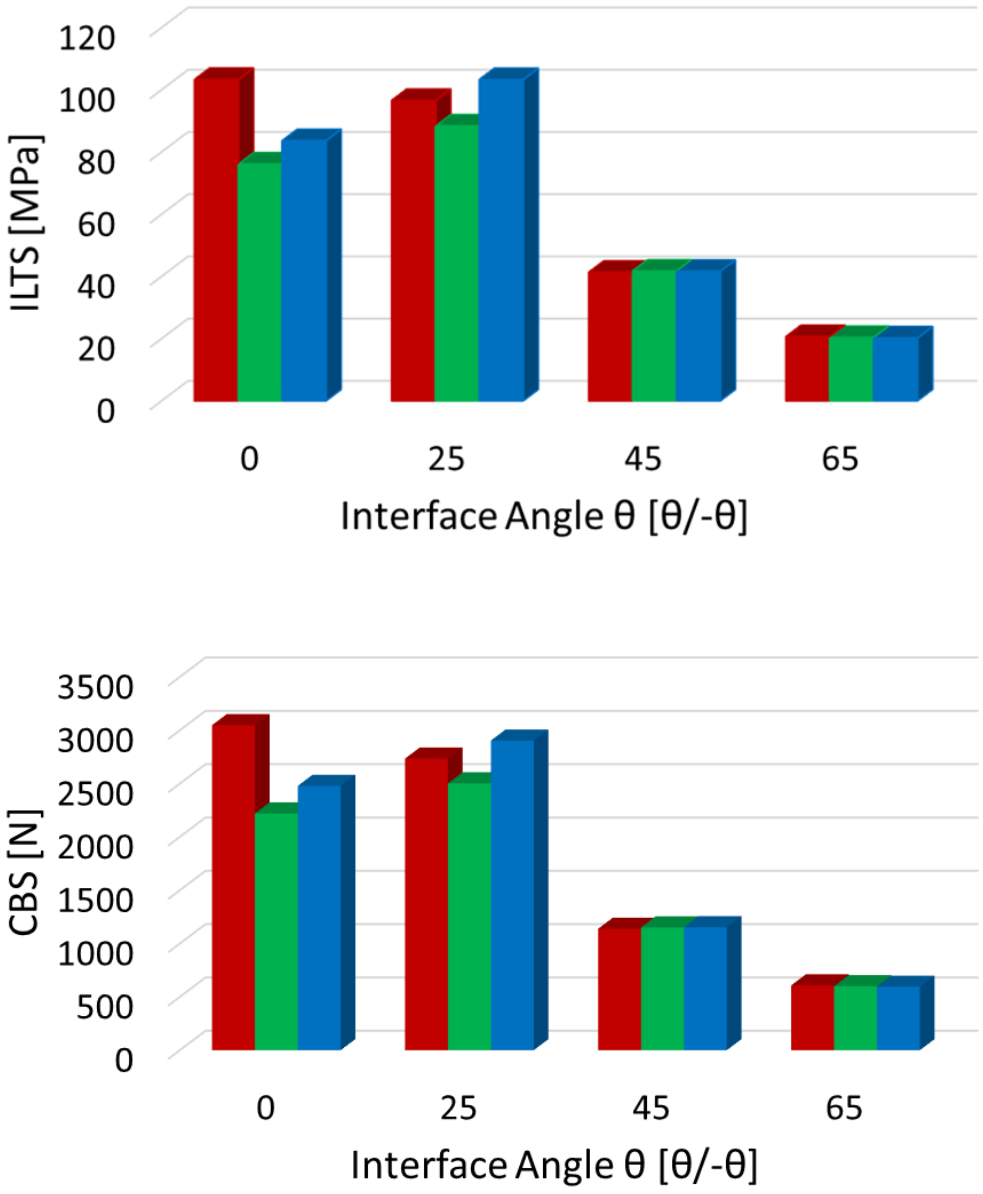

Figure 2.31. ILTS and CBS results for CFRP

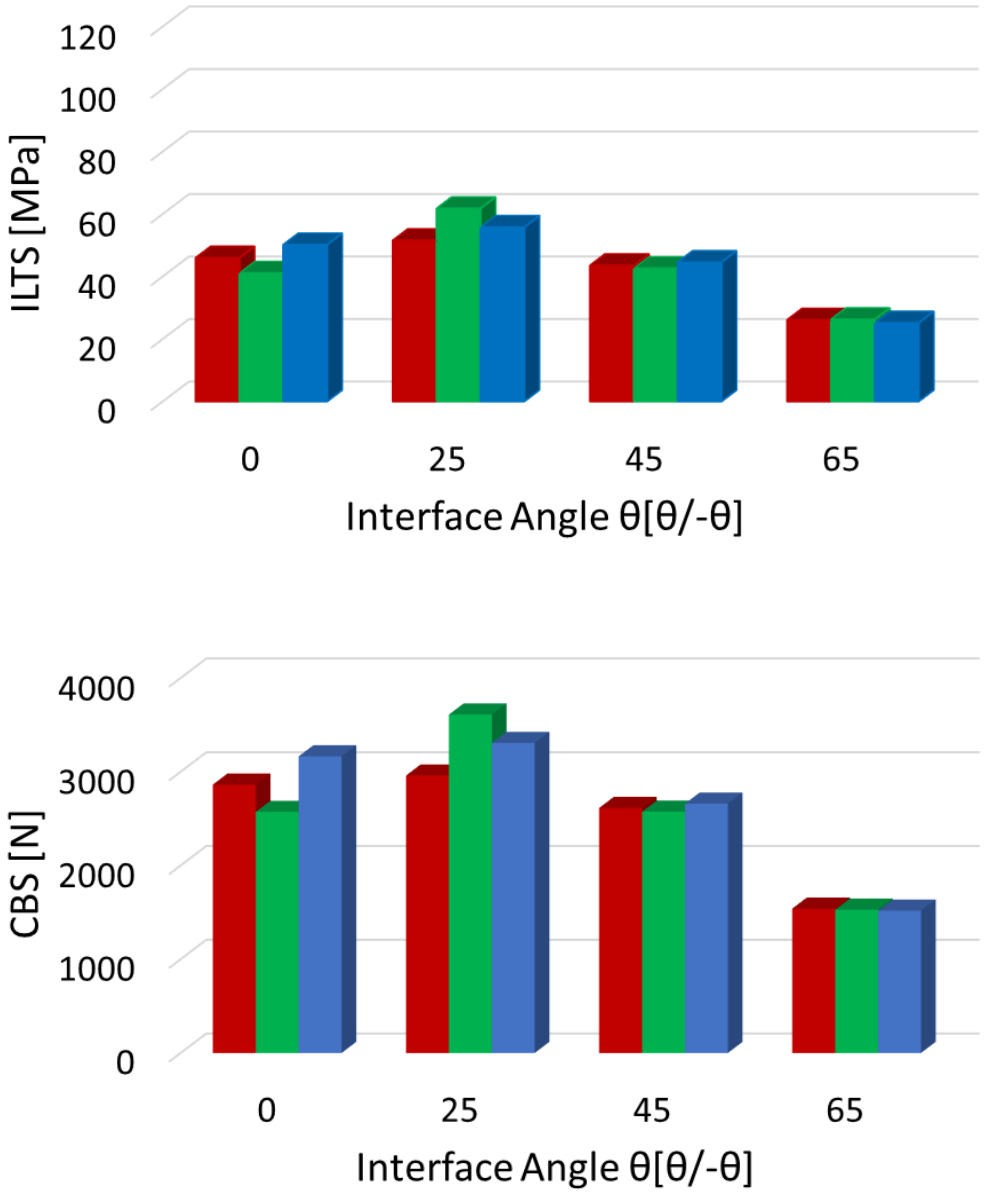

Figure 2.32. ILTS and CBS results for GFRP

When $[\pm 65]_{20}$ specimens are not taken into account, a lower variation in ILTS is observed for GFRP specimens, while there is a larger difference obtained for CFRP. CFRP 0/0 and 25/-25 ILTS is more than twice the values of CFRP 45/-45. 0/0, 25/-25 and 45/-45 ILTS of GFRP laminates. However, they are close to each other, there is about 16% variation from average ILTS as seen in Table 2.4. GFRP laminates have

an average ILTS value of 48.5 MPa when the 65/-65 interface result is removed (due to matrix cracks occurring before delamination). CFRP laminates have a 75 MPa average ILTS value when the 65/-65 interface is removed due to the same reason. The variation is 28 percent with respect to the average value for CFRP specimens.

Table 2.4. Average ILTS and CBS results for interfaces

ILTS AVG. RESULTS

Interface	CFRP [MPa]	GFRP [MPa]
0/0	87.6	45.7
25/-25	96	56.3
45/-45	41.5	43.5
65/-65	20.4	25.8

CBS AVG. RESULTS

Interface	CFRP [N]	GFRP [N]
0/0	2582	2866
25/-25	2713	3292
45/-45	1148	2615
65/-65	601	1528

2.4. Discussion

Micrographs of various layup angles are shown in Figure 2.33. The modes of failure shown in these pictures have a direct impact on test results. During the curing process, carbon fibers for $[0]_{40}$ specimens get closer easily due to fibers being in the same direction, which means there is less resin-rich area in the 0/0 interface. This increases the ILTS values due to stress being able to be transferred fiber to fiber at the interface. In one poorly produced carbon CBS specimen with 45/45/45/45/-45/45/-45 around the crack region, delamination occurred at 45/-45 interfaces instead of at the 45/45 interface in Figure 3.35 since it represents 0/0 ILTS value which is two times higher than that of the 45/-45 interface. The delamination did not occur at the area of maximum interlaminar tensile stress, because the interlaminar stress variation around 0.2 to 0.5 nondimensional r is about 20 percent according to Ko and Jackson in Figure 3.35, whilst the ILTS of the 45/45 interface is double the ILTS of the 45/-45 interface. Due to this, delamination occurs at the 45/-45 interface. Also, a richer resin region of the 45/-45 interface than the 45/45 interface is noticeable. On the other hand, this phenomenon does not occur for Glass $[0]_{40}$ due to its high resin ratio. Glass prepreg ply has a 50.4% fiber ratio while the carbon one has a 58.5% fiber ratio. Therefore, glass specimens are affected by resin-rich regions at the interface. This is also the reason for ILTS values of $[0]_{40}$ and $[\pm45]_{20}$ specimens being almost the same. Resin rich regions are illustrated in Figure 2.34.

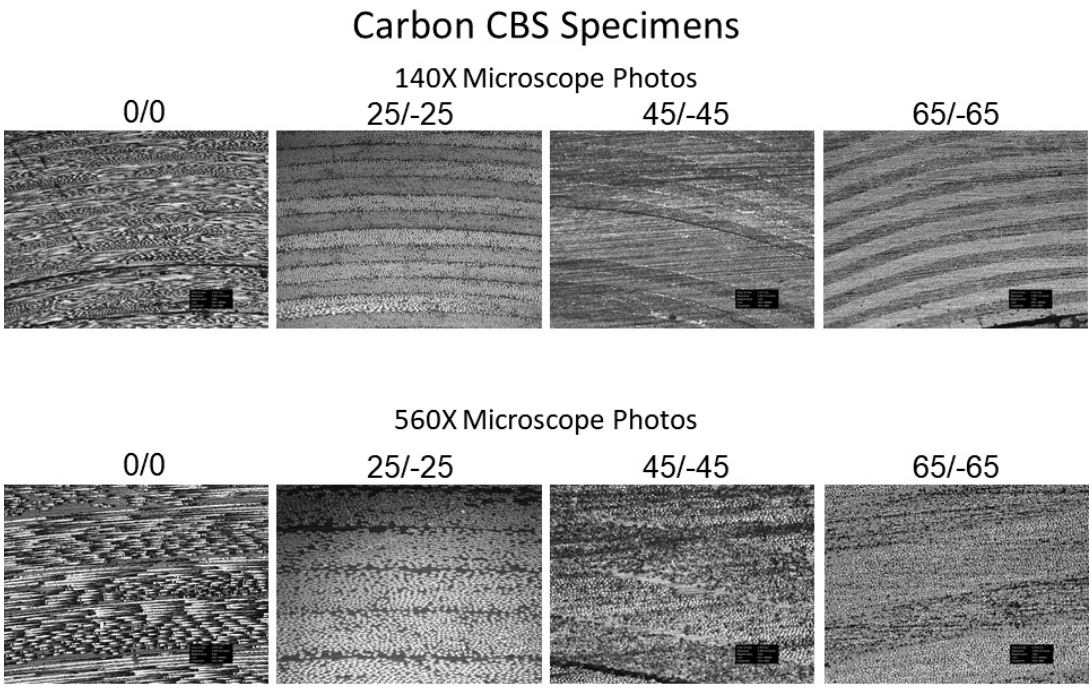

Figure 2.33. Microscopic views of carbon specimens

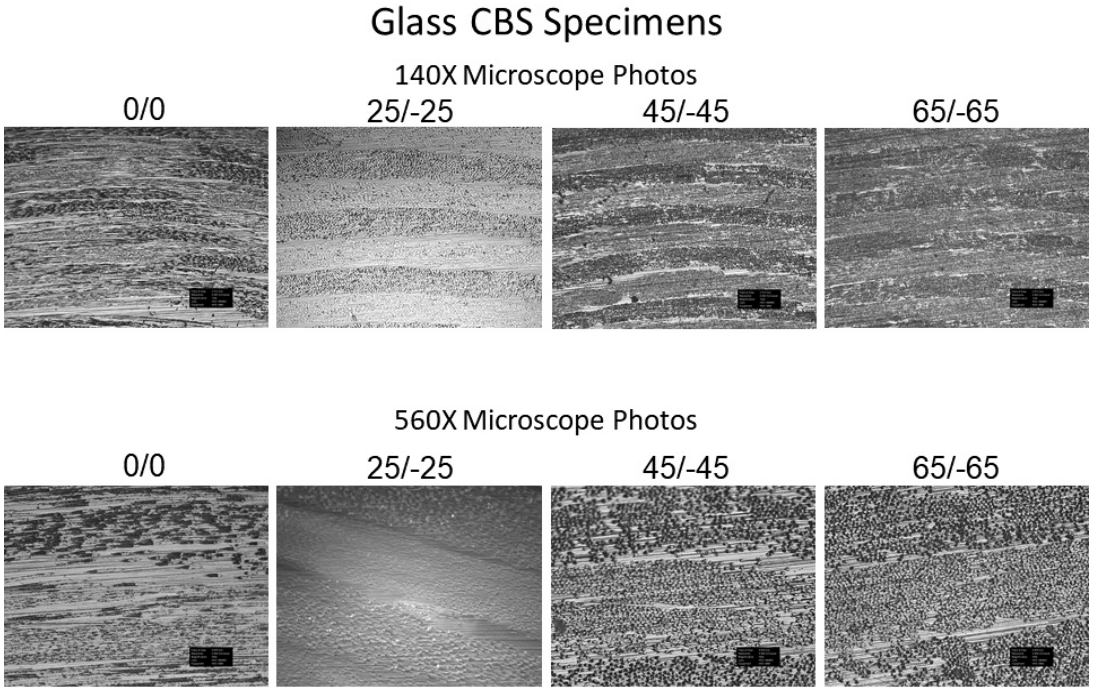

Figure 2.34. Microscopic views of glass specimens

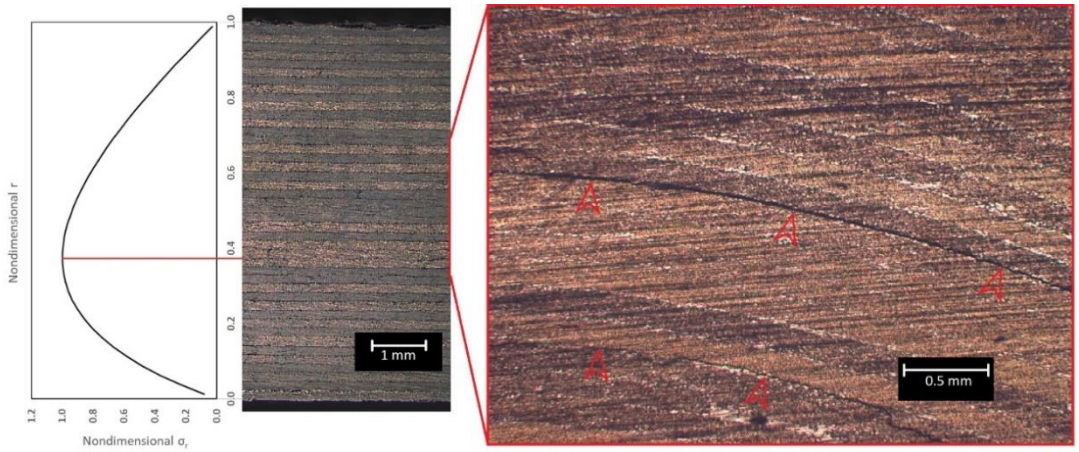

Figure 2.35. Interlaminar tensile stress curve with respect to nondimensional radius according to Ko and Jackson formulation and delaminations at 45/-45 interface which is above the four 45 layers

For both carbon and glass $[\pm 65]_{20}$ specimens ILTS values are very low relative to other interfaces. Matrix crack occurs for these specimens because their tensile load direction is almost perpendicular to the fiber direction. Delamination occurs as a propagation of a matrix crack. Therefore, these ILTS are not acceptable as an initiation value. Matrix crack preceding delamination is shown in Figure 2.30.

Both carbon and glass $[\pm 25]_{20}$ specimens were produced in different production batches. For glass specimens, the only difference is the ILTS of 25/-25 interface without taking account of the ILTS of 65/-65 interface. This is an indication of the difference in production. This may also apply to the CFRP specimens. In general, the delamination occurs at angle-ply interfaces like 25/-25 rather than at the 0/0 interface. However, the 25/-25 interface has more ILTS than the 0/0 interface for our CFRP specimens. This unexpected result could be due to the production difference.

2.5. Conclusions

In this study, four different interfaces, 0/0, 25/-25, 45/-45, and 65/-65, for CFRP and GFRP laminates were examined for their interlaminar tensile strength values. The following conclusions have been drawn:

1. The CFRP 0/0 interface has double the ILTS of the 45/-45 interface, 87.6 MPa, and 45.7 MPa respectively. 0-degree layers came closer during the curing process while 45-degree and -45-degree layers could not be closer due to the angle difference at the interface.
2. GFRP ILTSs were closer to each other than CFRP ones, having 48.5 MPa ILTS on average. GFRP specimens have an 8 percent more resin ratio than CFRP specimens. This resin difference corresponds to 19 percent more resin for GFRP ones when only resin volume is compared. This prevents those fibers from different layers from coming into close proximity. So, resin-rich regions occur at the interfaces and this decreases the ILTS value due to low-stress transfer. The resin in the composite structure transfers the stress fiber to the fiber. If the layers are too far from each other, stress cannot transfer from one to the other.
3. The lowest CFRP ILTS is 64 percent of the strength in the transverse direction, while it is 87 percent for GFRP. Because of this, it is important to use true ILTS values to create a good design and prevent unpredictable delamination. For these CFRP parts, using a 0/0 interface ILTS value for the other interfaces would be a reason for unpredictable delamination whilst in use.
4. If one value is to be used for all interfaces, for a safer design process, the 45/-45 ILTS can be used for all interfaces.
5. The same resin type was used for both glass and carbon laminates. According to the producer data, 65 MPa is the tensile strength of the resin only. It shows that using the resin tensile strength as an ILTS value is not conservative.
6. It was not expected to get the highest ILTS value for the 25/-25 interface. This may be indicative of the effect of production differences on ILTS.

CHAPTER 3

MODE I FRACTURE TOUGHNESS OF DIFFERENT ANGLE-PLY CFRP AND GFRP COMPOSITE

3.1. Introduction

Advanced composite parts have been used for years in very critical systems like aerospace vehicles, planes, high-performance cars to name a few. These high technology parts have become a subject of competition among large companies. This competition grows to a state where the manufacture of such parts require materials with enhanced properties of higher strength and lower weight. Although carbon fiber reinforced polymer (CFRP) and glass fiber reinforced polymers (GFRP) are such materials, they have very low strength in their interlaminar planes. Failure of such interfaces is called delamination which is mainly a crack growing along with the interface of two plies without causing any damage within them.

Interlaminar interfaces being the weakest plane in the composite structure, in the event of their failure, are the reason for a dramatic decrease in load-carrying capacity. These facts demonstrate that delamination properties are very important for the design processes of composite structures. Two crucial properties control delamination; one of them is the interlaminar strength for the onset of delamination and the other is the fracture toughness for the propagation of delamination. There are three modes in fracture toughness for the propagation of delamination which are opening, sliding, and tearing modes. In this study, we will focus on Mode I (opening) delamination failure of composite laminates.

In a study conducted by Gallagher et al. [14], they revealed that crack growth in different angle ply laminates could grow through a ply or between plies, so fracture

toughness values vary between laminates. Moreover, Chou et al. [15] realized that when the crack grows with zig-zag movement, G_I increases with crack size.

With the advent of this century, safety and reliability issues have become a very important topic. One of the most important values which determine the life of a CFRP or a GFRP part is the G_I value itself, so using 0//0 interface properties for the design of the multidirectional laminates is not suggested [16]. Following this recommendation, Hwang et al. [17] have tried to determine Mode I and Mode II fracture toughness in different angle ply laminates for safer and more reliable designs. Andersons [18] presented a comprehensive literature review classifying experiments according to their lamination sequences and material types. He showed that G_I value changes with the angle of plies (α) in which delamination grows as illustrated in Figure 3.1.

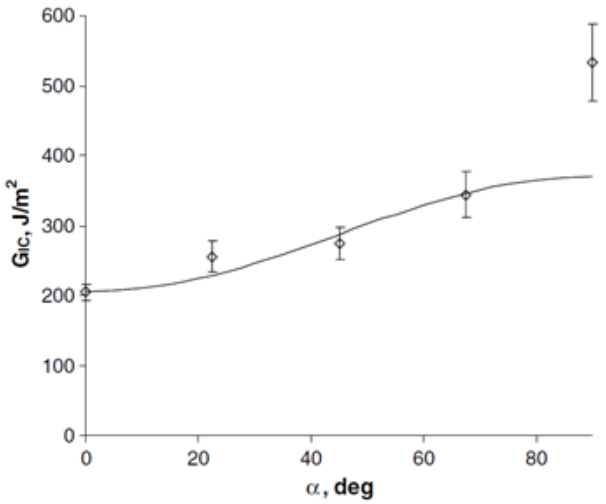

Figure 3.1. Variation of G_I with the ply orientation α [6]

Moreover, it is found that Mode I fracture toughness values increase partially with ply angle α for both 0/α and α/α interfaces [15]. The latest study about antisymmetric interfaces has been done by C. Blondeau, who emphasizes fracture toughness, fracture surface, and implementation of the fracture toughness in FEA [20].

Fracture toughness between laminates for composite material under opening loading has been studied for aramid/epoxy [21], glass/vinylester [22], glass/polyester [23], glass/epoxy [24-26], carbon/PEEK [27,28], carbon/nylon [29], and carbon/epoxy [17,20,28,30-50] composites. Experiments of crack propagation between different any-ply laminas are carried out with the hybrid short bar test technique [28], DCB with edge inserts [37,40], width-tapered DCB [17], and other common DCB tests [20,21,25,27,33,34,36,38,43,44,48,49].

Although there are many studies about Mode I fracture toughness with different lay-up, the effect of a wide range of different interfaces and different materials were not studied. The main objective of this study is to investigate the effect of lay-up orientation at the interface on the fracture toughness of certain CFRP and GFRP unidirectional laminates experimentally according to ASTM D5528 [19].

3.2. Experimental Procedure

Mode I experiments were conducted using a double cantilever beam (DCB) specimen according to ASTM D5528 [19]. Mode I fracture toughness tests are complicated since the crack length must be constantly measured during the experiment and the accurate recording of the crack length is important. The measurement requires utmost care. Specimen preparation, experimental protocol and post-processing data of the experimental study are mentioned in this section.

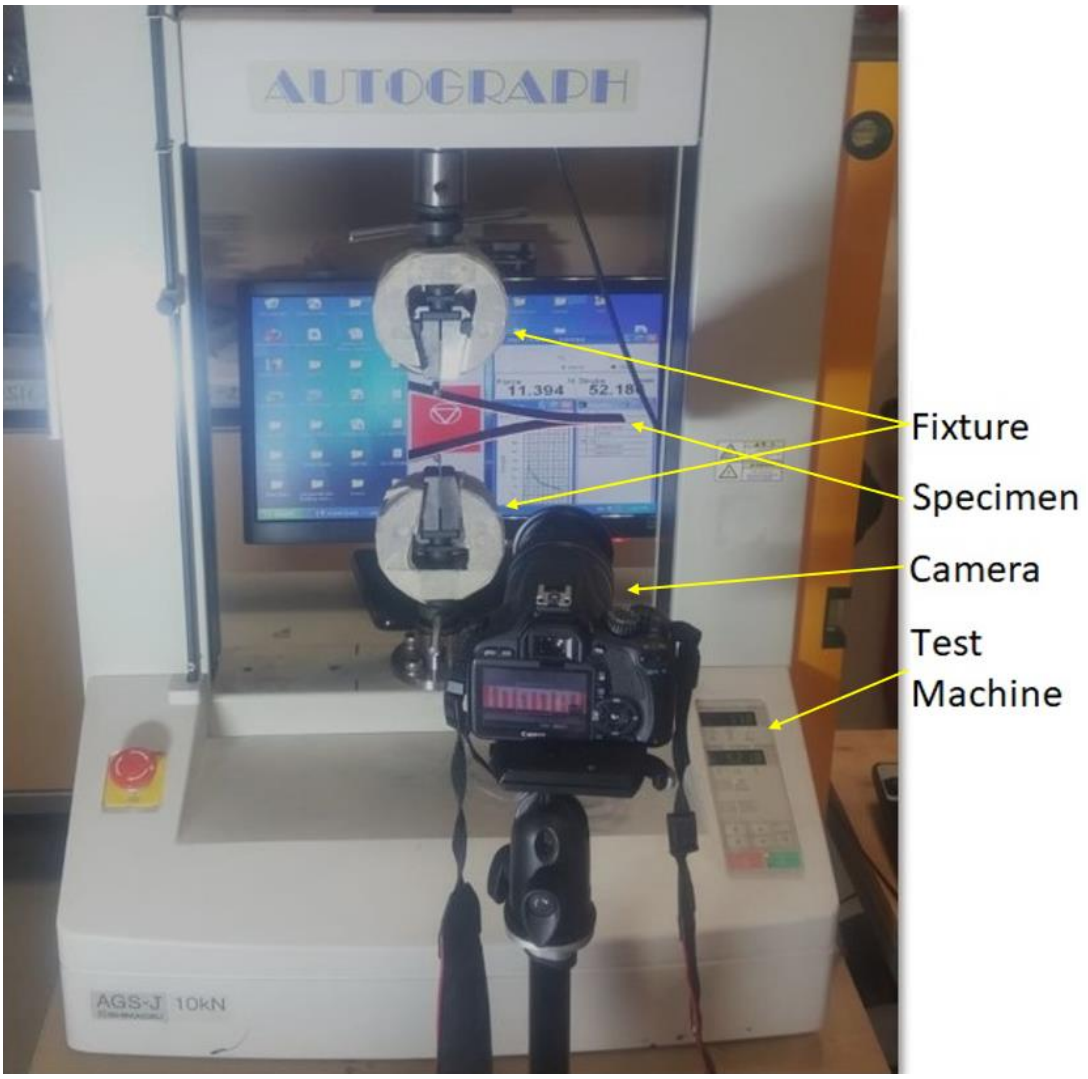

Figure 3.2. Experiment setup

3.2.1. Specimen Preparation

The specimens were produced with CFRP and GFRP unidirectional prepreg composites and their material properties are shown in Table 3.1 and Table 3.2. There are 6 different laminate layups, which are $[0_{10}//0_{10}]$, $[0_8/-25/25//-25/25/0_8]$, $[0_8/-45/45//-45/45/0_8]$, $[0_8/45/45//45/45/0_8]$, $[0_8/65/65//65/65/0_8]$ and $[0_8/90/90//90/90/0_8]$. The interface symbol, //, is used to denote the position of the initial crack. For introducing the initial crack, a 20-micron thick release film was used during the manufacturing of specimens. The release film location and example of the whole laminate before the cutting process is shown in Figure 3.5. The specimen dimensions were 200×25 mm, as illustrated in Figure 3.6, chosen according to ASTM D5528 testing standard (Ref 18). It contained a 75mm length release film for forming an initial crack.

*Table 3.1.*Material properties of CFRP UD prepregs (HEXPLY 913 132 HTA Carbon)

Density	ρ= 1.52 (g/cm^3)
Ply Thickness	0.136 mm
Fiber Volume Fraction	58.4 %
Elastic	E^t_{11}=140 GPa, E^t_{22}=E^t_{33} =9 GPa, E^c_{11}=110 GPa, E^c_{22}=E^c_{33} =10 GPa, ν_{12}=ν_{13}=0,35, ν_{23}=0,12, G_{11}=G_{22}=G_{33} =5 GPa
Strength	S^t_{11}=2000 MPa, S^t_{22}=65 MPa, S^c_{11}=1500 MPa, S^c_{22}=S^c_{33}=220 MPa, S_{12}= S_{13}=S_{23} =110 MPa

Table 3.2. Material properties of GFRP UD prepregs (Hexcel S2 Glass UD/913)

Density	ρ= 1.85 (g/cm^3)
Ply Thickness	0.244 mm
Fiber Volume Fraction	50.5 %
Elastic	E^t_{11}=50 GPa, E^t_{22}=E^t_{33} =12 GPa, E^c_{11}=40 GPa, E^c_{22}=E^c_{33} =12 GPa, ν_{12}=ν_{13}=0,3, ν_{23}=0,1, G_{11}=G_{22}=G_{33}=4 GPa
Strength	S^t_{11}=1400 MPa, S^t_{22}=50 MPa, S^c_{11}=1100 MPa, S^c_{22}=S^c_{33}=200 MPa, S_{12}= S_{13}=S_{23} =90 MPa

CFRP DCB Specimens

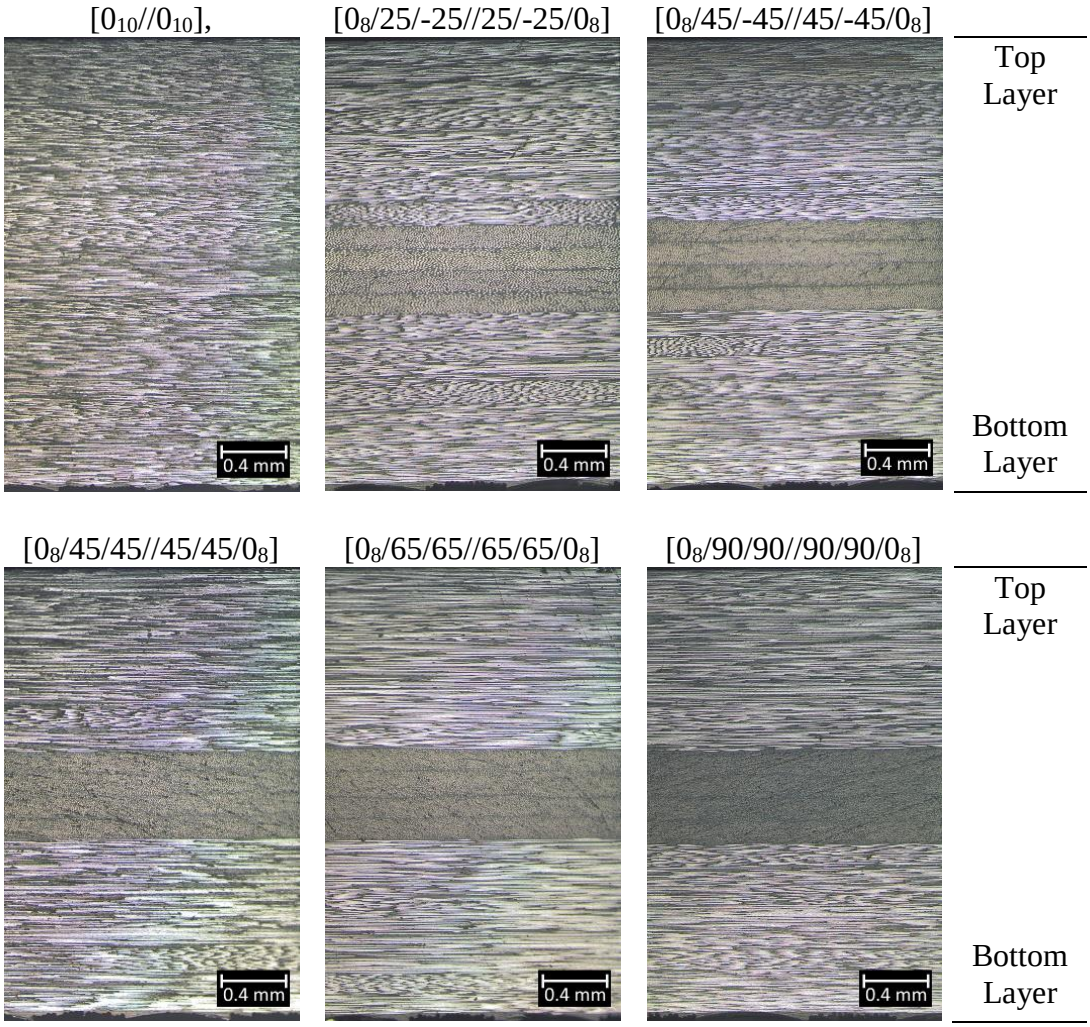

Figure 3.3. Microscopic Pictures of the Cross-sectional View of CFRP Specimens

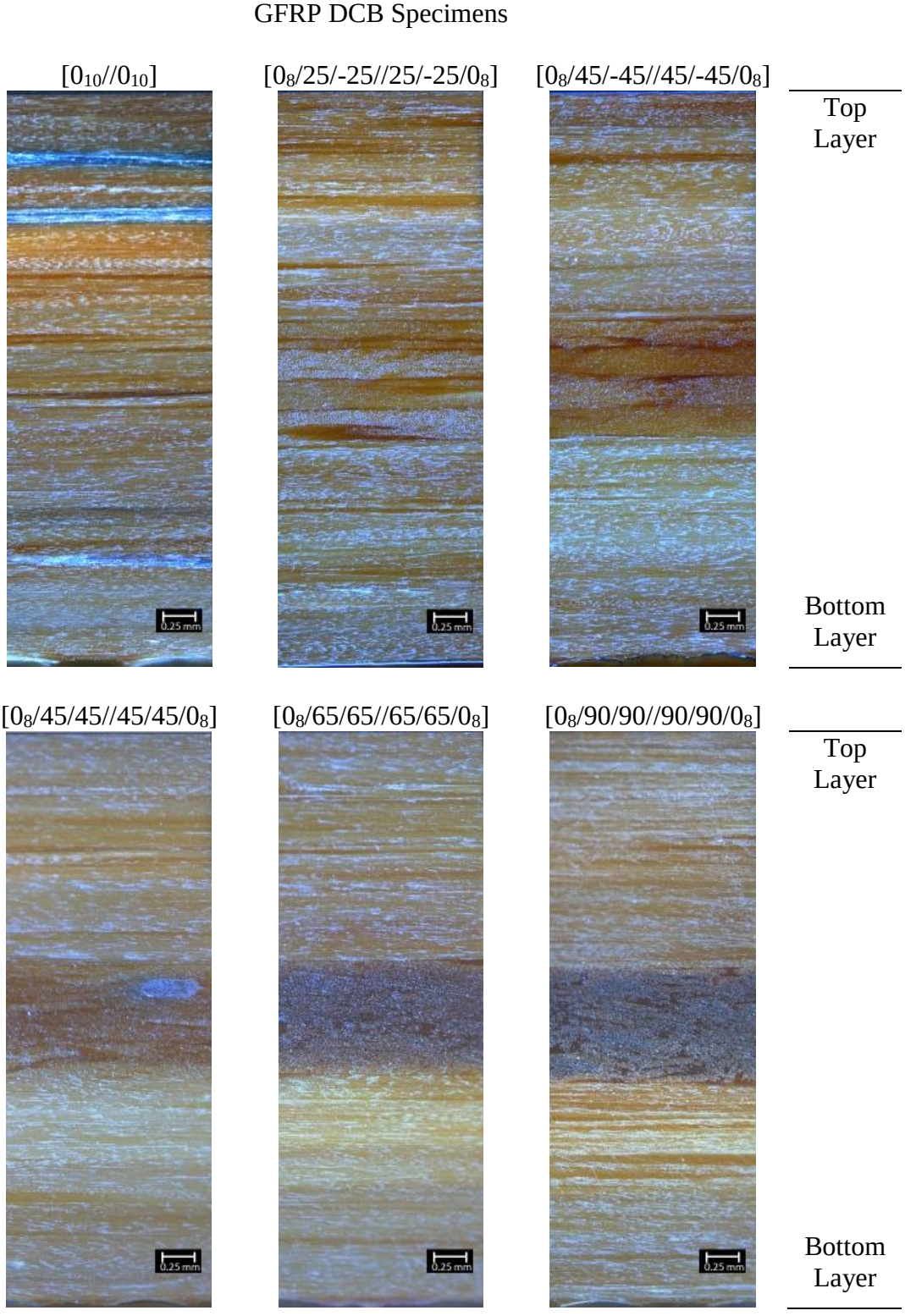

Figure 3.4. Microscopic Pictures of the Cross-sectional View of GFRP Specimens

All specimens were cut with a water jet machine. However, an initial opening hole machined with the water jet cutter can create delamination in the specimens as shown in Figure 3.7. Due to this, the opening hole must be machined with a drill machine, not with the water jet machine. Specimens were classified according to their material types, experimental modes, stacking sequence, specimen number, and manufacturer number, respectively, as in C-DCB-ENF-0-0-19-MF103735. The microscope pictures of all laminates in Figure 3.3 and Figure 3.4 were taken after a polishing process.

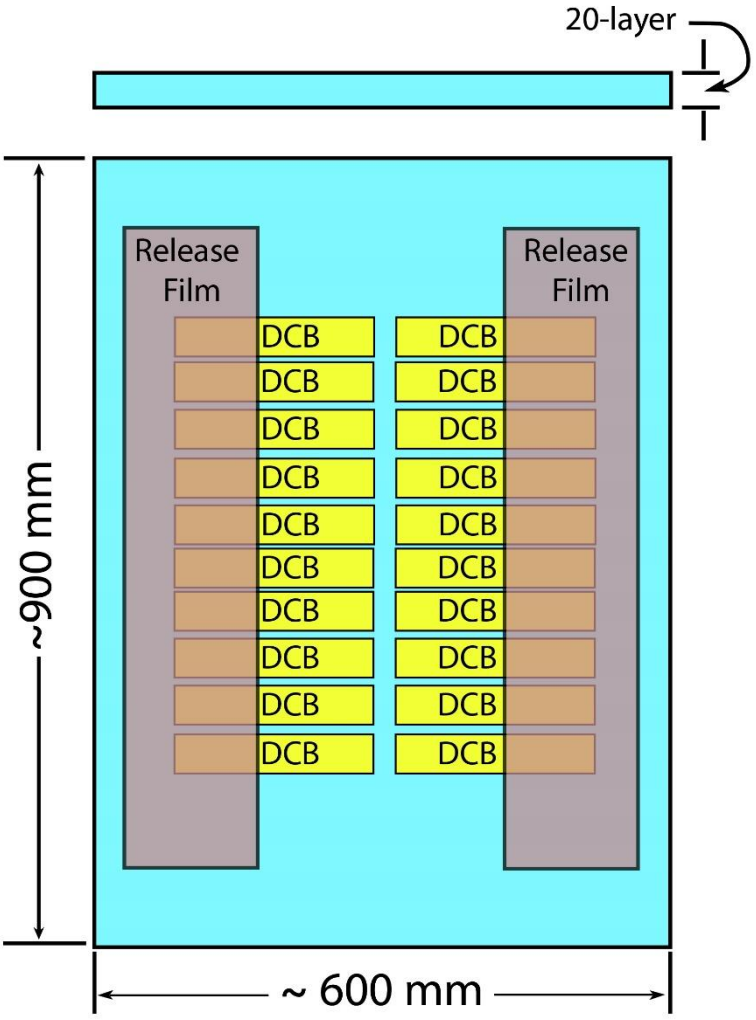

Figure 3.5. Produced laminate

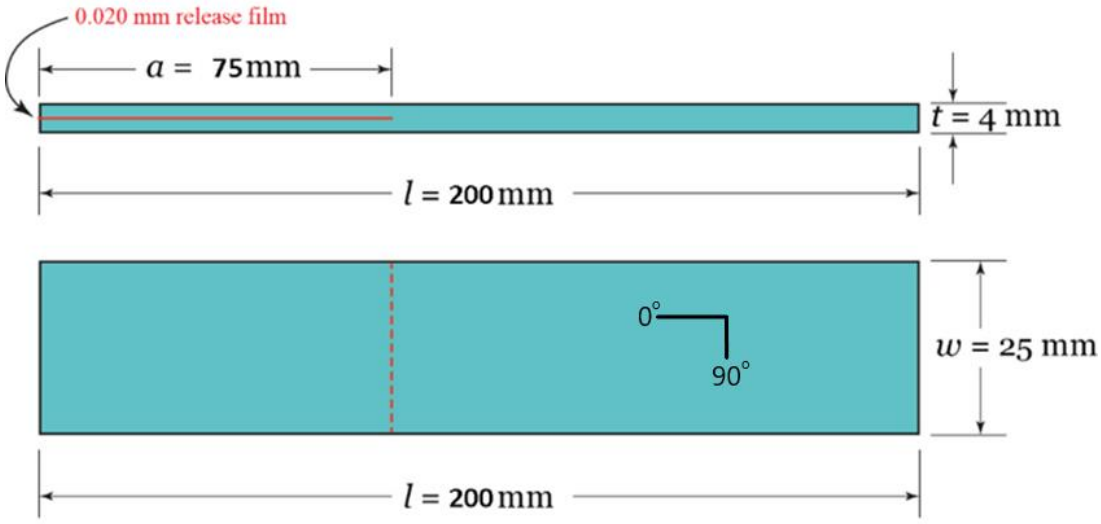

Figure 3.6. DCB specimen used in the study

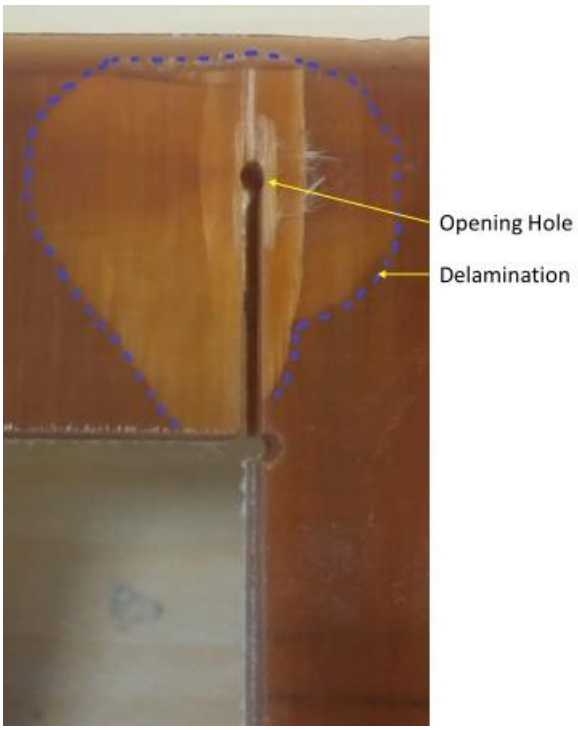

Figure 3.7. The delaminated hole opened with the water jet

The CFRP specimens were painted with a brittle, thin white paint at the long edge, which is important for the accurate visualization of crack length and its measurement. GFRP specimens were not painted with white color, because, in order to see the crack in GFRP specimens, very bright light is used to create a shadow over the crack. Afterwards, a detailed ruler (Figure 3.9) silhouette was sprayed on using a glossy red color as shown in Figure 3.8 for CFRP specimens, and a matt black color for the GFRP specimens, also in Figure 3.8. With this approach, the crack length can be easily seen and measured. In order to connect the DCB specimens to the tensile test machine, a hinge had to be combined with the specimen. For this operation, after the water-jet cutting of the specimens, sand-papering was carried out on areas of glue application. Sand papering was done with 100-grade sandpaper. Specimens and especially their edges were cleaned with acetone or alcohol. The hinge in Figure 3.10, used for gripping the specimen in the tensile test machine, was bonded onto the specimen using Pattex K2 fast glue. Other types of glues which have more strength, but longer curing times, can cause an alignment problem during curing. It is easy to fix the hinge into the right position with instant glue.

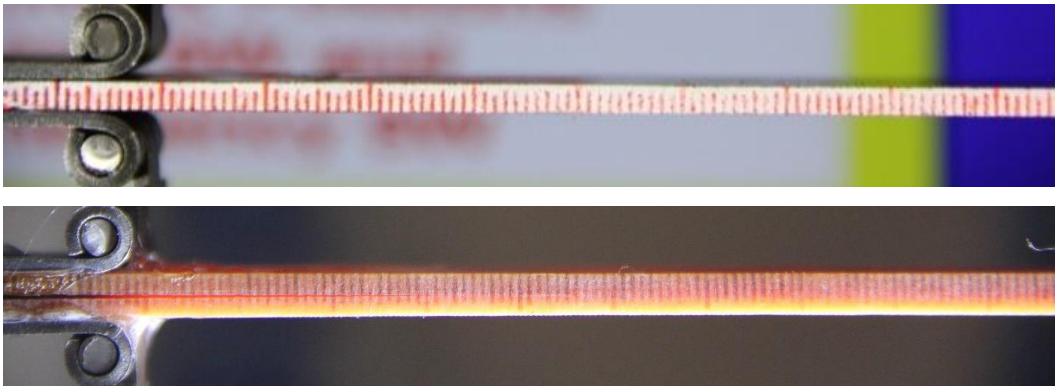

Figure 3.8. Painted DCB specimens (CFRP above, GFRP below)

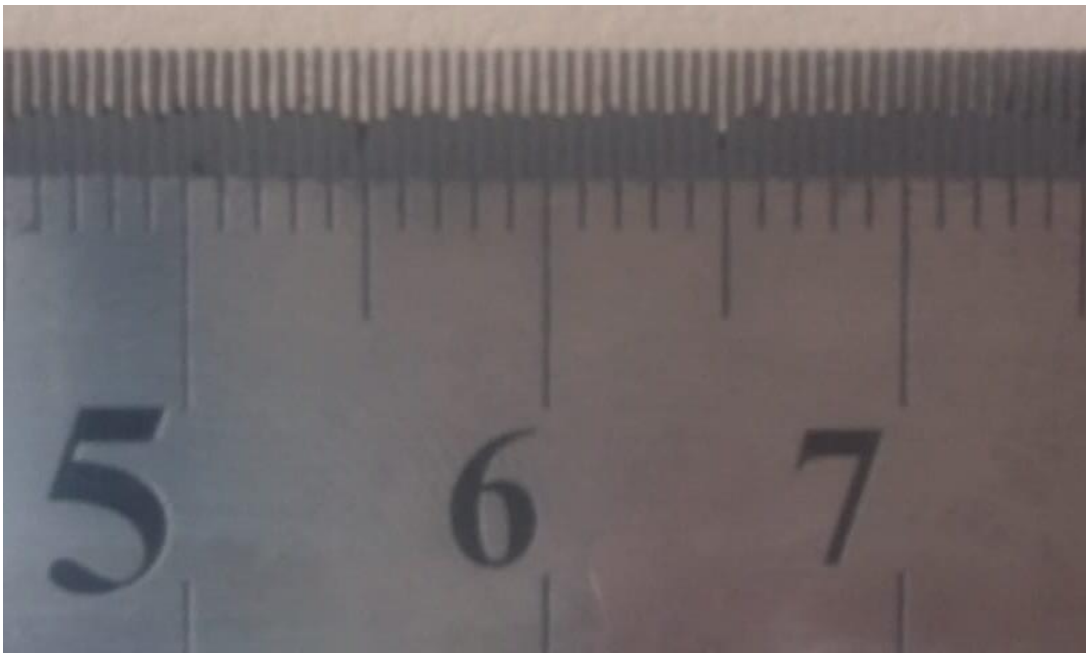

Figure 3.9. Apparatus which creates ruler silhouette

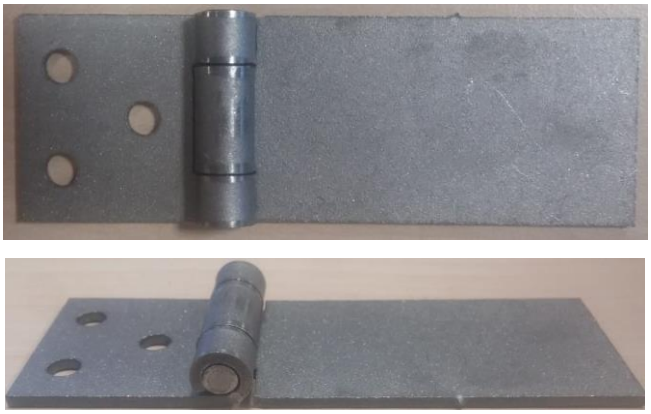

Figure 3.10. Hinge used in experiments

3.2.2. Experimental Protocol

All tests were conducted at room temperature and specimens were stored in normal room conditions. DCB tests were conducted with standard 25mm tensile test machine grips, under displacement control with 1mm/min crosshead speed. Before loading started, it was ensured that the specimen hinge was attached to the load line of the 10 KN Shimadzu (Figure 3.2) tensile test machine and it was as parallel as possible. Then loading was started at a speed of 1mm/min and the load-displacement data was

recorded by the computer. After the loading started, photos of the crack were taken for each 1 mm of crack growth for the first 15mm, then at each 5mm of further growth until the specimen broke. In order to catch the difference between dynamic crack propagation and stable crack propagation, data must be taken for each 1 mm crack growth until the specimen separated into two pieces. Crack lengths measured during tests are synced with corresponding displacement measurements. Except for the 0//0 interface specimen, crack length was measured from both sides for all CFRP specimens, since the location of the crack front may vary from one edge to the other. On the other hand, very bright light is put below the GFRP specimens to create a shadow of crack which can then be seen from above the specimen. Except for the 0//0 experiments, in order to allow taking the crack length data from both sides or examine the crack length shadow for GFRP specimens, the tensile test machine was stopped intermittently.

3.2.3. Post-Processing of Data

Load-displacement data was recorded in the test machine. The load-displacement graph is useful for the visualization of the progress of the experiment. Crack length data obtained from pictures were synced with the load-displacement data. The crack length data for all specimens at each stop were averaged since the locations of crack fronts from each side showed a variation. Then, the necessary calculations are performed; the area method, the load method, and the compliance method were used for determining G_I values.

3.2.3.1. Area Method

The area method is based on energy which is basically calculated from the area under the load-displacement graph. Formulation of the area method is seen in Equation (1). "B" is the width of the specimens which was 25 mm. "a" is the crack length of the specimen while "Δa" is the crack length difference between 2 data points. "U" is the energy dissipated during crack propagation, while "ΔU" is the energy dissipated between 2 data points. In order to calculate the dissipated energy from the load-displacement graph, it is assumed that the load-displacement data returns to 0 N and 0 displacement. The area of the triangular shape under the load-displacement is the dissipated energy during the crack length propagation between two data points which are at the corners of the triangular shape. After ΔU and Δa are calculated as mentioned above, fracture toughness was calculated according to Equation (1). The area method has scattering problems in the results section, it is probably due to the assumption done during determining the triangular area in the calculation method. As a reminder, the assumption is that the unloading curve at any crack length is linear and intersect at the (P=0;δ=0) point.

$$G_{Ic} = \frac{\Delta U}{B\,\Delta a} \tag{1}$$

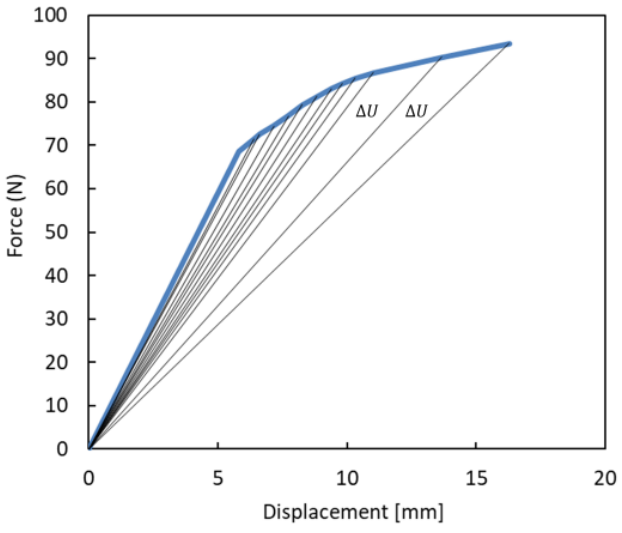

Figure 3.11. Dissipated energy calculation from load-displacement graph

3.2.3.2. Load Method

The load method uses the load (P) and displacement data (δ) from load displacement data taken from the test machine, a sample load displacement graph is seen in Figure 3.11. "B" is the width of the specimen, "a" is the crack length and "α" is the crack length correction. "α" is calculate from "$C^{1/3}$" vs "a" graph. "C" corresponds to compliance of one leg of the DCB specimen. "α" is the value where the curve fit equation of "$C^{1/3}$" vs "a" graph and y=0 line intersect as shown in Figure 3.12. "α" is a positive value. Fracture toughness values is calculated according to Equation (2).

$$G_{Ic} = \frac{3P\delta}{2B(a+\alpha)} \tag{2}$$

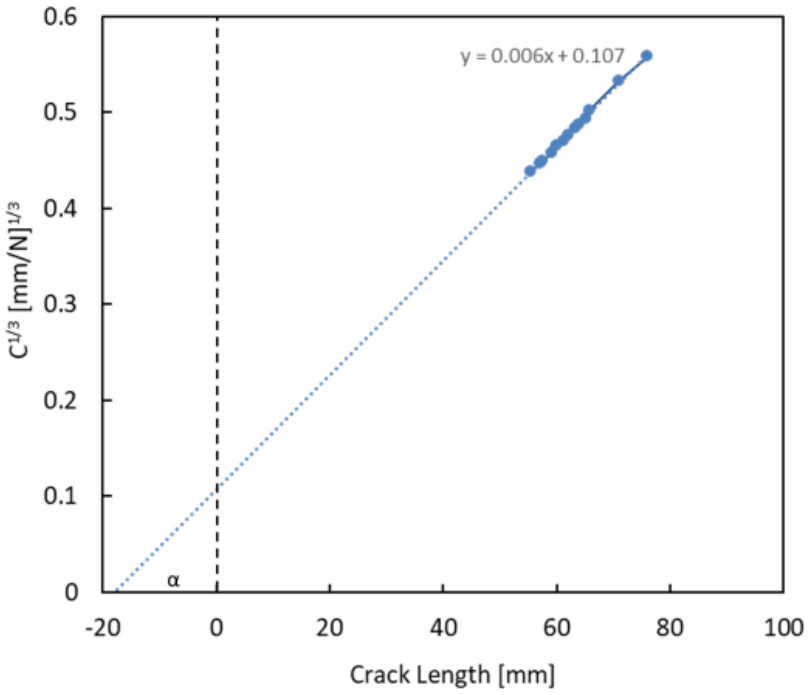

Figure 3.12. Graph of $C^{1/3}$ vs crack length

3.2.3.3. Compliance Method

The compliance method basically does not use crack length data. Crack length data is integrated into the "A_1" value which is the slope of the a/h vs "$C^{1/3}$" graph shown in Figure 3.13. "h" is the thickness of the leg of the DCB specimen. As mentioned above, "P" is the load applied to the specimen, "C" is the compliance of one leg of the DCB specimen. Fracture toughness is calculated at each crack length according to Equation (3). It can be seen in the results section, that there is good agreement between compliance and load method.

$$G_{Ic} = \frac{3P^2C^{2/3}}{2A_1Bh} \tag{3}$$

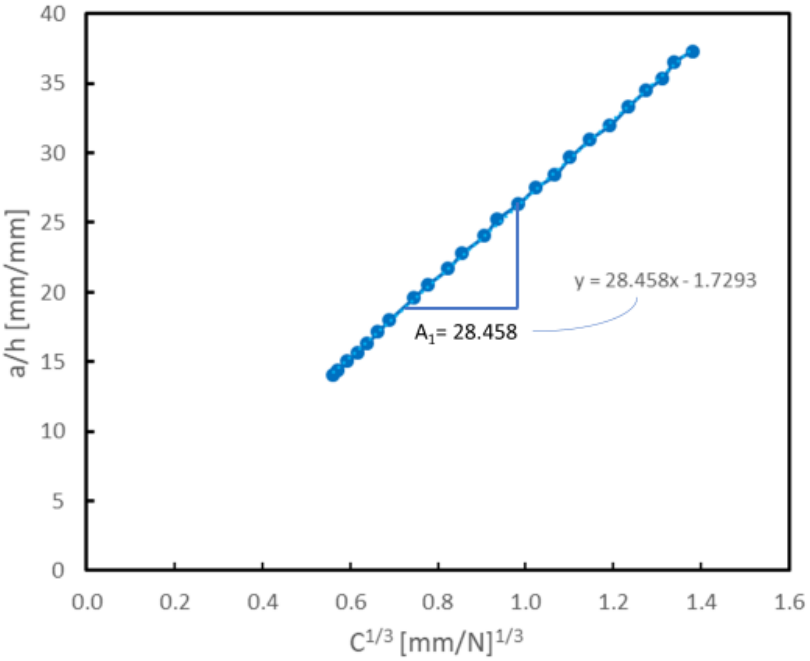

Figure 3.13. Graph of a/h vs $C^{1/3}$

3.3. Results

Three experiments were conducted for each interface. The results of the DCB tests for CFRP and GFRP will be discussed separately and results for each interface illustrated separately. In interface results of each material type, load-displacement graphs of three experiments are illustrated in the first figure. Pictures of the fracture surfaces of one of the experiment specimens are shown in the top of the second figure. Fracture toughness values of the experiments using the three different calculation methods are shown in the bottom of the second figure in order to explain the results. While one of the experiment's results and fracture toughness is shown in this section, the other results are shown in the appendix. In the last figure in each heading, the compliance method results with respect to the crack length of three experiments are illustrated in one graph in order to see the trend of the interface. The test matrix is seen in Table 3.3. Lay-up orientations, material types, and numbers of experiments that were accomplished are shown in the table. "//" shows where the initial crack was placed with release film in the lay-up orientations.

Table 3.3. Test matrix

Lay-up orientation	Material	Numbers of experiments
$[0_{10}//0_{10}]$	CFRP/GFRP	3/3
$[0_8/25/-25//25/-25/0_8]$	CFRP/GFRP	3/3
$[0_8/45/-45//45/-45/0_8]$	CFRP/GFRP	3/3
$[0_8/45/45//45/45/0_8]$	CFRP/GFRP	2/3
$[0_8/65/65//65/65/0_8]$	CFRP/GFRP	3/3
$[0_8/90/90//90/90/0_8]$	CFRP/GFRP	2/1

3.3.1. Mode I Results of CFRP Specimens

In this section, Mode I fracture toughness results of CFRP specimens are shown for 0//0, 25//-25, 45//-45, 45//45, 65//65, 90//90 interface angles. These specimens have $[0_{10}//0_{10}]$, $[0_8/-25/25//-25/25/0_8]$, $[0_8/-45/45//-45/45/0_8]$, $[0_8/45/45//45/45/0_8]$, $[0_8/65/65//65/65/0_8]$ and $[0_8/90/90//90/90/0_8]$ lay-up orientations as shown in Figure 3.3 and Figure 3.4. Tests were repeated for three specimens. The individual results of these experiments are shown with three different calculation methods which are load, compliance and area method. For one experiment, side photos of the experiment are illustrated in order to see fiber bridging. The results of three experiments for each interface are shown using only a compliance method.

3.3.1.1. Mode I Fracture Toughness of 0//0 Interface

Three CFRP 0//0 specimens' load-displacement graph is shown in Figure 3.14. All the experiments' graphs seem very close to each other. As a remainder, lay-up orientation is [0_{10}//0_{10}]. Firstly, the stiffness of specimens before the crack starts to propagate has the same slope which is dependent on the bending stiffness of one of the beams and the crack length of the specimen. Because the fracture toughness is related to energy release during the crack propagation, the area under the curve is related to fracture toughness. If the areas under the curves are close to each other this shows the fracture toughness values also will be close to each other which is illustrated in Figure 3.17.

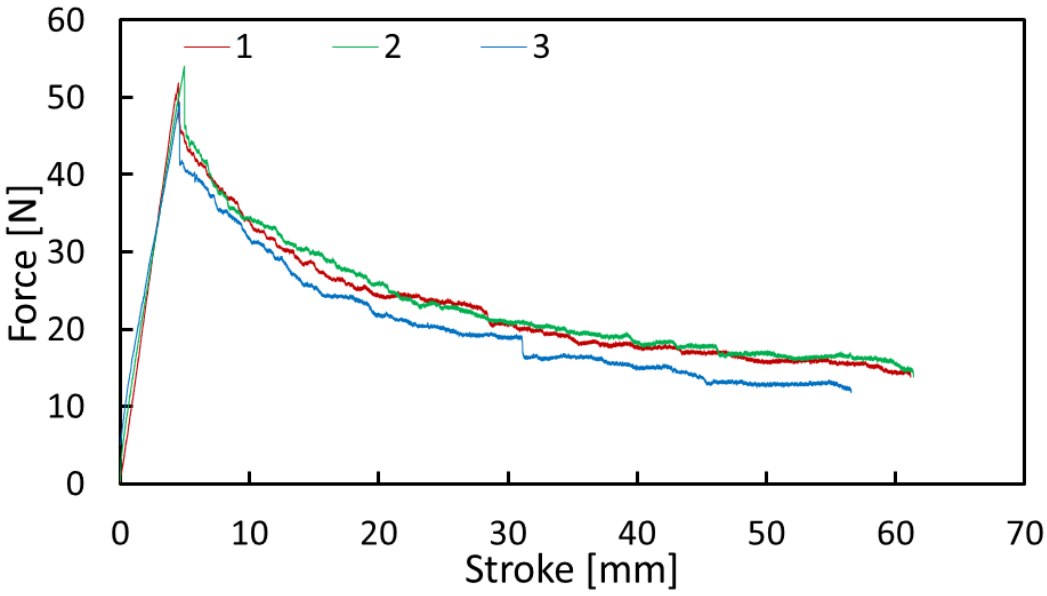

Figure 3.14. Load-displacement graph of CFRP 0//0 specimens

In Figure 3.15, fracture surface pictures and fracture toughness values of specimen number 2 (C-DCB-ENF-0-0-18-MF10727) are seen. In the fracture surface picture, there is no crack jump between layers, the crack propagates between two 0-degree layers. There is low fiber bridging which is shown in Figure 3.16. The fracture toughness value starts with 0.300 J/mm^2 at 42 mm crack length, increases a little bit with fiber bridging and reaches about 0.350 J/mm^2 at 150 mm crack length.

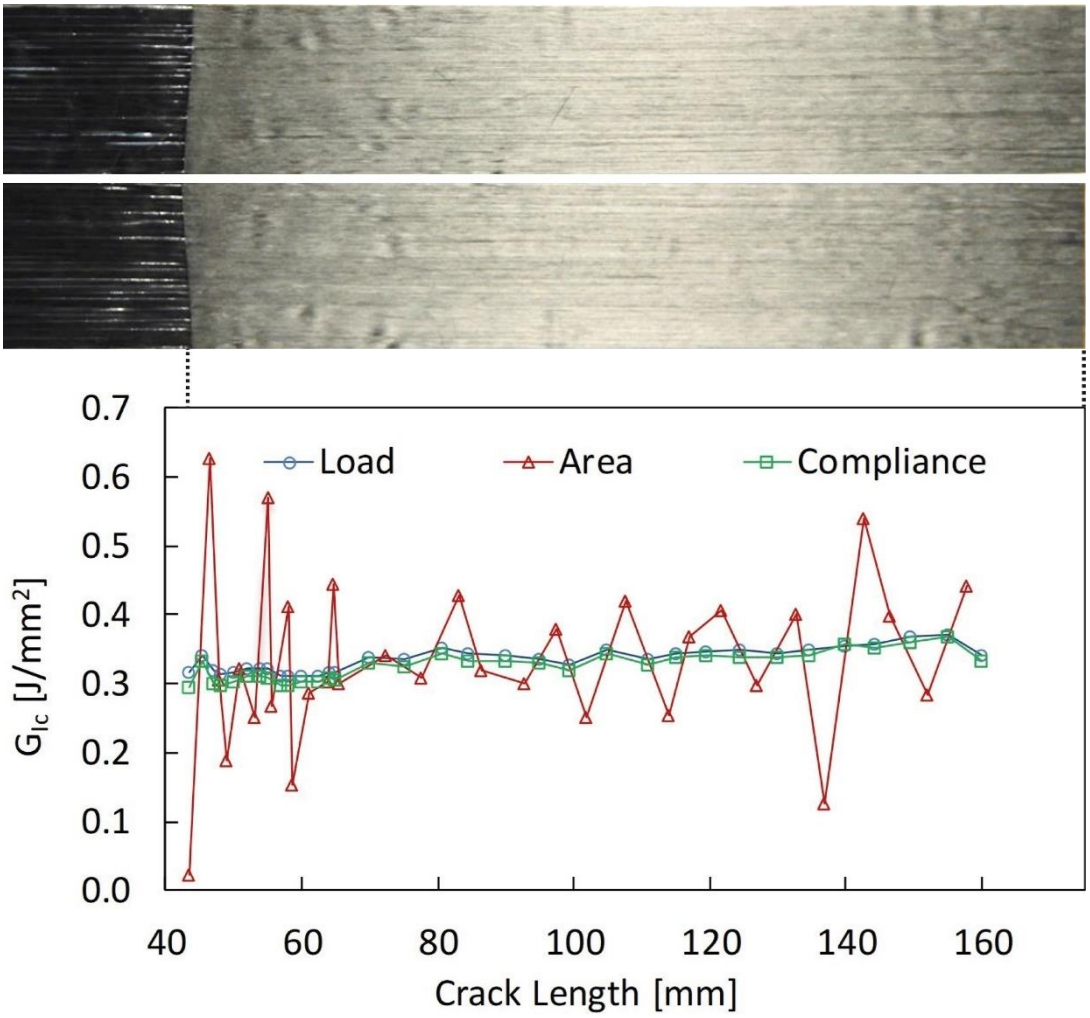

Figure 3.15. Fracture toughness results and fracture surface of specimen #2 (C-DCB-ENF-0-0-18-MF10727)

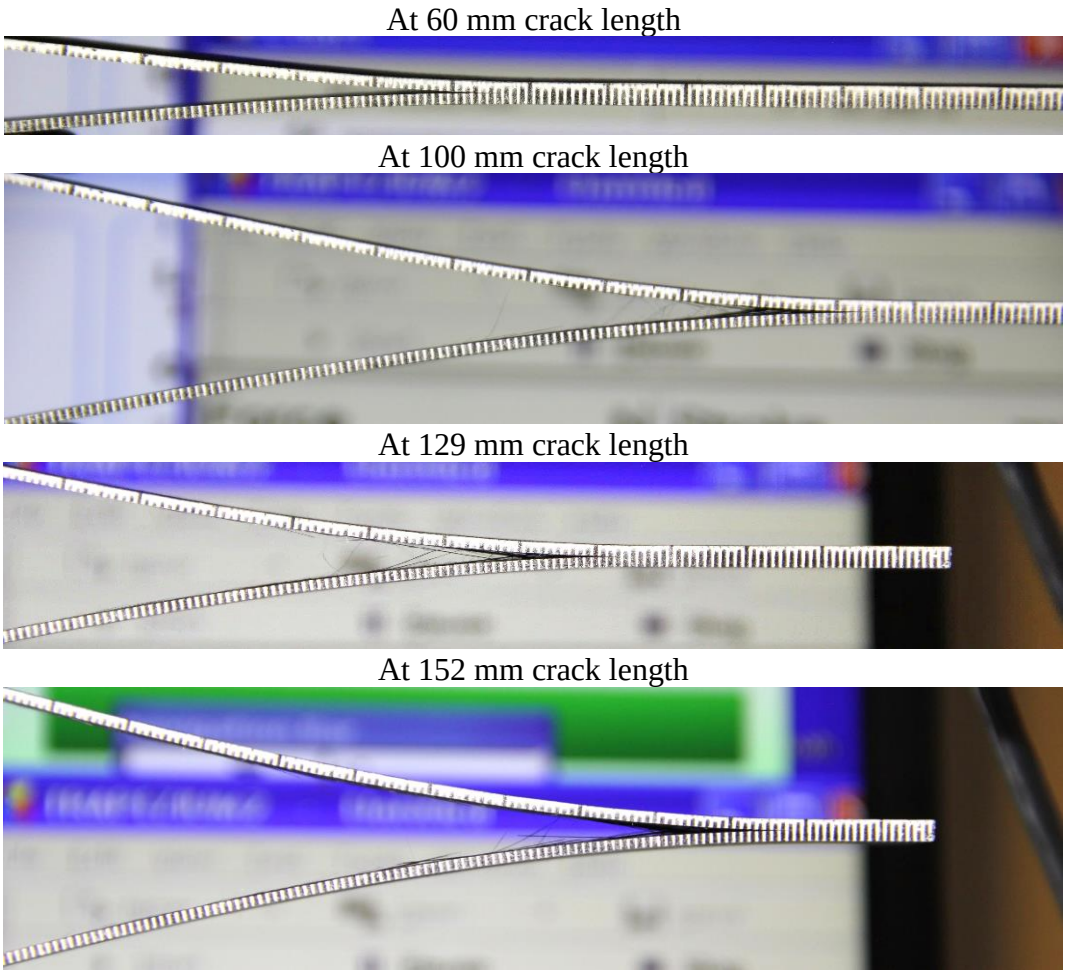

Figure 3.16. Side view of specimen #2 (C-DCB-ENF-0-0-18-MF10727) during DCB test

All experiment results using the compliance method for the 0//0 interface are illustrated in Figure 3.17. The crack started at about 42 mm in these specimens. The fiber bridging effect is less seen in this specimen than the other specimens. Also, the most stable experiment is that using 0//0 interfaces because layer jump of the crack is not possible. As seen in Figure 3.14 there is no dynamic crack propagation. This also reduces the fracture toughness change with propagation. So, the fracture toughness during crack propagation is only slightly changing. An initiation fracture toughness value is 0.280 J/mm^2 for these specimens. Then, due to the little fiber bridging effect, there is a linear increase in fracture toughness with the increase of the crack length. The formulation on the graph can be used as a crack length-dependent fracture

toughness; however, 0.300 J/mm^2 can be taken as a constant because there is a slight change. The individual results of the three experiments can be seen in Figure 3.15, Figure 0.5, and Figure 0.6. Furthermore, all values calculated with three methods, which are load, area, and compliance, can be seen also in these figures. The results in Figure 3.17 are calculated with the compliance method which is the most used one in the literature.

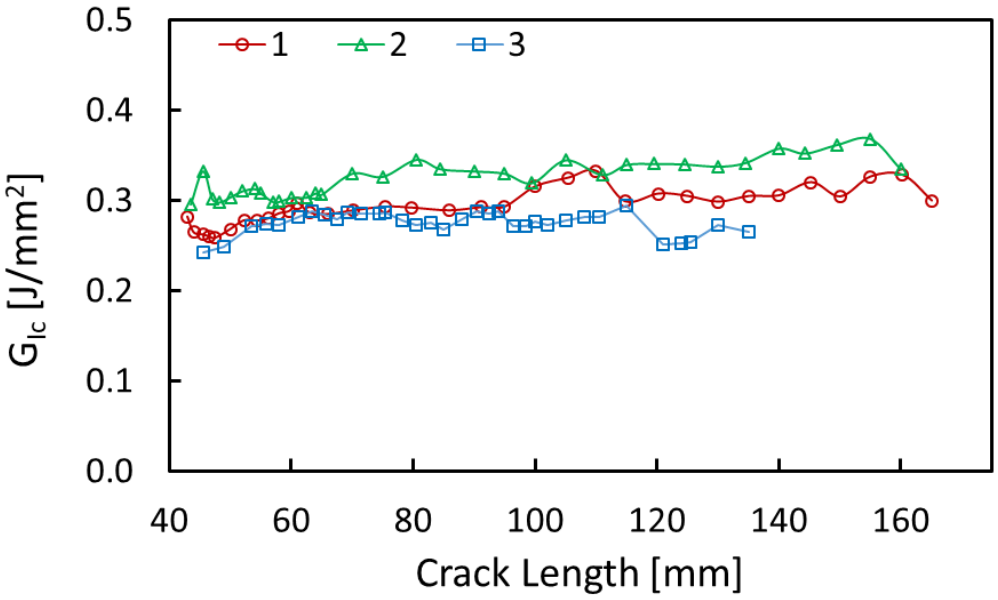

Figure 3.17. Fracture toughness vs crack length graph of three CFRP 0//0 specimens

3.3.1.2. Mode I Fracture Toughness of 25//-25 Interface

Load-displacement graphs of three CFRP 25//-25 DCB specimens, which have [0_8/25/-25//25/-25/0_8] lay-up orientation, are seen in Figure 3.18. All the load displacement graphs of experiments seem very close to each other. There is consistency for both stiffness and area under the curve for all experiments. There is no dynamic crack propagation for this interface.

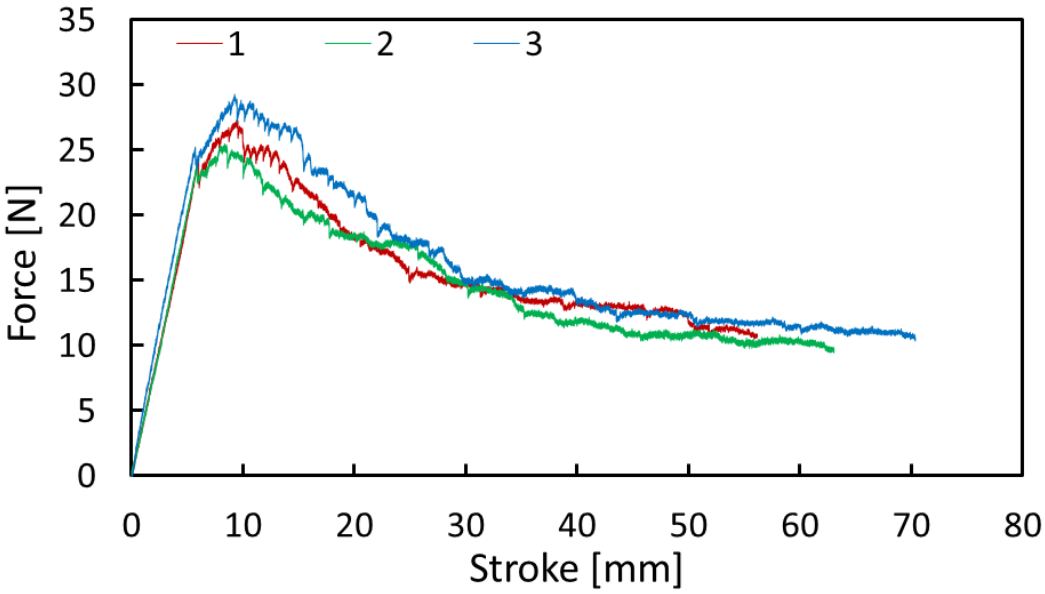

Figure 3.18. Load-displacement graph of CFRP 25//-25 specimens

Fracture toughness results and fracture surface of experiment number 2 are seen in Figure 3.19. Initial fracture toughness value is about 0.175 J/mm^2 at 50mm crack length, fracture toughness is stabilized around 0.250 J/mm^2 when the crack propagates 10 mm. There is no layer jump of the crack, which is seen in both load displacement graph and photos of the fracture surface. Also, fiber bridging is very low which is seen at side view pictures in Figure 3.20.

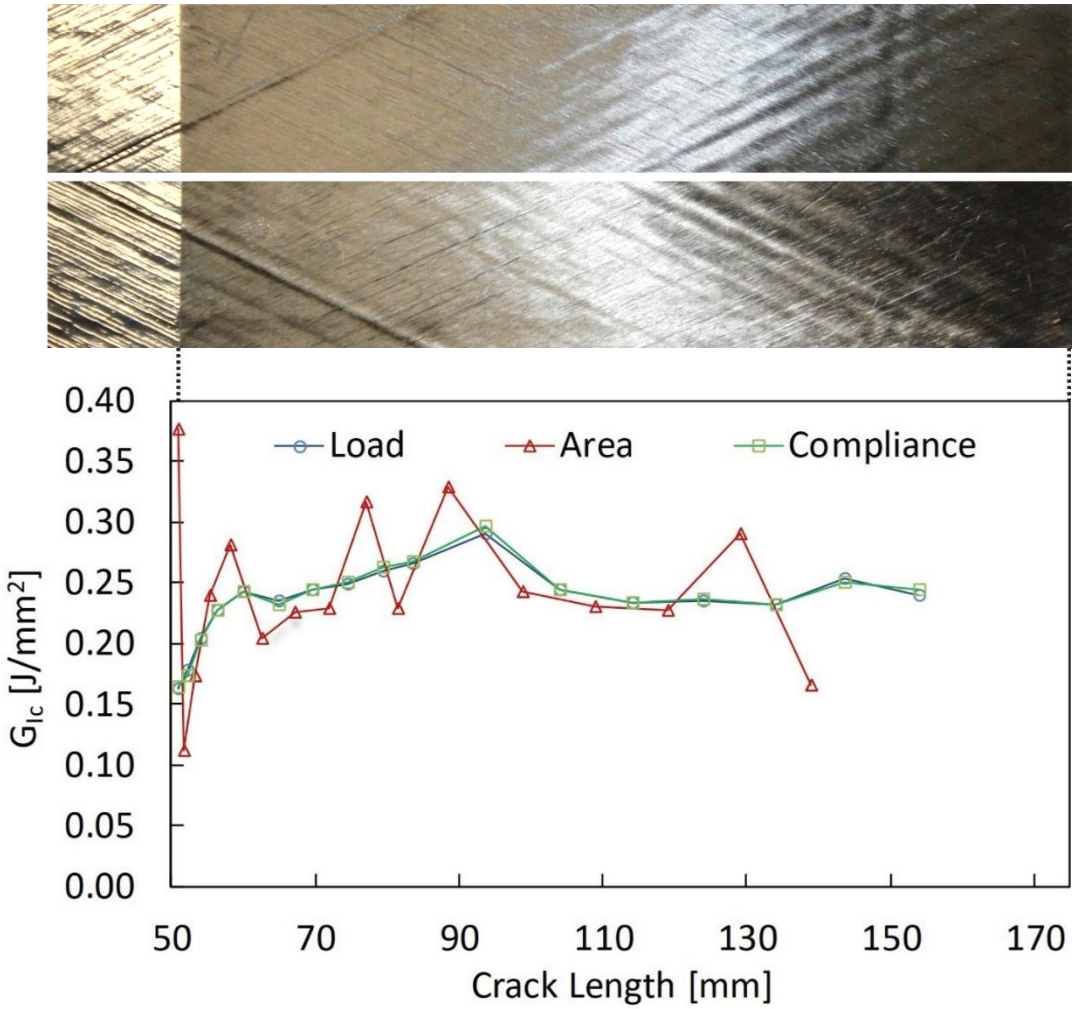

Figure 3.19. Fracture toughness results and fracture surface of specimen #2 (C-DCB-ENF-25--25-3-MF11603)

At 60 mm crack length

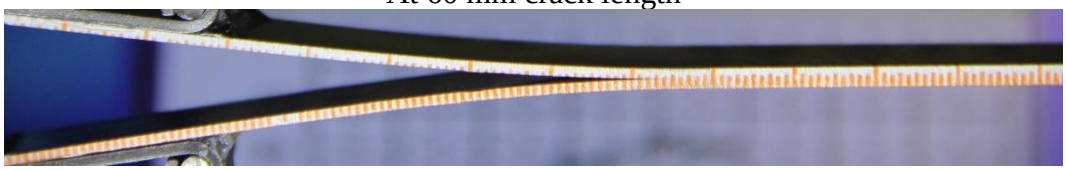

At 104 mm crack length

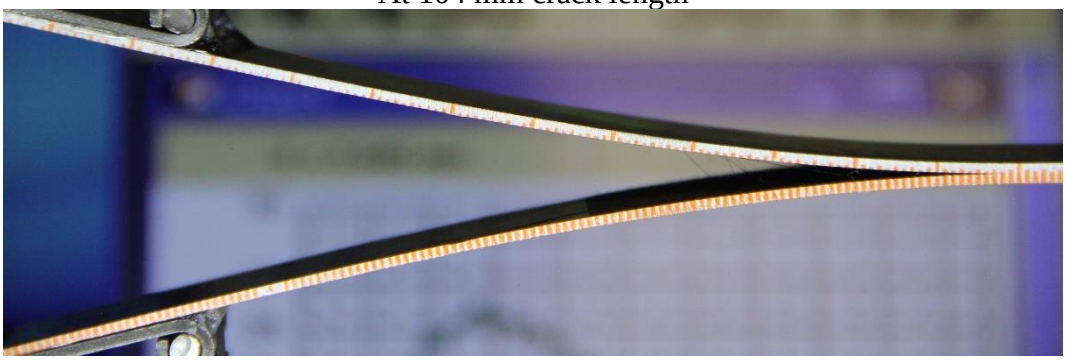

At 135 mm crack length

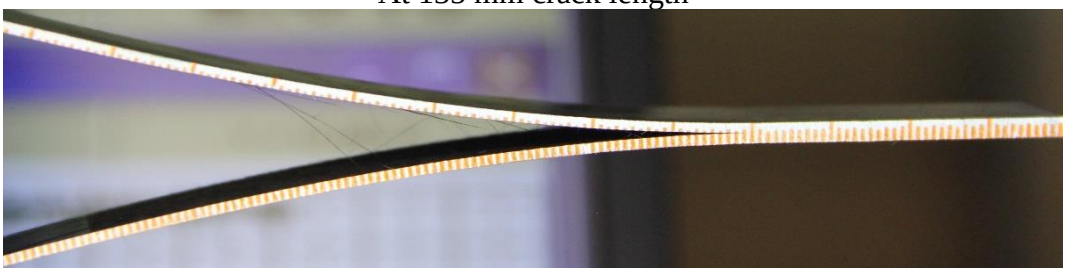

At 154 mm crack length

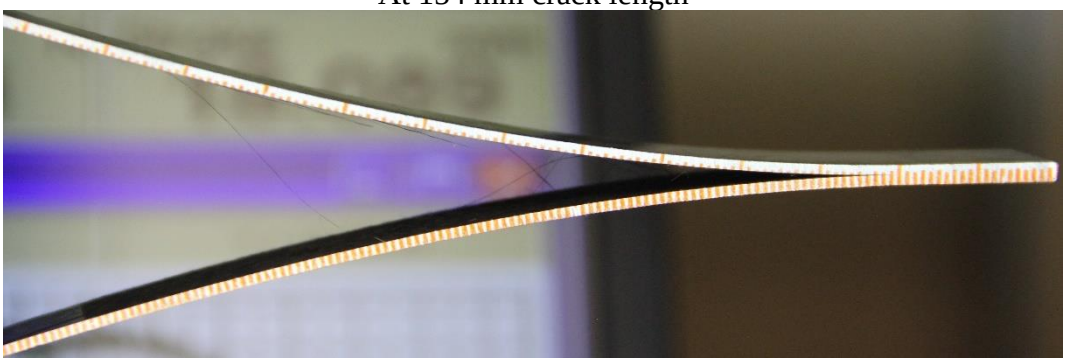

Figure 3.20. Side view of specimen #2 (C-DCB-ENF-25--25-3-MF11603) during DCB test

All experimental results for 25//-25 interfaces with the compliance method are shown in Figure 3.21. Rather like the 0//0 specimens, the huge bridging effect does not appear in the side picture so the increase in the first 20 mm could be due to creating new crack surfaces. After the new crack surfaces are created, fracture toughness seems stabilized as seen in Figure 3.21. This is the proof of no extra fiber bridging and no increase in the crack surface. The initiation fracture toughness value of the CFRP 25//-25 interface

is 0.170 J/mm^2. Then, the stabilized value (0.260 J/mm^2) can be used as the propagation value. Individual results of experiments are visualized in Figure 0.7, Figure 3.19, and Figure 0.8. with 3 different calculation methods and crack surfaces.

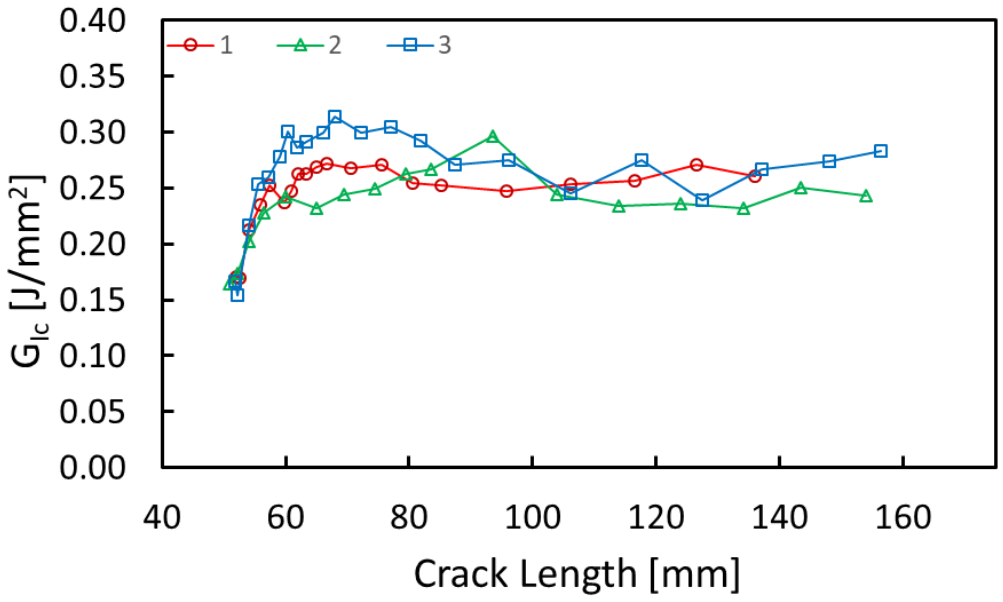

Figure 3.21. Fracture toughness vs crack length graph of three CFRP 25//-25 specimens

3.3.1.3. Mode I Fracture Toughness of 45//-45 Interface

Three experiments, of [0_8/45/-45//45/-45/0_8] lay-up-oriented specimens, are explained in this section with the load-displacement graph in Figure 3.22. Except for the linear part of the experiment, crack propagation parts of load-displacement graphs are not close to each other because of the dynamic crack propagation. The decrease in fracture toughness is the cause of this high-speed crack propagation. When the crack changes the propagation region or the fiber bridging finished due to fiber length, a huge fall in fracture toughness is seen. The dynamic crack propagation occurs when the energy around the crack tip is too high than the fracture toughness. The dynamic crack propagation continues until the energy around the crack tip equalizes the fracture toughness value at the weak zone. Then, the dynamic propagation is finished. In general, when this happens, the crack passes at a new interface or the huge fiber bridging is finished.

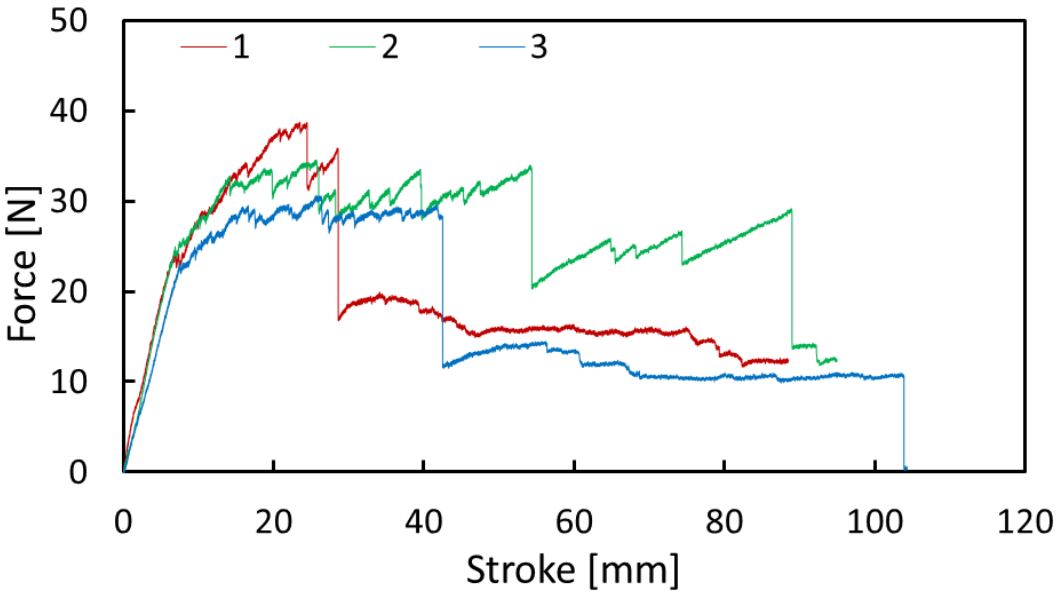

Figure 3.22. Load-displacement graph of CFRP 45//-45 specimens

Fracture toughness values and fracture surfaces of Experiment number 1 are seen in Figure 3.23. Fracture toughness value is 0.2 J/mm^2 at the beginning where the crack goes between 45/-45 interfaces. Due to high fiber bridging which is seen in Figure

3.24 at 70 mm crack length, fracture toughness increased to 0.6 J/mm^2. Then, the fiber bridging is broken which is seen in Figure 3.24 at 79 mm crack length and in Figure 3.22 where the first load drop of the red curve corresponds to the broken or separated fiber bridging. The huge load drop also agrees with the dynamic delamination and that crack passes to the inside of one of the 45 layers which is seen in Figure 3.23. Then, the fracture toughness value is stabilized at around 0.4 J/mm^2 until the specimen is divided into two pieces.

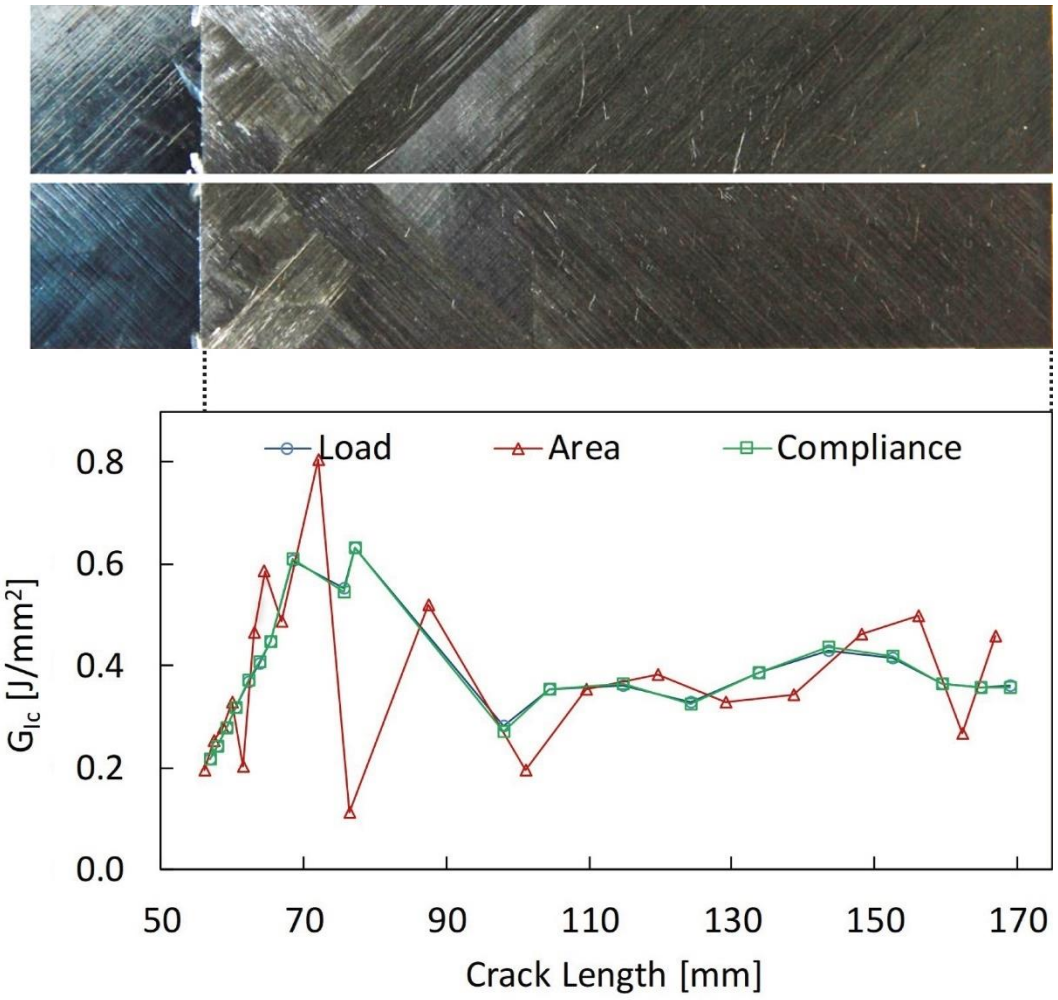

Figure 3.23. Fracture toughness results and fracture surface of specimen #1 (C-DCB-ENF-45--45-1-MF11610)

At 61 mm crack length

At 70 mm crack length

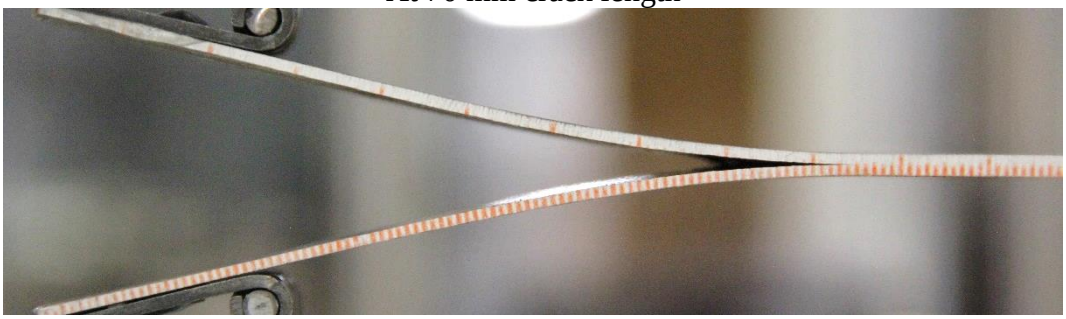

At 79 mm crack length

At 126 mm crack length

Figure 3.24. Side view of specimen #1 (C-DCB-ENF-45--45-1-MF11610) during DCB test

The dynamic part of delamination can also be seen in Figure 3.25 which shows 3 experiment's result with the compliance method. Without line connection between data shows that there is a dynamic crack propagation. The dynamic delamination generally means that crack passes from between 45//-45 interfaces into one of the 45 layers. Then it propagates into the 45-degree layer with fiber bridging. High fiber bridging and new surfaces created by the fiber bridging are reasons for the increase in fracture toughness. It starts with 0.100 J/mm^2 and increases to 0.800 J/mm^2 with

the huge fiber bridging at the beginning. After that, it jumps into one of 45 layers with 0.380 J/mm^2 fracture toughness. There is also fiber bridging where the crack goes into one of 45 layers. These crack jumps and individual fracture toughness can be seen in Figure 3.23, Figure 0.9, and Figure 0.10.

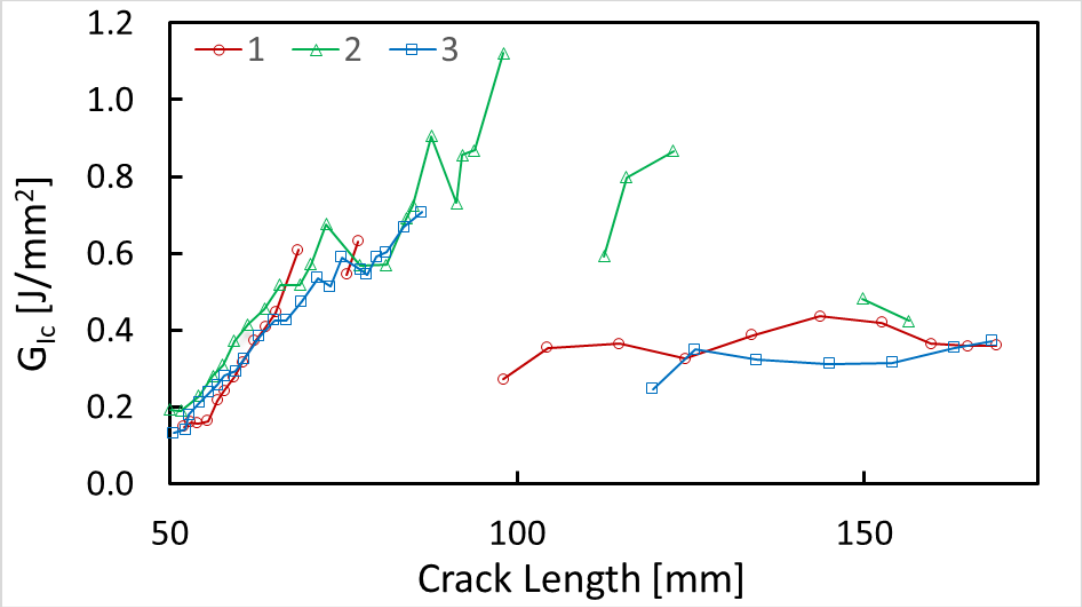

Figure 3.25. Fracture toughness vs crack length graph of three CFRP 45//-45 specimens

3.3.1.4. Mode I Fracture Toughness of 45//45 Interface

Load-displacement graphs of two CFRP 45//45 specimens are shown in Figure 3.26. One experiment is missing due to some experimental errors. Their lay-up orientation is [0_8/45/45//45/45/0_8]. A good match in the stiffness related part of the curve is observed for the specimens. Moreover, little dynamic crack propagation is also seen in these specimens. The load drop at the dynamic crack is less than the 45//-45 interface one because the drop in these specimens is from 0.500 J/mm^2 to around 0.380 J/mm^2 while in the 45//-45 specimens one jumps from 0.800 J/mm^2 to 0.380 J/mm^2.

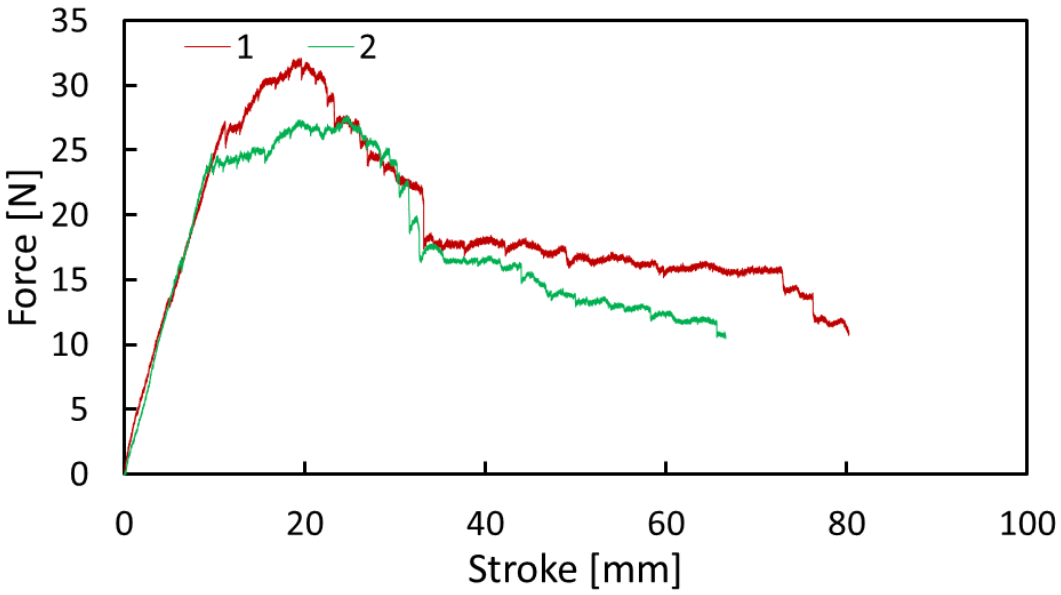

Figure 3.26. Load-displacement graph of CFRP 45//45 specimens

Fracture toughness values and fracture surface of experiment number 1 are seen in Figure 3.27. The initial fracture toughness value is about 0.275 J/mm^2. It increases with fiber bridging which is seen in Figure 3.28 at 80 mm crack length. The fibers which are bridging have a connection with the initial part of the crack. When their bridging is finished in Figure 3.28 at 93 mm, little dynamic crack propagation occurs. Then, delamination occurs with less fiber bridging, having the crack length inside one of the 45-degree layers. The fracture toughness is 0.400 J/mm^2 in this region.

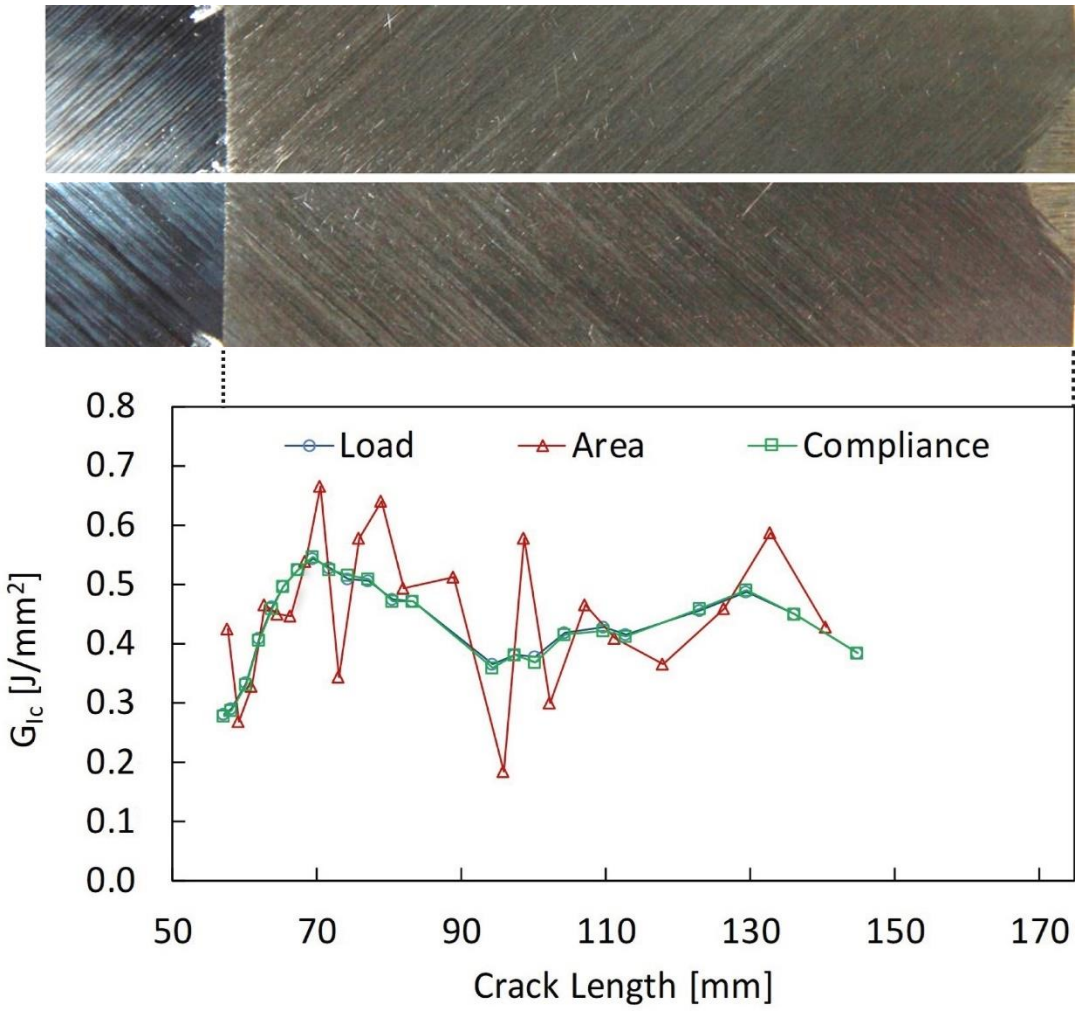

Figure 3.27. Fracture toughness results and fracture surface of specimen #1 (C-DCB-ENF-45-45-7-MF12048)

At 80 mm crack length

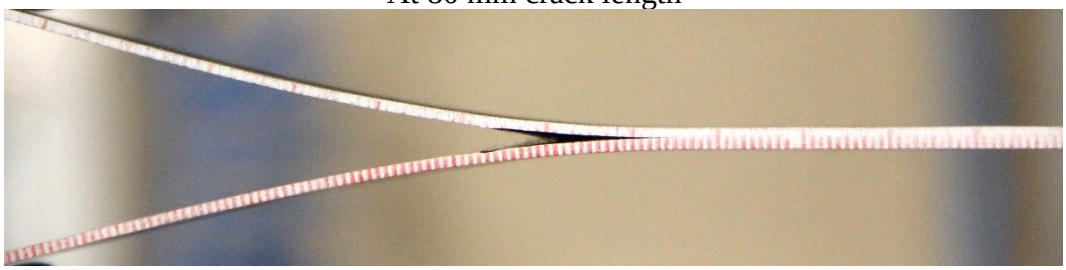

At 93 mm crack length

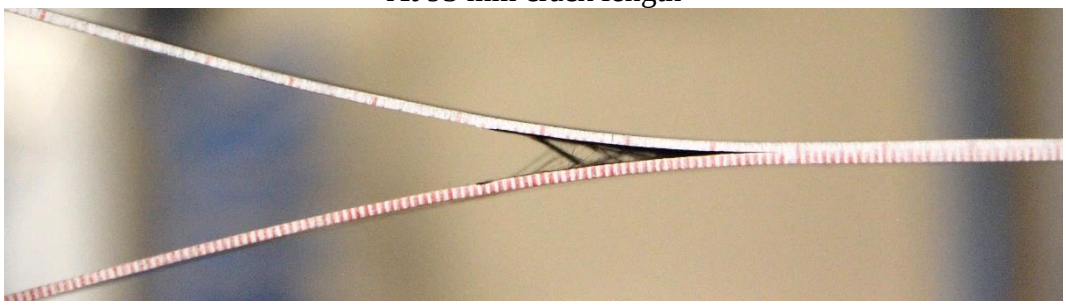

At 122 mm crack length

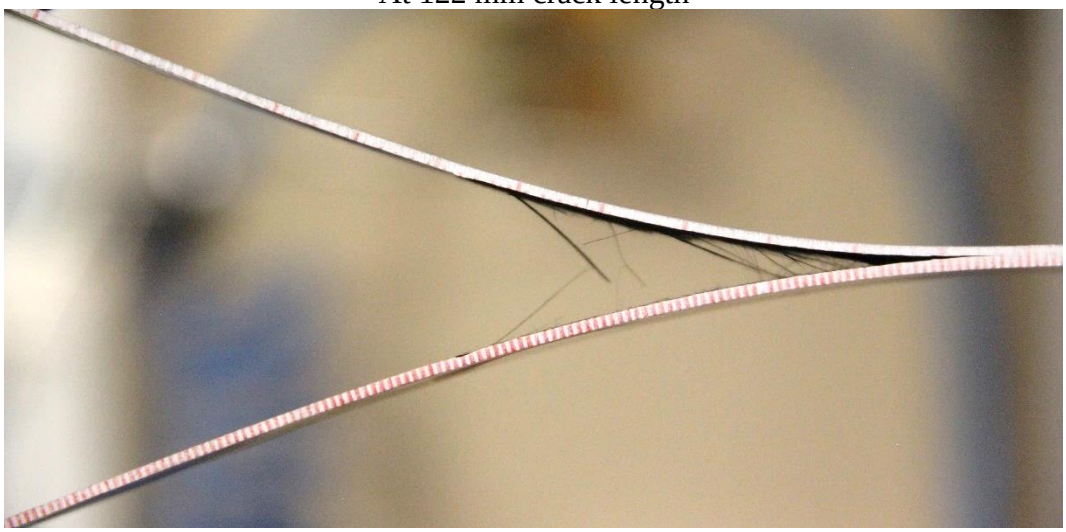

At 135 mm crack length

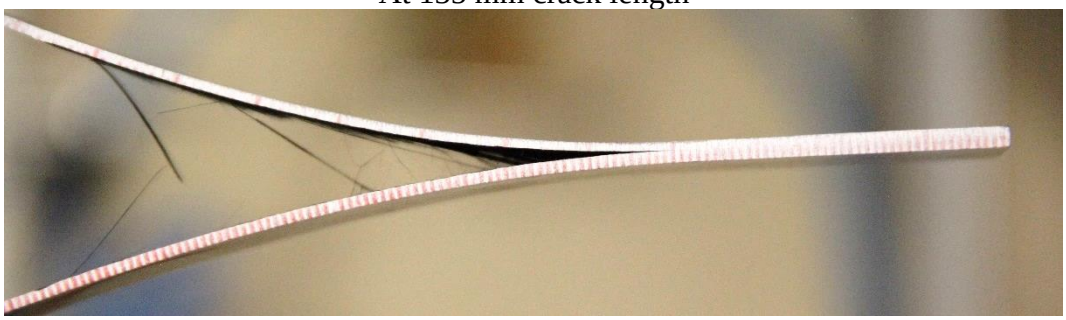

Figure 3.28. Side view of specimen #1 (C-DCB-ENF-45-45-7-MF12048) during DCB test

Fracture toughness values using the compliance method of two experiments are demonstrated in Figure 3.29. The little dynamic crack jump, which is at around 90 mm crack length, corresponds to the completed huge fiber bridging. The fracture toughness value decreases from 0.500 J/m^2 to 0.380 J/mm^2 which can be seen in Figure 3.29. After the crack jump, the crack propagates into a 45 layer rather than in the between two 45-degree layers. Furthermore, there is a good agreement of fracture toughness of the crack inside the 45-degree layer with 45//-45 experiments. The values are about 0.380 J/mm^2 for all specimens. Individual results are in Figure 3.27, and Figure 0.11.

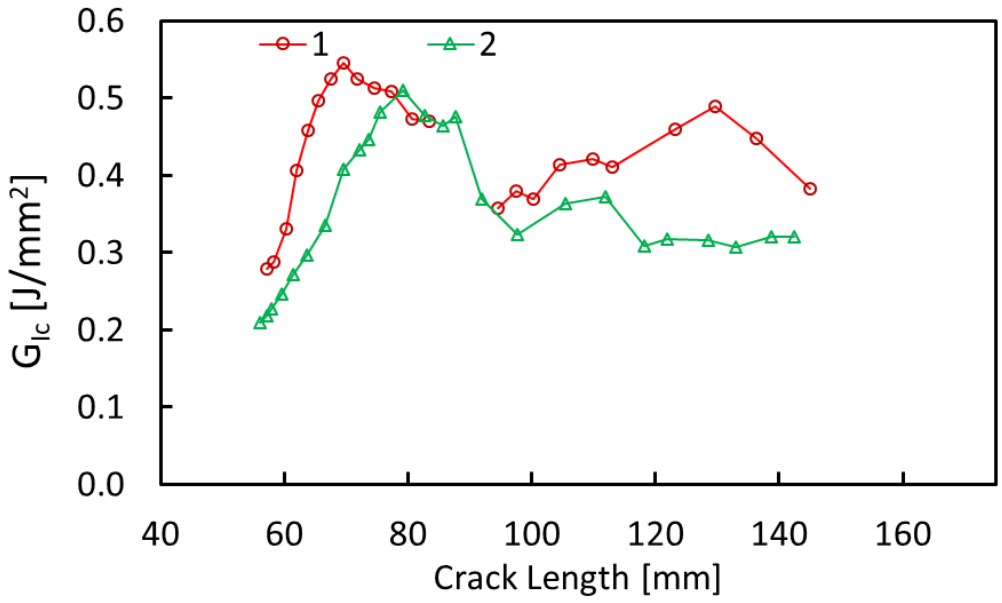

Figure 3.29. Fracture toughness vs crack length graph of three CFRP 45//45 specimens

3.3.1.5. Mode I Fracture Toughness of 65//65 Interface

The load-displacement graph of three experiments of CFRP 65//65 specimens which have [0_8/65/65//65/65/0_8] lay-up orientation is shown in Figure 3.30. Specimen number 1 has less stiffness than the others because its first crack length was about 54mm while the others started at 50 mm crack length. There are few dynamic cracks in these experiments like the 45//45 ones.

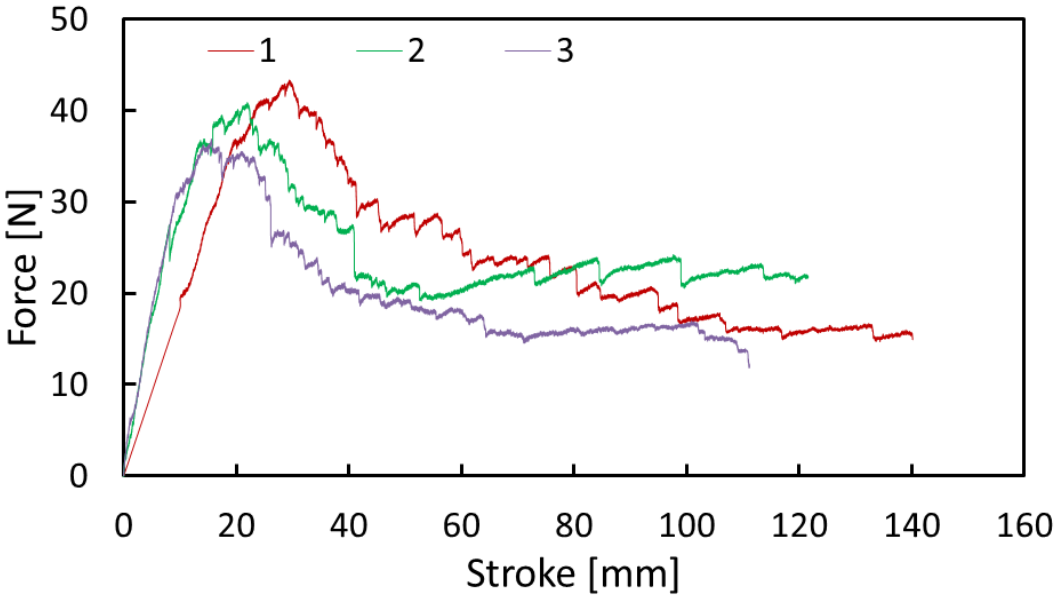

Figure 3.30. Load-displacement graph of CFRP 65//65 specimens

Fracture toughness values and fracture surface photos of specimen number 3 are seen in Figure 3.31. Initial fracture toughness starts around 0.150 J/mm^. Then, the fiber bridging has around one-layer thickness, which is seen in Figure 3.32 at 68 mm crack length, the fracture toughness value increases until crack length 80 mm. Then the steady-state region starts and continues until crack length 135 mm with a 0.500 J/mm^2 fracture toughness value. At 135 mm crack length, it is seen that some regions of the crack pass to 0/65 interface in Figure 3.31. It seems that fiber bridging or creating a new fracture surface at 0/65 interface increases the fracture toughness.

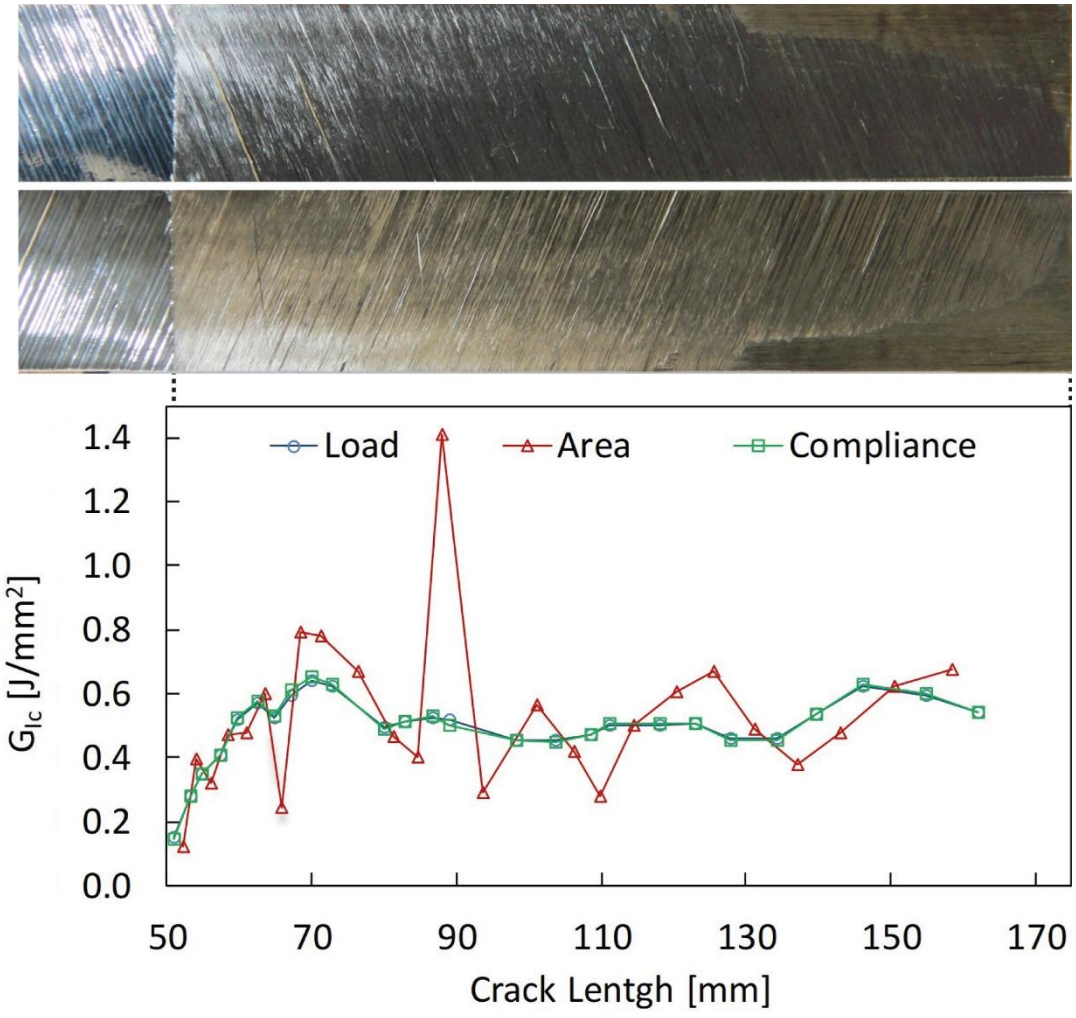

Figure 3.31. Fracture toughness results and fracture surface of specimen #3 (C-DCB-ENF-65-65-9-MF11999)

At 68 mm crack length

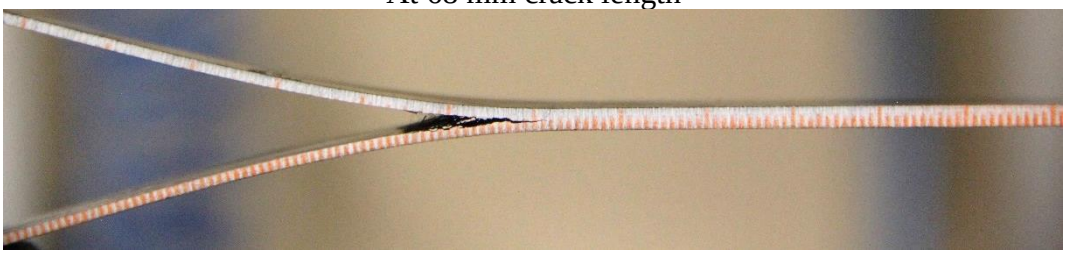

At 86 mm crack length

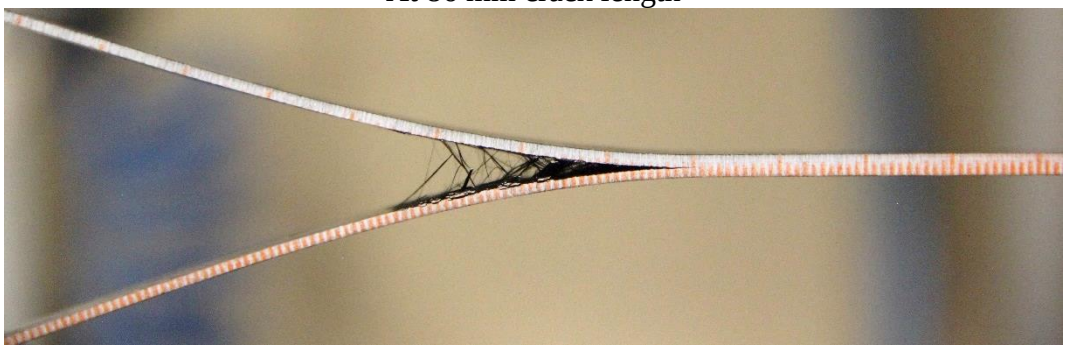

At 97 mm crack length

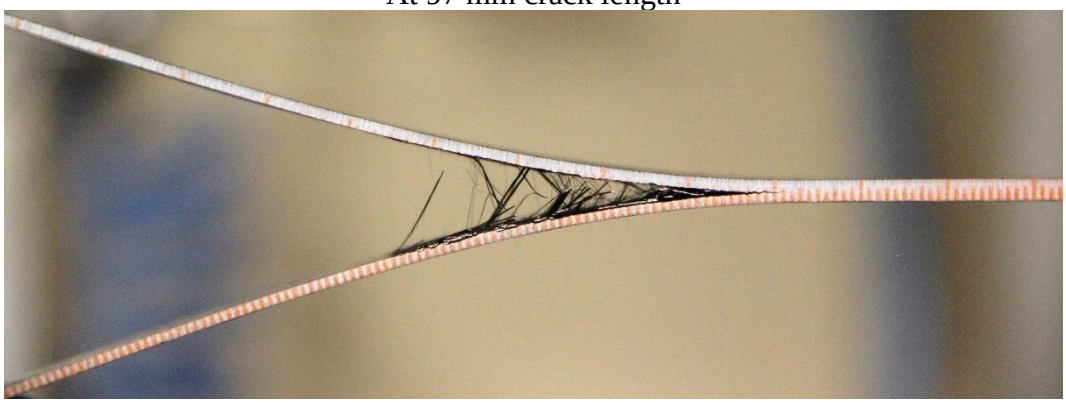

At 145 mm crack length

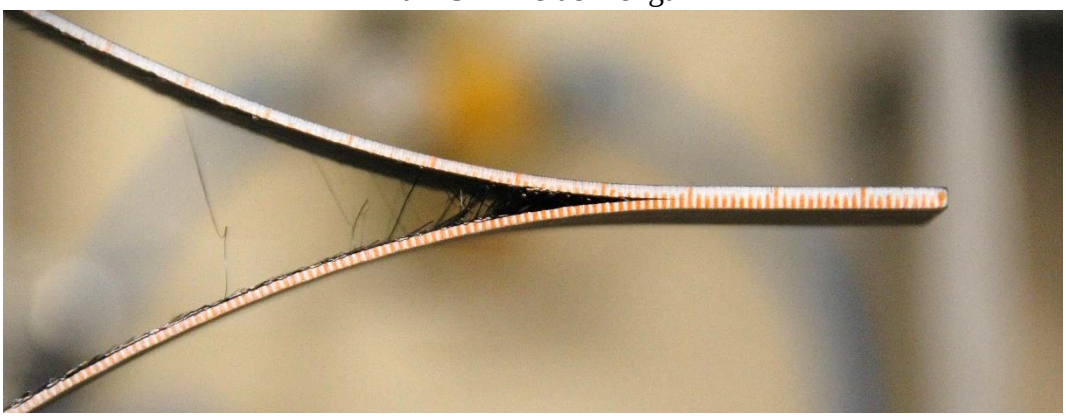

Figure 3.32. Side view of specimen #3 (C-DCB-ENF-65-65-9-MF11999) during DCB test

The compliance method results for all specimens are illustrated in Figure 3.33. The initial fracture toughness is about 0.150 J/mm^2 for all specimens. Then, the same increasing pattern as that of the 45//45 ones is seen. It reaches about 0.800 J/mm^2. Dynamic crack propagations are demonstrated as there is no connection between data points in Figure 3.33. The cracks go into one of the 65 layers in the laminate after 20 mm crack propagation. When the crack goes inside the 65-degree layer, the fracture toughness is about 0.700 J/mm^2. Some part of the crack also goes between the 0//65 interface around the end of the specimens. Their individual results and crack propagation surfaces can be seen in Figure 0.12, Figure 0.13, and Figure 3.31.

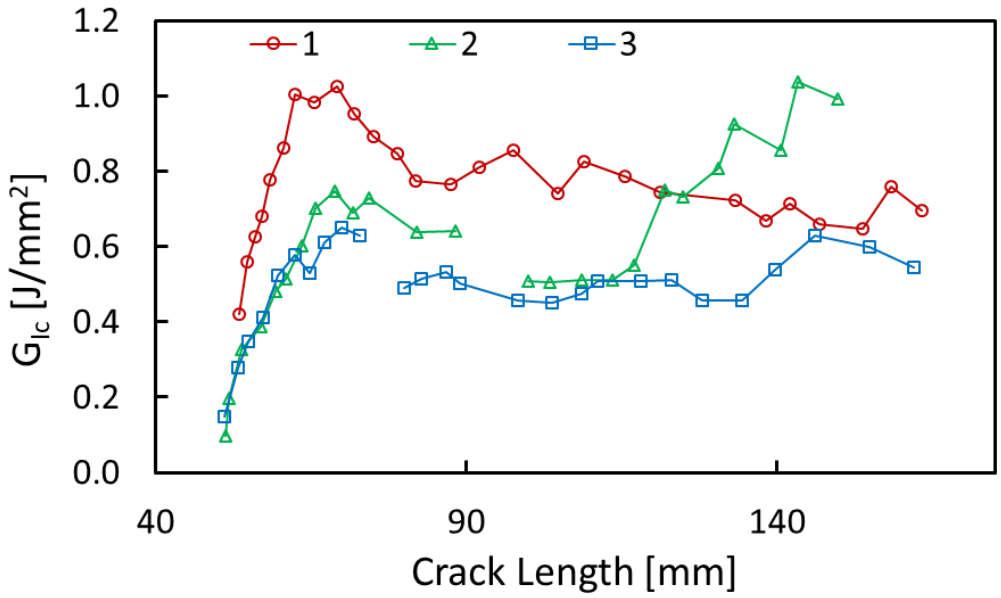

Figure 3.33. Fracture toughness vs crack length graph of three CFRP 65//65 specimens

3.3.1.6. Mode I Fracture Toughness of 90//90 Interface

Two experiments are conducted for the 90//90 interfaces which have [0_8/65/65//65/65/0_8] lay-up orientation. The load-displacement graphs of these experiments are seen in Figure 3.34. Many dynamic cracks are seen in these experiments, due to the crack propagation zone changing repetitively between inside the 90-degree layers and 0/90 interface. Also, the crack goes into a tooth shape, because of that there are many little load drops in the load-displacement curve.

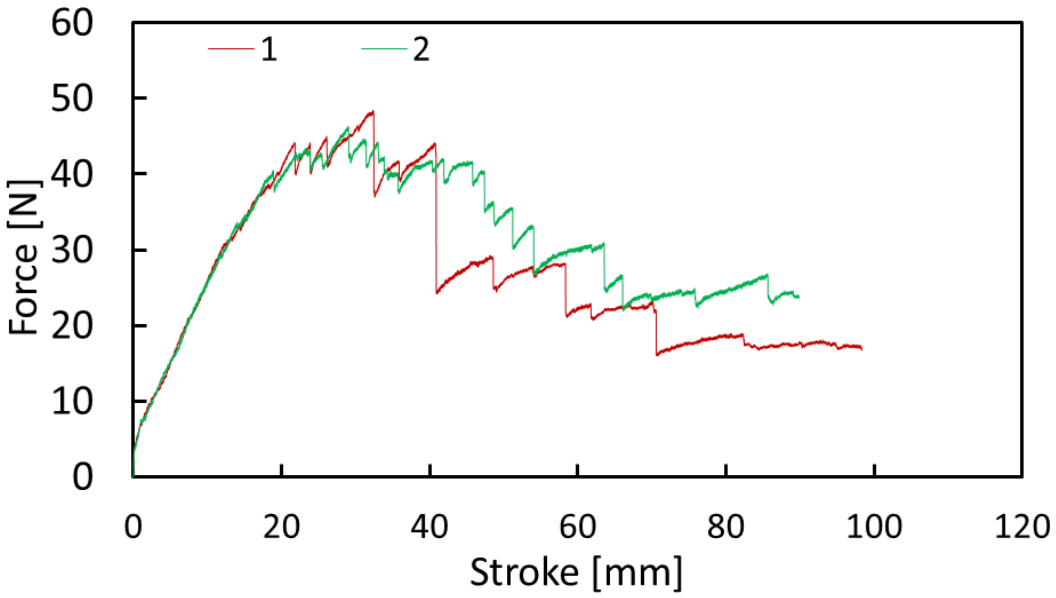

Figure 3.34. Load-displacement graph of CFRP 90//90 specimens

The result of experiment number two with three calculation methods and fracture surfaces are illustrated in Figure 3.35. Initial fracture toughness is about 0.400 J/mm^2. Then it is increasing with both fiber bridging and tooth shape movement of the crack which means the crack has much more length than is shown in the figures. The tooth shape movement is illustrated in Figure 3.36. With this phenomenon, fracture toughness is increased above 1 J/mm^2. Because of the two sides of the tooth shape crack propagation is different, fiber bridging occurs in Figure 3.36. Further delamination occurs in both the 0/90 interface and inside one of the 90-degree layers,

so making a comment on this region is not easy, however, toughness is around 1 J/mm^2.

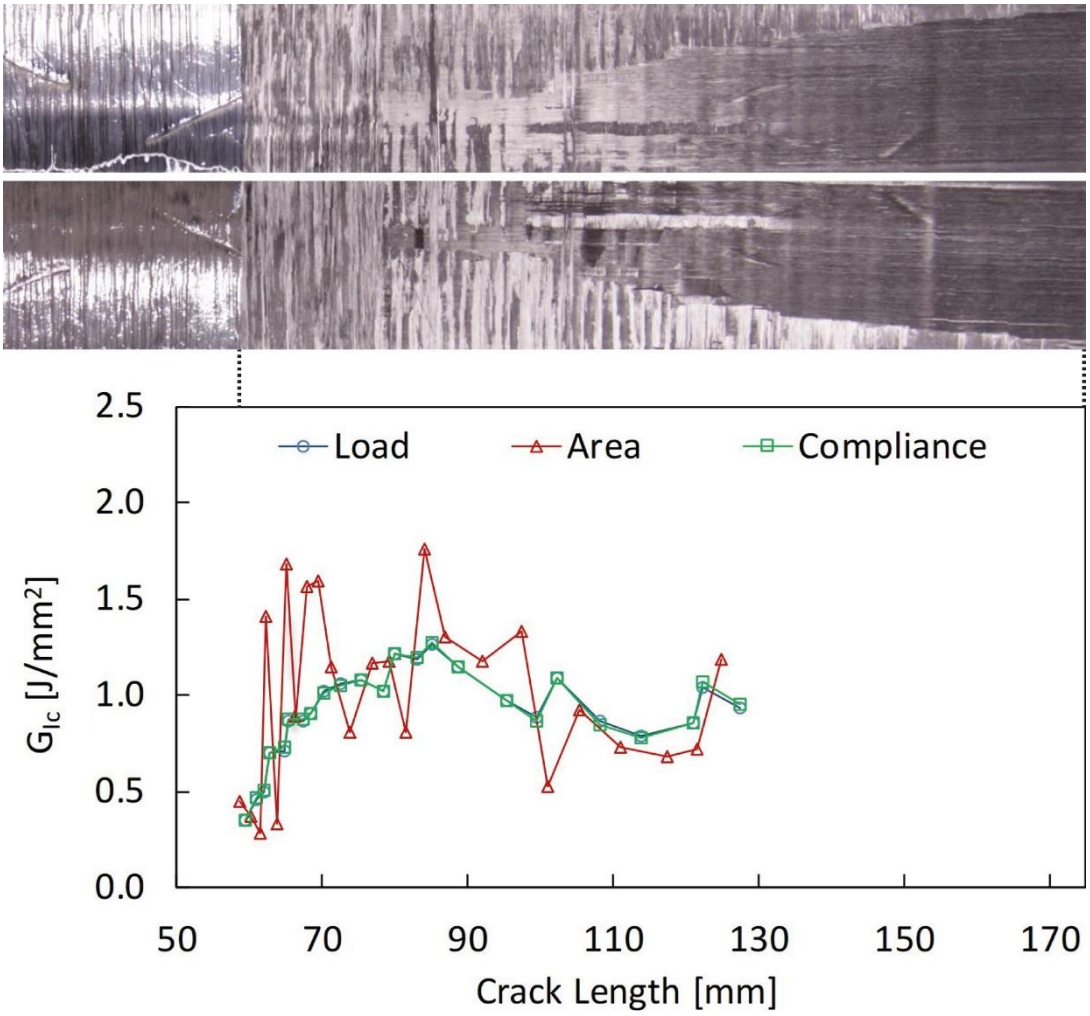

Figure 3.35. Fracture toughness results and fracture surface of specimen #2 (C-DCB-ENF-90-90-16-MF10725)

At 73 mm crack length

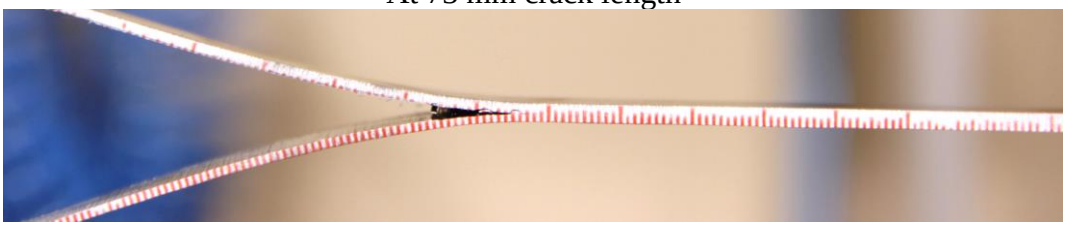

At 88 mm crack length

At 98 mm crack length

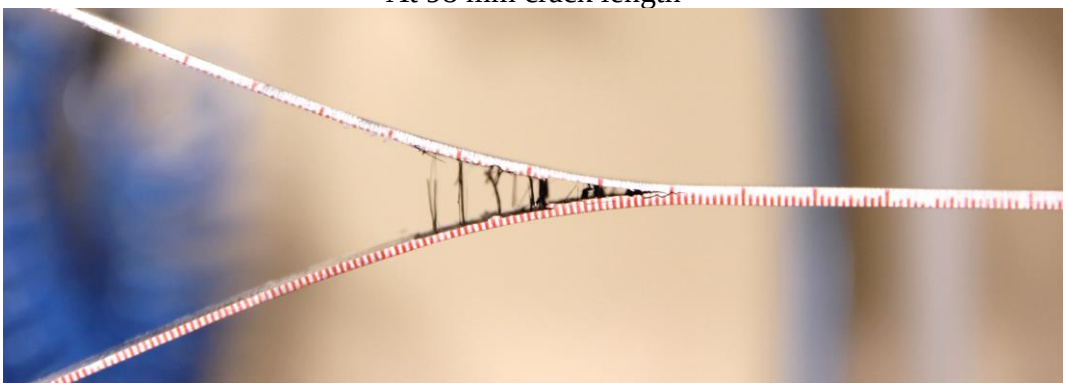

At 128 mm crack length

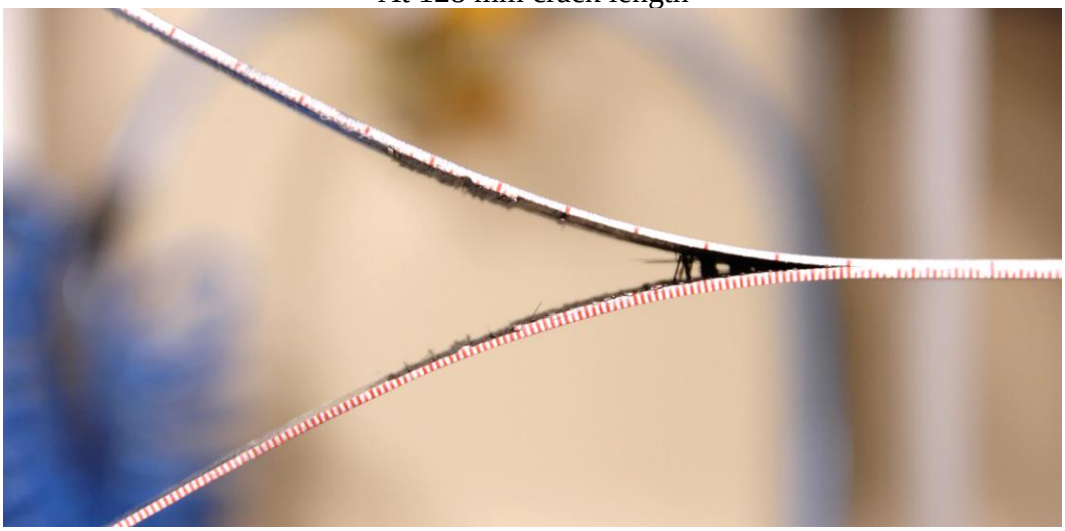

Figure 3.36. Side view of specimen #2 (C-DCB-ENF-90-90-16-MF10725) during DCB test

Fracture toughness with respect to crack length for two experiments is illustrated in Figure 3.37 with only the compliance method. Increasing fracture toughness with tooth-shaped crack propagation and fiber bridging for two specimens show close results at the beginning. When the value passes 1.0 J/mm^2, the crack is likely to pass the 0/90 interface which is weaker or has less fracture toughness value. This shows that a crack in 90-degree layers can propagate about 25 mm, then it jumps to a weaker interface. The other experiment result is illustrated in Figure 0.14 in the appendix.

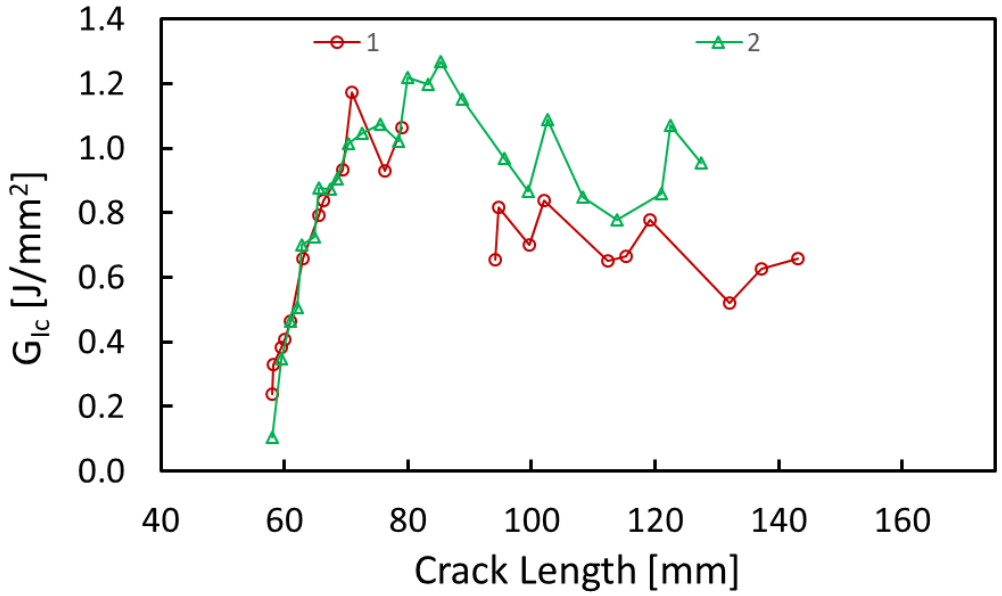

Figure 3.37. Fracture toughness vs crack length graph of three CFRP 90//90 specimens

3.3.1.7. General Trend of Mode I Fracture Toughness of CFRP Specimens

Cracks in the CFRP specimens hardly pass to other interfaces or other laminates. These cracks generally propagate between layers or inside the layer which is nearest to the initial crack. Most of the results start at a value of fracture toughness and increase with the crack propagation. The reasons for the increase are the zigzag movement of the crack front and fiber bridging between adjacent layers. Then it can be simplified like two fracture toughness values; one for initiation and one for propagation. For complex analysis, full resistance curve data can be inserted into an analysis program.

3.3.2. Mode I Results of GFRP Specimens

In this section only Mode I fracture toughness results of GFRP specimens is shown with 0//0, 25//-25, 45//-45, 45//45, 65//65, 90//90 interface angles. These specimens have $[0_{10}//0_{10}]$, $[0_8/-25/25//-25/25/0_8]$, $[0_8/-45/45//-45/45/0_8]$, $[0_8/45/45//45/45/0_8]$, $[0_8/65/65//65/65/0_8]$ and $[0_8/90/90//90/90/0_8]$ lay-up orientations respectively. The individual results of these experiments are shown with three different calculation methods which are load, compliance and area method. Results of 3 experiments for each interface are shown using only the compliance method. Side photos of one of the experiments are illustrated in order to show fiber bridging.

3.3.2.1. Mode I Fracture Toughness of 0//0 Interface

These specimens also have a good match with load-displacement graphs and fracture toughness graphics in Figure 3.38. This is because all layers are 0-degree layers, there is no crack jump. Also, the area under the curves are very close to each other, it shows that fracture values will be close to each other.

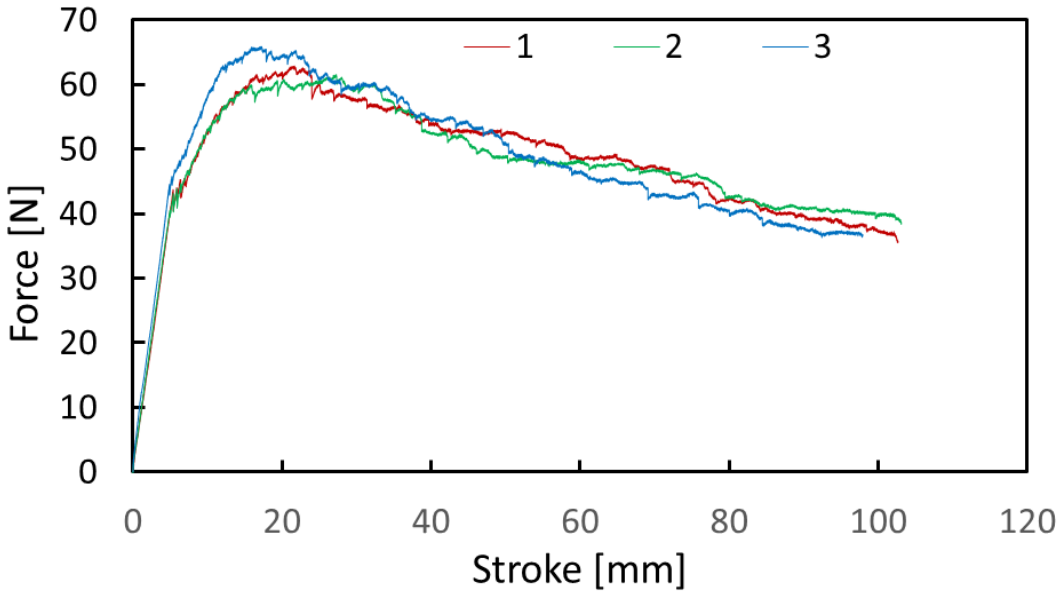

Figure 3.38. Load-displacement graph of GFRP 0//0 specimens

The result of experiment number three with three calculation methods and fracture surfaces are illustrated in Figure 3.39. The initial fracture toughness value is about 0.200 J/mm^2. It increases with fiber bridging and settles down at around 1.200 J/mm^2. Fiber bridging which is seen in Figure 3.40 is more than the carbon specimen with the same interface. Besides, crack jump at the interface is not observed. The crack propagates between 0-degree layers with fiber bridging.

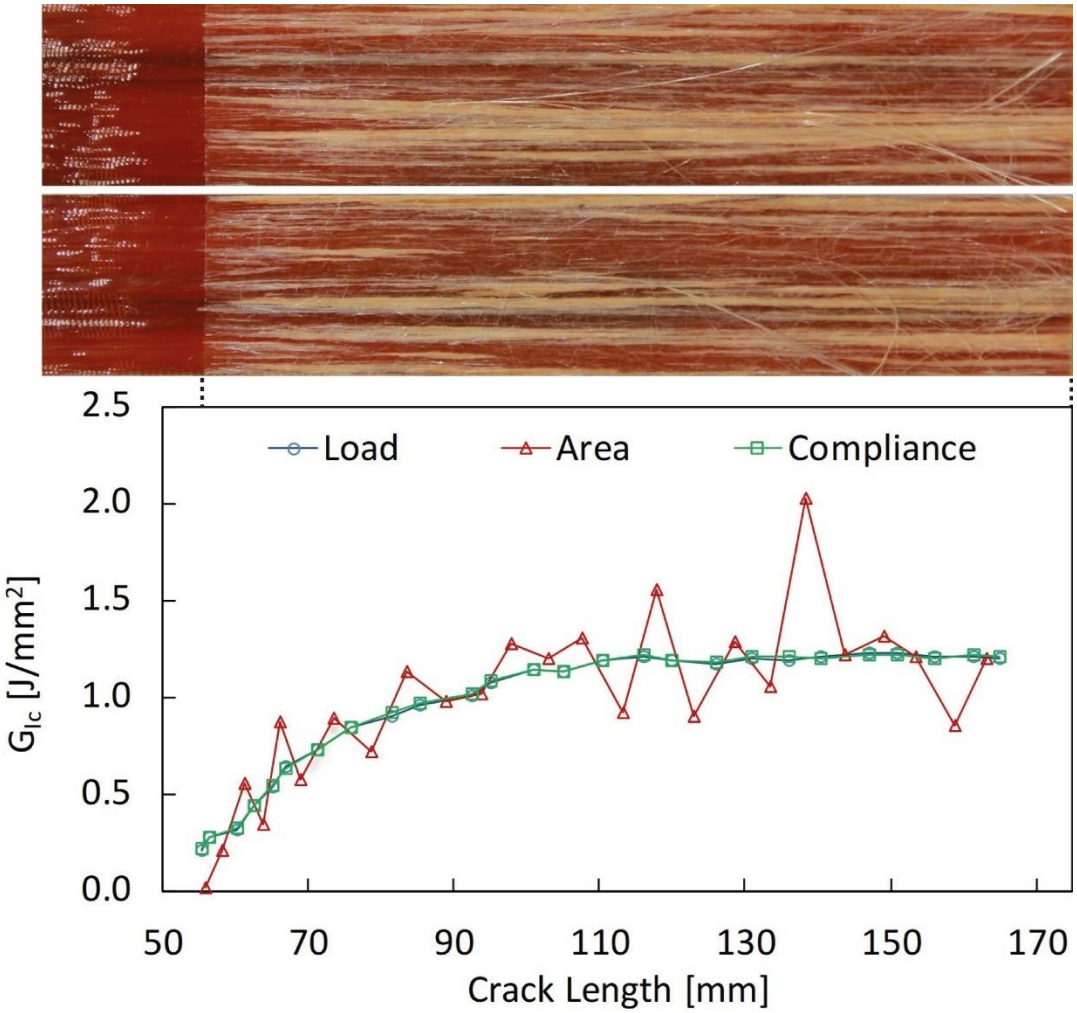

Figure 3.39. Fracture toughness results and fracture surface of specimen #3 (G-DCB-ENF-0-0-16-MF11609)

At 95 mm crack length

At 112 mm crack length

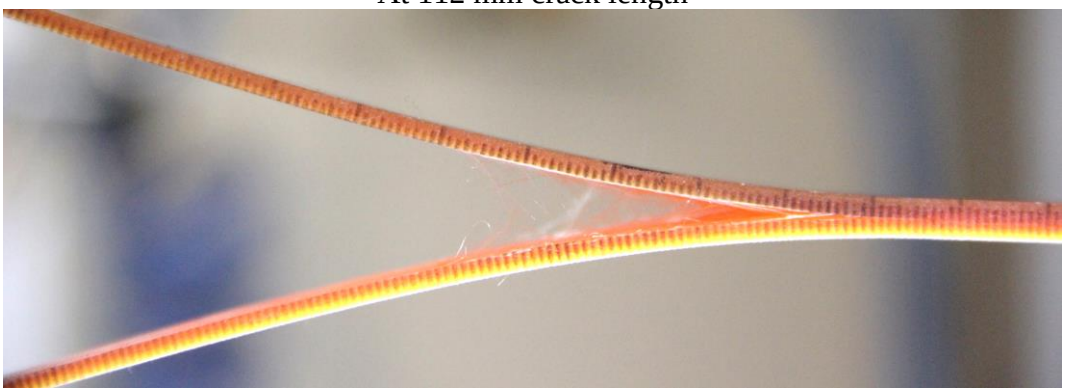

At 141 mm crack length

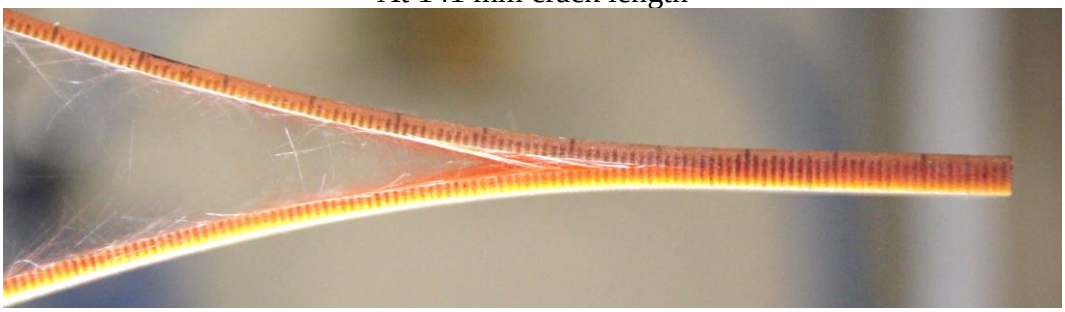

At 165 mm crack length

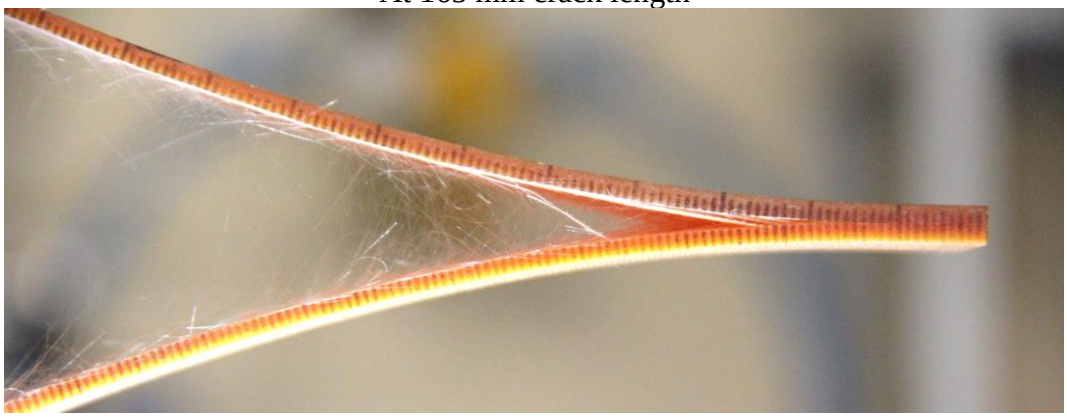

Figure 3.40. Side view of specimen #3 (G-DCB-ENF-0-0-16-MF11609) during DCB test

Fracture toughness values for all specimens using the compliance method are shown in Figure 3.41. As it is mentioned above, fracture toughness values are consistent with each other and very low scattering is observed. Initial fracture toughness values are about 0.200 J/mm^2. Then, they increase with large fiber bridging and stabile around 1.250 J/mm^2. Therefore, the curve fit equation can easily be used as a function of fracture toughness. Furthermore, the fiber bridging areas are seen on these specimens as a color change. Their color is closer to white rather than orange-red in Figure 0.15, Figure 0.16, and Figure 3.39.

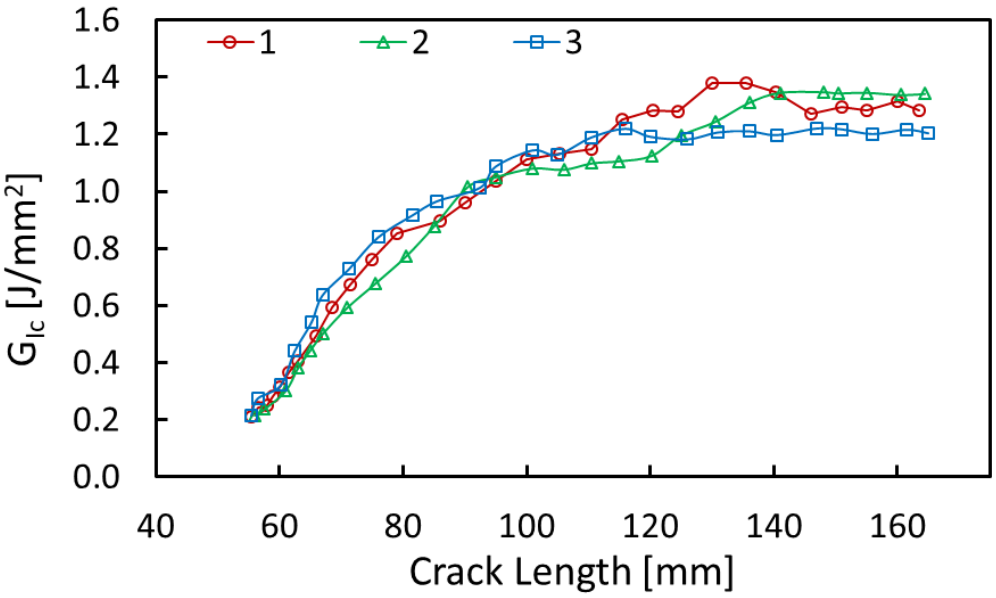

Figure 3.41. Fracture toughness vs crack length graph of three GFRP 0//0 specimens

3.3.2.2. Mode I Fracture Toughness of 25//-25 Interface

Results of three [08/25/-25//25/-25/08] lay-up DCB specimens are shown in this section. The elastic parts of the load-displacement graphs are well-matched in stiffness value in Figure 3.42. There is a little dynamic crack propagation in the experiments, yet crack jump is not observed in Figure 3.43, Figure 0.17, and Figure 0.18.

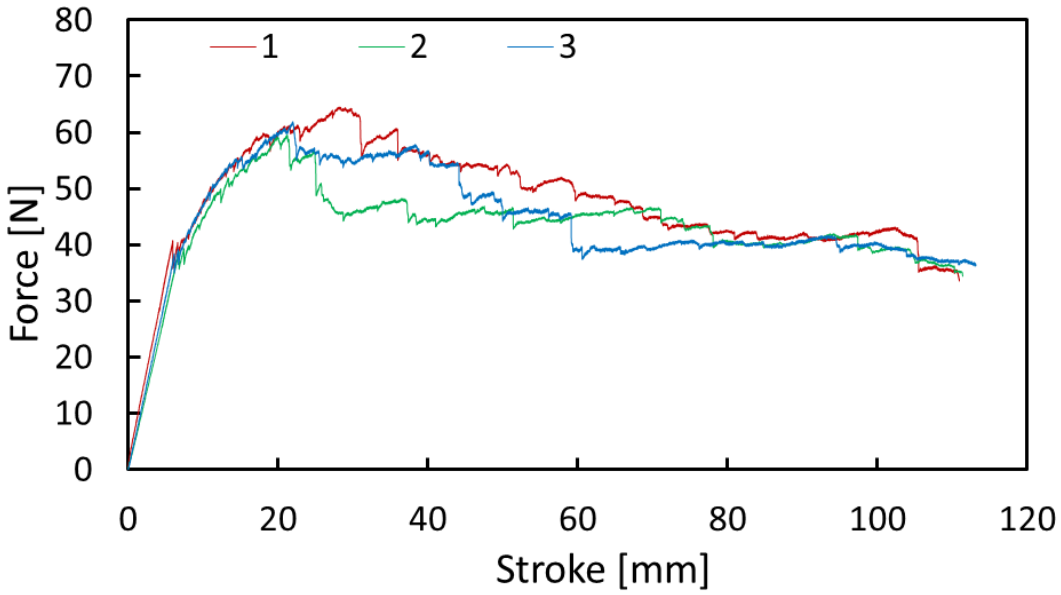

Figure 3.42. Load-displacement graph of GFRP 25//-25 specimens

Experiment number one is demonstrated in Figure 3.43. Initial fracture toughness is about 0.100 J/mm^2. Fiber bridging is seen in the figure with color change of the fibers to white. The fracture toughness has a constant value which is about 1.400 J/mm^2 when crack length passes 110 mm. The little dynamic crack propagation does not reverberate on the fracture toughness graph. Bridging fibers are also seen in Figure 3.44.

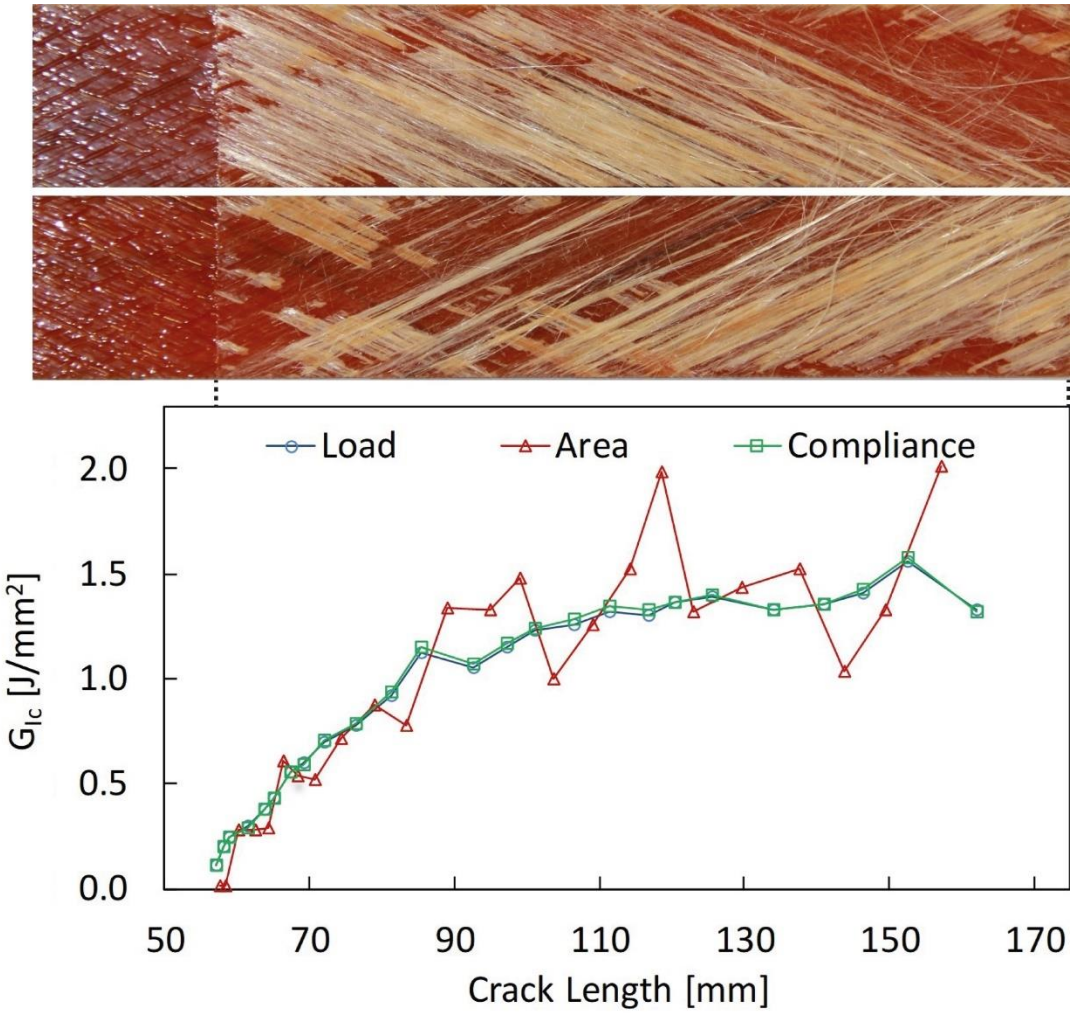

Figure 3.43. Fracture toughness results and fracture surface of specimen #1 (G-DCB-ENF-25--25-4-MF10724)

At 85 mm crack length

At 101 mm crack length

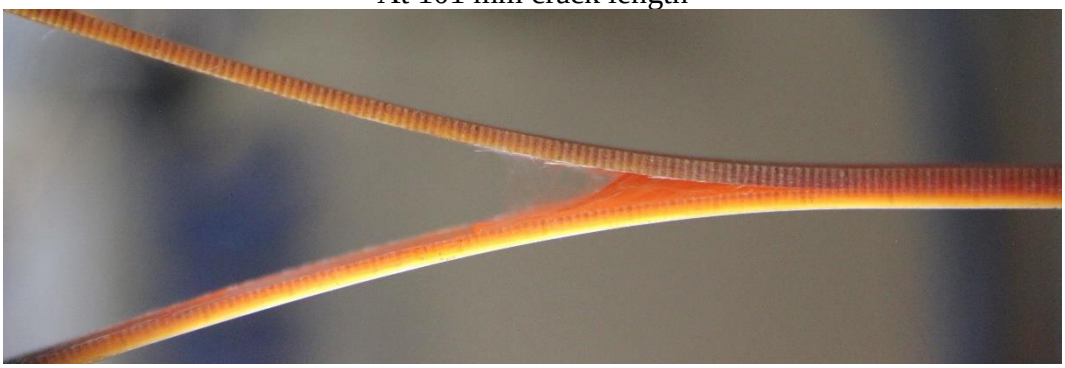

At 116 mm crack length

At 152 mm crack length

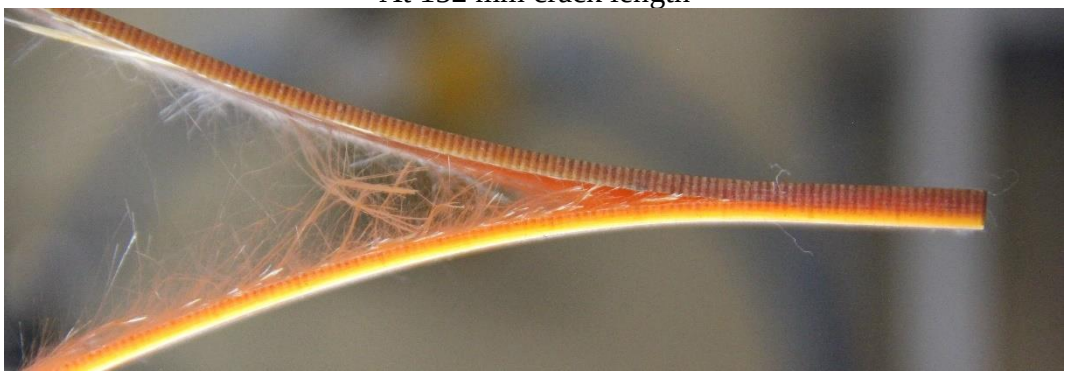

Figure 3.44. Side view of specimen #1 (G-DCB-ENF-25--25-4-MF10724) during DCB test

Three experiment's results are shown in Figure 3.45 using only the compliance method. Initiation fracture toughness value is about 0.100 J/mm^2 and it is increased with greater fiber bridging and as more fracture surface is created. It is increased with low scattering until 80 mm crack length. Crack morphology changes a little bit after 80 mm crack length varies from specimen to specimen and cracks propagate between 25-degree and -25-degree plies across the specimen. Some fibers which bridge between layers, stay on the counter layer, as seen in Figure 3.43, Figure 0.17, and Figure 0.18.

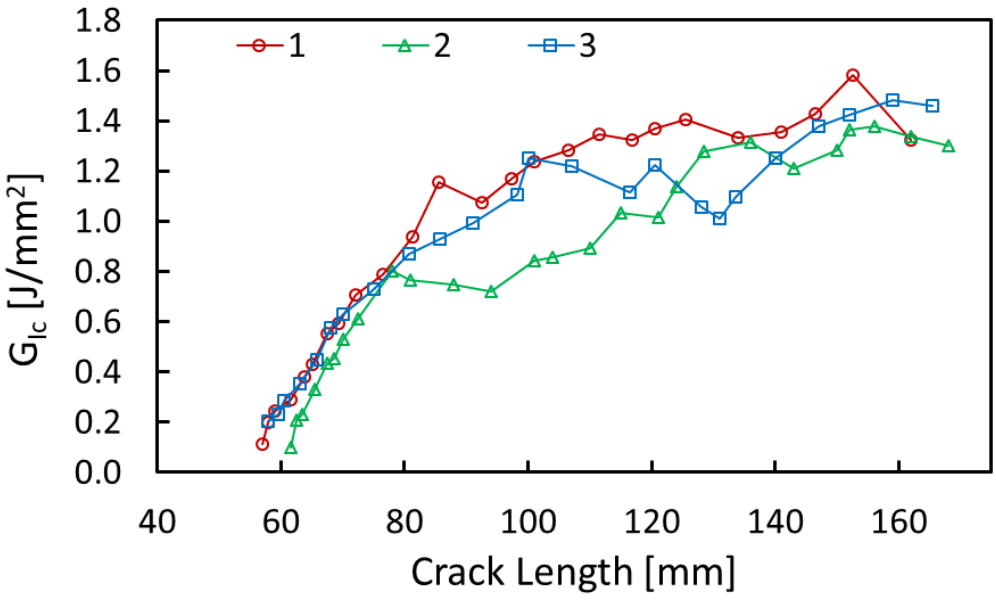

Figure 3.45. Fracture toughness vs crack length graph of three GFRP 25//-25 specimens

3.3.2.3. Mode I Fracture Toughness of 45//-45 Interface

Three experiments were done for samples with 45//-45 interface which had [0_8/45/-45//45/-45/0_8] lay-up orientation. The graph of the first experiment, which has a different slope at the no crack propagation region, suggests it had a crack length less than the others,, however, according to experimental notes, all crack lengths are close to each other. Furthermore, the crack propagation parts of the graphs of experiments are not close to each other. Whilst one has a big dynamic crack, the others have little dynamic cracks.

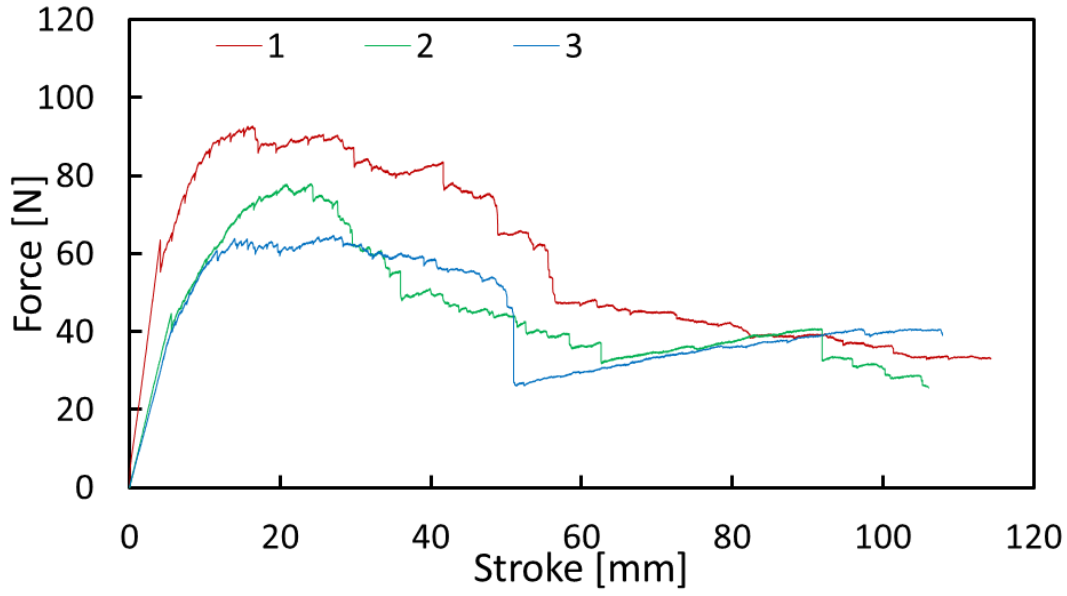

Figure 3.46. Load-displacement graph of GFRP 45//-45 specimens

The individual result of experiment number two is seen in Figure 3.47 using the three calculation methods. Initial fracture toughness starts about 0.250 J/mm^2 and it reaches 1.500 J/mm^2 with the high fiber bridging. The fiber bridging is related to the angle of the layer at the interface. The huge fiber bridging continues until the fiber comes from the initial crack surface which is clearly seen in fracture surface photos of Figure 3.47. Even if there are two crack jumps between layers, one is from the 45/-45 to -45/45 interface the other is from the -45/45 to 45/90 interface, the fracture toughness value is about 1.200 J/mm^2. Changes in fracture toughness correspond to

these crack jumps. Fiber bridging and stiffness change of the specimen are seen in Figure 3.48. When the stiffness of one leg of a DCB specimen is increased due to these crack jumps, the specimen end rotates to the weaker leg direction.

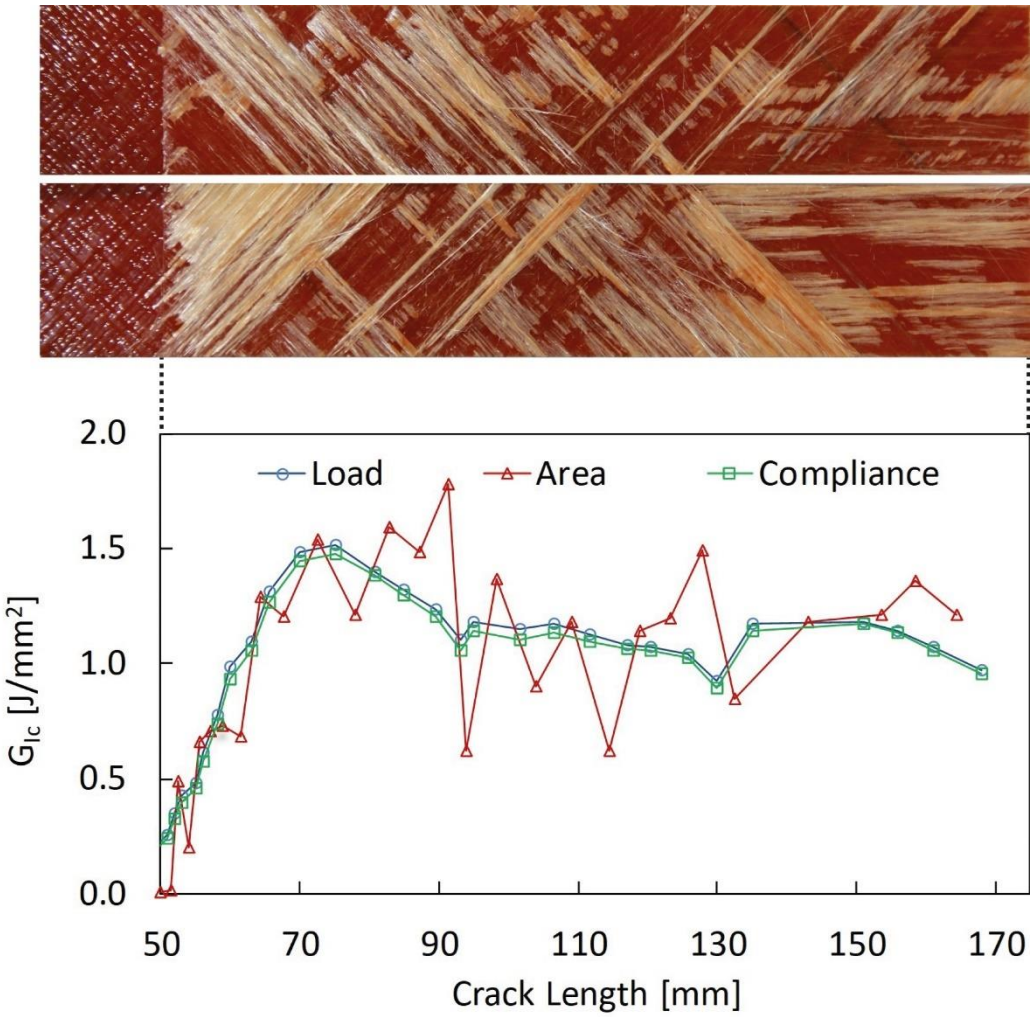

Figure 3.47. Fracture toughness results and fracture surface of specimen #2 (G-DCB-ENF-45--45-10-MF11608)

At 94 mm crack length

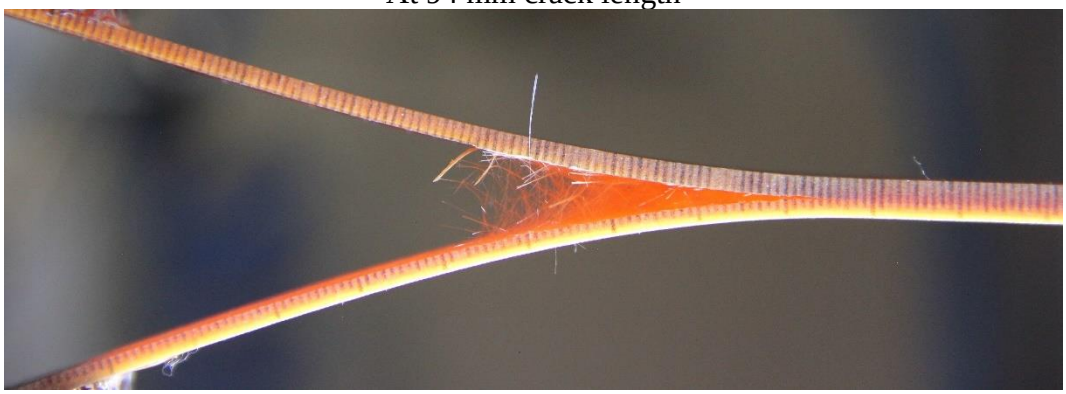

At 103 mm crack length

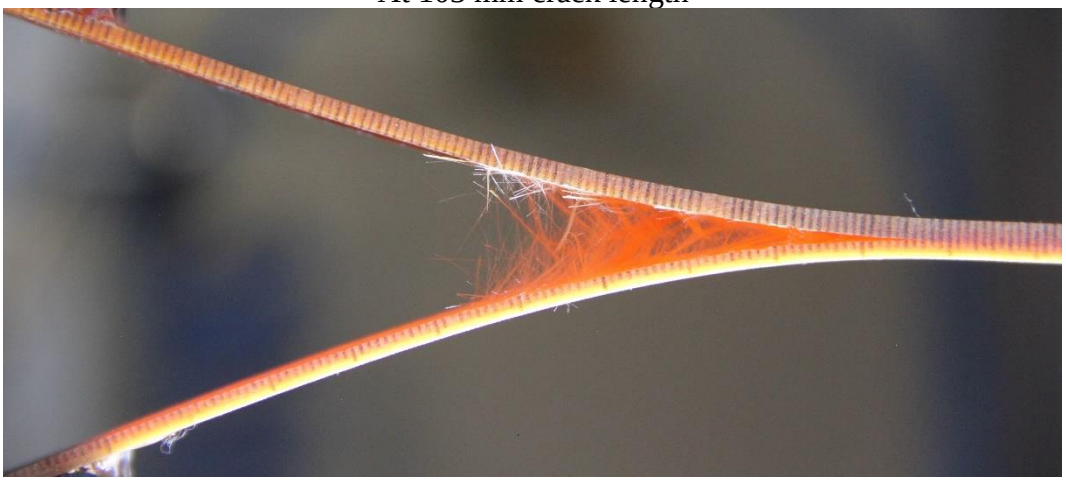

At 129 mm crack length

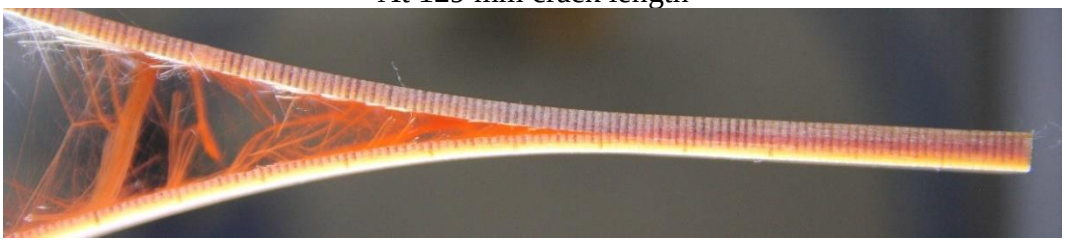

At 150 mm crack length

Figure 3.48. Side view of specimen #2 (G-DCB-ENF-45--45-10-MF11608) during DCB test

Three experimental results using the compliance method are shown in Figure 3.49. As seen in the load-displacement graph, fracture toughness values have differences from each other. The initiation value is about 0.200 J/mm^2. It is increased up to 1.400 J/mm^2 at 80 mm crack length. However, it is hard to get information from any further crack length due to crack propagation in a different region for these experiments. In experiment number one, the crack generally goes between the 45-degree and -45-degree layers. In experiments number two and three, the crack goes between the 45-degree and -45-degree layers, then it propagates between the -45-degree and 45-degree layers, and then goes between the 0-degree and 45-degree layers. Even though these differences affect the fracture toughness value, 1.100 J/mm^2 can be assumed as a propagation value.

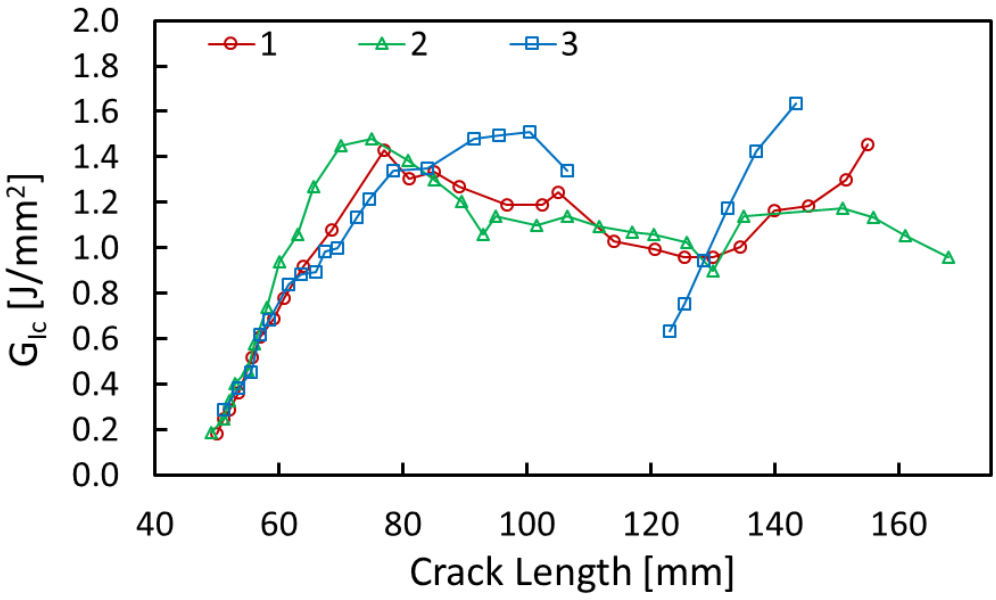

Figure 3.49. Fracture toughness vs crack length graph of three GFRP 45//-45 specimens

3.3.2.4. Mode I Fracture Toughness of 45//45 Interface

As in the CFRP 45//-45 experiment, the load-displacement graphs of the GFRP [0_8/45/45//45/45/0_8] laminated experiments are very close the each other as shown in Figure 3.50 and also in the fracture toughness graph in Figure 3.53. Three dynamic propagations for three experiments are at different crack lengths seen as a huge load drop.

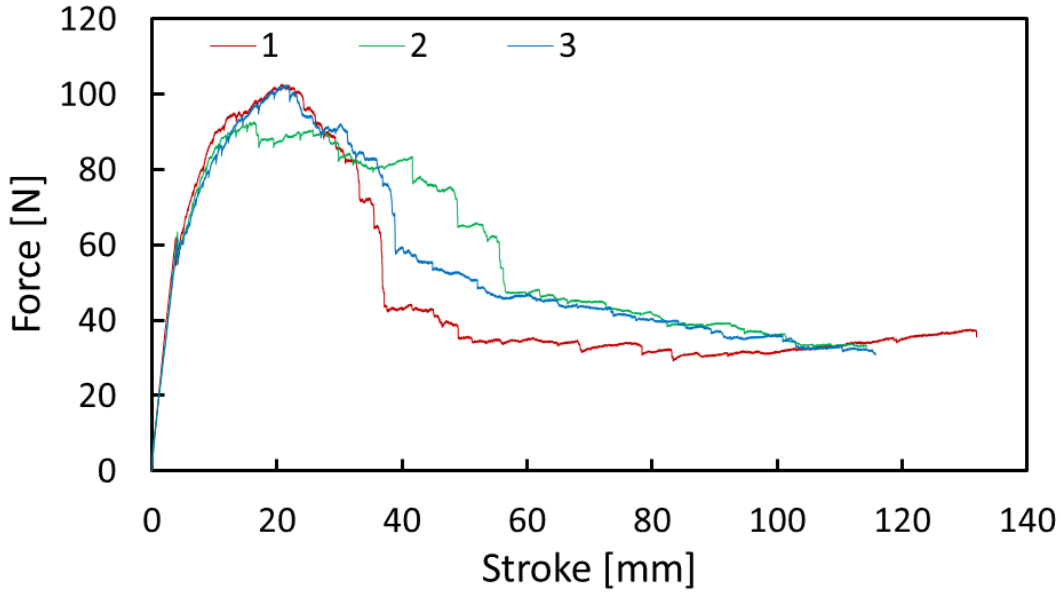

Figure 3.50. Load-displacement graph of GFRP 45//45 specimens

The individual experiment result of specimen number 3 is shown in Figure 3.51. The fracture toughness starts with 0.250 J/mm^2 and with huge fiber bridging, which has almost 2 layer thickness in Figure 3.52 at 94 mm crack length, the fracture toughness values increased to 2.000 J/mm^2. When the crack jumps to the 0/45 interfaces, the values stabilized at around 1.500 J/mm^2. The correlation between crack jumps and the fracture toughness is seen in Figure 3.51.

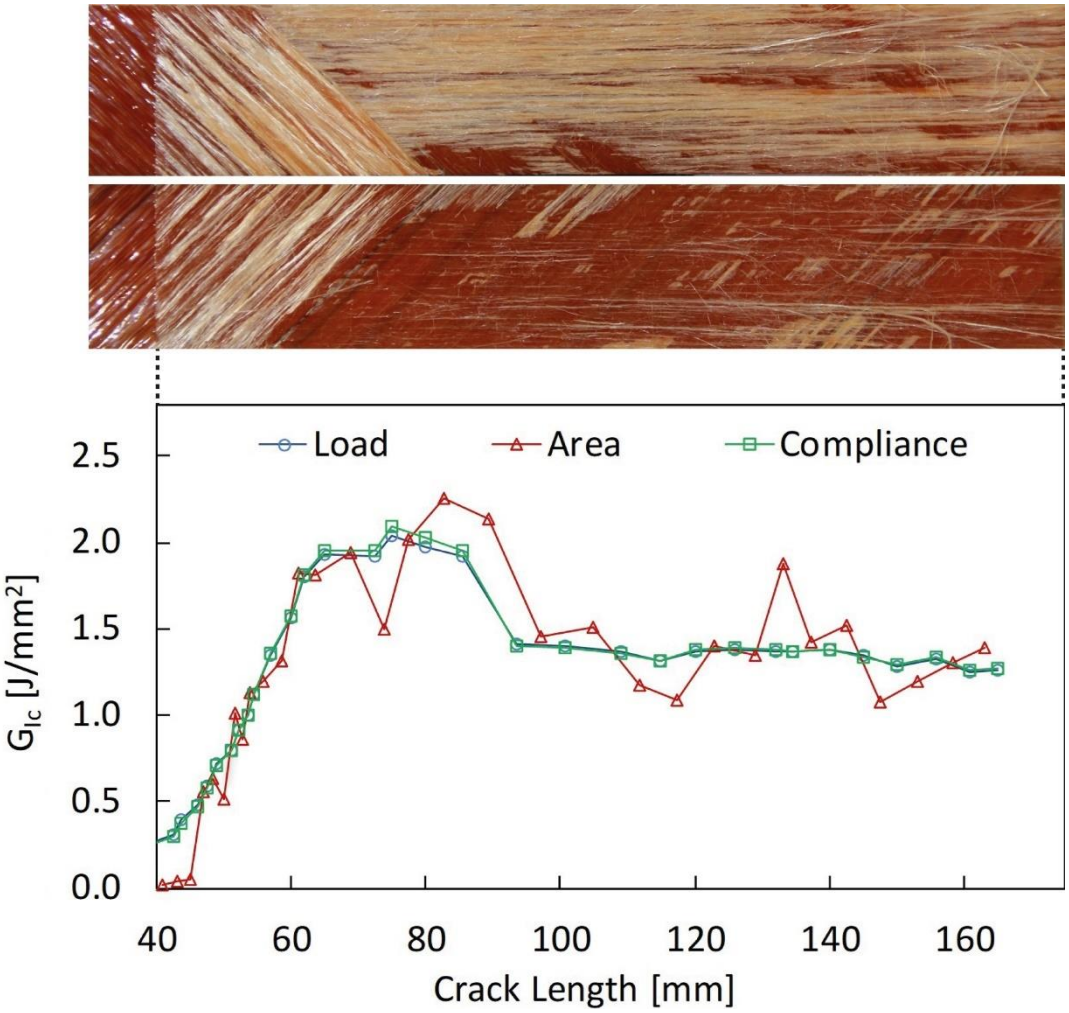

Figure 3.51. Fracture toughness results and fracture surface of specimen #3 (G-DCB-ENF-45-45-7-MF10745)

At 79 mm crack length

At 94 mm crack length

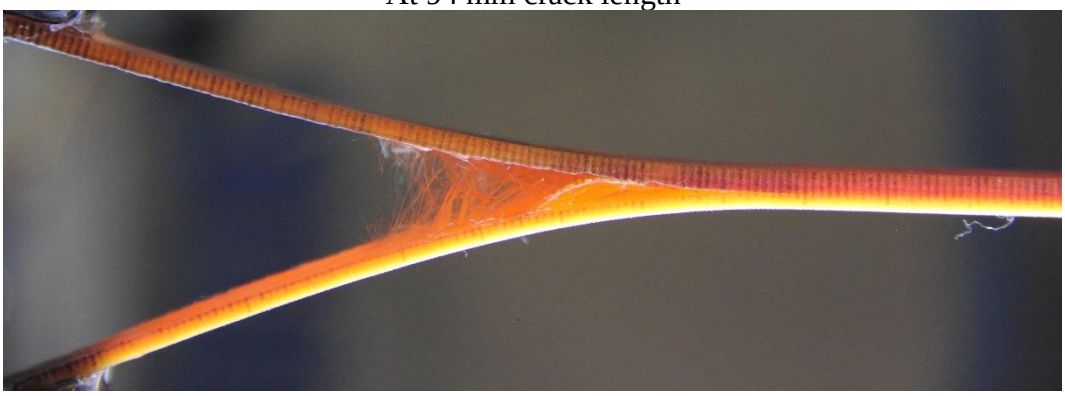

At 120 mm crack length

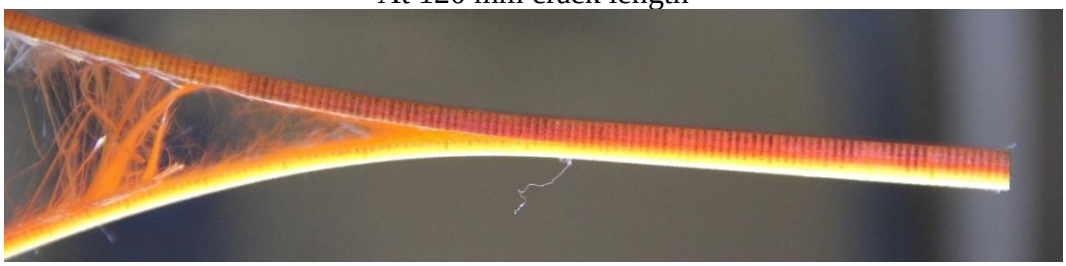

At 145 mm crack length

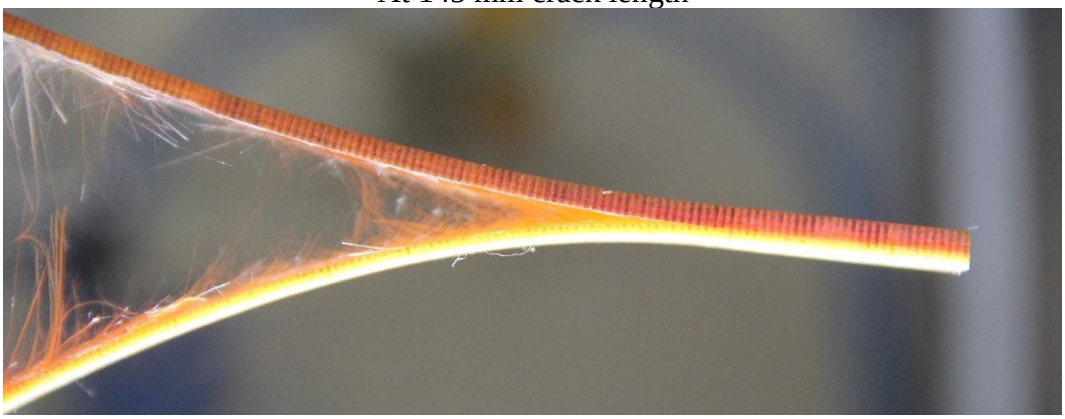

Figure 3.52. Side view of specimen #3 (G-DCB-ENF-45-45-7-MF10745) during DCB test

Three experimental results are illustrated using the compliance method in Figure 3.53. As an initiation value, 0.100 J/mm^2 can be used for this interface. Due to two layers of 45-degree layers, fiber bridging thickness is equal to two layers' thickness. This phenomenon is seen as an increase in fracture toughness up to 2 J/mm^2. Then, the crack jumps to the 45//0 interfaces and has 1.4 J/mm^2 fracture toughness in Figure 3.53. The crack jumps (dynamic crack propagation) correspond to no line connection between data points. Also, individual results can be seen in Figure 0.21, Figure 0.22, and Figure 3.51.

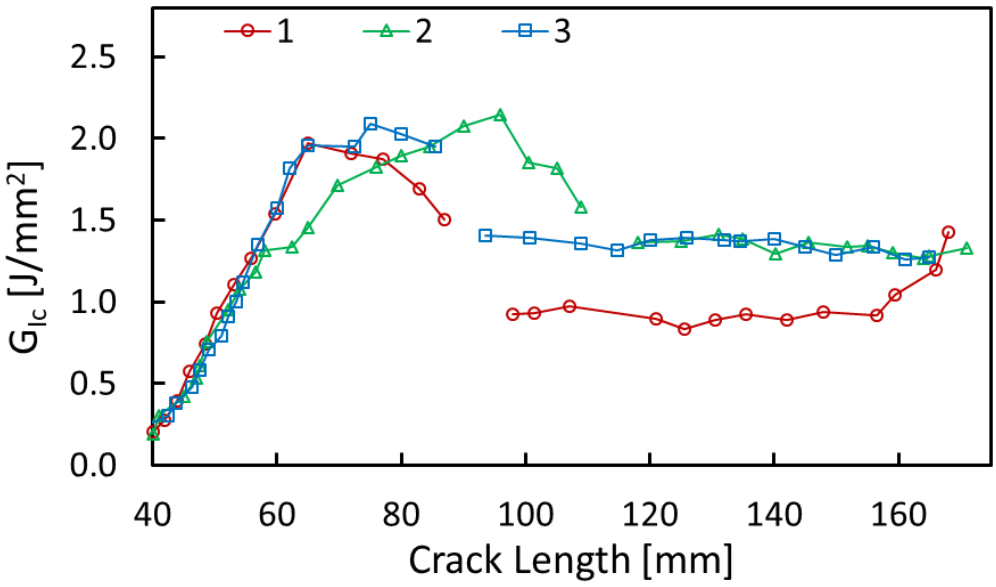

Figure 3.53. Fracture toughness vs crack length graph of three GFRP 45//45 specimens

3.3.2.5. Mode I Fracture Toughness of 65//65 Interface

For all 65//65 specimens which have [0_8/65/65//65/65/0_8] lay-up orientation, the crack propagates between the 65-degree layers for about 20 mm. This fiber bridging length is related to interface angle and specimen width. The crack jumps are not seen clearly in the load-displacement graphic in Figure 3.54, because fracture toughness between the 65-degree layers and 65/0 interface are very close to each other.

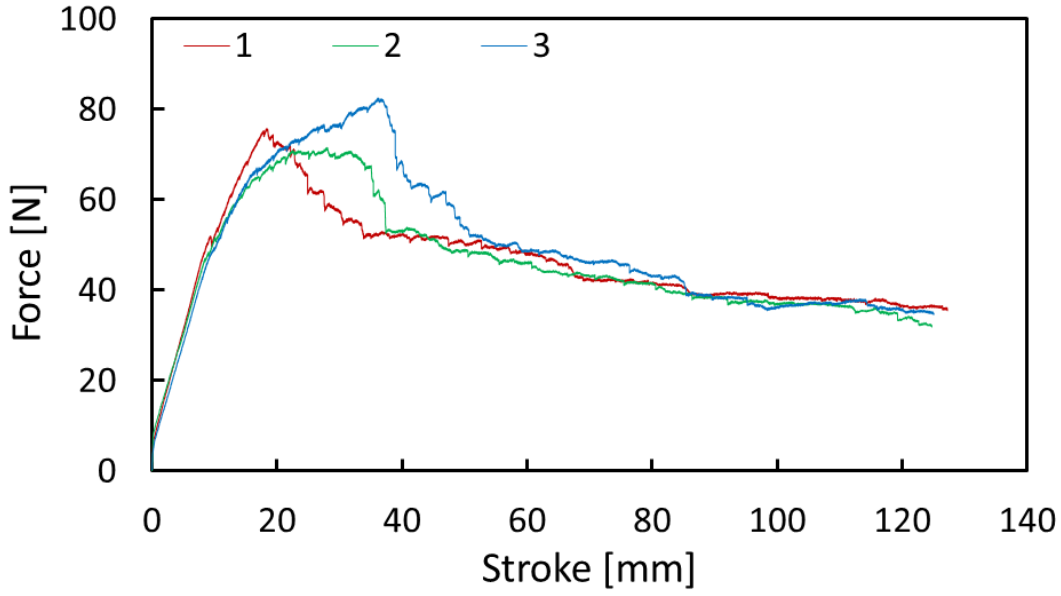

Figure 3.54. Load-displacement graph of GFRP 65//65 specimens

The result of experiment number three is illustrated in Figure 3.55. Initial fracture toughness is about 0.250 J/mm^2. With the huge fiber bridging at the beginning, it reaches 1.900 J/mm^2. The huge fiber bridging with a thickness of 2 layers is seen in the 96 mm crack length photo in Figure 3.56. The crack jumps the weaker region which is the 65/0 interface after the huge fiber bridging which is connected to the initial crack region. The fracture toughness values are stabilized at about 1.500 J/mm^2 while the cracks propagate in the 65/0 interface.

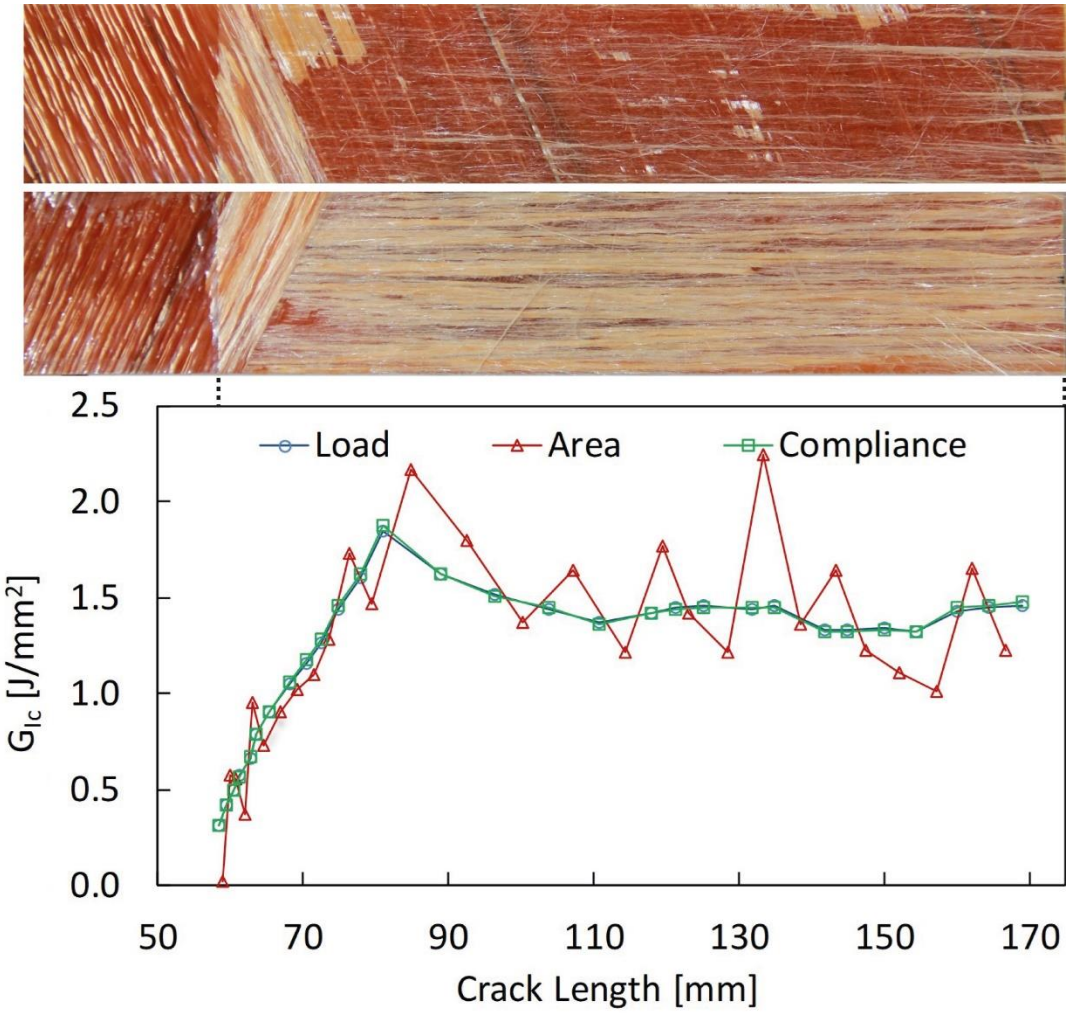

Figure 3.55. Fracture toughness results and fracture surface of specimen #3 (G-DCB-ENF-65-65-3-MF12060)

At 74 mm crack length

At 96 mm crack length

At 121 mm crack length

At 146 mm crack length

Figure 3.56. Side view of specimen #3 (G-DCB-ENF-65-65-3-MF12060) during DCB test

As it is seen in Figure 3.57, fracture toughness at the crack jumps are almost equal for all specimens. The initiation values are about 0.250 J/mm^2 and it reaches 1.5 J/mm^2 with the huge fiber bridging. The starting the fracture toughness value of the 0//65 interface is 1.2 J/mm^2 and it increases with little fiber bridging up to 1.5 J/mm^2.

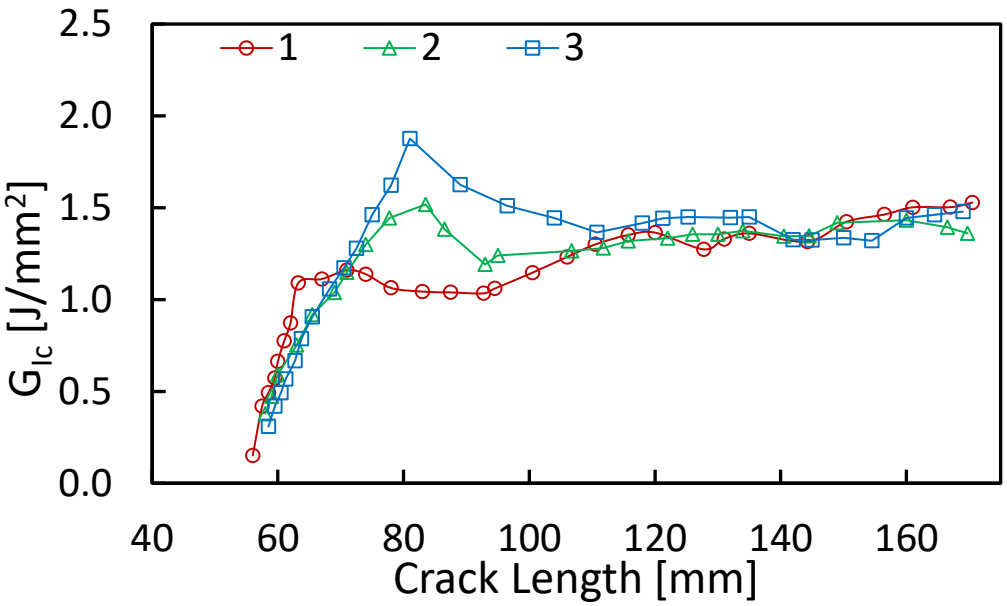

Figure 3.57. Fracture toughness vs crack length graph of three GFRP 65//65 specimens

3.3.2.6. Mode I Fracture Toughness of 90//90 Interface

For the GFRP 90/90 interface specimens with [08/90/90//90/90/08] lay-up orientation, only one experiment was conducted because the crack does not propagate between 90-degree layers. There is no dynamic crack propagation in the load displacement graph in Figure 3.58 since the crack immediately jumps to the 0/90 interface and continues between them until the specimen is separated into two pieces.

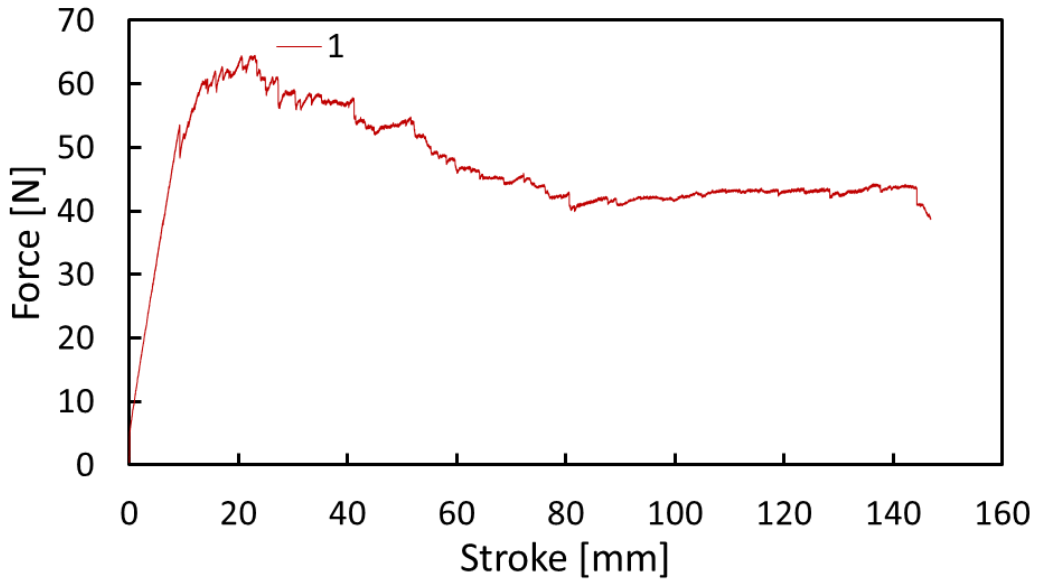

Figure 3.58. Load-displacement graph of GFRP 90//90 specimens

The experiment result is shown in Figure 3.59. The crack jump which is mentioned above is seen in both fracture surface photos and 55 mm crack length photo in Figure 3.60. Initial fracture toughness is about 0.250 J/mm^2 while the propagation value is about 1.500 J/mm^2. The only information which can be taken from the experiment is θ/0 interfaces fracture toughness values are close to each other which is at about 1.500 J/mm^2

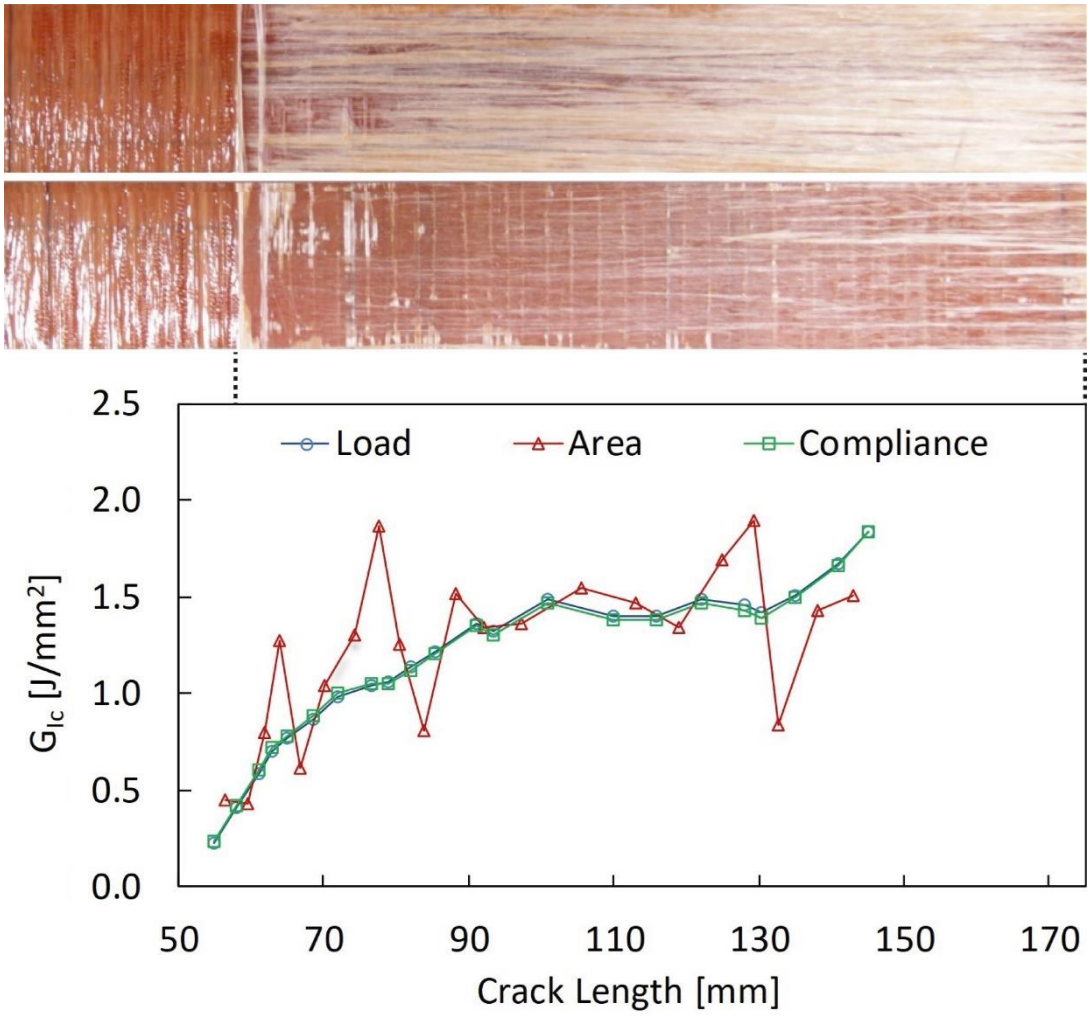

Figure 3.59. Fracture toughness results and fracture surface of specimen #1 (G-DCB-ENF-90-90-11-MF10723)

At 55 mm crack length

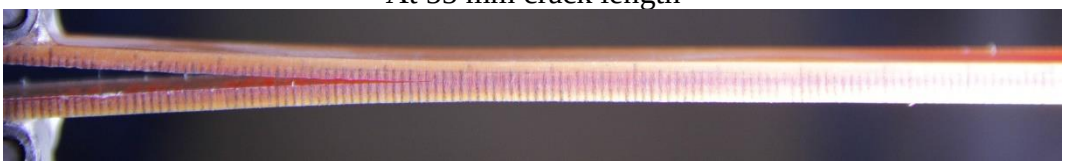

At 86 mm crack length

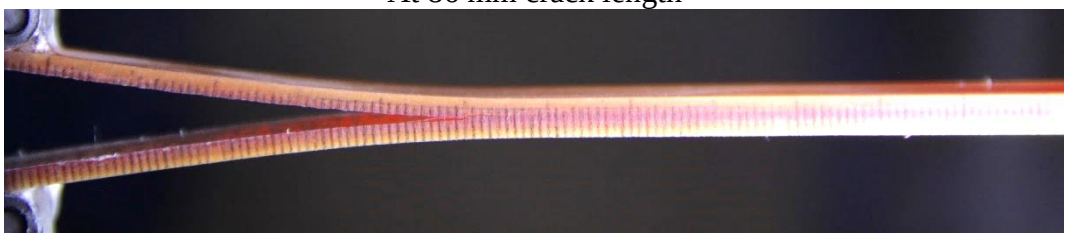

At 116 mm crack length

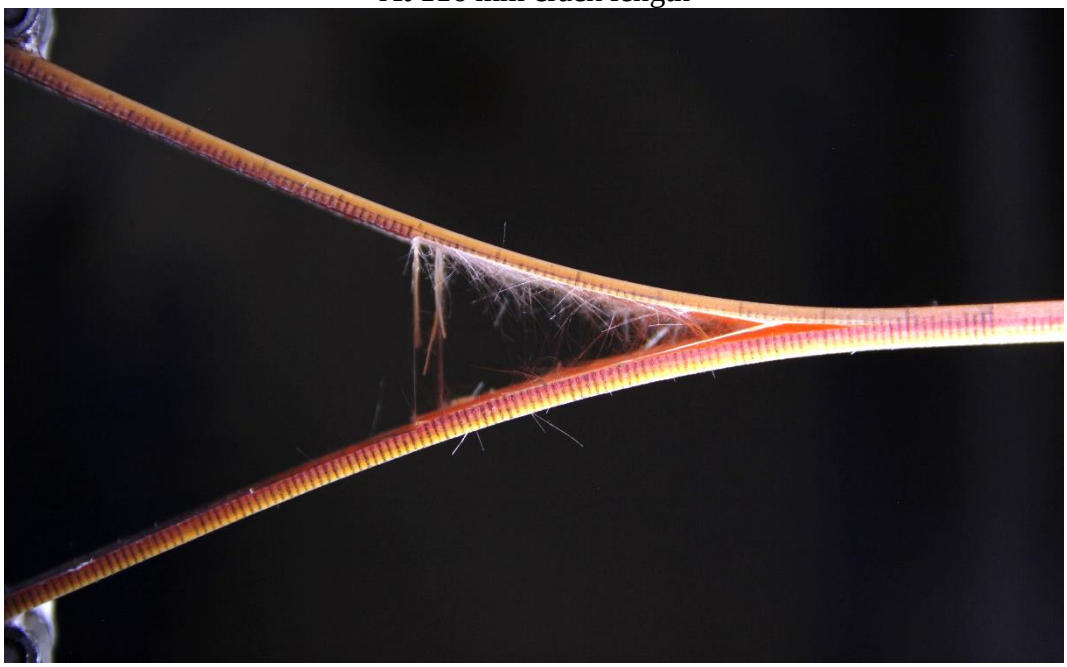

At 160 mm crack length

Figure 3.60. Side view of specimen #1 (G-DCB-ENF-90-90-11-MF10723) during DCB test

3.3.2.7. General Trend of Mode I Fracture Toughness of GFRP Specimens

Cracks in the GFRP specimens are more likely to pass to other interfaces or other laminates than in CFRP laminates. They generally propagate between layers until the connection of fibers with the initial crack is finished. Then, with the increase of the angle, crack jumping gets close to the initial crack area. Huge fiber bridging is observed in the GFRP specimens. The fiber bridging thickness reaches two times the thickness of a layer because, after fiber bridging of two layers, there are 0-degree layers at the top and bottom. So, the crack jump is finished when it faces the 0-degree layer. Then it can be simplified like two fracture toughness trends; one before the crack jump and one after the crack jump. For complex analysis, full crack propagation data can be inserted into an analysis program.

3.4. Discussion

In this section, the results of these tests are compared. In the first part, comparisons are made between GFRP and CFRP for each interface orientation. In the second part, comparisons are made for different interface orientations for CFRP and then for GFRP.

3.4.1. Comparison of CFRP and GFRP Fracture Toughness for 0//0 Interface

0//0 interface is the suggested orientation in the literature because there is no crack jump during the experiment. These stable experiments are seen in the fracture toughness graphs with low scattering values in Figure 3.61. As an initiation value, there is nearly no difference between CFRP and GFRP specimens. Their initiation values are 0.280 mm^2 and 0.200 J/mm^2 respectively. With increasing crack-length, GFRP fracture toughness is increasing enormously up to 1.2 J/mm^2 until the fiber bridging stabilizes at high crack lengths. However, CFRP fiber bridging has not much effect on fracture toughness which increases from 0.280 J/mm^2 to 0.325 J/mm^2. Less fiber bridging shows that carbon fiber-resin bonding has more strength than glass fiber resin strength because glass fiber easily separates from their layer and creates the fiber bridging effect. Fiber bridging is also the reason for the creation of new fracture surfaces. In order to create these surfaces, more energy is needed. While using constant fracture toughness values are proper for CFRP specimens, resistance values must be used for GFRP specimens.

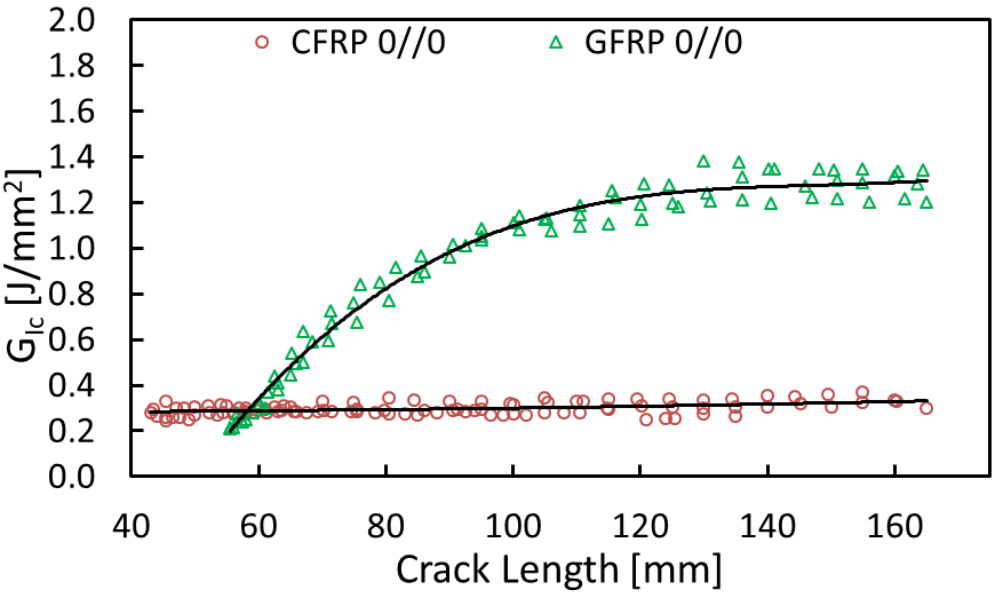

Figure 3.61. Comparison graph of CFRP and GFRP fracture toughness for 0//0 interface

3.4.2. Comparison of CFRP and GFRP Fracture Toughness for 25//-25 Interface

The 25//-25 interface fracture toughness results are close to 0//0 interface results. CFRP specimens start with 0.2 J/mm^2 and GFRP specimens start with 0.100 J/mm^2. The propagation part is also very close to the 0//0 interface. Fracture toughness of GFRP is increasing enormously up to 1.4 J/mm^2 in Figure 3.62. The huge fiber bridging difference is also seen in fracture surface pictures. Using a constant fracture toughness value is good enough for these CFRP specimens while crack length-dependent fracture toughness values must be used for GFRP ones.

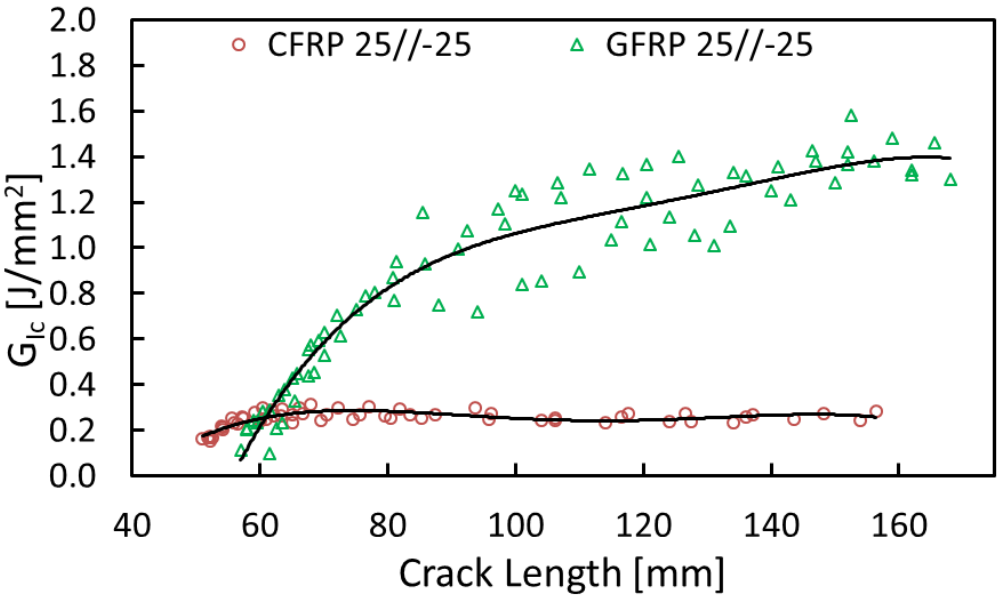

Figure 3.62. Comparison graph of CFRP and GFRP fracture toughness for 25//-25 interface

3.4.3. Comparison of CFRP and GFRP Fracture Toughness for 45//-45 Interface

Unlike the 0//0 and 25//-25 interfaces, in this experiment, the crack changes the region of propagation. This phenomenon is seen in both CFRP and GFRP specimens with a close trend. The effect of differences in the interface angles is clearly seen for these specimens. Cracks for both CFRP and GFRP specimens start at the 45//-45 interface, then both jump into one of the 45-degree layers. Whilst for CFRP specimens, the crack continues into the 45-degree layer, some of the cracks in GFRP specimens jump to the 0//45 interface. So, the propagation part of the GFRP specimen is not clear and has much more scatter value than CFRP ones. Initiation values are very close to each other at about 0.2 J/mm^2. For the propagation part, the glass specimen is again dominated by huge fiber bridging in Figure 3.63. CFRP specimen also has huge fiber bridging, however, fracture toughness of CFRP specimens is about half of the glass fracture toughness. This huge fiber bridging is the main reason for the crack jumps. For both results, curve-fit values must be used for the fracture data used in the analysis.

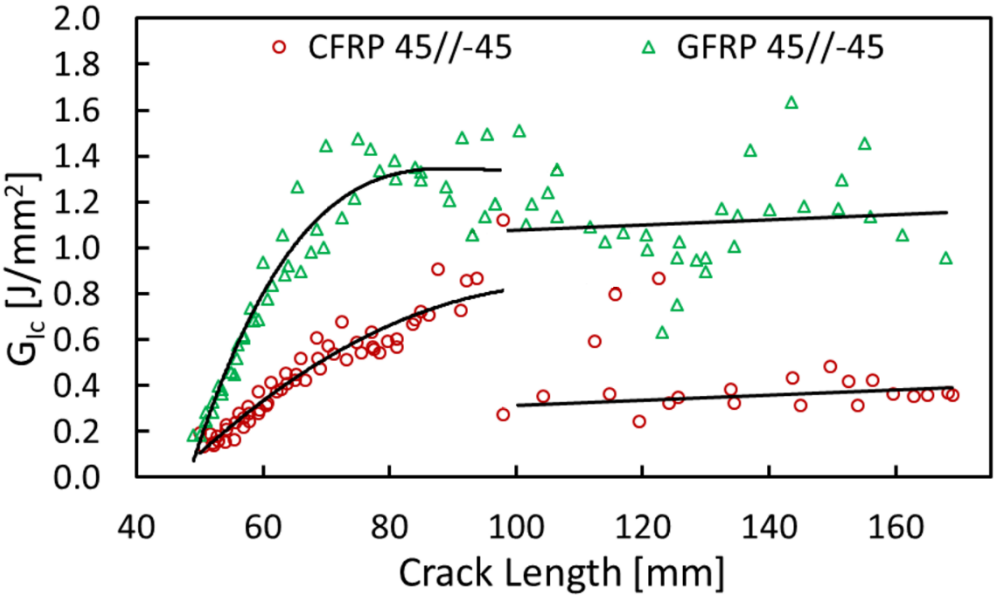

Figure 3.63. Comparison graph of CFRP and GFRP fracture toughness for 45//-45 interface

3.4.4. Comparison of CFRP and GFRP Fracture Toughness for 45//45 Interface

Close trends are also seen in this comparison. GFRP fracture toughness values are like scaled values of CFRP fracture toughness. The initiation values are again very close to each other at about 0.2 J/mm^2 in Figure 3.64. Rather than the plus-minus interfaces, these plus-plus interfaces are prone to crack jump into the adjacent interface. Both CFRP and GFRP first propagate in the 45//45 interface, then they jump to the 0//45 interface. Hence, before and after the jump, trends are very close to each other as a curved shape. However, the fracture toughness of glass specimens is always higher than carbon specimens. For the fracture toughness of 0//45 interface, constant fracture toughness values can be used but for initiation and propagation until the crack jump, crack length-dependent values must be used.

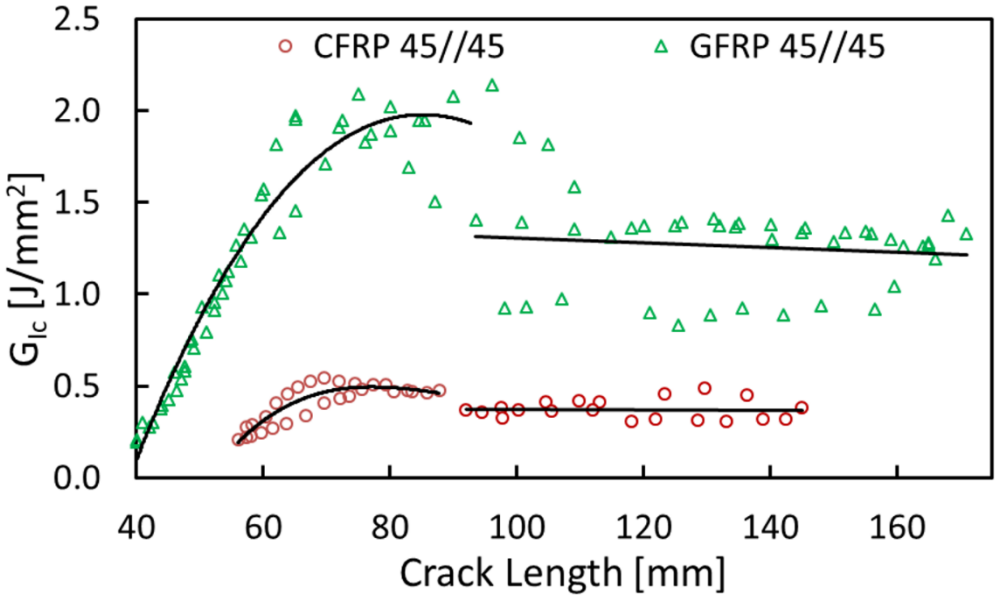

Figure 3.64. Comparison graph of CFRP and GFRP fracture toughness for 45//45 interface

3.4.5. Comparison of CFRP and GFRP Fracture Toughness for 65//65 Interface

Compared with the 45//45 interface, a crack in the 65//65 interface is more prone to jump into the adjacent interface at shorter crack length, due to their interface angles. Curve-fit shapes are similar to each other, like the other interfaces, GFRP specimens' fracture toughness is double the CFRP one in Figure 3.65. Cracks of both CFRP and GFRP specimens start at the 65//65 interface and then jump into the 0//65 interfaces. For the fracture toughness of the 0//65 interface, constant fracture toughness values can be used but for initiation and propagation until the crack jump, crack length-dependent values must be used.

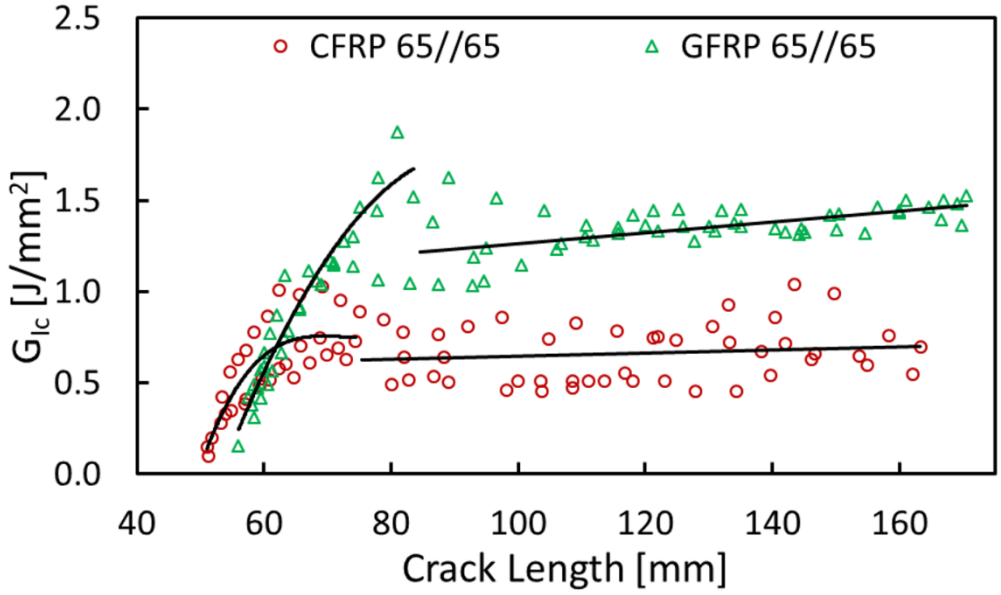

Figure 3.65. Comparison graph of CFRP and GFRP fracture toughness for 65//65 interface

3.4.6. Comparison of CFRP and GFRP Fracture Toughness for 90//90 Interface

Making a comparison on this interface is not relevant, because the crack in the GFRP specimen immediately jumps to the 0/90 interface while the crack in the CFRP specimen propagates much more in the 90-degree layers. This is the only interface that trends of CFRP and GFRP are different, as seen in Figure 3.66.

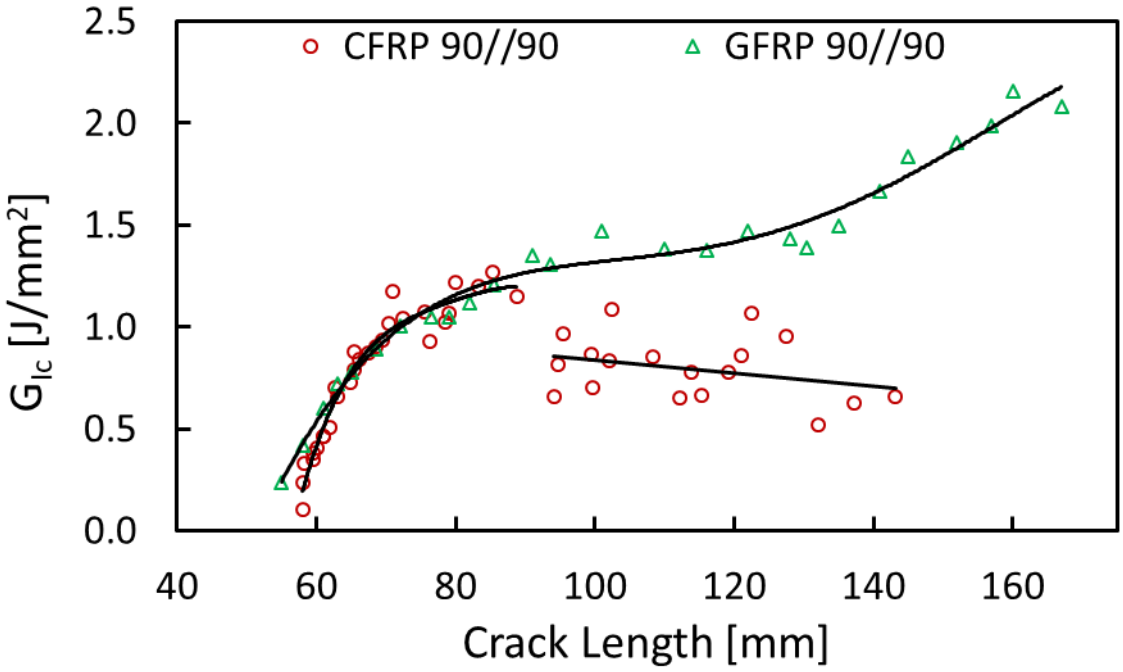

Figure 3.66. Comparison graph of CFRP and GFRP fracture toughness for 65//65 interface

3.4.7. Comparison of Fracture Toughness for All CFRP Interfaces

Effect of interface change for fracture toughness of CFRP laminates is shown in Figure 3.67. Fracture toughness results of 0//0, 25//-25, 45//-45, 45//45, 65//65, and 90//90 interfaces are shown using red, orange, green, blue, black and purple colored curves respectively. All fracture toughness values are illustrated as cracks starting at zero crack length in order to see the differences clearly. First of all, it is clearly shown that all fracture toughness values for all interfaces are not equal to each other. Except for the 0//0 specimens, all specimens' initiation values are close to each other and is about 0.18 J/mm^2. However, the fracture toughness of propagation and crack jump locations are different from each other. Fracture toughness values of cracks which are propagated into 0//0 and 25//-25 are similar to each other. Furthermore, after the crack jump, fracture toughness values of the 45//-45 and 45//45 specimens are highly close to each other because both cracks propagate into a 45-degree layer at these regions.

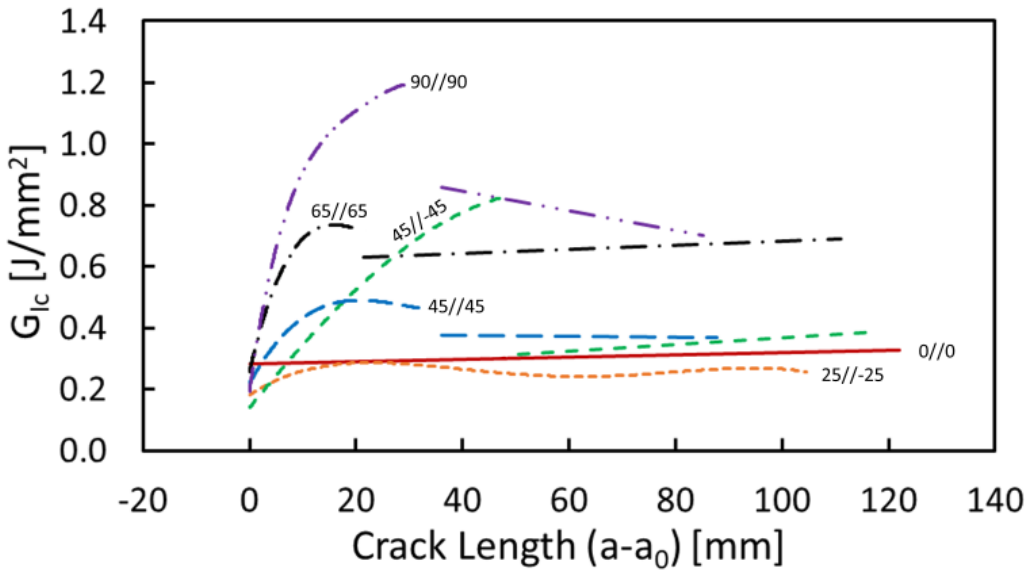

Figure 3.67. Comparison graph of different interfaces for CFRP laminates

Fiber bridging is observed excessively in the 65//65 interface, which is shown with the black curve. After it jumps into the 65//0 interface, the value is stabilized. Interestingly, fracture toughness values of the 65//0 interface are much higher than the 0//0 interface. The enormous increase in fracture toughness of the 90//90 interface proves that if the interface angle is closer to 90-degrees, the slope of increase of fracture toughness will be higher.

3.4.8. Comparison of Fracture Toughness for All GFRP Interfaces

Effect of interface change for fracture toughness of GFRP laminates is shown in Figure 3.68. Fracture toughness results of 0//0, 25//-25, 45//-45, 45//45, and 65//65 interfaces are shown using red, orange, green, blue and black colored curves respectively. The result of the 90//90 interface is not put into the figure, because the crack in this experiment immediately jumps to the 90/0 interface. All fracture toughness values are illustrated as cracks starting at zero crack length in order to see the differences clearly. Firstly, the fiber bridging effect of the 0//0 and 25//-25 interfaces are close, also the fiber bridging effect of the 45//-45 and 45//45 interface are similar to each other. Like CFRP specimens, the highest-fiber bridging effect is in the 65//65 interface. Further delamination values are alike because one of their interface layer degrees is 0, which is 0//0, 0//45 and 0//65. Only the 25//-25 specimens' crack does not jump near to the 0-degree layer. Similar to the CFRP specimens, 0//0 fracture toughness values and 25//-25 fracture toughness values are very close to each other. For glass specimens, using crack length-dependent fracture toughness values is essential because they are highly affected by the crack length and fiber bridging.

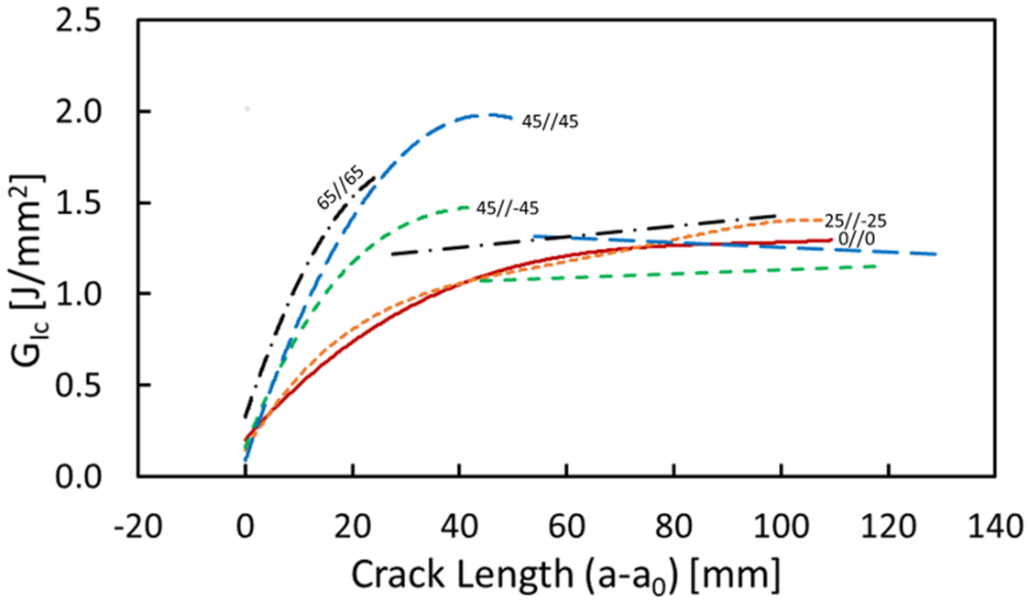

Figure 3.68. Comparison graph of different interfaces for GFRP laminates

3.5. Conclusions

In this study, Mode I fracture toughness of six different interfaces was examined for two different materials; CFRP and GFRP. Results are calculated using three different methods; load, compliance, and area method. The following conclusions were drawn:

1. Cracks in 0//0 and 25//-25 interfaces for both CFRP and GFRP laminates do not jump into other interfaces or into a lamina, so fracture toughness of these interfaces have one resistance trend curve. With the increase of the interface angle, fracture toughness of 45//-45, 45//45, 65//65 and 90//90 interfaces have two resistance trend curves.
2. After crack length propagated 50 mm in GFRP specimens, fracture toughness stabilized around 1.250 J/mm^2 for all interfaces. For crack length between 0 mm and 50 mm, all interfaces had unique resistance curves. However, resistance curves of 0//0 and 25//-25 interfaces for GFRP laminates were very close to each other.
3. Resistance curves of 0//0 and 25//-25 interfaces for CFRP laminates were also very close to each other with one trend curve. Fracture toughness of 45//-45, 45//45, 65//65 and 90//90 interfaces have two trend curves. Fracture toughness of the first 50 mm crack length for all interfaces had unique resistance curves. Fracture toughness values of further delamination for 0, 25 and 45 degree angles were very close to each other and had a constant fracture toughness value of around 0.300 J/mm^2, while 65 and 90 degree interfaces had higher constant toughness values which rose with increase in interface angle.
4. The crack at 90//90 interface immediately jumps to the adjacent interface for GFRP laminates. For CFRP laminates, the crack propagates about 25 mm, then it jumps to the adjacent interface which is 0/90.
5. Initial fracture toughness values of both GFRP and CFRP are low and close to each other. Fracture toughness of GFRP laminates increases with crack length more than that of CFRP, with also more fiber bridging than CFRP. We presume that the bonding between glass and resin is weaker than carbon and

resin, which could be the reason that GFRP specimens have more fiber bridging than CFRP specimens. This could also be the reason that GFRP specimens have a tendency to exhibit crack jump while CFRP ones hardly do.

6. Using a constant fracture toughness value for analyzing a crack would give wrong results, so the resistance curve must be used for all interfaces. However, fracture toughness of CFRP 0//0 and CFRP 25//-25 specimens with respect to crack length are almost constant. So, using constant fracture toughness for these interfaces would not give wrong results.
7. Using these fracture toughness values is relevant when the width of the part is close to these specimens. If it is not, fiber bridging length will rise with increasing width. For example, if the width of the specimens is doubled, the crack jump starts at double the previous delta crack length.
8. Results using the compliance and load methods are very close to each other, while those using the area method are more scattered. We claim that this is due to the assumption done during the calculation of area method which is that the unloading curve is assumed linear and intersects with (0,0) point. However, the average and total fracture toughness values for all calculation methods are very close to each other which shows that the area method has only a scattering error.

REFERENCES

1. Kedward, K. T., Wilson, R. S., & Mclean, S. K. (1989). The flexure of simply curved composite shapes. *Composites, 20*(6), 527-536. doi:10.1016/0010-4361(89)90911-7

2. Hara, E., Yokozeki, T., Hatta, H., Iwahori, Y., Ogasawara, T., & Ishikawa, T. (2012). Comparison of out-of-plane tensile strengths of aligned CFRP obtained by 3-point bending and direct loading tests. *Composites Part A: Applied Science and Manufacturing,43*(11), 1828-1836. doi:10.1016/j.compositesa.2012.06.016

3. Moroni, F., Pirondi, A., Pernechele, C., Gaita, A., & Vescovi, L. (2018). Comparison of tensile strength and fracture toughness under mode I and II loading of co-cured and co-bonded CFRP joints. *Frattura Ed Integrità Strutturale,13*(47), 294-302. doi:10.3221/igf-esis.47.22

4. Cui, W., Liu, T., Len, J., & Ruo, R. (1996). Interlaminar tensile strength (ILTS) measurement of woven glass/polyester laminates using four-point curved beam specimen. *Composites Part A: Applied Science and Manufacturing,27*(11), 1097-1105. doi:10.1016/1359-835x(96)00071-1

5. Standard test method for measuring the curved beam strength of a fiber-reinforced polymer-matrix composite, ASTM International, D 6415/D 6415 M.

6. Hao, W., Ge, D., Ma, Y., Yao, X., & Shi, Y. (2012). Experimental investigation on deformation and strength of carbon/epoxy laminated curved beams. *Polymer Testing,31*(4), 520-526. doi:10.1016/j.polymertesting.2012.02.003

7. Arca, M. A., & Coker, D. (2014). Experimental investigation of CNT effect on curved beam strength and interlaminar fracture toughness of CFRP laminates. *Journal of Physics: Conference Series,524*, 012038. doi:10.1088/1742-6596/524/1/012038

8. Ranz, D., Cuartero, J., Miravete, A., & Miralbes, R. (2017). Experimental research into interlaminar tensile strength of carbon/epoxy laminated curved beams. *Composite Structures,164*, 189-197. doi:10.1016/j.compstruct.2016.12.010

9. Seon, G., Makeev, A., Nikishkov, Y., & Lee, E. (2013). Effects of defects on interlaminar tensile fatigue behavior of carbon/epoxy composites. *Composites Science and Technology, 89*, 194-201. doi:10.1016/j.compscitech.2013.10.006

10. Murri G. B., O'Brien T. K., and Rousseau C. Q. (1998), Fatigue life methodology for tapered composite flexbeam laminates, *J. Am. Helicopter Soc.* 43, 146–155.

11. Gulasik, H., & Coker, D. (2014). Delamination-Debond Behaviour of Composite T- Joints in Wind Turbine Blades. *Journal of Physics: Conference Series,524*, 012043. doi:10.1088/1742-6596/524/1/012043

12. Armanios, E. A., & Parnas, L. (1991). Delamination Analysis of Tapered Laminated Composites Under Tensile Loading. *Composite Materials: Fatigue and Fracture (Third Volume),3*, 340-358. doi:10.1520/stp17726s

13. Celik, O., & Parnas, L. (2017). Maximization of Ultimate Strength of Unidirectional Tapered Composite Structures Considering Different Failure Modes. *58th AIAA/ASCE/AHS/ASC Structures, Structural Dynamics, and Materials Conference*. doi:10.2514/6.2017-0893

14. Nicholls, D., & Gallagher, J. (1983). Determination of GIC in Angle Ply Composites Using a Cantilever Beam Test Method. *Journal of Reinforced Plastics and Composites, 2*(1), 2-17. doi:10.1177/073168448300200101

15. Chou I. (1998). Effect of fiber orientation and moisture absorption on the interlaminar fracture toughness of CFRP laminates, *Advanced Composite Materials*, 7 (4), 377–94.

16. Pereira, A., & Morais, A. D. (2006). Mixed mode I II interlaminar fracture of glass/epoxy multidirectional laminates – Part 2: Experiments. *Composites Science and Technology*, *66*(13), 1896–1902. doi: 10.1016/j.compscitech.2006.04.008

17. Hwang J.H., Lee C.S., and Hwang W (2001). Effect of crack propagation directions on the interlaminar fracture toughness of carbon/epoxy composite materials, *Applied Composite Materials*, Vol. 8, 411–33.

18. Andersons, J., and König, M (2004). Dependence of fracture toughness of composite laminates on interface ply orientations and delamination growth direction *Composites Science and Technology*, 64 (13-14), 2139-2152.

19. Standard test method for mode I interlaminar fracture toughness of unidirectional fiber-reinforced polymer matrix composites, ASTM International, D5528.

20. Blondeau, C., Pappas, G., & Botsis, J. (2019). Influence of ply-angle on fracture in antisymmetric interfaces of CFRP laminates. *Composite Structures,216,* 464-476. doi:10.1016/j.compstruct.2019.03.004

21. Bolotin V.V., Bolotina K.S., Radin V.P., Shchugorev V.N., (1996). Fracture toughness characteristics of laminated composites. *Mech Compos Mater*, 32:14–20.

22. Davies P., Rannou F., (1995). The effect of defects in tubes: Part 1. Mode I delamination resistance. *Appl Compos Mater*, 1:333–349.

23. Ozdil F., Carlsson L.A., (1999). Beam analysis of angle-ply laminate DCB specimens. *Compos Sci Technol*, 59:305–315.

24. Ozdil F., Carlsson L.A., (2000) Characterization of mode I delamination growth in glass/epoxy composite cylinders. *J Compos Mater*, 34:398–419.

25. Laksimi A., Benyahia A.A., Benzeggagh M.L., Gong X.L., (2000). Initiation and bifurcation mechanisms of cracks in multi-directional laminates. *Compos Sci Technol*, 60:597–604.

26. Hwu C., Kao C.J., Chang L.E., (1995). Delamination fracture criteria for composite laminates. *J Compos Mater*, 29:1962–1987.

27. Jordan W., (2000). Changing the toughness of graphite fiber/resin based composites by changing their internal structure. *Composites: Part B* 31:245–252.

28. Lachaud F., Piquet R., Michel L., (1999). Delamination in mode I and II of carbon fibre composite materials: fibre orientation influence. In: *Proceedings of ICCM-12*, Paris, July 5th–9th, paper 1284.

29. Tohgo K., Hirako Y., Ishii H., Sano K., (1996). Mode I interlaminar fracture toughness and fracture mechanism of angle-ply carbon–Nylon laminates. *J Compos Mater*, 30:650–661.

30. Blackman B.R.K., Brunner A.J., (1998). Mode I fracture toughness testing of fibre-reinforced polymer composites: unidirectional versus cross-ply lay-up. In: Proceedings of *ECF 12 – Fracture from Defects*, 1471–1476.

31. Li Yong, Li Shunling, Xiao Jun, Tao Jie (1997). Study on the mode I interlaminar fracture toughness of multi-directional laminates. In: *Proceedings of ICCM 11*, vol. 2, 431–437.

32. Gilchrist M.D., Svensson N., (1995). A fractographic analysis of delamination within multidirectional carbon/epoxy laminates. *Compos Sci Technol*, 55:195–207.

33. Chou I., Kimpara I., Kageyama K., Ohsawa I., (1992). Effect of fiber orientation on the mode I interlaminar fracture behavior of CF/ epoxy laminates. *J Soc Mater Sci Jpn*, 41:1292–1298.

34. Chou I., Kimpara I., Kageyama K., Ohsawa I., (1995). Mode I and mode II fracture toughness measured between differently oriented plies in graphite/epoxy composites. *ASTM STP*, 1230:132–51.

35. Olsson R., Thesken J., Brandt F., J€onsson N., Nilsson S., (1996). Investigation of delamination criticality and the transferability of growth criteria. *Compos Struct*, 36:221–47.

36. Fish J.C., Malaznik S.D., (1996). Fracture of double beam specimens containing 90-degree plies. *Key Engrg Mater*, 121–122:347–360.

37. Trakas K., Kortschot M.T., (1997). The relationship between critical strain energy release rate and fracture mode in multidirectional carbonfiber/ epoxy laminates. *ASTM STP*, 1285:283–304.

38. Russell A.J., Street K.N., (1982). Factors affecting the interlaminar fracture energy of graphite/epoxy laminates. In: *Proceedings of ICCM IV*, Tokyo, 279–300.

39. Chai H., (1984). The characterization of Mode I delamination failure in non-woven, multidirectional laminates. *Composites*, 15:277–290.

40. Robinson P., Song D.Q., (1992). A modified DCB specimen for mode I testing of multidirectional laminates. *J Compos Mater*, 26:1554–1577.

41. La Saponara V., Muliana H., Haj-Ali R., Kardomateas G.A., (2002). Experimental and numerical analysis of delamination growth in double cantilever laminated beams. *Engrg Fract Mech*, 69:687–99.

42. Choi N.S., Kinloch A.J., Williams J.G., (1999). Delamination fracture of multidirectional carbon-fiber/epoxy composites under mode I, mode II and mixed-mode I/II loading. *J Compos Mater*, 33:73–100.

43. Laksimi A., Benzeggagh M.L., Jing G., Hecini M., Roelandt J.M., (1991). Mode I interlaminar fracture of symmetrical cross-ply composites. *Compos Sci Technol* ,41:147–164.

44. Schon J., Nyman T., Blom A., Ansell H., (2000). A numerical and experimental investigation of delamination behavior in the DCB specimen. *Compos Sci Technol*, 60:173–184.

45. Lucas J.P., (1992). Delamination fracture: effect of fiber orientation on fracture of a continuous fiber composite laminate. *Engrg Fract Mech*, 42:543–562.

46. Allix O., Leveque D., Perret L., (1998). Identification and forecast of delamination in composite laminates by an interlaminar interface model. *Compos Sci Technol*, 58:671–678.

47. Rubbrecht P.h., Verpoest I., (1993). The development of two new test methods to determine the mode I and mode II fracture toughness for varying fibre orientations at the interface. In: *Proceedings of the 38th International SAMPE Symposium*, Anaheim, CA, 875–887.

48. Polaha J.J., Davidson B.D., Hudson R.C., Pieracci A., (1996). Effects of mode ratio, ply orientation and precracking on the delamination toughness of a laminated composite. *J Reinf Plast Compos*, 15:141–173.

49. Hudson R.C., Davidson B.D., Polaha J.J., (1998). Effect of remote ply orientation on the perceived mode I and mode II toughness of θ/θ and θ/-θ interfaces. *Appl Compos Mater,* 5:123–138.

50. de Morais A.B., de Moura M.F.,Marques A.T., de Castro P.T., (2002). Mode I interlaminar fracture of carbon/epoxy cross-ply composites. *Compos Sci Technol*, 62:679–686.

51. Olsson, R. (2012). Modelling of impact damage zones in composite laminates for strength after impact. *The Aeronautical Journal*, *116*(1186), 1349–1365. doi: 10.1017/s0001924000007673

APPENDICES

A. Results

a. ILTS Experiment Results

i. ILTS Result of 0/0 Specimens

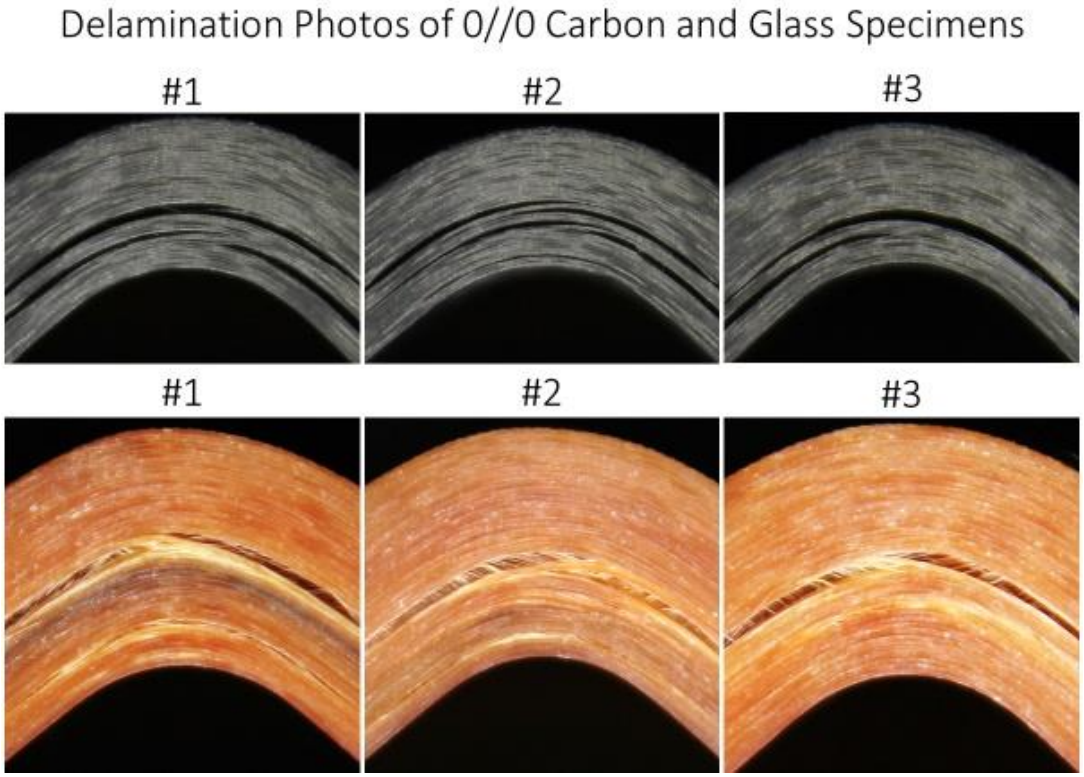

Figure 0.1. Delamination photos of 0/0 specimens

ii. ILTS Result of 25/-25 Specimens

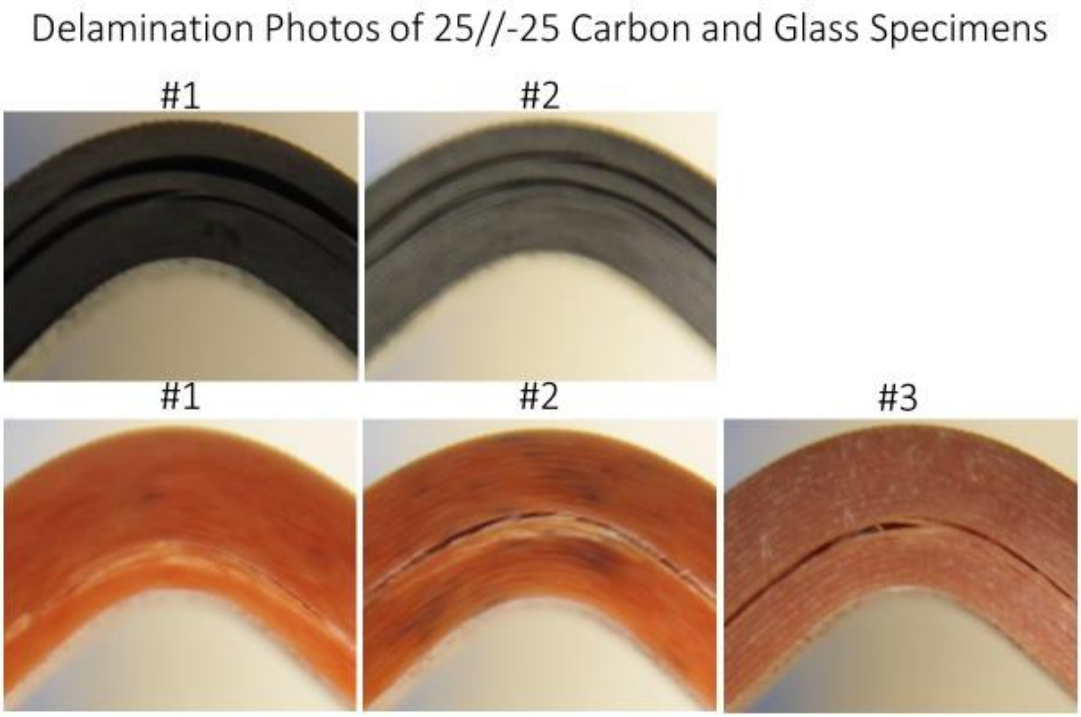

Figure 0.2. Delamination photos of 25/-25 specimens

iii. ILTS Result of 45/-45 Specimens

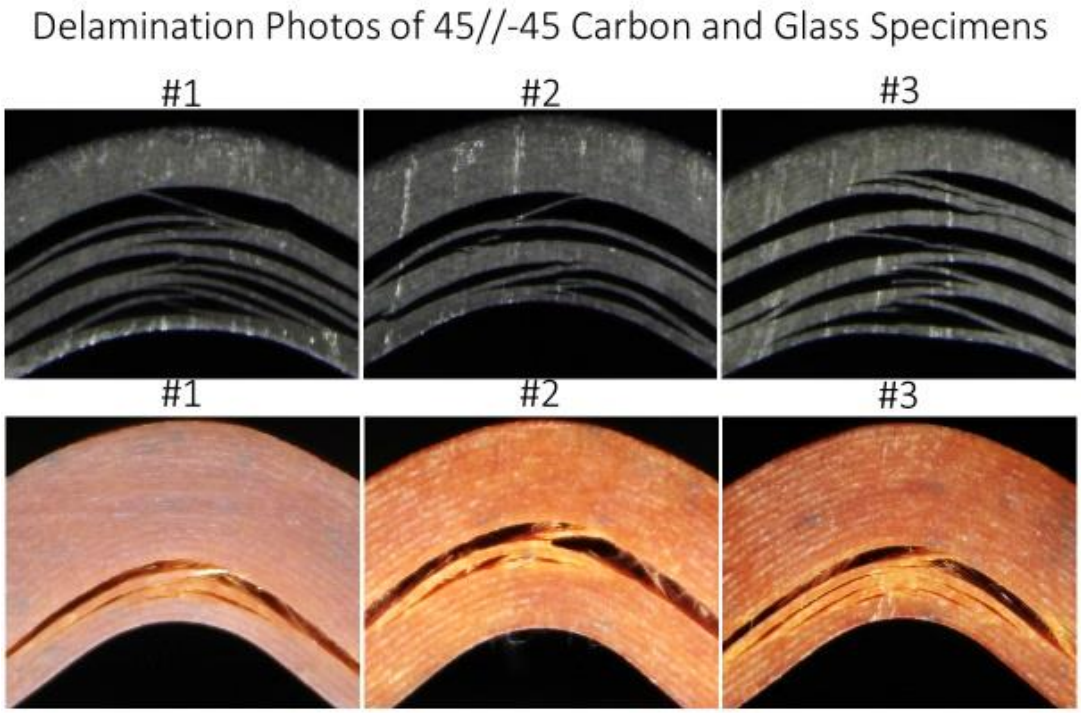

Figure 0.3. Delamination photos of 45/-45 specimens

iv. ILTS Result of 65/-65 Specimens

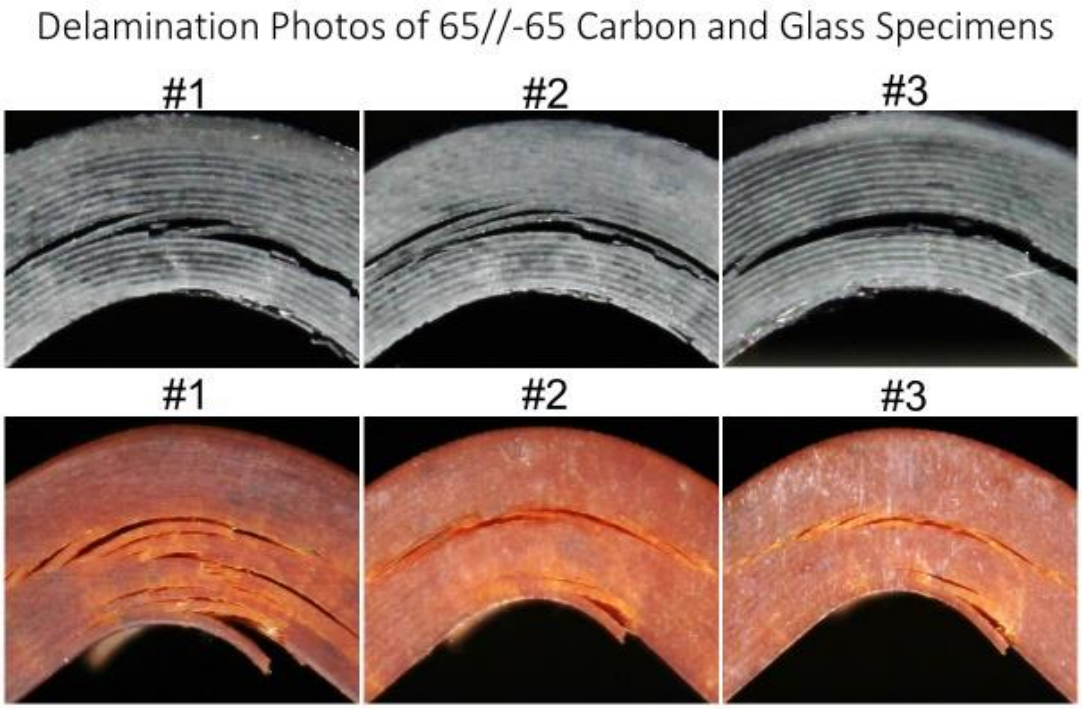

Figure 0.4. Delamination photos of 65/-65 specimens

b. Mode I Experiment Results

i. Mode I Result of CFRP Specimens

1. Mode I Fracture Toughness of 0//0 Interface

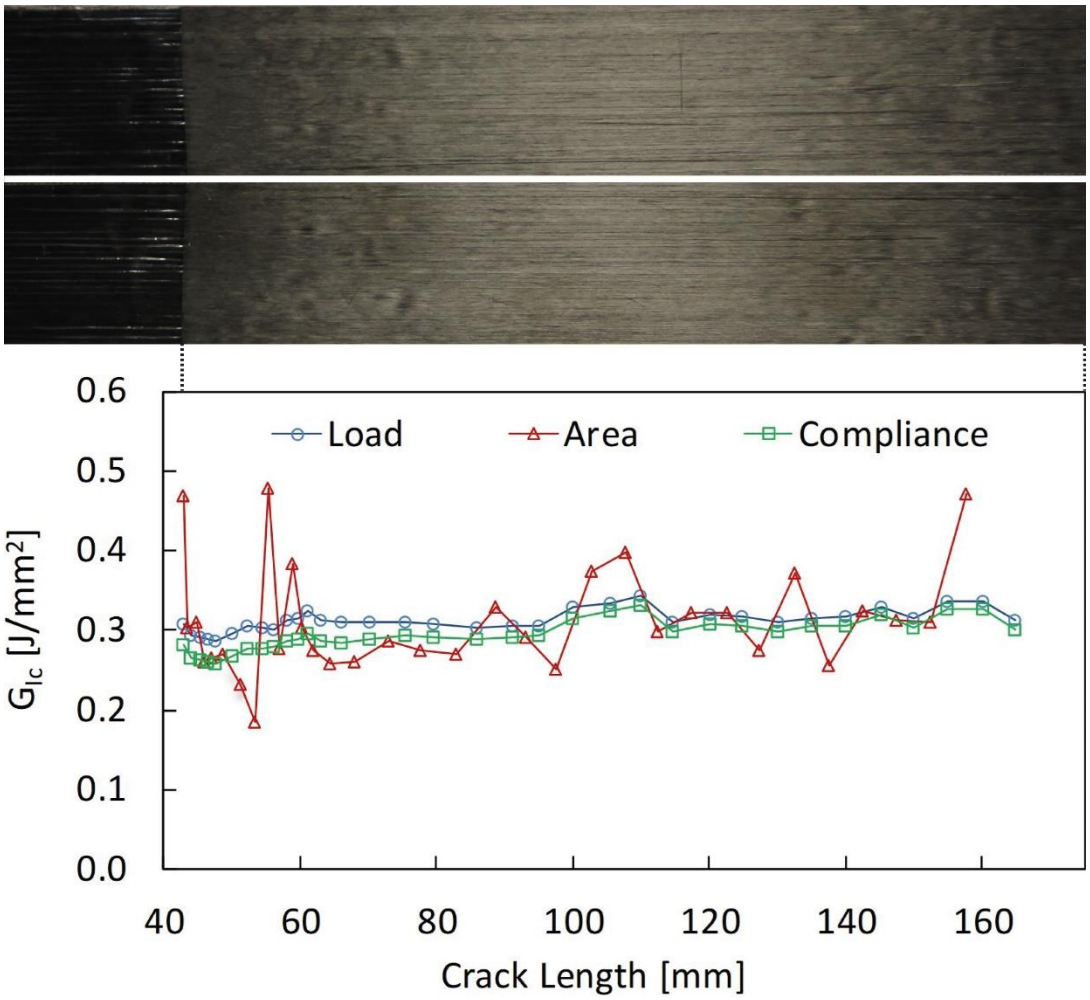

Figure 0.5. Fracture toughness results and fracture surface of (#1) C-DCB-ENF-0-0-17-MF10727

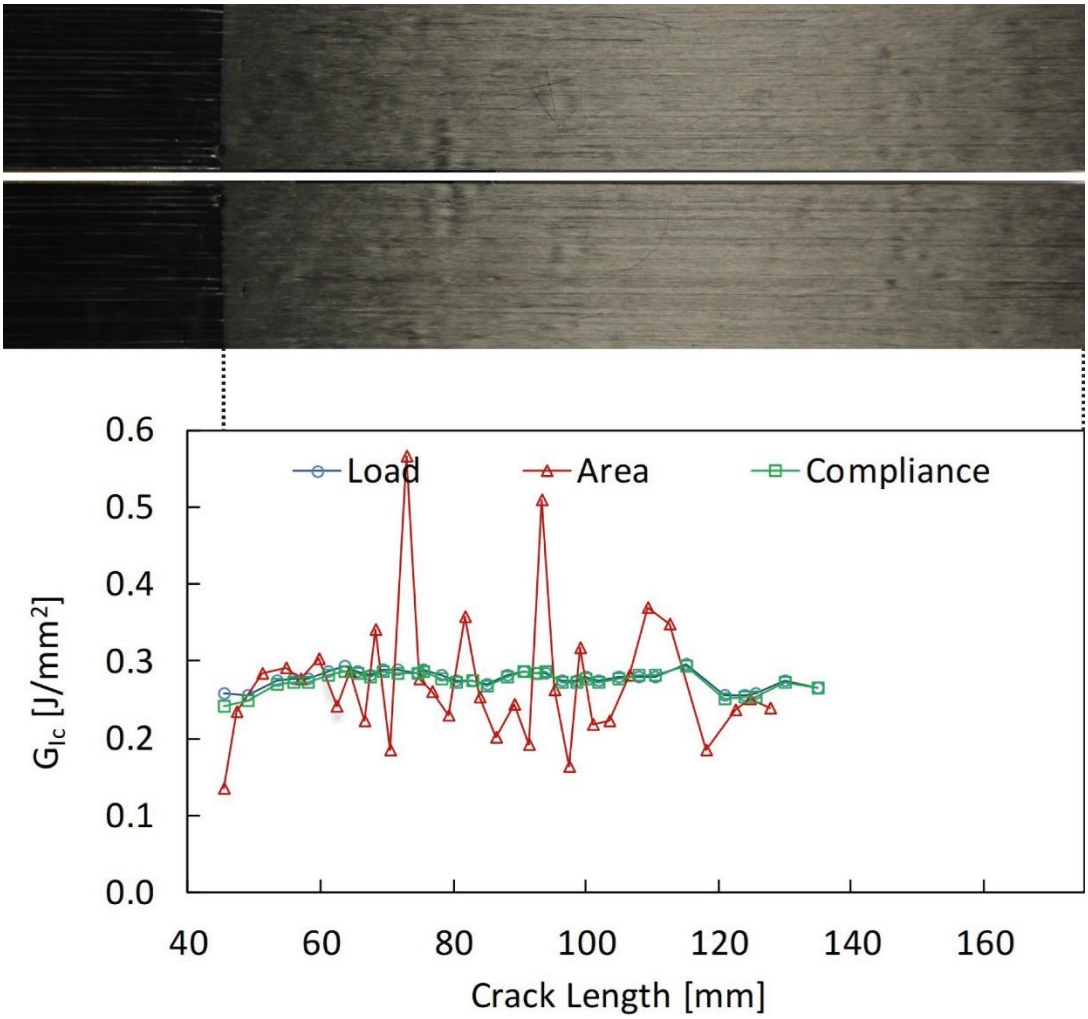

Figure 0.6. Fracture toughness results and fracture surface of (#3) C-DCB-ENF-0-0-19-MF10727

2. Mode I Fracture Toughness of 25//-25 Interface

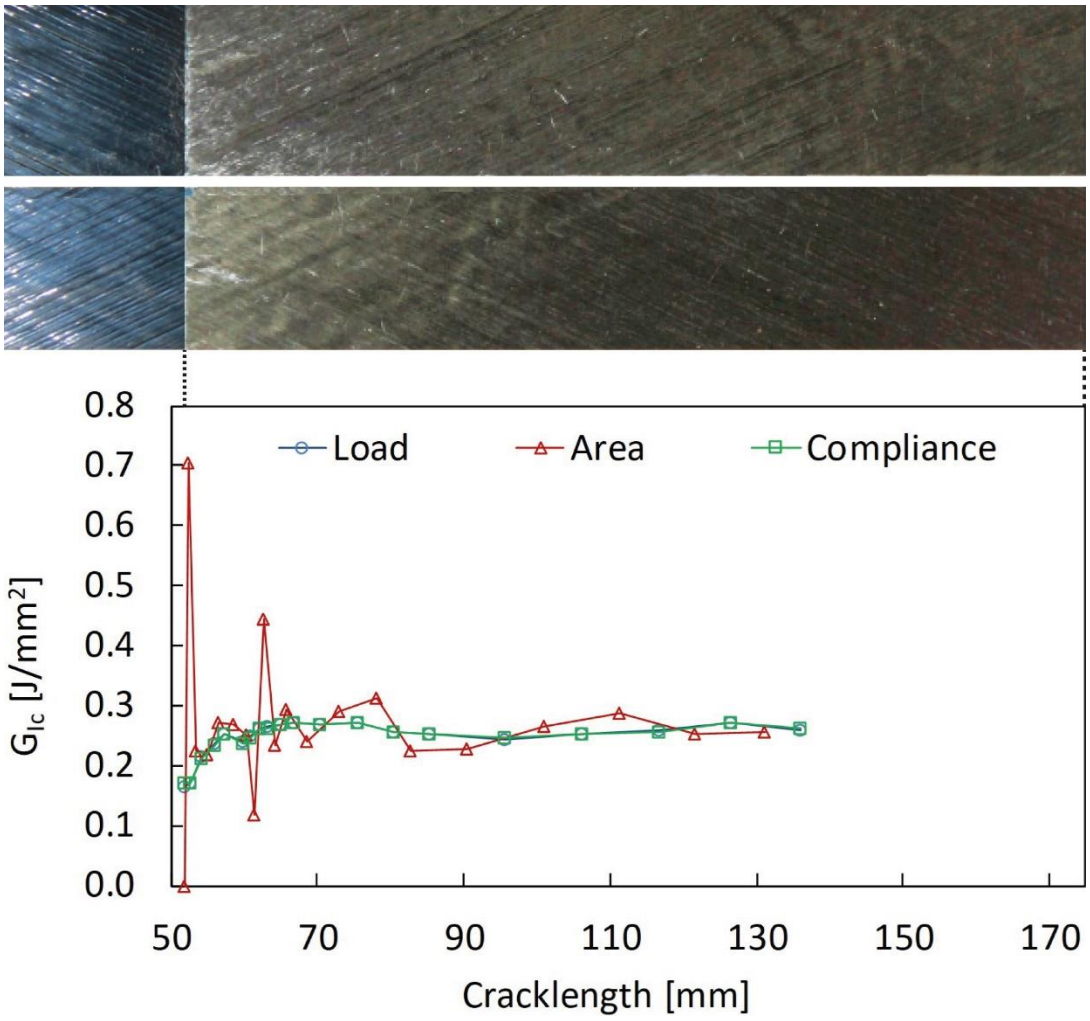

Figure 0.7. Fracture toughness results and fracture surface of (#1) C-DCB-ENF-25--25-2-MF11603

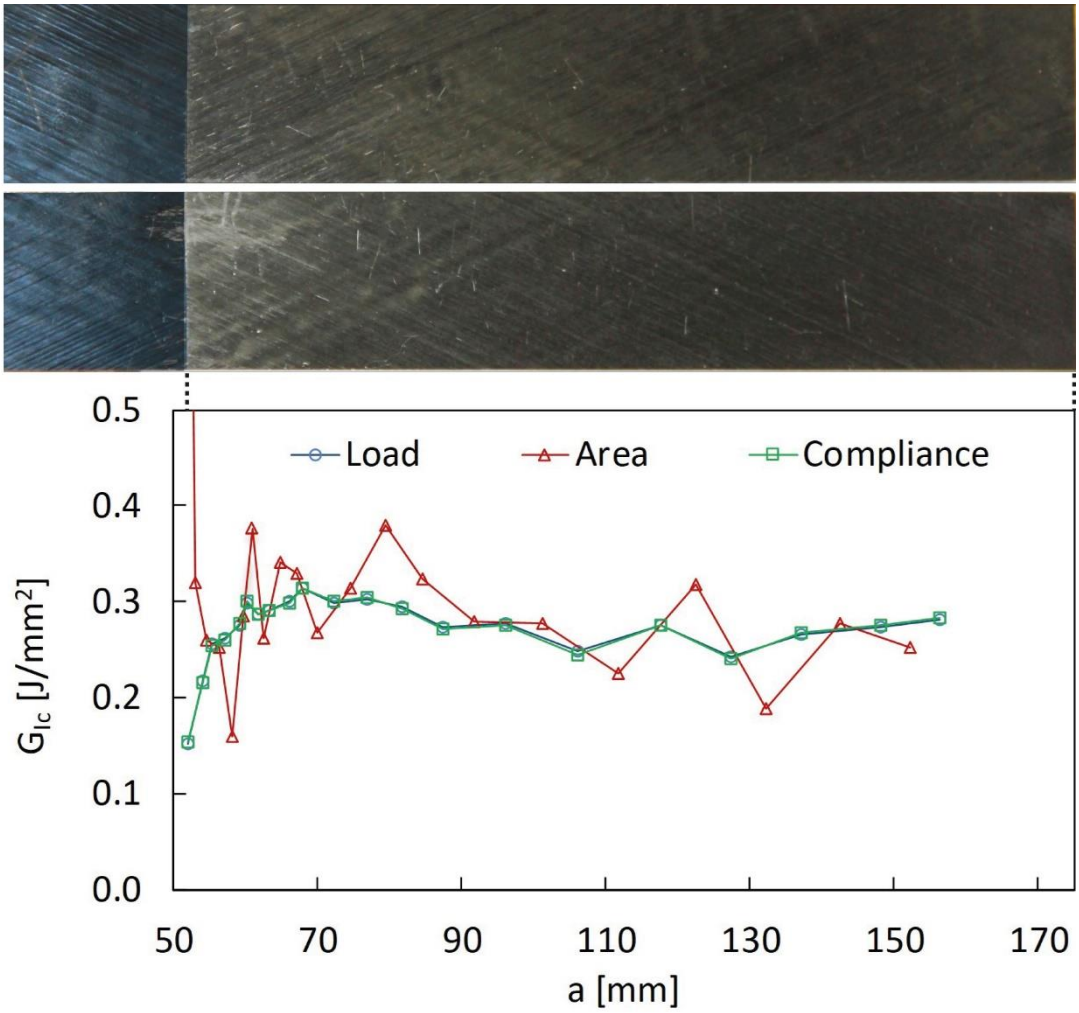

Figure 0.8. Fracture toughness results and fracture surface of (#3) C-DCB-ENF-25--25-4-MF11603

3. Mode I Fracture Toughness of 45//-45 Interface

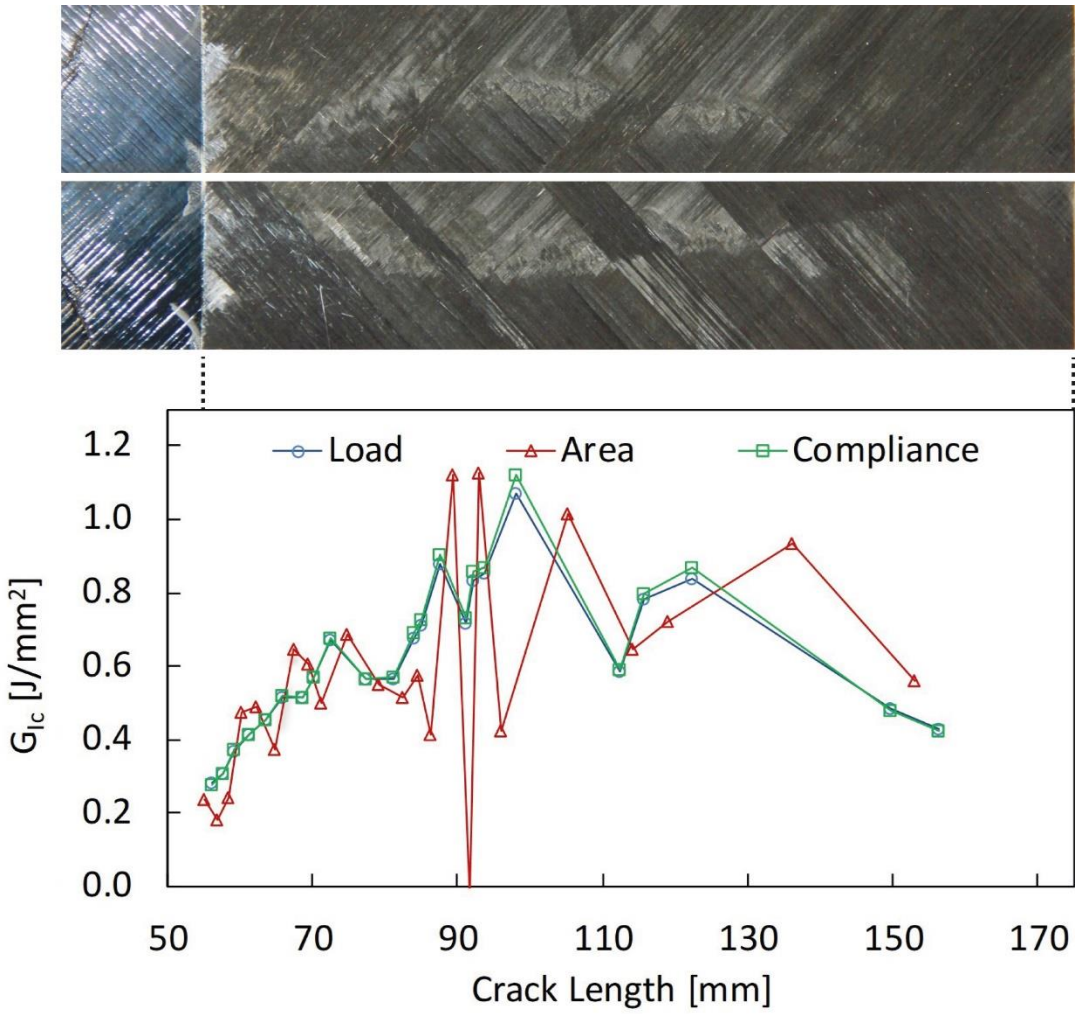

Figure 0.9. Fracture toughness results and fracture surface of (#2) C-DCB-ENF-45--45-2-MF11610

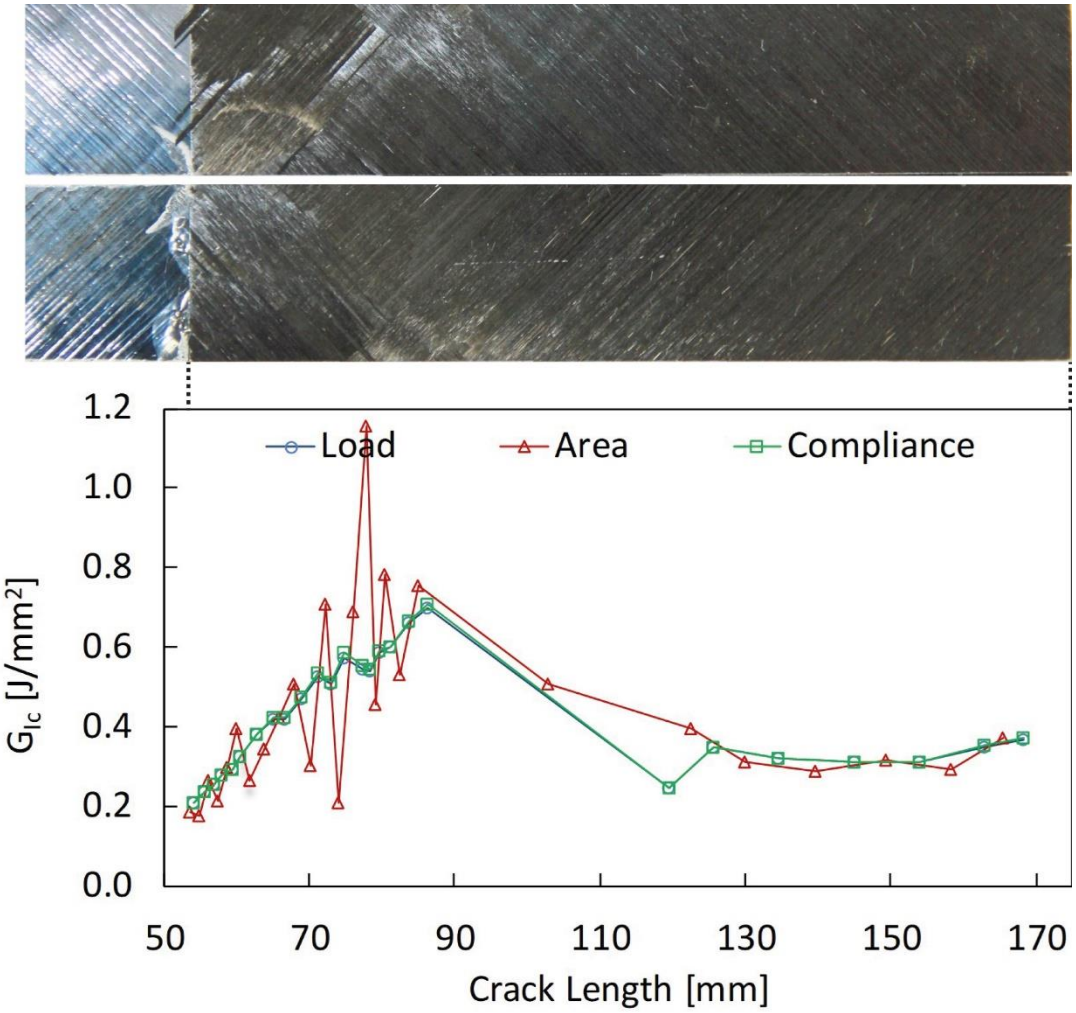

Figure 0.10. Fracture toughness results and fracture surface of (#3) C-DCB-ENF-45--45-3-MF11610

4. Mode I Fracture Toughness of 45//45 Interface

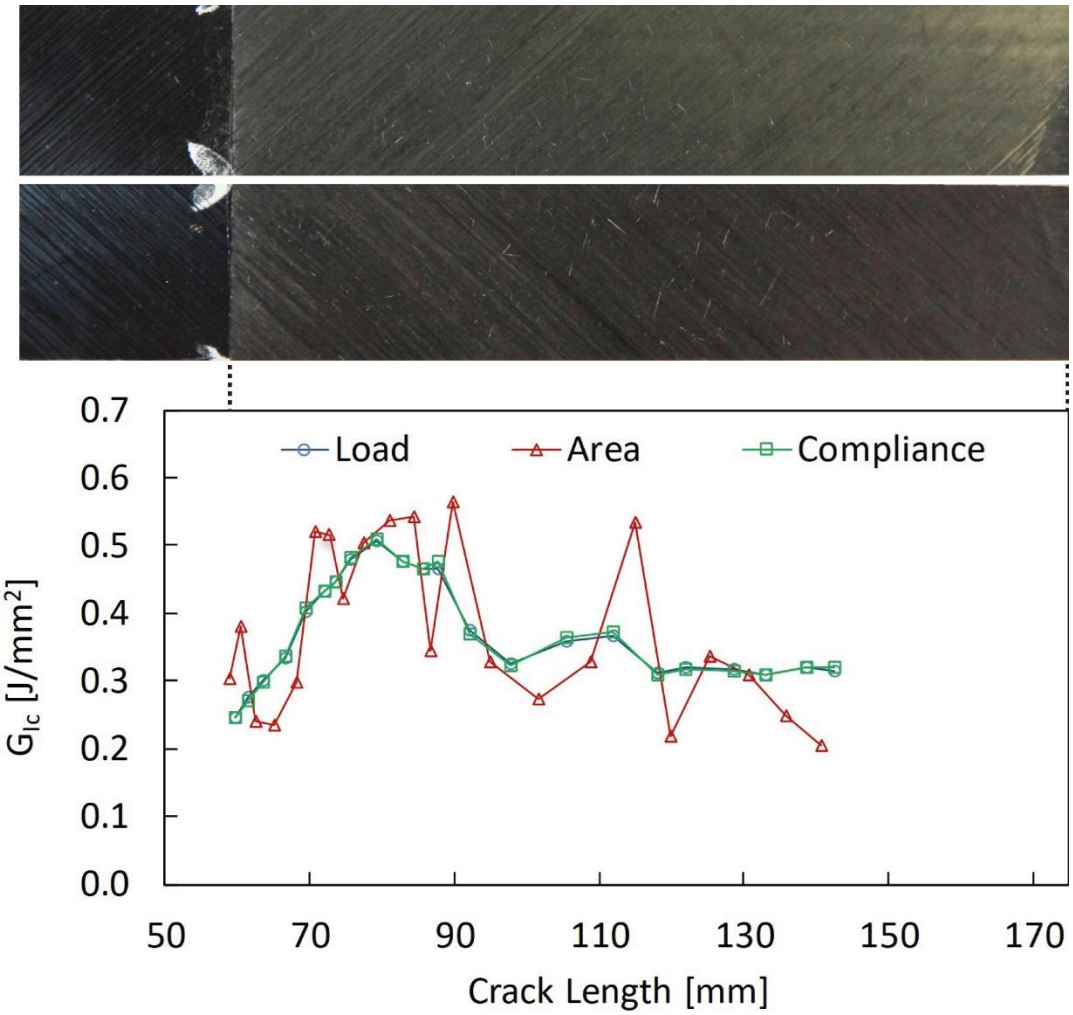

Figure 0.11. Fracture toughness results and fracture surface of (#2) C-DCB-ENF-45-45-17-MF12048

5. Mode I Fracture Toughness of 65//65 Interface

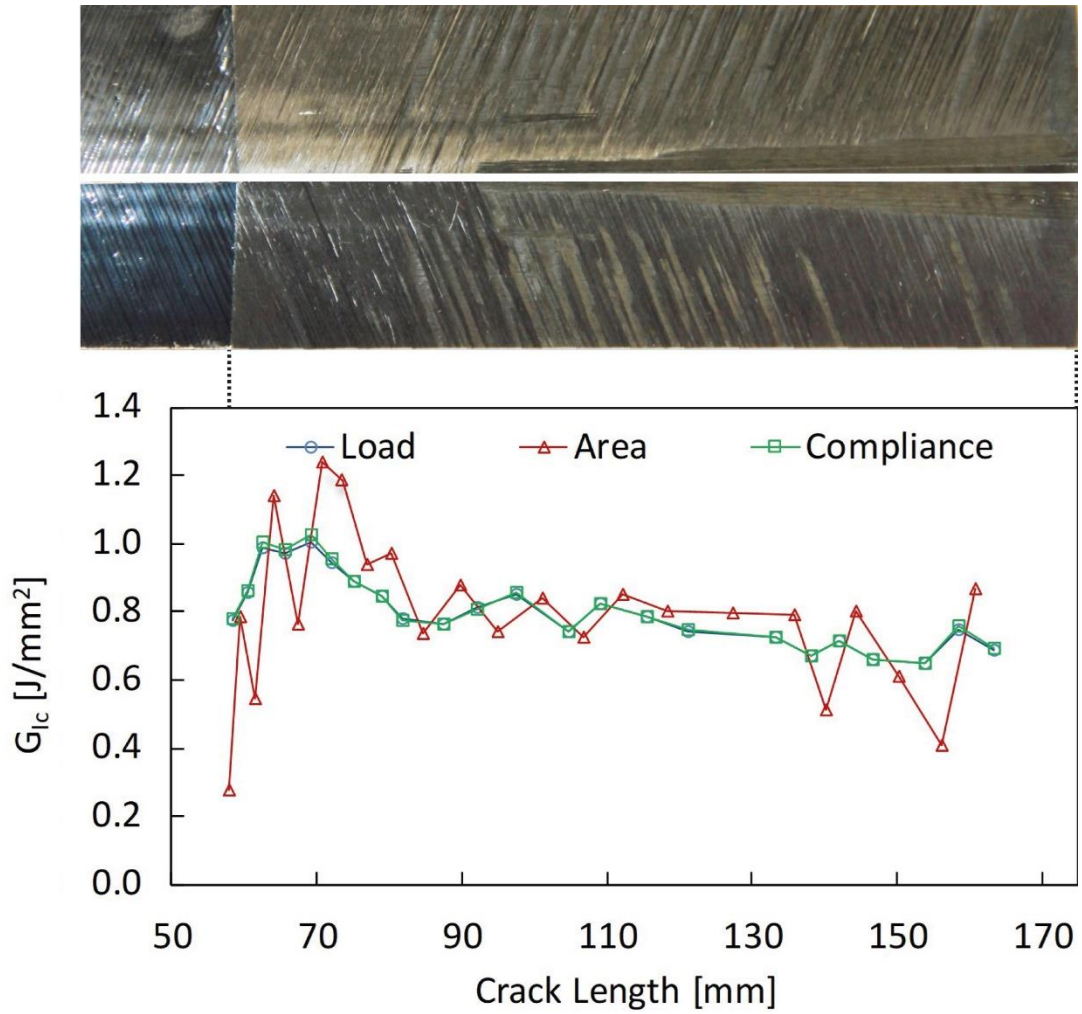

Figure 0.12. Fracture toughness results and fracture surface of (#1) C-DCB-ENF-65-65-5-MF11999

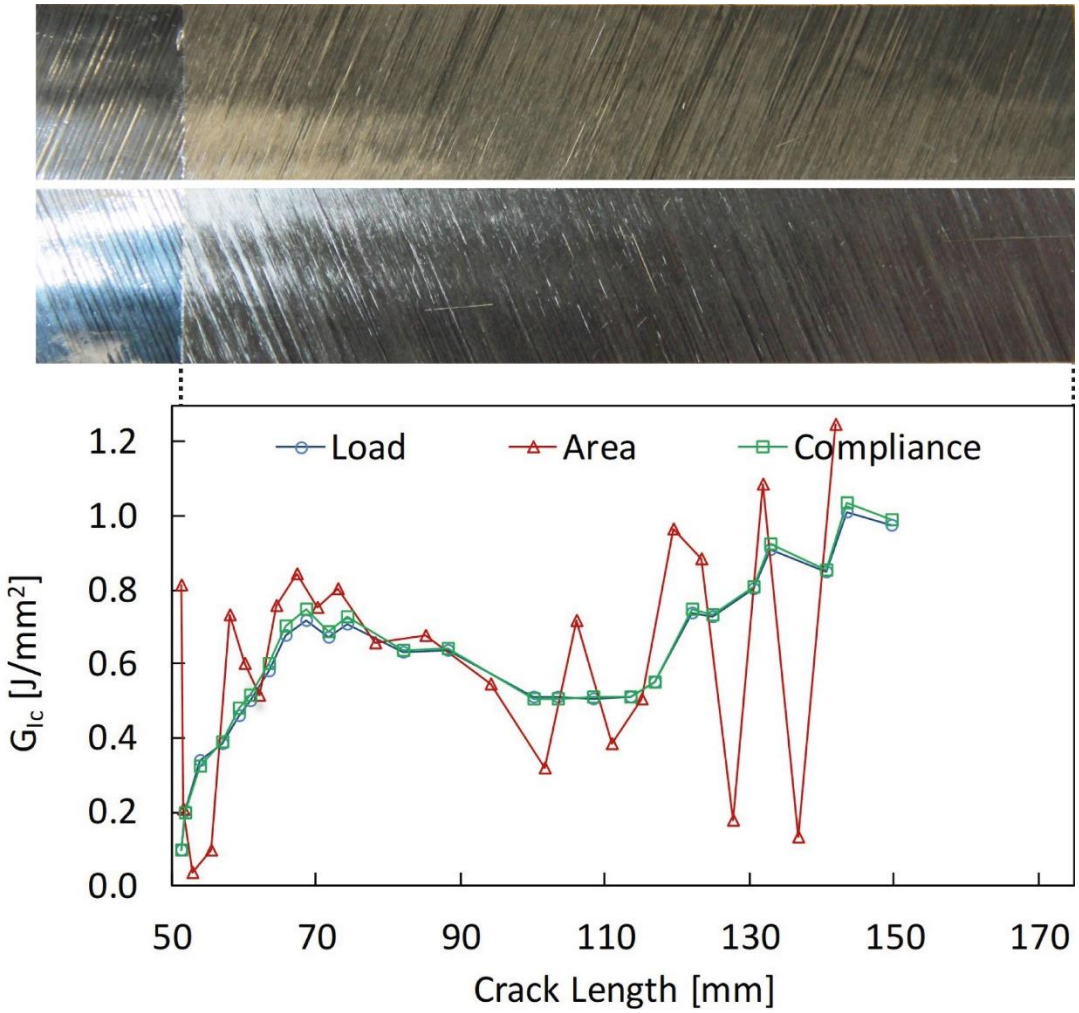

Figure 0.13. Fracture toughness results and fracture surface of (#2) C-DCB-ENF-65-65-7-MF11999

6. Mode I Fracture Toughness of 90//90 Interface

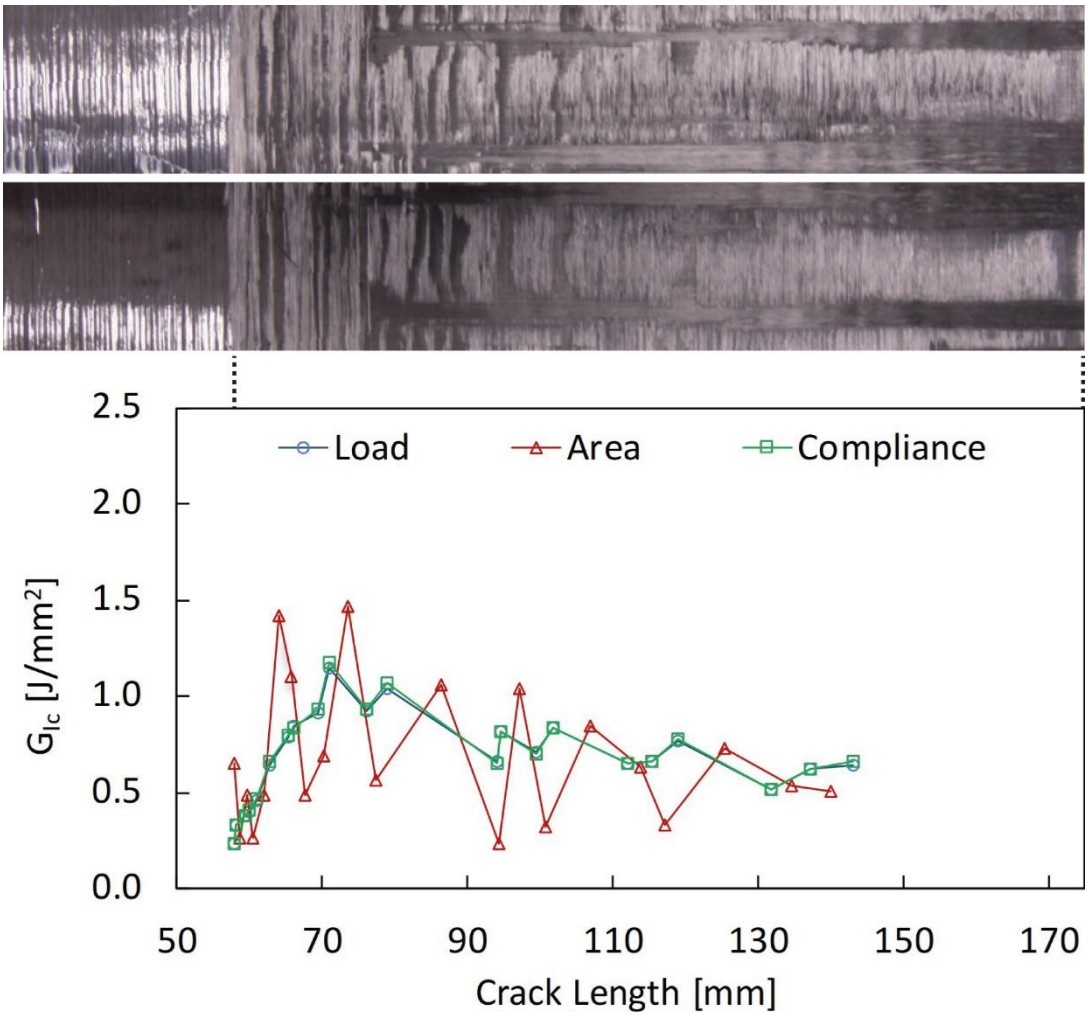

Figure 0.14. Fracture toughness results and fracture surface of (#1) C-DCB-ENF-90-90-11-MF10725

ii. Mode I Result of GFRP Specimens

1. Mode I Fracture Toughness of 0//0 Interface

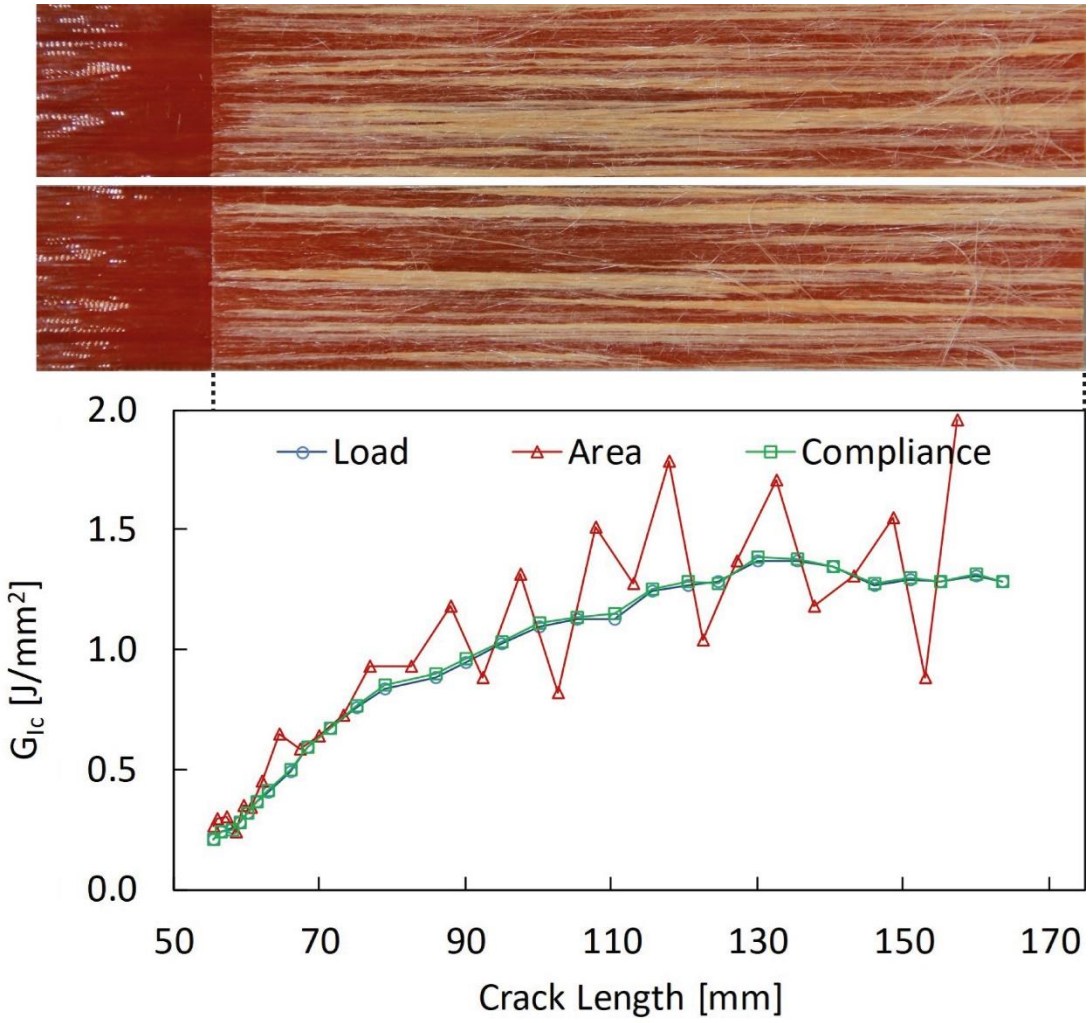

Figure 0.15. Fracture toughness results and fracture surface of (#1) G-DCB-ENF-0-0-5-MF11609

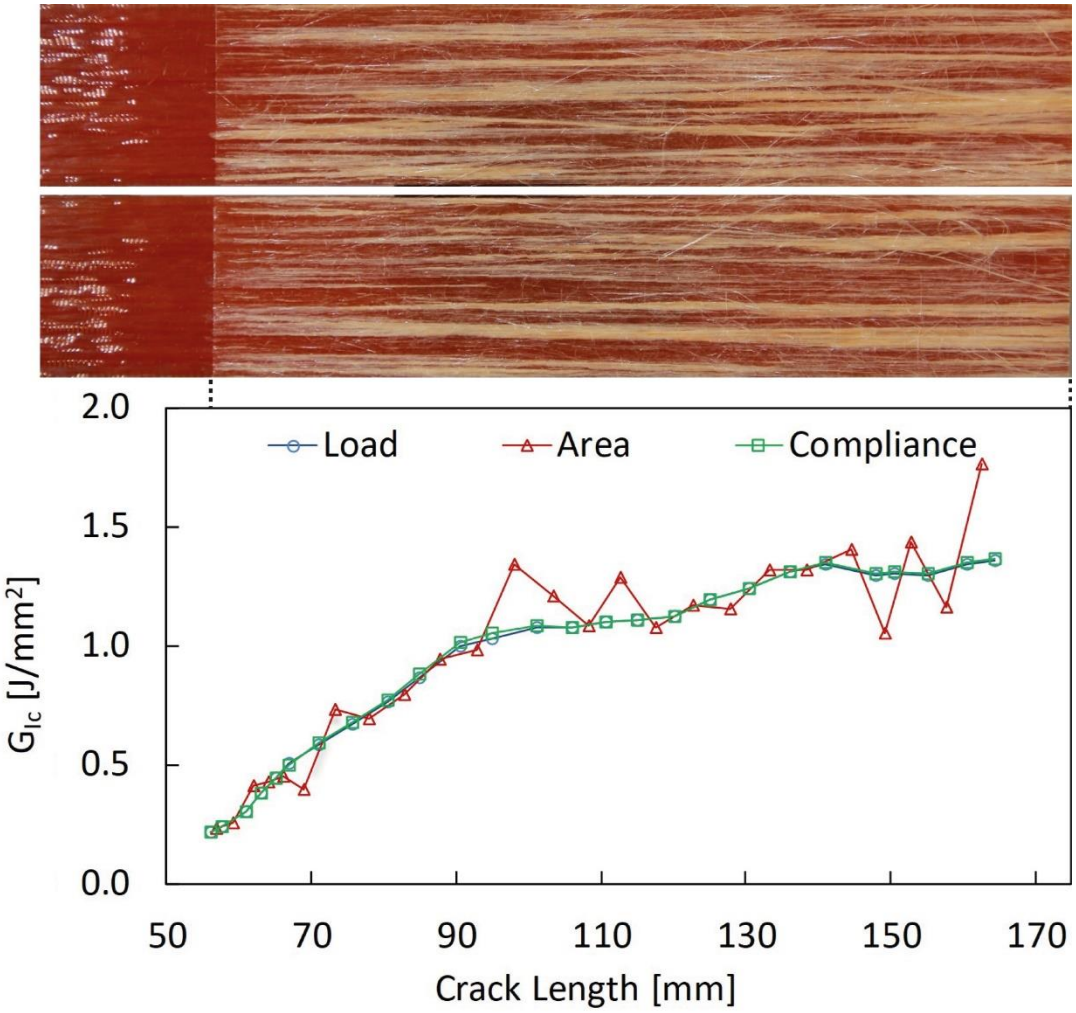

Figure 0.16. Fracture toughness results and fracture surface of (#2) G-DCB-ENF-0-0-11-MF11609

2. Mode I Fracture Toughness of 25//-25 Interface

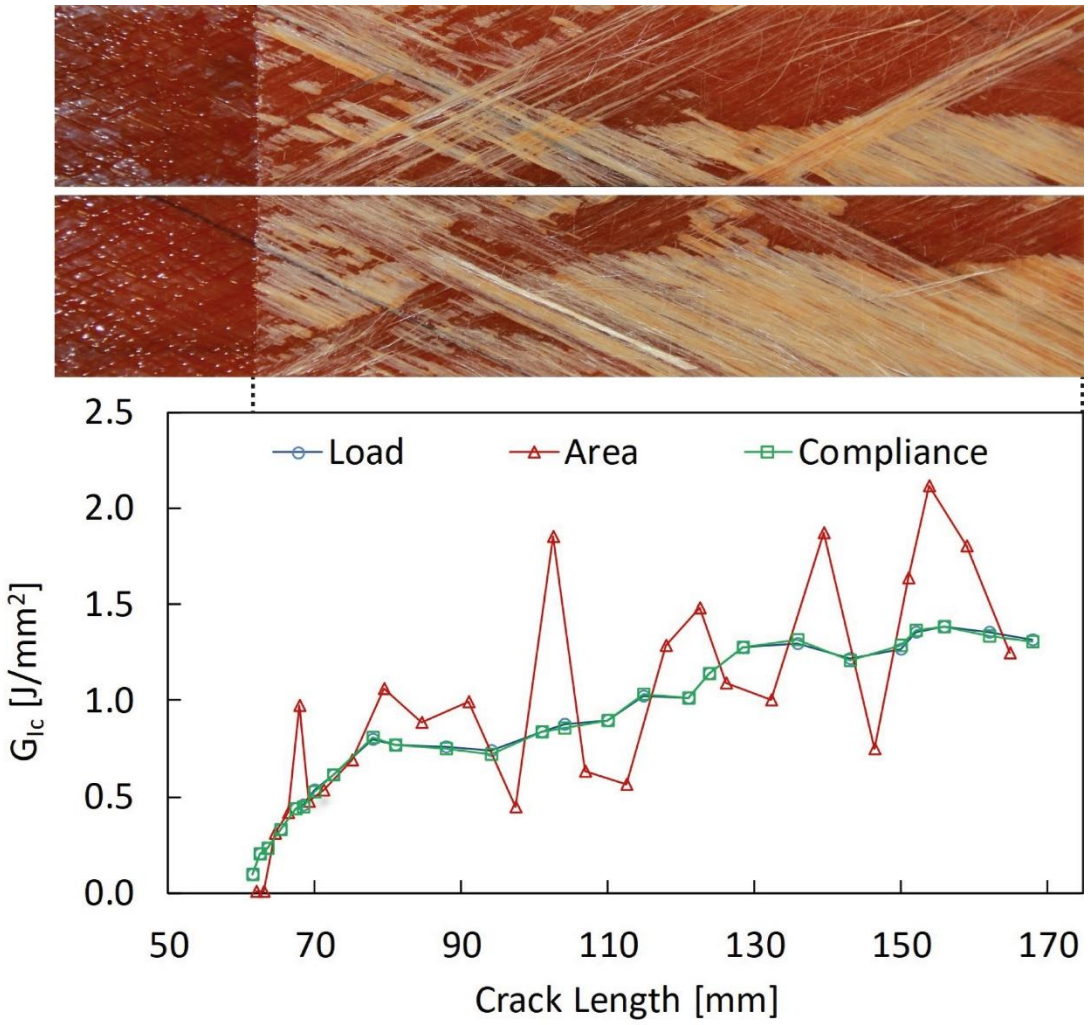

Figure 0.17. Fracture toughness results and fracture surface of (#2) G-DCB-ENF-25--25-5-MF10724

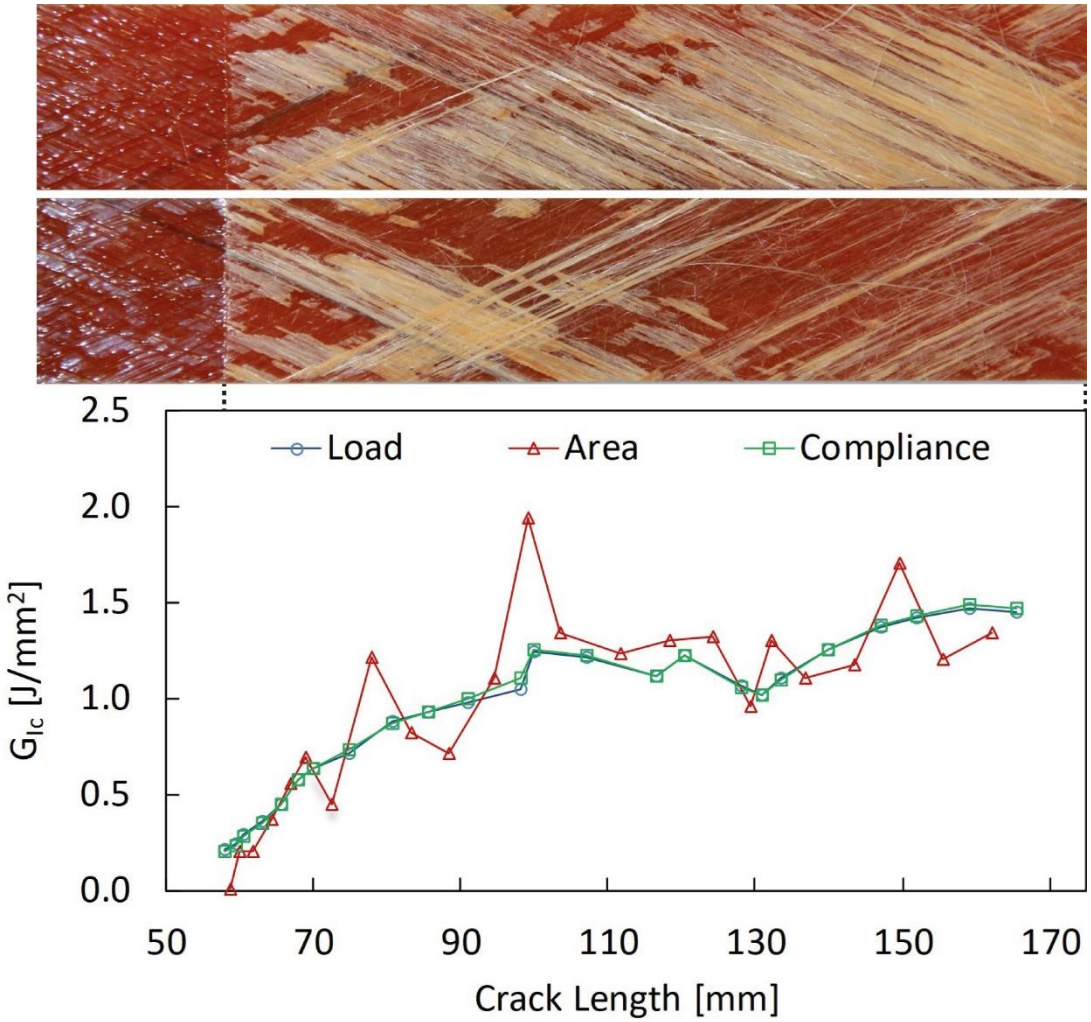

Figure 0.18. Fracture toughness results and fracture surface of (#3) G-DCB-ENF-25--25-16-MF10724

3. Mode I Fracture Toughness of 45//-45 Interface

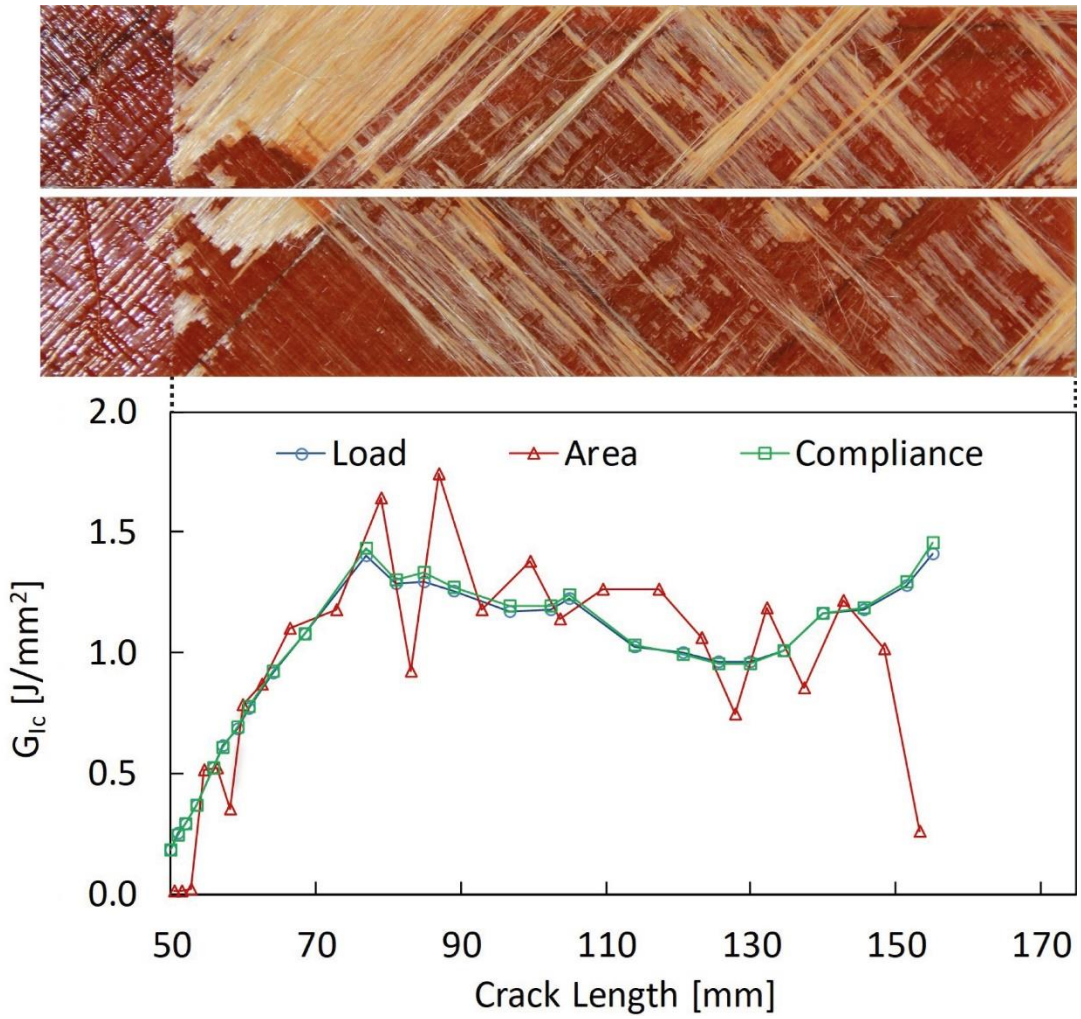

Figure 0.19. Fracture toughness results and fracture surface of (#1) G-DCB-ENF-45--45-5-MF11608

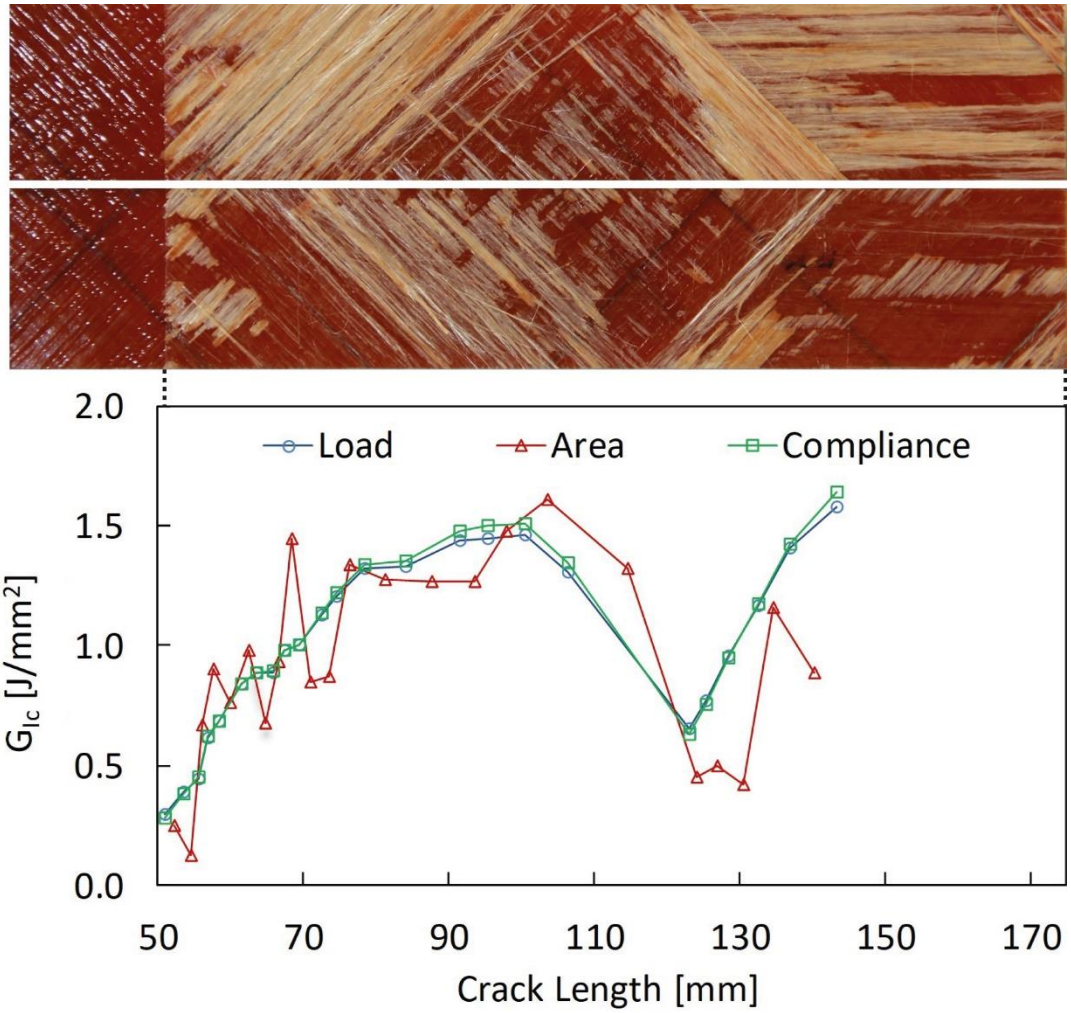

Figure 0.20. Fracture toughness results and fracture surface of (#3) G-DCB-ENF-45—45-11-MF11608

4. Mode I Fracture Toughness of 45//45 Interface

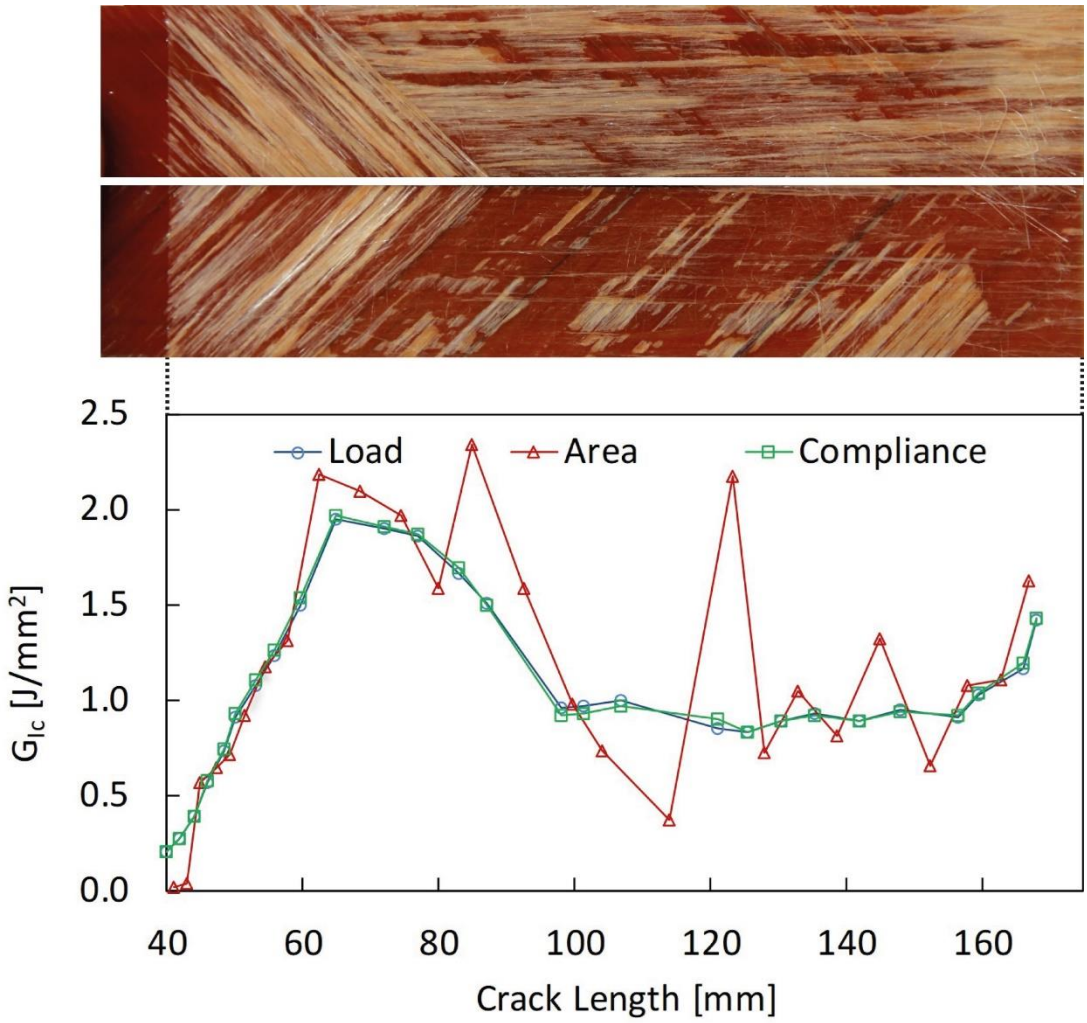

Figure 0.21. Fracture toughness results and fracture surface of (#1) G-DCB-ENF-45-45-4-MF10745

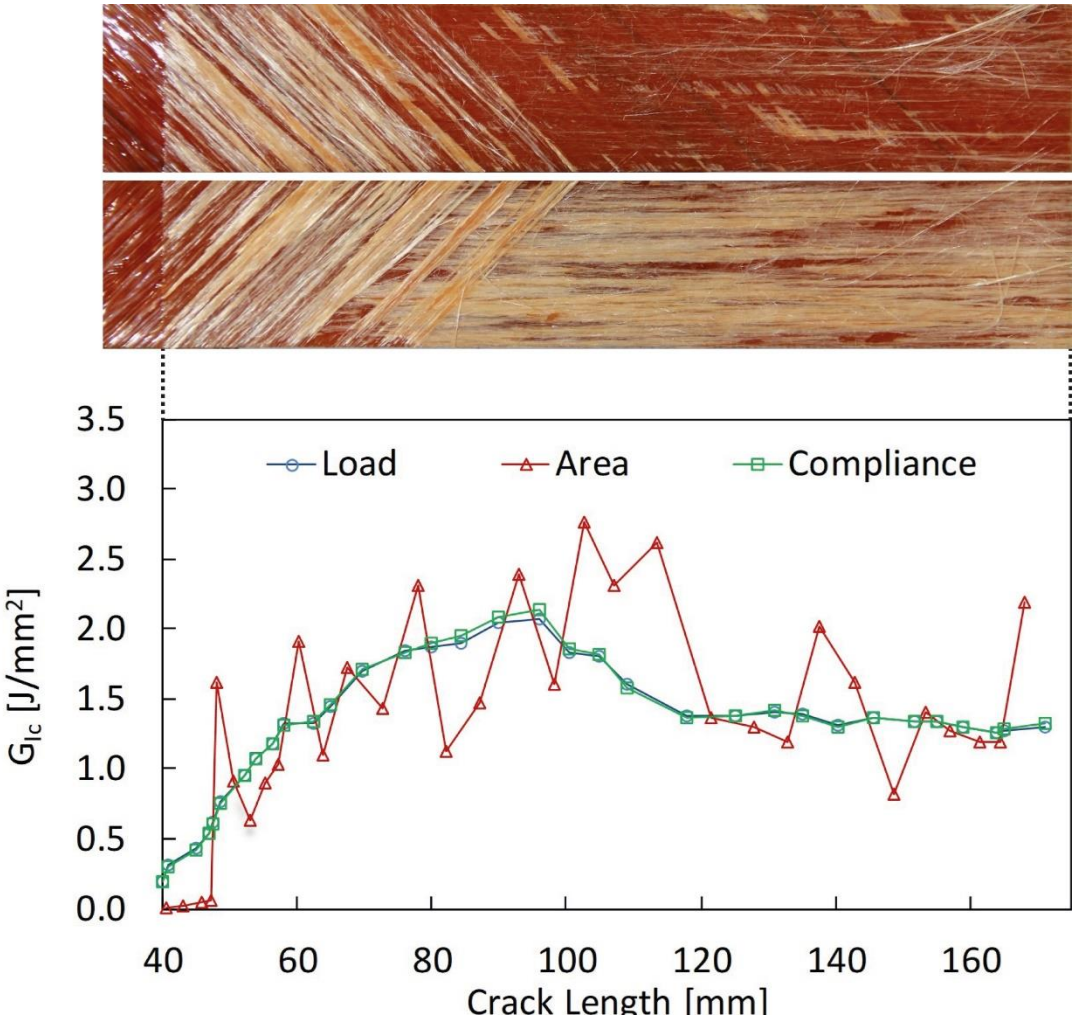

Figure 0.22. Fracture toughness results and fracture surface of (#2) G-DCB-ENF-45-45-5-MF10745

5. Mode I Fracture Toughness of 65//65 Interface

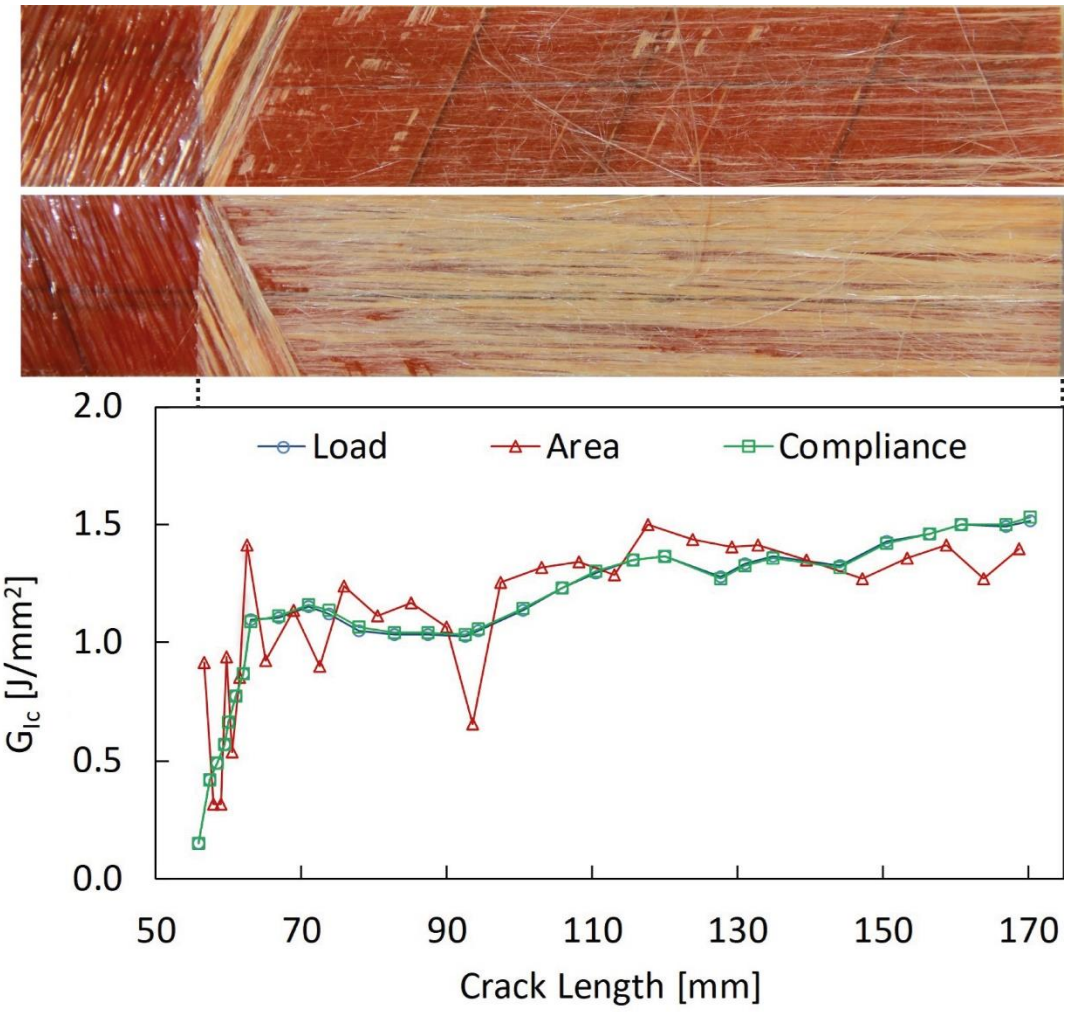

Figure 0.23. Fracture toughness results and fracture surface of (#1) G-DCB-ENF-65-65-1-MF12060

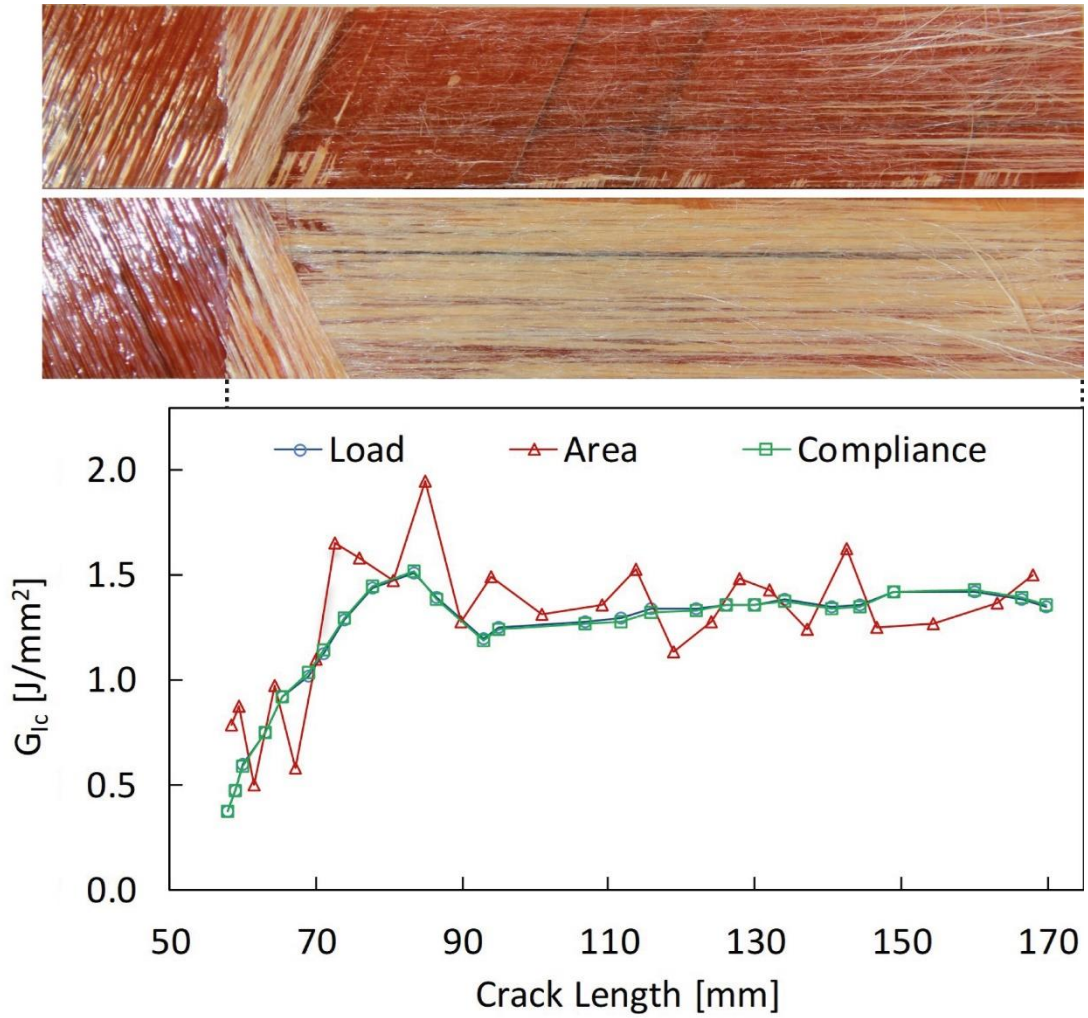

Figure 0.24. Fracture toughness results and fracture surface of (#2) G-DCB-ENF-65-65-2-MF12060